Master's thesis

NTNU
Norwegian University of Science and Technology
Faculty of Engineering
Department of Civil and Environmental Engineering

Elias Waage Helstad

A laboratory study of the mechanical behavior of Tiller-Flotten quick clay

Master's thesis in Bygg- og miljøteknikk
Supervisor: Steinar Nordal
June 2023

NTNU
Norwegian University of
Science and Technology

Elias Waage Helstad

A laboratory study of the mechanical behavior of Tiller-Flotten quick clay

Master's thesis in Bygg- og miljøteknikk
Supervisor: Steinar Nordal
June 2023

Norwegian University of Science and Technology
Faculty of Engineering
Department of Civil and Environmental Engineering

NTNU
Norwegian University of
Science and Technology

Preface

This master's thesis are performed during spring 2023 at the Geotechnical Divison of the Department of Civil and Environmental Engineering at the Norwegian University of Science and Technology. The thesis is the final individual work of the five-year-long Civil and Environmental Engineering M.Sc programme "Bygg- og miljøteknikk".

The extensive laboratory work during this semester has been time-consuming, but truly instructive and educative. The execution of the laboratory study, as well as the thereafter data interpretation, has enlightened several aspects of quick clay behavior which I am grateful to carry forward into the work as a geotechnical engineer.

Several people have been truly helpful during my work, and I am truthfully thankful for their input and advice. I would especially like to express my sincere gratitude to my supervisor, Professor Steinar Nordal, for his theoretical and educational talents throughout my time at NTNU, and especially during the work on this master's thesis. His affection for geotechnics has been truly inspiring. Professor Gustav Grimstad and Sigurdur Mal Valsson have been very helpful with their theoretical and practical visions on my thesis subject. A big thanks to laboratory engineer Espen Andersen Torsæter for his positivity and skilled fieldwork, providing me with the relevant samples needed for accomplishing this laboratory study.

Finally, I extend my gratitude to the individuals at *Geohjørnet 2023* for contributing to a motivating and pleasant working atmosphere throughout the entire semester.

Elias Waage Helstad

Trondheim, June 2023

Abstract

The results from this master thesis supplement laboratory data and identify collapse and yield characteristics for quick clay from Tiller-Flotten. Special emphasis on the identification and determination of the material behavior for the quick clay through an extensive geotechnical laboratory study with oedometer and triaxial tests. Regarding the responsibility of laboratory work and the reliability of results, different procedures for reconsolidation to in situ conditions are studied as a comparison of isotropic versus anisotropic to p'. An improvement of saturation and corresponding pore pressure response during undrained conditions are as well studied through different procedures during the B-value tests. The field and laboratory work are carried out with both traditional 54 mm piston samples and modern mini block samples. The quick clay from Tiller-Flotten shows a characteristic material behavior for highly sensitive clays.

Undrained and drained triaxial tests reveal an especially progressive behavior and collapse after reaching the ultimate strength. The failure does often develop in a localized shear band. CRS oedometer tests conducted with various strain rates uncover rate dependencies for the quick clay, both in terms of stiffness and the preconsolidation yield plateau.

Several oedometer tests also reveal a peculiar decrease of the effective stress after reaching the preconsolidation level by a pore overpressure at collapse. This is perceived as a ”snap-back” and shows how quick clay behaves in an oedometer when it’s strain-controlled and sufficiently fast brought past the preconsolidation stress. The clay reveals an increasing stiffness after the ”snap-back” effect. This happens when the sample has lost around 5 - 15 % of its initial sample volume. The ”snap-back” behavior is especially clear when testing the mini block samples on quick clay, but less visible for the piston samples. By all accounts, this has to do with the sample disturbance caused by the piston sampling method.

The triaxial test series also reveal significant differences between mini block and 54 mm piston samples. The obtained stress paths from undrained triaxial tests on mini block samples reveal a distinctive, temporary dilative behavior prior to reaching the ultimate strength and contractive collapse. Shear tests conducted on piston samples distinctively reveal a pure contractive behavior when reaching the ultimate strength. The ultimate strength is substantially lower for piston samples than for the mini block samples. An approximately 75 % higher failure strain is also observed for the piston samples.

The preconsolidation obtained from the oedometer tests may be understood as a yield point,

i.e. a point on a yield surface. The yield surface is attempted to be identified through various triaxial tests, both undrained and drained. Shear tests, as well as drained K_0' compression tests, are conducted to interpret yielding and yield characteristics for the quick clay. The resulting yield points coincide approximately with earlier proposed yield surfaces for clays with roughly the same friction angle. Missing isotropically compression tests and triaxial extension tests during this laboratory study makes it difficult to define the total form for the Tiller-Flotten quick clay yield surface.

Concerning the comparative study of isotropic versus anisotropic reconsolidation to in situ effective average stress, p', the study reveals that the high-quality mini block samples accomplish roughly the same undrained shear strength independently of the two procedures. On the contrary, piston samples indicate higher undrained strength values for the anisotropically consolidated samples. Similar for both sample types are higher failure strains for the isotropically consolidated to p'. These findings corroborate the use of the anisotropic reconsolidations to in situ conditions and suggest that even if isotropic consolidations to the same average stress level are simpler and yield relatively similar results, anisotropic reconsolidations are superior.

During this study, it is a consistent conclusion that block samples exhibit significantly better sample quality than 54 mm piston samples.

During undrained triaxial tests, subsequent increases of the back pressure were done if the system and specimen revealed unsatisfactory saturation. Following the back pressure increase from 700 to 1000 kPa, the clay specimens were allowed to rest for 180 minutes prior to the next B-test being conducted. Each sample subjected to this procedure showed an increased pore pressure response. Acceptable B-values around 0.95 was normally achieved. Air bubbles in vents and cranes contribute to unsatisfactory pore pressure response and are considered to be accountable for low B-values. Effective procedures for satisfactory saturation of cranes and vents together with substantial back pressure and resting time for the specimen are recommended.

Sammendrag

Resultatene fra denne masteroppgaven supplementerer laboratoriedata og identifiserer kollaps- og fytekarakteristikk for kvikkleire fra Tiller-Flotten. Spesiell vekt er lagt for å undersøke og identifisere materialoppførsel for kvikkleira gjennom en serie av ødometer og treaksialforsøk. For å kunne gi relevante og pålitelige resultater må leirprøvene før testing bringes til en tilstand som representerer in situ forhold. Det er derfor gjennom laboratorieforsøkene utprøvd ulike prosedyrer for rekonsolidering til in situ spenningsnivå, både anisotropt og isotropt til effektiv middelspenningsnivå, p'. En forbedring av metning og poretrykksrespons er i tillegg studert gjennom ulike prosedyrer for såkalt B-verdi testing. Felt- og laboratoriearbeidet er gjennomført både på moderne miniblokkprøver og på tradisjonelle 54 mm stempelprøver. Kvikkleira fra Tiller-Flotten viser en karakteristisk materialoppførsel for høysensitive leirer.

Udrenerte- og drenerte treaksialforsøk viser en særlig kontraktiv oppførsel og kollaps etter styrketaket nås. Bruddet utvikles ofte i et lokalisert skjærbånd. CRS ødometerforsøk gjennomført med ulike tøyningshastigheter avdekker rateavhengighet for både stivhet og prekonsolideringsspenning. Dette fremkommer av ulik stivhet og prekonsolideringsspenning ved CRS ødometerforsøk.

Flere ødometerforsøk viser en signifikant kollapsmekanisme rundt prekonsolideringen som preges av avtagende effektivspenning og poreovertrykk etter oppnådd prekonsolidering for kvikkleira fra Tiller-Flotten. Dette fremstår som et ”snap-back” og viser hvordan kvikklera oppfører seg i et ødometer når den tøyningskontrollert og tilstrekkelig raskt bringes forbi prekonsolideringsspenningen. Leira viser etter ”snap-back” igjen en økende stivhet. Dette skjer etter leira har mistet porevann tilsvarende 5 til 15 % av sitt opprinnelige prøvevolum. Denne oppførselen er særlig tydelig ved testing av blokkprøver på kvikkleire, men er i mindre grad synlig på prøver tatt med 54 mm prøvetaker. Dette skyldes etter alt å dømme prøveforstyrrelsen ved stempelprøvetakingen.

Ved treaksialforsøk ser en også betydelige forskjeller mellom blokkprøver og 54 mm prøver. Spenningsstiene fra udrenerte treaksialforsøk på miniblokkprøvene viser en markant, temporær dilaterende oppførsel før bruddtaket nås og prøven kollapser kontraktant. Skjærforsøk gjennomført på stempelprøver viser distinktivt en kontraktiv oppførsel etter oppnådd bruddtak. Bruddtaket er markert lavere for prøver tatt med stempelprøvetaker enn for prøver tatt med blokkprøvetaker. Sammenlignet med miniblokkprøvene avdekkes det en omtrentlig 75 % høyere bruddtøyning for stempelprøvene.

Prekonsolideringsspenningen i fra ødometerforsøkene kan forstås som et flytepunkt, d.v.s. et punkt på en flyteflate. Flyteflaten er også forsøkt identifisert i udrenerte og drenerte skjærforsøk. Videre er det gjennomført drenerte K_0' belastningsforsøk kvikkleiras for tolkning av flytepunkter og flytekarakteristikk. Resulterende flytepunkter sammenfaller omtrentlig med tidligere foreslåtte flyteflater for leirer med omtrentlig lik friksjonsvinkel. Manglende isotrope trykkforsøk og skjærforsøk i strekk gjør det problematisk å definere hele flyteflatens form.

Vedrørende sammenligningsstudien for isotrope og anisotrope rekonsolideringer til kvikkleiras effektive middelspenningsnivå, p', viser studien at høykvalitets miniblokkprøver oppnår omtrentlig lik udrenert skjærstyrke uavhengig av valg av konsolideringstype. I motsetning viser 54 mm stempelprøver høyere udrenert skjærstyrke for anisotropt konsoliderte prøvestykker. Likt for både stempelprøver og miniblokkprøver er en gjennomgående høyere bruddtøyning for prøvestykker isotropt konsolidert til p'. Disse resultatene støtter bruken av anisotrop konsolidering og antyder at selv om isotrop konsolidering til samme midlere effektivspenning er enklere og gir relativt like resultater, så er anisotrop konsolidering bedre og bør foretrekkes.

Det er en gjennomgående konklusjon i dette studiet at blokkprøver er av betydelig bedre prøvekvalitet enn 54 mm stempelprøver.

For prøvestykker som initielt viste utilfredsstillende metning ved gjennomføring av udrenerte skjærforsøk, ble det foretatt en påfølgende oppjustering av baktrykket. I etterkant av oppjustering av baktrykket fra 700 kPa til 1000 kPa, fikk leirprøvene hvile under oppnådd baktrykk i 180 minutter før neste B-test ble foretatt. Samtlige prøvestykker viser en forbedret poretrykksrespons etter nevnte tiltak. Akseptable B-verdier på omtrent 0.95 ble normalt oppnådd. Luftbobler i ventiler og kraner bidrar til utilfredsstillende poretrykksrespons og vurderes å bære mye ansvar for lave B-verdier. Kraner og ventiler som reduserer faren for å fange luftbobler bør brukes. Gode prosedyrer for å mette opp kraner, ventiler og slanger er viktig. Bruk av et betydelig baktrykk med en påfølgende hvilefase etter påført baktrykk anbefales.

Table of content

Figures

Tables

Notations

A_0	Initial cross-section area
A_{kons}	Cross-section area change after consolidation
A_{shear}	Continous updated cross-sectional area during shearing
B	Skemptons pore pressure parameter
E_u	Undrained stiffness
G	Shear modulus
H_0	Initial sample height
H	Sample height
I_L	Liquidity index
I_P	Plasticity index
K_0'	Earth pressure coefficient at rest
K	Bulk modulus
M_0	In-situ oedometer stiffness
M_L	Smallest oedometer stiffness after preconsolidation
M_{oed}	Oedometer stiffness
M	Slope of CSL in p':q space
OCR	Overconsolidation ratio
P	Piston force
S_r	Degree of saturation
S_t	Sensitivity
V_0	Initial sample volume
V_{kons}	Sample volume change after consolidation
V_p	Pore volume
V_s	Volume of solids
W	Work
ΔA	Cross-section area change
ΔV	Expelled pore water / Change in sample volume
$\Delta\sigma$	Stress change
Δe	Void ratio change
Δr	Change in radial strain
Δu_b	Pore pressure change
δ_a	Axial deformation

$\dot{\varepsilon}$	Strain rate
γ_s	Unit weight
ρ_d	Mineral density
ρ	Density
σ'_m	Average stress in oedometer condition
σ'_{cv}	Vertical preconsolidation stress
σ'_{h0}	In-situ effective horizontal stress
σ'_{v0}	In-situ effective vertical stress
σ_1	Largest principle stress
σ_3	Smallest principle stress
σ_a	Axial stress
σ_c	Cell pressure in triaxial cell
σ_r	Radial stress
τ	Shear stress
ε_a	Axial strain
ε_f	Failure strain
ε_p	Volumetric strain
ε_q	Shear strain
ε_r	Radial strain of sample
ε_{v0}	Axial strain at σ'_{v0}
ε_{vol}	Volumetric strain
ε	Strain
φ'	Friction angle
a	Attraction
c_u	Undrained shear strength
c_v	Consolidation coefficient
c_{uA}	Active, undrained shear strength
c_{ufc}	Undrained shear strength by falling cone
c_{urfc}	Remoulded shear strength by falling cone
c_{ur}	Remoulded shear strength
c	Constant when performing falling cone tests
e_0	Initial void ratio
e	Void ratio
g	Gravity
m_s	Mass of solids
m_w	Mass of water
m	Modulus number
p'_0	Isotropic preconsolidation stress
p'	Effective average stress
p	Average stress
q	Deviator stress
r_0	Initial radius of sample
t	Time

u_b	Pore pressure
v	Spesific volume
w_L	Liquid limit
w_P	Plastic limit
w	Water content
z	Depth from terrain surface

Abbreviations

CADC Consolidated anisotropic, drained compression test.

CAUC Consolidated anisotropic, undrained compression test.

CIDC Consolidated isotropic, drained compression test.

CIUC Consolidated isotropic, undrained compression test.

CPTU Piezocone penetration test.

CRS Oedometer test by constant rate of strain.

In-situ The samples actual situation in its natural location.

MCCM Modified Cam Clay Model.

NGF Norwegian Geotechnical Society.

NGTS Norwegian GeoTest Sites.

NGU Norway's National Geological Survey.

NVE Norwegian Water Resources and Energy Directorate.

SVV The Norwegian Public Roads Administration.

Chapter 1

Introduction

1.1 Background

Quick clay along Norwegian fjords and in regions below the marine limit may cause disastrous consequences if retrogressive or progressive landslides are triggered. After the well-known quick clay landslide in Rissa, in 1978, extensive work has been done to identify hazardous quick clay zones across the country, (Gregersen, 2008). Natural erosion along rivers and streams impose risks for landslide triggering, but human activity and construction work has induced the biggest threat towards triggering quick clay landslides, as in Rissa and at Skjeggestad, (Helle, 2017). Thus, maintaining stability and safe design around areas characterized by quick clay requires a wide understanding and knowledge concerning the behavior of this complex soil material.

Our knowledge concerning the material behavior of quick clay is mostly based on laboratory tests, where the clay samples are subject to controllable stresses, relevant to their natural origin or design issue. Various geotechnical laboratory tests that are carried out in the laboratory follow thoroughly prepared guidelines, both nationally and internationally. Laboratory work is crucial for our understanding of the material and interpretation of engineering properties. The interpretation of laboratory tests provides an understanding of the material's strength, stiffness, and deformation properties.

To be able to utilize the material behavior observed in the laboratory for providing safe design and measures, it's crucial to apply relevant loads and stresses to the clay samples when performing laboratory tests. Laboratory results must be representative of the in-situ behavior. This requires high-quality samples and high-quality testing procedures at the geotechnical laboratory.

This master's thesis presents a comprehensive laboratory study of high-quality quick clay samples from Tiller-Flotten for identification of the material behavior when subjected to different loadings. The yielding characteristics for the quick clay, extracted from around 9-12 meters depth, are obtained during the laboratory work and further correlated to proposed soil models and earlier research regarding clay behavior. The thesis challenges some procedures of

geotechnical special tests, such as obtaining proper undrained conditions in the triaxial cell and how to handle rate dependencies in oedometer tests. The effect of the overall sample disturbance, from the extrusion of the soil samples from the test site to performing laboratory investigations, is as well studied due to the modern high-quality sampling methods.

1.2 Objectives and purpose

The present master's thesis investigates and interprets mechanical behavior for the Tiller-Flotten quick clay, such as stress history, yielding characteristics, and strength data. The material behavior is identified through conducting a wide laboratory test program, including different types of triaxial compression tests as well as oedometer and routine tests. The laboratory work has been carried out on both high-quality mini block samples, as well as traditional 54 mm piston samples, to further identify differences regarding strength envelopes and yielding characteristics. Throughout the laboratory study, procedures for triaxial consolidations back to in-situ conditions and how to achieve undrained conditions are studied during the implementation of undrained shear tests. In addition, the effect of anisotropic versus isotropic consolidation to the effective mean stress, p', is studied.

The laboratory test results are interpreted using several material models proposed and used in the geotechnical industry for simulating soil response. The effect of the modern high-quality sampling methods and rate dependencies are as well studied to reveal a wider characteristic of the Tiller-Flotten quick clay. Routine and index tests performed do correlate the clay properties to an overall geotechnical categorization of the deep clay deposit at Tiller-Flotten.

1.3 Limitations

The basis for this laboratory study is relatively wide, with a large number of available samples. Nevertheless, additional high-quality samples would be desirable. The performed compression tests could be supplemented with tension tests, as well as drained stress path testing, to further investigate yielding characteristics for the Tiller-Flotten quick clay. An extended study regarding the different rate dependencies would also expand the knowledge from this laboratory study.

1.4 Thesis structure

The present master's thesis is structured to cover the relevant phases from the soil sampling in situ, through the different steps prior to executing the laboratory investigations, and until the test results are interpreted. Chapter 2 presents characteristics regarding clay, especially quick clay, through the geotechnical index, strength, and deformation parameters. A basis for the definition of yielding characteristics is described. Chapter 3 reviews the different sampling methods and the differences in resulting sample quality, and addresses the procedures for the different geotechnical test procedures. Chapter 4 presents the geological history and geotechnical characterization of the current test site, Tiller-Flotten. A description of how the

laboratory test program is meant to answer the research questions is described in Chapter 5. The test results and interpretations are given in Chapter 6 and discussed in Chapter 7. A short summary and conclusions may be found in Chapter 8.

Chapter 2

Geotechnical characterization of clay samples

2.1 Routine- and index parameters

Routine and index parameters are used to identify natural soils into soil types like sand, moraine, clay, quick clay, etc. In addition, routine and index parameters may help in estimating mechanical properties based on experience. For a geotechnical classification of clay materials, there are several relevant index parameters to consider. However, chapter 2.1 presents the most central parameters relevant to the thesis topic, such as water content, density, plasticity, and falling cone strength.

Water content

The complex behavior of clays is to a large extent affected by the existence of water. The water content, together with the clay particles and their arrangements and applied stresses influence the soil structure, (Helle, 2017). The natural water content is found to typically span from $20-50$ % for Norwegian clays and is discovered to link with several mechanical properties of the soil, both strength and deformation properties. One example may be seen in Figure 2.1, which relates the natural water content to the undrained shear strength. The water content is defined as shown in Equation (2.1), as the relation between the dry mass, m_s, and the weight of water in the sample, m_w, (Sandven et al., 2017). Soil below the groundwater table is often assumed fully saturated, ($S_r = 100\%$), which suggests that the pore volume is filled with water and has no presence of air or gasses, (Emdal, 2022).

$$w = \frac{m_w}{m_s} \tag{2.1}$$

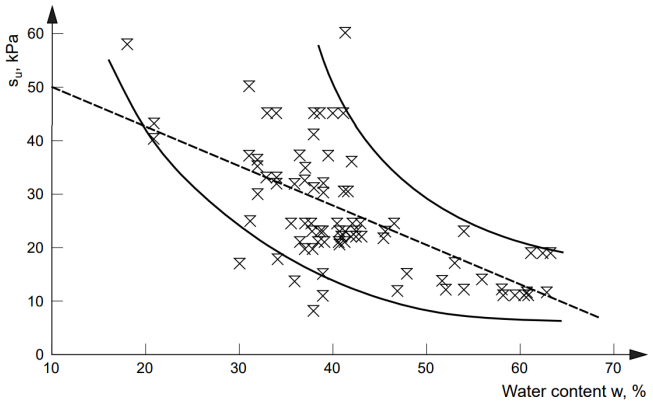

Figure 2.1: The natural water content correlated to the undrained shear strength. Taken from Sandven et al. (2017).

Density and weight

Norwegian clays often reveal a unit weight, γ_s, around $17-21\ kN/m^3$, which corresponds to a density, ρ, around $1.7-2.2\ g/cm^3$. The densities of soil deposits significantly impact the weights of overlaying soil, the corresponding stress situation, and the in situ state of soil deposits. An obtainment of these parameters is especially important and forms a basis for geotechnical evaluations of the in-situ state for soil deposits. Since the mineral density for saturated Norwegian clays is found to be in the range between $\rho_d \approx 2.6-2.8\ g/cm^3$, the density measures the porosity of the void ratio. The void ratio relates to geotechnical properties.

Liquid- and plastic limit

For investigations on which water contents the behavior of clays change, the liquid and plastic limits are identified. These parameters have been correlated to strength data in later studies, and empirically linked to strength-, deformation- and other mechanical properties. One example is Skemptons well-known expression from 1957, Equation (2.4), linking strength data to the plasticity index (Wood, 1990). The liquid limit, w_L, correlates to the water content of clayey soils when it's on the limit to behave like a liquid. The plasticity limit, w_P, correlates to the water content of the clay when it's crumbling and behave like a soft, deformable, plastic mass. This mostly depends on the fines content (Sandven et al., 2017). The liquidity- and plasticity index is further calculated as shown in 2.2 and 2.3.

$$I_L = \frac{w - w_P}{w_L - w_P} = \frac{w - w_P}{I_P} \qquad [\%] \tag{2.2}$$

$$I_P = w_L - w_P \qquad [\%] \tag{2.3}$$

$$\frac{c_u}{\sigma'_{cv}} = 0.11 + 0.37 \cdot I_P \tag{2.4}$$

The liquidity index is found to be of great value when comparing both the structure and history of clay deposits (L'Heureux et al., 2019). For fine-grained materials, especially clayey soils, the liquidity index may be used to correlate strength values. According to Leroueil et al. (1983), the remolded shear strength may be expressed as seen in Equation (2.5) if the water content of the sample is exceeding the liquid limit. By this expression, if the liquidity index exceeds 1.6, the remolded shear strength will be less than $0.5kPa$, indicating that the residual strength of the material is close to the definition of a quick clay (*def:* $c_{ur} < 0.33$ kPa). Clays are further classified from plasticity as shown in table 2.1. The plasticity index, I_P, expresses the clay particles' ability to bind water. A high I_P imply a highly plastic material that behaves plastic for a large variation in water content. The clay classification in terms of plasticity may be seen in Table 2.1.

$$c_{ur} = \frac{1}{(I_L - 0.21)^2} \qquad [\text{kPa}] \tag{2.5}$$

Clay	**Plasticity**	I_P
Low plastic	Low plasticity	< 10
Medium plastic	Medium plasticity	10 - 20
Highly plastic	High plasticity	> 20

Table 2.1: Classification from plasticity (Statens Vegvesen, 2016).

2.2 Strength parameters

Undrained- and remolded shear strength

Natural soil deposits retain quite different characteristics. For fine-grained soils, especially natural clays, the ability for water to maneuver through the soil is very limited, and may thereby take a long time. To be able to evaluate and interpret the soil strength and stiffness for design after an immediate load application, it's, therefore, a necessity to obtain the soil strength in undrained conditions (Nordal, 2020). Undrained conditions are representative of low permeable soils, such as clayey and silty materials. Performing undrained laboratory tests, where the pore water cannot escape from the soil structure, is essential for obtaining the short-term strength parameters for low permeable soils. The pore water and clay particles will in such load circumstances behave as one material, where the pore water carries the main proportion of the applied load, also denoted an excess pore pressure (Sandven et al., 2017).

For undrained conditions, the undrained shear strength, c_u, is the strength-defining parameter. Normally, the undrained shear strength is obtained through the implementation of different laboratory tests where clay samples are subjected to axial compression or tension. We

know that soil responds differently in compressive and tensile loadings and that the undrained strength varies for different load directions (Lunne et al., 2011). The dissimilarity between compression- and extension strength is further discussed in section 3.5. The remolded shear strength characterizes the residual material strength after a significant structural collapse, without any change in the natural water content, further described in Section 2.3. Table 2.2 shows the classification of clays based on their undrained shear strength and corresponding sensitivity, and equation (2.6) defines the material sensitivity.

$$S_t = \frac{c_u}{c_{ur}} \tag{2.6}$$

c_u (kPa)	**Shear strength**
< 25	Low
25 - 50	Medium
> 50	High

(a) Shear strength classification.

S_t (-)	**Sensitivity**
< 8	Little sensitive
8 - 30	Medium sensitive
> 30	Highly sensitive

(b) Sensitivity classification.

Table 2.2: Classification from shear strength and sensitivity (Statens Vegvesen, 2016).

Strength on an effective stress basis

Strength described in an effective stress state separates from short-term undrained analysis and takes into account the permeability of soils in a time aspect of the design situation. Under an applied surface load, pore water is allowed to drain, the excess pore pressures will decrease, and the material strength will over time be affected by a denser soil skeleton due to an effective stress increase. To be able to find and obtain the soil strength when the in-situ stresses increase, an effective stress analysis based on the material friction angle, φ', and material attraction, a, is necessary.

The material friction angle and the material attraction are parameters used in the effective stress analysis, often combined with the Coulumb-criterion or other proposed material models defining a strength envelope. The material attraction is mainly used as a curve-fitting parameter, for a reliable coupling with the failure line seen from triaxial tests, to define a failure surface for the soil material. The friction angle defines the inclination of the critical failure line observed from the same triaxial test and describes how the effective stress condition impacts the material's ability to mobilize shear stresses without going to failure as a shear strength envelope.

2.3 Quick clay

Different attributes of clayey soils are to be identified all over the world. For countries localized in the northern hemisphere, especially Scandinavia, Russia, and Canada, highly sensitive, brittle clays are typical due to glaciation, saltwater deposition, land uplift, and freshwater leaching. Quick clays are originally deposited and situated below the marine limit. Due to the long-lasting land uplift after the last ice age, significant amounts of these marine deposits are nowadays situated above the marine limit and affected by freshwater infiltration. The freshwater infiltrates these marine deposits, and in the long run, washes away the natural salts which ensure the strong bond between the clay particles.

After the salty pore water is substituted by the fresh groundwater, the clay deposit is sensitive to an overload, which may cause a structural collapse and the clay particles to float in their own pore water (NVE, 2019). The ability to become liquefied, when subjected to loadings, is a major factor governing post-failure behavior. Initial quick clay landslides often leave an unstable scarp behind and thereby behave in a retrogressive matter (L'Heureux, 2012), as seen from Figure 2.2. The retrogressive behavior of quick clay landslides is commonly acknowledged, initially proposed by Bjerrum (1955). Thus, in an undisturbed manner, quick clay is a fairly stable and strong material. Collapses and overloads, which lead to quick clay landslides and failures, are often linked to human activity, in terms of construction works and redistribution of masses, or natural causes such as river erosion or an increase in pore pressure.

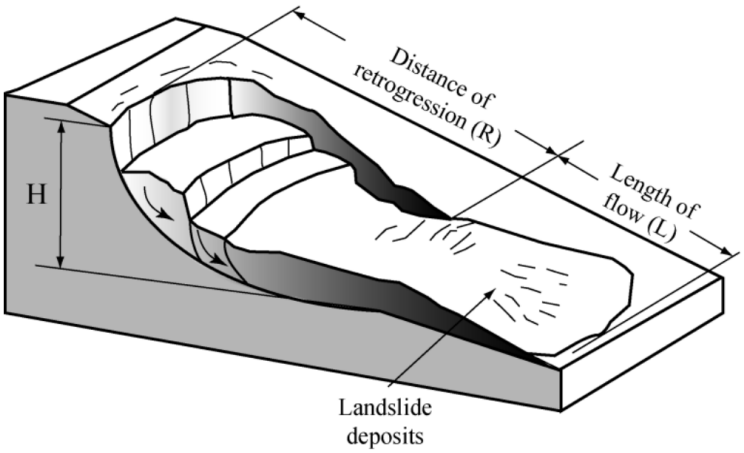

Figure 2.2: Retrogressive model of quick clay landslides. Taken from L'Heureux (2012).

Quick clay is a highly brittle material. Brittle materials are low ductile materials, with a low level of residual strength. Norwegian regulations, hereby the guidelines presented by The Norwegian Water Resources and Energy Directorate (NVE), define quick clay by a remolded shear strength of $c_{ur} \leq 0.33$ kPa, according to ISO 17892-6:2017 (Standard Norge, 2017). Older guidelines used $c_{ur} \leq 0.5$ kPa as the definition of quick clay. In general, brittle clays- are defined by a remolded shear strength ≤ 1.27 kPa, (NVE, 2019). Several other index parameters, such as salinity and sensitivity, as well as results of in situ field tests, characterizes quick clay.

Water content above the liquid limit, $w \geq w_L$ and salt content below $5g/L$ may indicate a highly sensitive material. In situ investigations, such as Piezocone penetration test (CPTU)- and total soundings, as well as field vane tests, may be useful to identify brittle behavior. Such methods provide powerful tools for further evaluation and investigation, to a precise and effective matter be able to identify these hazardous quick clay locations.

Because of its low residual strength, landslides in areas containing quick clay may be disastrous. Geotechnical engineers have a unique responsibility to identify and localize possible quick clay zones and thereby assure a safe design to prevent any retrogressive landslides. It's hereby of central importance to understand the mechanical and structural behavior of these highly sensitive natural clays, to be able to predict and model a safe design. Laboratory tests have over the years provided a lot of experience on strength properties and other mechanical parameters for us to be able to correlate and identify brittle clays. Because of the potentially catastrophic and horrendous consequences, it's important to provide further research on quick clay to be able to avoid future frightful disasters.

2.4 Deformation properties and stress conditions

Deformation of materials is a central issue in geotechnics and requires an understanding of the soil response due to different load cases. Knowledge and understanding of stress conditions and mechanical properties of soil layers enable us to predict deformations. A combination of strength-, stiffness-, and deformation data gives us powerful tools for proper design (Sandven et al., 2017).

The degree of overconsolidation, defined by equation (2.7), expresses stress history based on the largest previously experienced overburden, also called vertical preconsolidation stress, σ'_{cv}. An overconsolidation ratio above 1, $OCR > 1$, suggests that the soil sample has previously experienced higher stresses than the current in situ effective stress. If $\sigma'_{cv} > \sigma'_{v0}$, a relaxation of the stresses will affect the structure of soils, and cause swelling of clayey soils (Statens Vegvesen, 2022). The preconsolidation stress, σ'_{cv}, is often interpreted from oedometer tests, and coincides with a clear drop in the $\sigma'_{v0} - \varepsilon_a$ curve, as shown in figure 3.16.

$$OCR = \frac{\sigma'_{cv}}{\sigma'_{v0}} \tag{2.7}$$

The preconsolidation stress is hereby a result of the loading- and time history for the given clay. Loading beyond the preconsolidation plateau will lead to the accumulation of large strains while loading below σ'_{cv} cause modest strains and deformation since this will be a reloading. Rate dependencies complicate this complex behavior (Länsivaara, 1999).

The consolidation effects for low-permeable soils are immensely important, both for understanding the stress history for soil deposits, as well as for interpreting the soil response when subjected to loadings. Regarding stress history, normally consolidated (NC) clays are only seen to have been consolidated for their own weight and thereby the present overburden (σ'_{v0}). An

overconsolidated (OC) deposit has earlier been exposed and consolidated to an additional stress level ($\sigma'_{v0} + \Delta\sigma$) (Sandven et al., 2017).

The consolidation process describes the interaction between the soil particles and pore water, as well as how this interaction develops over time seen on the basis of stresses and soil structure. In low-permeable soils, loading beyond the in situ condition will cause the pore water to, in an undrained matter, initially carry the load as an excess pore pressure. When time passes, slow drainage of the pore water will decrease the excess pore pressure. Figure 2.3 shows the development of excess pore pressure in undrained conditions. The dissipation leads to a tighter connection between the soil particles and an increase in the effective stress. The consolidation procedure takes place until the excess pore pressure is fully dissipated (Nordal, 2020).

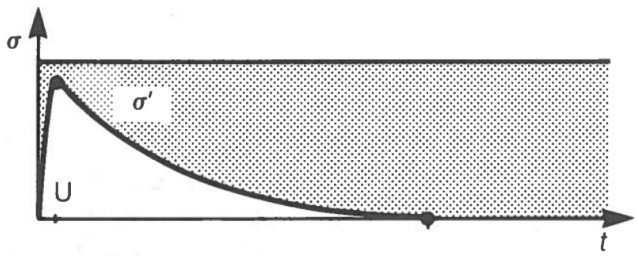

Figure 2.3: Excess pore pressure (U) dissipation by time for an undrained load application for low-permeable soils. Taken from Sandven et al. (2017).

2.5 Yield surfaces and mechanical behavior of clays

One of the most central challenges in geotechnical engineering has been to fully understand and predict the complex soil behavior when subjected to various loading scenarios. The soil response has been a research topic for a long time, and in the mid 20's century, computational models based on the theoretical plasticity approach were proposed (Wood, 1990). These methods resulted from numerous laboratory tests of different soils and may simulate soil behavior in complex design issues. Several models have been proposed for different soil materials and different loading scenarios. A complex scientific work of laboratory testing, categorization of soil parameters, and further development of calculation methods is the basis for the advanced computational simulations we're able to perform nowadays, especially by the use of the finite element method (Länsivaara, 1999).

2.5.1 Yielding of clays

To form a conventional basis for understanding general material behavior, it's stated that the preconsolidation stress, σ'_{cv}, marks the start of yielding for natural clays, and further that the stiff response which is seen from the oedometer curve for stresses below this yield point may be assumed elastic (Wood, 1990). If the stresses on the clay sample exceed the preconsolidation plateau and are later unloaded, a stiffer response is characteristic of the stress path in this

elastic region. The same effect also appears in the triaxial cell, when clay samples are subjected to isotropic loading and unloading. The exact point which identifies the start of yielding for natural clays may be seen as a moving memory, in situ given by stress- and geologic history, and in the laboratory given by controllable loading patterns by execution of different special tests. In principle, it is the highest stress state the sample has experienced previously. Thus, the definition of yielding and development of plastic mechanisms has to be interpreted in correlation to the applied initial and boundary conditions.

Yielding of undisturbed clay samples may therefore by execution of different compression tests be determined by a significant drop in the material stiffness, (Yong & McKyes, 1971). The two-dimensional stress condition which is achieved in axisymmetric laboratory tests is thus a limitation for our insight into the true three-dimensional, anisotropic in situ condition. The oedometer condition, characterized by initial conditions as described in section 3.6, may define one singular yield point due to its stress- and strain condition. Additionally, different types of triaxial tests give the opportunity to impose different load combinations and initial conditions to the clay sample, and further identify several yield states for identification and understanding of the yield locus of the undisturbed, natural clay, (Wood, 1990).

The mechanical behavior of natural clays differs from other pure isotropic and elastic materials, due to the complex interaction of the soil particles and pore water. The identification of yielding may therefore not be as straightforward as for other materials, and the utilization of several various stress-, strain- and other relations has to be interpreted to obtain the start of yielding (Wood, 1990). The p':q - plane may be used for conventional drained- and undrained triaxial tests, where coinciding q-ε_a an p'-v - plot substantiates the location for the yield point (Wood, 1990). Equation 2.8 to 2.10 defines the effective average and deviator stress by the principle stresses, as well as the specific volume by the void ratio, e.

$$p' = \frac{1}{3}(\sigma_1 - 2\sigma_3) - u_b \tag{2.8}$$

$$q = \sigma_1 - \sigma_3 \tag{2.9}$$

$$v = 1 + e \tag{2.10}$$

There are proposed several different methods for on a general matter interpreting yield points from different tests, where Tavenas et al. (1978) shows that the definition of work, W, may give reliable identification to support conventional stress-strain curves. Equation (2.11) shows the expression for the work done in the triaxial cell, given by the p'-q - space and coinciding volumetric- and shear strains. Graphical visualizations of the work, W, correlated with strain parameters may be of significant assistance to substantiate the localization of the yield point. On a general basis, Wood (1990) points out that identification and localization of yield points should be obtained by several relations for optimal yield point detection.

$$W = \int (p' \cdot d\varepsilon_p + q \cdot d\varepsilon_q) \tag{2.11}$$

2.5.2 Elastic- and plastic strains

Based on several performed scientific laboratory studies regarding the mechanical behavior of clay, various elastoplastic material models are proposed to simulate the material behavior. The different models are based on moving yield surfaces and take into account the preconsolidation stress as a memory-based parameter for the given soil (Graham et al., 1983). Popular models, such as for instance various Cam Clay models, are developed to describe and simulate the soil response for fairly different design purposes. In common, all models take into account an elastic response for stress states defined inside the yield surface. If a stress change in the two-dimensional stress space hit the yield surface, it will move outward and the response characterizes as both elastic- and plastic (Nordal, 2020).

When the response inside the defined yield surface is assumed isotropic and elastic, as earlier studies support (e.g. Länsivaara, 1999; Días-Rodríguez et al., 1992; Graham et al., 1983), equation (2.12) describes the relation between the elastic strains and stress changes. Equation (2.13) and 2.14 express the plastic volumetric- and shear strains as a superposition when pushing the defined yield surface outward as both elastic- and plastic contributions (Wood, 1990).

$$\begin{bmatrix} \delta {\varepsilon_p}^{el} \\ \delta {\varepsilon_q}^{el} \end{bmatrix} = \begin{bmatrix} 1/K & 0 \\ 0 & 1/3G \end{bmatrix} \begin{bmatrix} \delta p' \\ \delta q \end{bmatrix} \tag{2.12}$$

$$d\varepsilon_p = d{\varepsilon_p}^{el} + d{\varepsilon_p}^{pl} \tag{2.13}$$

$$d\varepsilon_q = d{\varepsilon_q}^{el} + d{\varepsilon_q}^{pl} \tag{2.14}$$

The strain components described above, and their corresponding directions, reveal the clay material response as irretrievable when expanding or translating the yield surface. Correspondingly irreversible shear strains develop. The directions of these strain increments are from studies interpreted to have a somehow orthogonal direction to the yield envelope (Wood, 1990). Yielding is therefore associated with the development of irreversible plastic strains, $d{\varepsilon_p}^{pl}$ and $d{\varepsilon_q}^{pl}$.

The size of these strain increments, which by definition is parallel to the p' and q axis, defines the direction of the total strain increment, $d\varepsilon^{pl} = d{\varepsilon_p}^{pl} + d{\varepsilon_q}^{pl}$. This behavior is further correlated with different yield points along the yield envelope to either enlarge or reduce the size of the yield surface, also defined as the flow rule and plastic potential in the proposed elastoplastic mathematical material models (Nordal, 2020). Figure 2.4 shows a typical yield surface and its enlarged plastic potential.

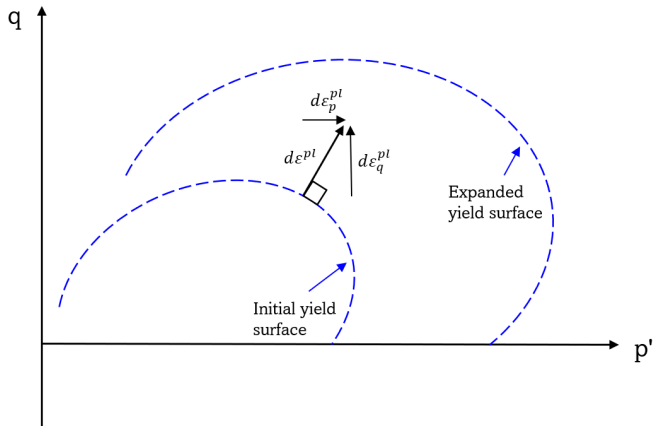

Figure 2.4: Typical yield surface and illustrated flow rule, plastic potential, and the correlated strain increments.

2.5.3 Typical yield surfaces and earlier research

The elastoplastic material models, proposed to simulate and predict the mechanical behavior of soils, are outcomes of comprehensive scientific laboratory studies. Figure 2.5 shows two examples of earlier reported yield surfaces identified by the execution of different loading scenarios in the triaxial apparatus. Earlier studies reveal that the yield surface for clays with an equal friction angle, φ', holds a strikingly similar form when visualized in a normalized p'-q - space (Länsivaara, 1999).

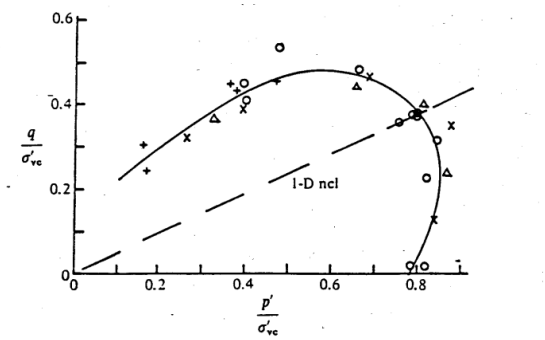

(a) Normalized yield surface reported by Wood (1990).

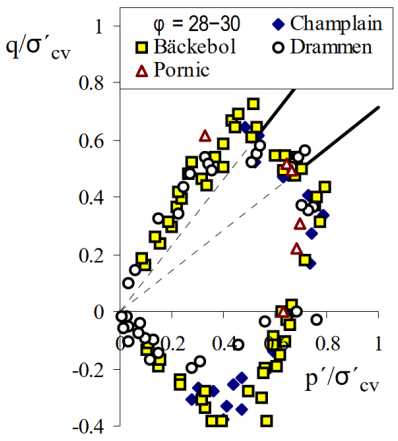

(b) Normalized yield points reported by Länsivaara (1999).

Figure 2.5: Earlier reported, normalized yield properties of clay.

The typical rotated elliptic form of the yield surface is characteristic of clayey soils and enables the understanding of the complex behavior of a sedimented material when subjected to vari-

ous loadings. The behavior of natural clays is well categorized and described in the literature. However, discoveries documented by Cotecchia and Chandler (2000) relate the sensitivity of clays to their behavior when surpassing the yield surface. Coteccia & Chandler report that sensitive clays experience a significant pore water volume decrease when crossing the yield surface, which further significantly reduces the sensitivity. The sensitivity, which defines the residual mechanical strength, is further shown to illustrate the deformation pattern for different loading scenarios. The mechanical behavior of quick clay when getting close to the yield surface is not too well described in the literature, but may seem to reveal its low residual strength by distinctive yield behavior (L'Heureux et al., 2019).

2.5.4 Proposed material models

Several mathematical models are proposed for simulating complex soil behavior. The rotated, elliptical yield surface, which is from laboratory studies seen to correlate well for various clayey soils, represents a yield loci that seems reasonable with the reported yield mechanisms observed from laboratory tests. Commonly used models, such as the Modified Cam Clay Model, (MCCM), utilizes a non-rotated ellipse for a simplified description of the yield loci (Wood, 1990). Equation (2.15) presents the equation for the symmetric ellipse as the basis for the MCCM, where M is the slope of the critical state line in the p':q space. Equation (2.16) presents how to obtain the inclination of the CSL. The elastic material stiffness, described by K and G, relates the elastic strains by utilization of the relation presented in Equation (2.12).

$$F = q^2 - M^2[p'(p'_0 - p')] = 0 \tag{2.15}$$

$$M = \frac{6sin\varphi'}{3 \pm sin\varphi'} \tag{2.16}$$

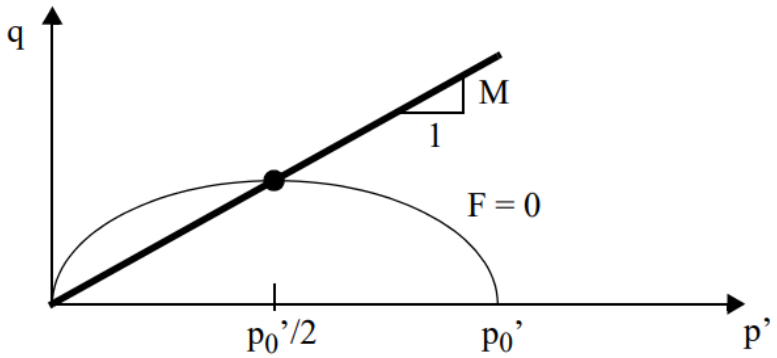

Figure 2.6: The MCCM yield surface and corresponding critical state line. Taken from Nordal (2020).

Länsivaara (1995) proposed a yield surface as a rotated ellipse to best fit experimental data for several natural clays. The yield surface is expressed by a shape-fitting parameter, α, and the

correlated isotropic triaxial preconsolidation stress p'_0. Based on the yield point, expressed in the p':q plot as (p'_k, q_k) from the K'_0-line, and the slope of the CSL line, M, the shape parameter can be obtained. Equation 2.17 describes the definition of the proposed yield surface seen in Figure 2.7. α is derived based on the associated flow rule and expressed in Equation (2.19). The yield points at the K'_0-line is obtained by assuming that the earth pressure coefficient at rest, K'_0, is given by Jâkys equation, $K'_0 = 1 - sin(\varphi')$ (Länsivaara, 1995).

$$F = q^2 - [sin(\alpha]p' + cos(\alpha)M\sqrt{p'(p'_0 - p')}]^2 \tag{2.17}$$

$$p'_0 = \frac{1}{M^2 cos(\alpha)^2 p_k}(q_k - sin(\alpha)p_k)^2 + p_k \tag{2.18}$$

$$\alpha = asin\left(\frac{1}{2p'_k}\frac{3p'_k - \sqrt{9p'^2_k + 4q_k{}^2 - 4M^2 p'^2_k + 12p'_k q_k - 4M^2 q_k{}^2 + 4M^4 p'^2_k - 12M^2 p'_k q_k}}{M^2 - 1}\right) \tag{2.19}$$

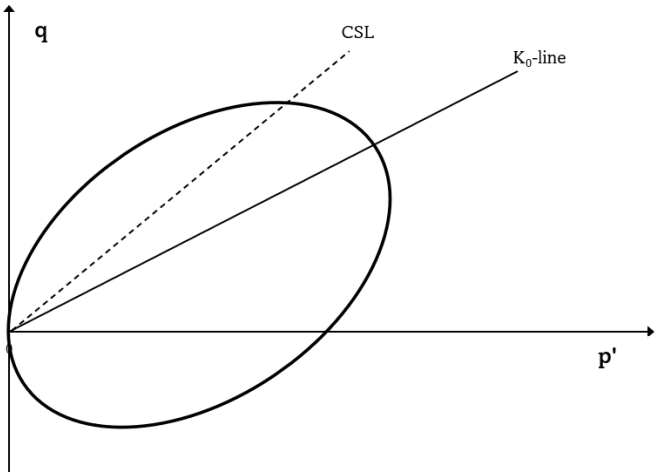

Figure 2.7: The rotated yield surface proposed by Länsivaara. Figure inspiration from Länsivaara (1995).

Dadras-Ajirloo et al. (2022) presented an isotache viscous model for simulating clay behavior using the hyperplasticity approach, presented as several convex yield surfaces. Former clay models, as stated by Dadras-Ajirloo, violate the rate and creep-dependent effects that are observed in natural clays. Therefore, a hyper-viscoplastic formulation of these effects is employed in the thermodynamic framework for the proposed yield locis. The force potential used in this framework, proposed by Grimstad et al. (2020), replaces the conventional force potential used in MCCM which does not make the free energy dissipation observable, (Dadras-Ajirloo et al., 2022).

The procedure developed by Dadras-Ajirloo attains a family of isotropic models on the basis of the non-associated flow rule. A short description of the different yield surfaces is presented in Equation 2.20 to 2.22, based on implicit functions. Figure 2.8 presents a graphical view

of the proposed model. The use of the dissipative stresses, χ_p and χ_q, is of importance due to the introduction of the non-associated flow rule, unlike the MCCM. In that way, both the deviatoric and mean stress affects the plastic potential in the model. The γ-parameter, seen in Figure 2.8, specifies the degree of non-associativity. Thus, as γ increases, the model describes a more strain-softening behavior on the compressive side of the stress space (Dadras-Ajirloo et al., 2022).

$$T = \frac{R}{2} + \left(\frac{R-2}{2}\right) tanh(S) \tag{2.20}$$

$$S = \left(\frac{M}{\eta}\right)^2 - \left(\frac{\eta}{M}\right)^2 \tag{2.21}$$

$$p_{eq} = \frac{R\chi_p \sqrt{\left(\chi_p^2 M^2 - \chi_q^2\right)^2 + \chi_q^2 [MT\chi_p + \sqrt{\chi_p^2 M^2 + (T^2-1)\chi_q^2}]^2}}{T\left(\chi_p^2 M^2 - \chi_q^2\right) + \sqrt{\left(\chi_p^2 M^2 - \chi_q^2\right)^2 + \chi_q^2 [MT\chi_p + \sqrt{\chi_p^2 M^2 + (T^2-1)\chi_q^2}]}} \tag{2.22}$$

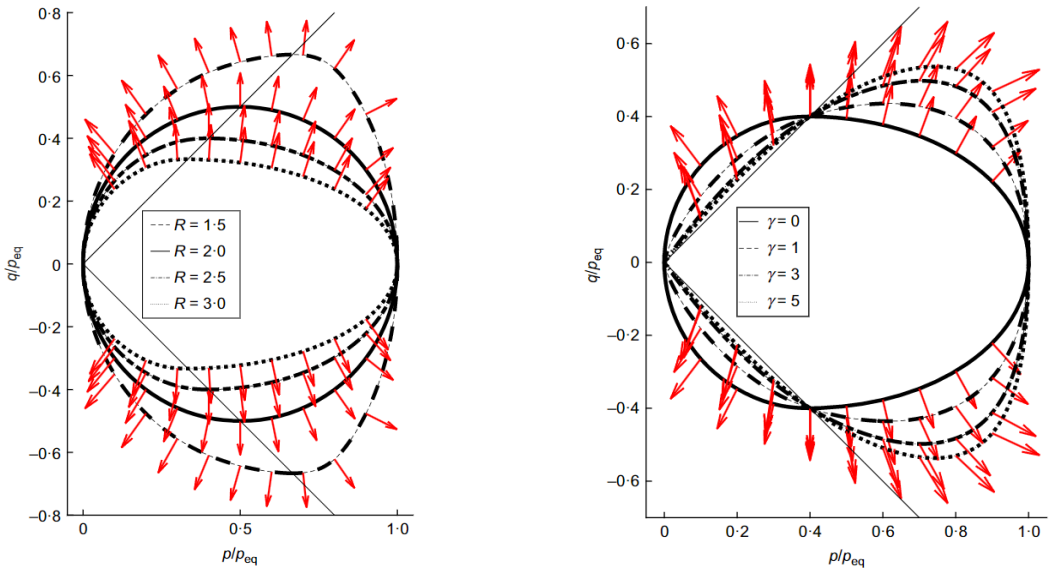

(a) Convex loci with the inelastic flow directions for different values of R, while $M = 1$.

(b) Convex loci with the inelastic flow directions for different values of γ, while $M = 1$ and $R = 2.5$.

Figure 2.8: The convex loci family presented by Dadras-Ajirloo et al. (2022).

Chapter 3

Sampling methods and laboratory tests

This chapter provides a general explanation of geotechnical sampling methods and laboratory experiments relevant to this master's thesis. The experimental procedures, equipment, and implementations are described in particular. Various options and alternatives for experimental conditions are also presented.

3.1 Piston samples

In Norway, ø54 mm piston samplers have long been used as the preferred sampling method for undisturbed soil samples (NGF, 2013). However, for undisturbed clay samples, particularly sensitive, soft clays, a considerably lower sample quality has been observed for geotechnical special tests such as triaxial and oedometer tests (NGI, 2013). The sample disturbance, compared to ø75 mm, ø95 mm, and block samples (cf. Amundsen et al. (2015)), has recently been shown so significant that ø54 mm piston samplers are not the optimal choice when conducting geotechnical special tests in soft, sensitive soils. Geotechnical routine tests, such as determination of water content, liquid- and plasticity limits, falling cone tests, etc., are less affected by sample disturbance as long as the sample cylinder is properly sealed to prevent any changes in water content before laboratory testing takes place (NGF, 2013).

Sampling method

The sample cylinder is lowered to the desired depth for sampling and is continuously fed at a cutting rate of 2-3 cm per second during the sampling process. The cylinder is pushed without rotation, and the feeding is stopped prior to the full sample length being obtained to prevent the sample from being additionally compressed. For sampling in soft and sensitive soils, the loss of sample material when lifting the cylinder may be prevented by allowing the cylinder to rest for a few minutes after the desired sample length is attained. The extraction procedure of the sample cylinder should be done without jerks and vibrations to prevent unnecessary

sample disturbance as much as possible (NGF, 2013). As soon as the sample cylinder is out of the ground, the cylinder is sufficiently sealed at both ends prior to being prepared for transport to the laboratory. Figure 3.1 shows the cylinder's downward pressure and the associated influences on the material being extracted.

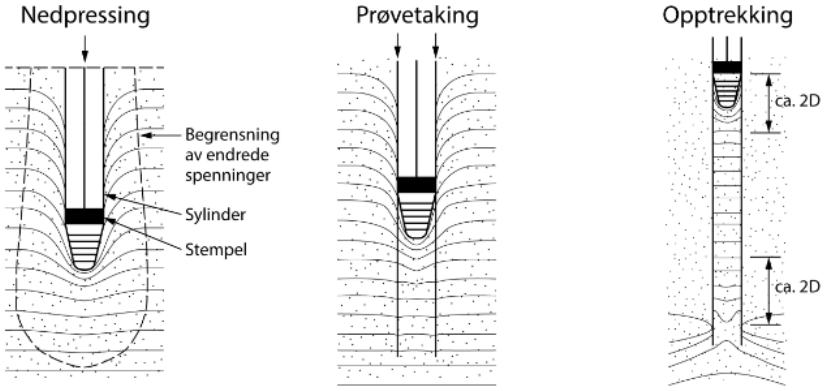

Figure 3.1: Piston sampling and its disturbing effects. Taken from NGF (2013).

Freight and storage

The cylinder samples should be exposed to minimal physical impact after sampling. Specially designed boxes should be utilized to prevent temperature changes, shocks, and vibrations for the cylinder samples (NGF, 2013). Cooling chambers should be used for storing cylinder samples upon arrival at the geotechnical laboratory to maintain the in-situ temperature for the sample. The Norwegian Geotechnical Society (NGF) points out that to minimize disturbances to the sample's mechanical structure, it is recommended to open the samples 2-4 weeks after sampling if the sample is to be tested for strength and deformation properties (NGF, 2013). These effects are widely reported by Amundsen et al. (2015).

Extortion and division

A specialized apparatus is used for extracting the sample material from the cylinder prior to conducting the laboratory experiments. The seals on both ends are removed, and the test cylinder is weighed to determine the mean density prior to the extraction of the sample material. To ensure an even extrusion of the sample material, a pulling piston at the top and a pushing piston at the bottom of the cylinder is mounted. The sample is then pushed out with a smooth movement onto a plate that is in advance covered in aluminum foil to avoid friction between the sample content and the plate. The extruded sample content is immediately covered with plastic film to prevent drying.

The sample material is divided into suitable lengths for the intended laboratory tests. Determination of water content should be performed at several locations along the length of the sample to reveal local differences. It should be attempted to use the minimized disturbed part,

often the middle part, of the sample for conducting geotechnical special tests, such as oedometer and triaxial tests. This is based on visual classification, but also due to the impact of the sampling method on the extracted material, according to Figure 3.1.

3.2 Block samples

Block samples represent soil samples extracted with a special type of sampler which differs from traditional piston sampling. Several block samplers have been developed, which may generally extract cylindrical soil samples up to approximately 27 cm in diameter and up to 35-40 cm in height. The use of block samplers has, from the beginning of the 1990s to the present day, shown improved sample quality compared to piston sampling (NGI, 2013). It has been particularly documented that block sampling provides better sample quality for sensitive clays, extracted deeper than 10 meters below terrain level (NGI, 2013).

The block sampler used to obtain block samples tested in this master thesis was obtained through NTNU's self-developed mini-block sampler. The sampler is attached to the drilling rig and lowered to the pre-drilled depth before the water supply is connected, and the actual block sampling can begin. Figure 3.2b shows NTNU's geotechnical drilling rig, and figure 3.2a shows the mini-block developed by NTNU.

(a) NTNUs mini block sampler. **(b)** NTNUs geotechnical drilling rig.

Figure 3.2: Mini block sampler and drilling rig.

Sampling method

The sampling process first involves a pre-drilling procedure to the desired depth for sampling. The borehole should be as pure and stable as possible prior to the sampling, often accom-

plished using a Ø45 mm soil auger. For the actual sampling procedure, the water sprays, cutting blades, and a very slow rotational penetration are utilized until the maximum depth of the block sampler is met. The soil sample is cut free at the bottom by the attached blades, and further raised out of the borehole (NGF, 2013). The rotation of the block sampler should be adjusted so that the penetration does not exceed 2 cm per minute (NGI, 2013). Essentially, only the rotation of the sampler itself, and the accompanying water flushing, should ensure that particularly soft clay samples are gently cut. This will provide a gentle sampling method with no significant disturbance to the clay sample. To best avoid any swelling and unnatural unloading of the clay samples extracted using block samplers, it is important that the edges of the block sample are supported, wiped clean and ”dry”, and sealed immediately after lifting out of the ground. Figure 3.3 shows the block sampler attached to the drilling rig, as well as a fresh block sample immediately after retrieval.

(a) Mini block sampler before sampling.

(b) Mini block sample immediately after sampling.

Figure 3.3: Mini block sampler attached to the rig before and after sampling.

Freight and storage

The transportation of block samples from the sampling area to the laboratory should be adapted to prevent vibrations and shocks. The sealing and storage of the block samples during transport require particular caution not to disturb the soil. Figure 3.4 shows a fresh block sample wrapped in a generous amount of plastic film, as well as the setup for transporting the block samples back to the laboratory. The block samples are supported in specially adapted cylindrical tubes, which in addition are filled with tiny polystyrene balls to prevent internal movement of the block sample.

In general, the storage of block samples after arrival at the laboratory should be under essentially the same conditions as for piston samples. Cooling chambers with high humidity and a temperature around 6-7 °C are required to simulate the in situ conditions and to prevent drying out of the sample. To best avoid the soil sample from reconsolidating and changing its mechanical structure during storage, NGF recommends that block samples should not be stored for more than 2-4 weeks after extraction (NGF, 2013). Testing immediately after sampling is, however, preferred.

(a) Mini block sample wrapped in plastic film.

(b) Block sample placed in the transport container.

(c) Block samples placed in the gentle supported container.

Figure 3.4: Procedure after mini block sampling.

Extortion and cutting

NTNU's cutting device is utilized for cutting and division of the mini-block samples according to which laboratory experiments are to be performed. The block sample is placed in the device and adjusted to the desired cutting height. A generous amount of silicone oil is applied to the upper surfaces of the device so that the cuts can slide smoothly without any friction after cutting. Prior to the cutting process, the upper edge of the block sample is supported with a custom foam rubber band. A large, pre-tensioned wire saw is used to cut the various parts by driving the wire saw gently back and forth in the cutting plane. The sample parts are gently rotated away from the mini-block to the pre-greased top surface. Figure 3.5 shows how the upper centimeter of the mini-block is cut off in this process.

The main part(s) of the mini-block are cut using the same method. As the different specimens are cut from the mini-block, the remaining mini-block sample should be covered with plastic to prevent drying out during the cutting process. The specimens of the mini-block are then cut using the longitudinal angles of the device. Here, each main part can potentially be cut into four different specimens, so that four different triaxial tests can be performed from each main part. Furthermore, a trimming device is used to trim each sample's geometry to an approximately cylindrical shape with a 54 mm diameter for adaptation to triaxial testing. Figure 3.6 shows

this process, and 3.8 shows the finished cut sample for conducting triaxial tests.

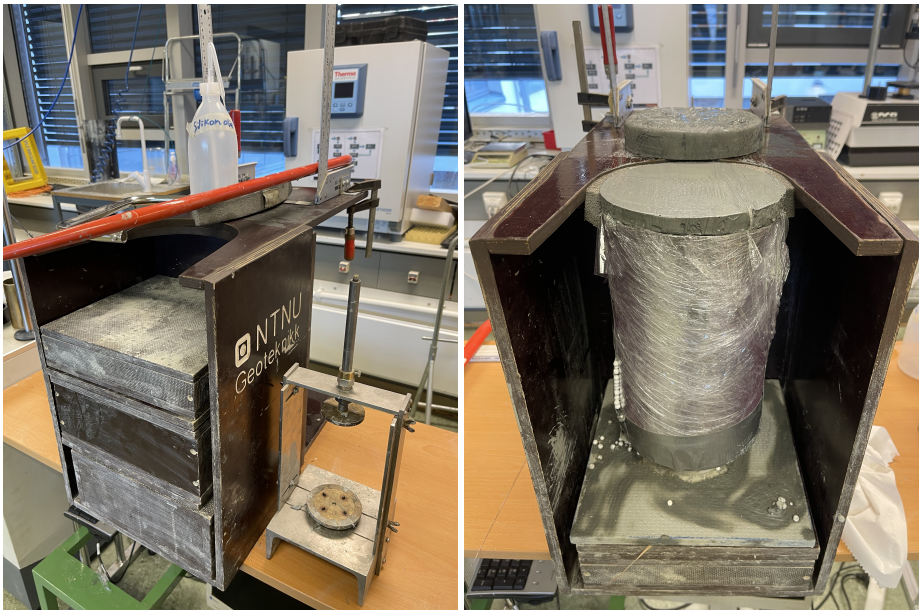

(a) Equipment for cutting the mini block sample.

(b) Removal of the upper disturbed, top layer.

Figure 3.5: Equipment and procedure of gentle cutting of the mini block sample.

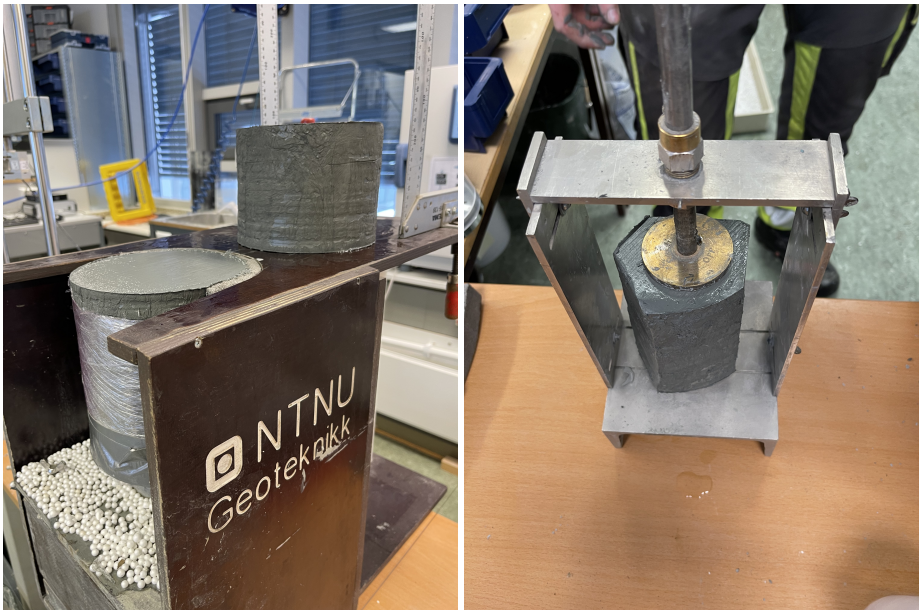

(a) Gentle trim for triaxial samples.

(b) Trim to 54 mm triaxial sample.

Figure 3.6: Procedure for preparing triaxial samples from mini block samples.

3.3 Sample disturbance

The effect of sample disturbance across the different sampling methods are relatively known and thoroughly investigated by several authors (e.g. Lunne et al., 2011; Amundsen et al., 2015; Lunne et al., 1997; Emdal, Amundsen, and Thakur, 2016). The superior quality of block samples compared to traditional piston tube samples is well documented and established. Especially for soft clays, the sample disturbance is of high importance when performing special laboratory tests, such as oedometer and triaxial tests, for obtaining reliable and representative soil parameters, (Emdal, Amundsen, & Thakur, 2016).

As stated in the above sections, handling-influenced sample disturbances are minimized when using block samplers to extract the soil specimens. However, the subsequent reduction of the block samples' effective overburden pressure is inevitable and causes a reconsolidation process of the extracted specimens, especially when the block samples are introduced to storage (Emdal, Amundsen, Kåsin, et al., 2016).

When storing the soil samples, suction and swelling effects will dominate the further developed stress state in the soil sample. As stated per Bjerrum and Aitchison (1973), the internal swell may cause a decrease in the measured undrained shear strength only hours after extraction from the field. Sampling from large depths remains still a challenge for soft and sensitive clays as discussed by L'Heureux et al. (2018), as well as procedures and effects from storage and handling (Emdal, Amundsen, & Thakur, 2016). The literature and official guidelines for geotechnical sample extrusion do state the importance of gentle handling, transport, and storage for the different sampling methods to avoid any unnecessary temperature changes, shocks, leaks, and drying of the samples. Thus, the criteria proposed for evaluation of the sample quality are based on actual laboratory investigations, where obtained results and expelled pore water during reconsolidation procedures are central.

There have been proposed different criteria for evaluating the sample disturbance when performing both oedometer and triaxial tests in the laboratory. Lunne et al. (1997) proposed a criterion based on the samples' volume change during reconsolidation to its in situ-effective stresses. The criterion is expressed in Equation (3.1), whereas the overconsolidation ratio also is taken into account in Table 3.1.

$$\frac{\Delta e}{e_0} = \varepsilon_{v0} \cdot \left(\frac{1 + e_0}{e_0} \right) = \varepsilon_{v0} \cdot \left(\frac{1 + \rho_d w}{\rho_d w} \right) \tag{3.1}$$

For assessment of the sample quality when performing oedometer tests, Karlsrud and Hernandez-Martinez (2013) proposed a criterion based on the quality of the oedometer modulus, M. The stiffness ratio, M_0 / M_L takes into account the max constrained modulus in the overconsolidated range and the lowest modulus identified at the preconsolidation pressure (Amundsen et al., 2015). These parameters are presented in Figure 3.16. Both proposed methods are widely used in geotechnical sample quality assessments when performing laboratory tests.

Sample quality	$1 < OCR < 2$ $\Delta e/e_0$	$2 < OCR < 4$ $\Delta e/e_0$	M_0/M_L
Very good to excellent	< 0.04	< 0.03	> 2.0
Good to acceptable	0.04-0.07	0.03-0.05	1.5-2.0
Bad	0.07-0.14	0.05-0.10	1.0-1.5
Very bad	> 0.14	> 0.10	< 1.0

Table 3.1: Sample quality criteria, on the basis of $\Delta e/e_0$, (Lunne et al., 1997) og M_0/M_L (Karlsrud & Hernandez-Martinez, 2013).

The effect of sample quality may also be evaluated based on the criteria of expelled pore water during reconsolidation in the triaxial cell, shown in Table 3.2 (Statens Vegvesen, 2022). These criteria apply to trimmed 54 mm triaxial samples with a sample height of 100 mm.

Expelled pore water, ΔV cm^3	**Expelled pore water,** $\Delta V/V_0$ *(%)*	**Classification**
0-5	0-2	Good
5-10	2-4	Acceptable
> 10	> 4	Bad

Table 3.2: Assessment of sample quality, on the basis of expelled pore water, (NGF, 2013).

3.4 Rutine tests

Routine tests are a common term for laboratory tests carried out on soils to characterize the overall composition, water content and index parameters, and other general strength properties. Results obtained from routine tests enable us to identify and compare the properties and behavior of the soil. Based on routine results, soil can be categorized and correlated to other mechanical properties. Section 3.4 describes the routine tests carried out for the experimental study in this master's thesis.

Determination of water content

The water content for each specimen is determined by the weight ratio before and after drying (Statens Vegvesen, 2016). Immediately after extraction of the specimen, the moist sample material is placed in bowls with a known weight. The wet weight of the sample is determined by instantaneous weighing, before placing it in a drying cabinet. The drying cabinet maintains a temperature of 105^oC, and dries the sample until a constant weight is achieved. After a constant mass of the specimen is achieved, the weight of evaporated water, m_w, and dry mass of the sample material, m_s, are determined. The water content is determined by equation (3.2).

$$w = \frac{m_w}{m_s} \cdot 100\% \tag{3.2}$$

Density measurement

The density measurement is done by gently pressing a cylinder with known weight and volume into the soil. After using the trim saw to flatten the ends, the weight of the cylinder and the soil can be obtained. Equation 3.3 to 3.5 present the procedure for obtaining the densities, ρ and ρ_d, and the unit weight, γ_s, of the soil specimen. The procedure for obtaining the dry density may be performed by drying the clay sample in the drying cabinet for 24 hours to obtain the weight of only the clay particles.

$$\rho = \frac{m_s + m_w}{V_0} \tag{3.3}$$

$$\rho_d = \frac{m_s}{V_0} \tag{3.4}$$

$$\gamma_s = \frac{(m_s + m_w) \cdot g}{V_0} \tag{3.5}$$

Liquid limit by Casagrande

The liquid limit of a material describes the moisture content at which the consistency of the specimen changes from a solid (plastic) to a liquid state (Statens Vegvesen, 2016). The liquid limit, along with the plastic limit, is used for further classification and correlation to other strength and deformation parameters described in Section 2.1. The liquid limit is determined using a special device developed by Arthur Casagrande in 1932 (Barnhart, 2014). The soil material is positioned in the bottom of the bowl before a groove is made in the center of the material. The bowl is raised and lowered at a steady frequency, and the number of revolutions required to close the groove over a distance of 3.2 mm is recorded, along with the corresponding moisture content of the soil material. Valid results are obtained with 15-40 revolutions. At least four tests are to be carried out, with an effort to perform two tests with 15-25 revolutions and two tests with 25-40 revolutions. The principle of the semi-graphic multi-point determination is used subsequently to identify the moisture content that corresponds to 25 revolutions, which is designated as the material's liquid limit.

$$w_L = \frac{m_w}{m_s} \cdot 100\% \tag{3.6}$$

Plasticity limit by rollout

Approximately 20 grams of the sample material is separated and rolled into two balls. Using a glass plate, the balls are rolled with smooth movements between the plate and the fingers to form a thread with a uniform diameter. If the threads become thinner than 3.2 mm without breaking, the process is repeated until the water content in the sample material decreases sufficiently for the threads to break either earlier or until the threads reach a diameter of 3.2 mm. The broken threads are collected in a bowl with a known weight and placed in a

drying cabinet until a constant mass is achieved. The sample is weighed after drying, m_s, and the mass of the evaporated water is thus known, m_w. The plasticity limit is determined by Equation (3.7).

$$w_P = \frac{m_w}{m_s} \cdot 100\% \tag{3.7}$$

Index strength by falling cone

The cone penetration test is based on releasing cones from the top surface of the material. The falling cone test is performed at both undisturbed and disturbed soil material. The penetration into the soil material is measured instantaneously after the drop and is subsequently utilized to determine both undrained shear strength, c_{ufc}, and remolded shear strength, c_{urfc}. The choice of cone weight and corresponding cone angle is determined by the length of the penetration. Valid tests reflect penetrations between 4-20 mm (Standard Norge, 2017). To determine the undrained shear strength, three different tests are performed, where the penetration should not vary by more than 0.5 mm between the different tests (Statens Vegvesen, 2016). Remolded shear strength is determined by conducting two different tests. The calculation of the undrained shear strength by cone penetration test is estimated according to equation (3.8), where i denotes the average value of the penetrations and m_{cone} is the weight of the cone used for penetration. c is a constant based on the cone angle, and found from Standard Norge (2017).

$$c_{u(r)fc} = c \cdot g \cdot \frac{m_{cone}}{i^2} \tag{3.8}$$

3.5 Triaxial tests

The triaxial test is within geotechnics considered one of the most reliable tests for reproducing soil materials' strength properties and behavior (Länsivaara, 1999). The triaxial test is based on the idea that soil materials experience the same stresses and strains as those close to in-situ conditions, as opposed to, for example, uniaxial compression tests, where soil samples do not experience horizontal stresses during loading. Soil samples tested in the triaxial apparatus are placed in a cell assembly filled with pressurized water, and the water supply into and out of the cell is controlled by a control unit. The control unit's water supply to the triaxial cell is controlled by user instructions, depending on the specified pressures that the soil sample is to be subjected to.

Compressive triaxial tests refer to tests where soil samples are subjected to axial compressive stress during the shear phase. The compressive stress is predetermined by the operator, often at a constant axial strain rate, causing increasing axial stresses on the soil material until it eventually fails. This thesis has conducted various types of triaxial tests during the experimental study, where undrained and drained compression tests, along with triaxial consolidations, both K_0'-consolidations and general loading paths with a constant K_0'.

3.5.1 Equipment

Figure 3.7 shows both NTNU's equipment for performing triaxial tests, as well as a schematic diagram of the setup taken from Statens Vegvesen (2016). The test specimen is enclosed by a tight rubber membrane and porous filter stones, both at the top and bottom surfaces. The rubber membrane is sealed at both ends by paired O-rings to ensure that water does not leak in or out of the test specimen. The top piece and pedestal are connected to the pore pressure gauge and back pressure system, which is controlled by a pressure-regulating control unit. The back pressure system is further connected to an air trap, which allows for flushing the system when the specimen is mounted in the triaxial cell. The cell itself is connected to a control unit for the cell pressure, as well as an external water tap for easy water supply both into and out of the cell. The control unit for the cell pressure controls the user-defined input for the internal pressure in the cell. An axial, digital deformation gauge is mounted at the top of the cell and records the axial deformation of the test specimen throughout the test. The piston is controlled by the GDS program to apply a user-defined axial load to the test specimen.

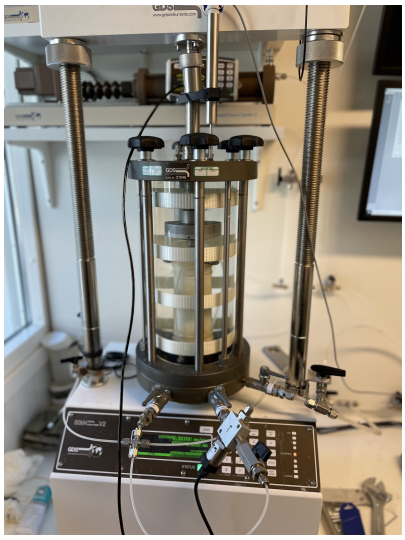

(a) GDS triaxial setup. Sample mounted in the cell filled with pressurized water.

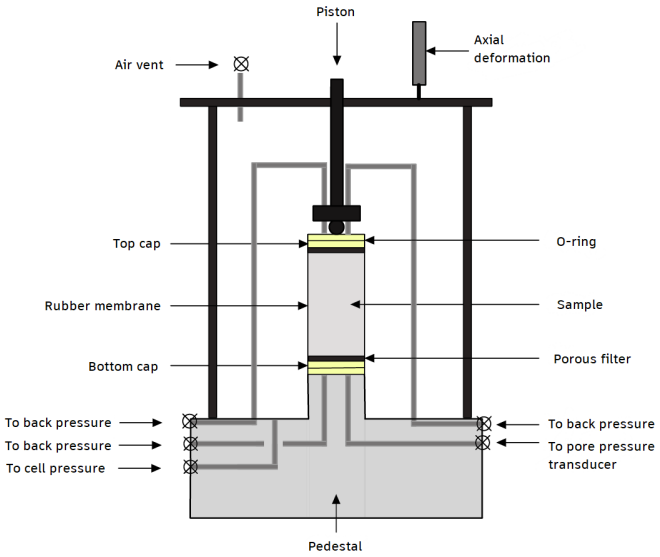

(b) General sketch of the triaxial setup. Figure inspired by Statens Vegvesen (2016).

Figure 3.7: Triaxial cell setup.

3.5.2 Mounting and preparation

Before placing the specimen on the pedestal, the end faces of the specimen shall be ensured to be cut flat with a wire saw, in accordance with ISO 17892-2 (Standard Norge, 2018). For specimens obtained with a mini-block sampler, each specimen is carefully cut both horizontally and longitudinally so that the specimen's cylindrical geometry corresponds to 100 mm in height and 54 mm in diameter, as for the specimens obtained from Ø54 mm piston samplers.

Figure 3.8 shows the gentle cutting process of specimens from mini-block samples, as well as the finished embedded specimen in the triaxial apparatus. After achieving the specimen's geometry, the specimen is weighed to be able to evaluate the sample quality after the test.

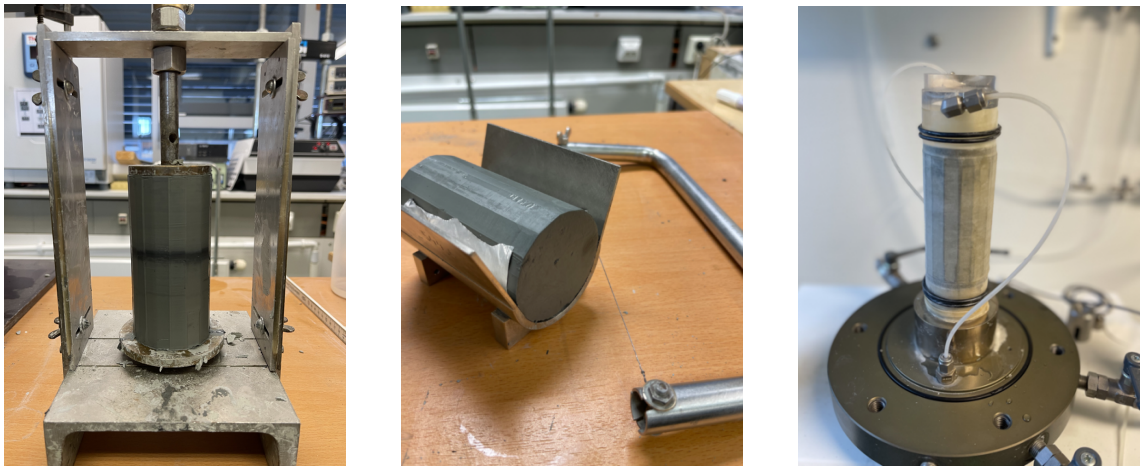

(a) Gentle trim for obtaining a cylindrical shape by use of special apparatus.

(b) Adaption to 10 cm sample height by use of a thin wire saw.

(c) Mounted triaxial sample, sealed with membrane and paired o-rings.

Figure 3.8: Process for gentle cutting of mini block samples to cylindrical triaxial sample.

The test specimen is placed in the triaxial cell, with water-saturated porous filter stones and filter paper at both ends. The stone filters should have been pre-saturated in an ultrasonic bath and desiccator, according to (Statens Vegvesen, 2016). The rubber membrane, which is checked to be impenetrable before the test, is carefully pulled over the test specimen using a vacuum pump and sealed both at the top and bottom with O-rings to prevent leakage. The triaxial cell is filled with water, and a cell pressure of about 10 kPa is applied to the test specimen immediately to prevent swelling when the filter stones are flushed, according to (Standard Norge, 2018). The valves for access to distilled, air-free water is opened, and the filter stones at the top and bottom of the test specimen are flushed. This is done to prevent accumulation and expulsion of air in the system, which can cause inaccurate pore pressure measurements and hence deviate from undrained conditions. This flushing procedure also ensures that volume changes during the consolidation phase can be accurately measured. After the flushing procedure, the installation is considered complete, and the consolidation phase can be initiated.

3.5.3 Consolidation procedures

Several consolidation procedures may be performed for different types of loadings in the triaxial cell. The traditional consolidation procedure to apply the relevant in-situ stresses to the soil sample is widely used when conducting conventional shear tests. Other consolidation procedures, like K_0'-consolidations or general loadings with a constant K_0', may reveal the effect of anisotropy and yielding characteristics.

Traditional isotropic- or anisotropic consolidation

The predefined stresses to be applied to the specimen in the consolidation phase are applied to the specimen through a slow change in stress. The Norwegian Public Roads Administration, (SVV), states that horizontal stress application (σ_3) should not exceed 2 kPa/min. In the case of anisotropic consolidation, the axial stress application (σ_1) should not exceed 0.5 kPa/min. After achieving the consolidation stresses, the consolidation phase continues until the specimen's volume change (expelled pore water) satisfies $\Delta V < 5mm^3/min$ (Standard Norge, 2018). If the requirement for expelled pore water is not met within 24 hours, the consolidation phase can be considered complete. Norwegian clay samples are typically consolidated over a period of around 16-24 hours (Statens Vegvesen, 2016).

An isotropic loading scenario applies equal stresses radially and axially to the test specimen, $\sigma_a = \sigma_r$. On the other hand, an anisotropic loading applies a radial stress that is different from the axial stress, $\sigma_a \neq \sigma_r$. Isotropic loading is usually not representative of soil conditions since the stress situation in-situ is typically higher axially than radially. On the other hand, anisotropic loading applies shear stresses to the test specimen, which may be undesirable for soil samples taken from shallow depths during laboratory tests. Such soil samples may retain low shear strength and may fail during an anisotropic consolidation phase. Therefore, both isotropic and anisotropic triaxial tests are carried out to best restore the specimen to the stresses that characterize the in-situ loading scenario. For the implementation of anisotropic consolidations, an earth pressure coefficient at rest, $K_0' = \sigma_{h0}'/\sigma_{v0}'$, is often specified to define the desired stress level. The earth pressure coefficient at rest can be identified through both laboratory and in-situ tests.

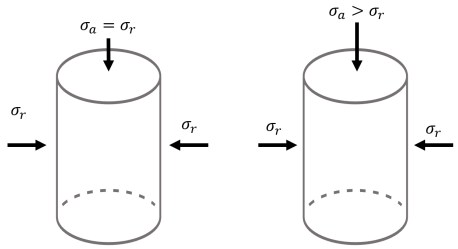

Figure 3.9: General difference between isotropic and anisotropic loading of the test sample.

Constant K_0' procedure

Cutting, as well as installation and assembly, are carried out according to section 3.5.2. The tests with constant K_0' were defined as a single step, with loading to the ultimate stress level that determines a constant K_0' throughout the test. The K_0' tests were used in this master's thesis to identify the yield point at different initial stress coefficients. The tests were carried out under drained conditions, with a slow application of stress that did not generate significant pore pressures. The stress rate was set to 0.2 kPa per minute after the test experiments were conducted.

K_0'-consolidation

The K_0' consolidations are carried out by loading the test specimen to a predetermined cell pressure. During loading, care is taken to ensure that the specimen does not develop radial strains and therefore does not change its cross-sectional area during the test. In this context, the K_0' consolidation can be related to the oedometer test, where the soil is prevented from expanding sideways due to the oedometer ring. Therefore, the K_0'-consolidations are also known as ”oedo-triaxial” tests. The K_0' consolidation ensures a defined transition between the elastic and plastic regions, and thus a simpler interpretation and localization of the developed yield mechanism, based on changes in both stiffness and strains.

3.5.4 Saturation and back pressure

Following the consolidation phase, the saturation phase ensures that the pore pressure system, connected to the sample, is subjected to a pressure load that eliminates any air bubbles that may interfere with pore pressure measurements in the shear phase. The pressure applied to the pore pressure system is hereby called "back pressure" and is applied to the system with a stress change equivalent to $2-10kPa/min$. There is different practice on how much back pressure is applied to the system, but 200 - 500 kPa is specified by SVV as satisfactory for full saturation of the pore pressure system (Statens Vegvesen, 2016). To maintain the same effective stress level as achieved in the consolidation phase, the cell pressure is also adjusted in parallel with the application of back pressure. After achieving the back pressure, the sample is "rested" to stabilize the stress state.

3.5.5 Undrained pore pressure response

After the rest period following the attainment of the back pressure increase, a so-called B-test is carried out. The B-test is performed to ensure that the specimen has a satisfactory pore pressure response prior to the undrained shear test, which correlates with the theoretical undrained conditions. For saturated soils, a stress change in undrained conditions would imply a change in the pore pressures equivalent to Equation (3.9), where A defines a pore pressure parameter that depends on the stress history and overconsolidation ratio for the sample (Bishop & Bjerrum, 1960).

$$\Delta u_b = B\left[\Delta\sigma_3 - A(\Delta\sigma_1 - \sigma_3)\right] \tag{3.9}$$

Because of the stress state in the triaxial cell, and the fact that superposition has to be restrictively applied for pore water pressure in soils, the A-parameter for saturated soils has earlier been proven to be neglected for triaxial tests (Bishop & Bjerrum, 1960). The change in cell pressure when measuring the pore pressure response for saturated soils is further found by Equation (3.10), and takes account of the even increase in the cell pressure surrounding the sample.

When performing the B-test, drainage valves are closed, and the cell pressure is instantaneously increased by $\Delta\sigma = 10$ kPa (Statens Vegvesen, 2016). The pore pressure change, Δu,

is continuously measured throughout the B-test. The B-value, expressed in equation (3.10), represents the pore pressure response in relation to the increase in stress, and according to ISO 17892-9, it should satisfy $B > 0.95$ to consider the pore pressure response satisfactory. The B-value is recorded over a period of 10 minutes, and if the pore pressure response does not meet the requirement, a new increase in back and cell pressure is recommended before a second B-test is carried out.

$$B = \frac{\Delta u_b}{\Delta \sigma} \tag{3.10}$$

SVV emphasizes that if the B-value does not meet the requirements and does not vary significantly after two B-tests, this is considered as evidence that the shear test can be initiated (Statens Vegvesen, 2016).

3.5.6 Shear test

Undrained shearing

The execution of the undrained triaxial tests in this master's thesis follows procedures developed by the Norwegian Public Roads Administration (SVV), (Statens Vegvesen, 2016). Figure 3.10 shows a summarized visualization of how the operator-selected stresses and the sample's response vary through the consolidation phase to the completion of the shear test.

As the shear test is initiated, the specimen is continuously loaded until a predefined strain, often $10-15$ % is reached. Drainage out from the sample is closed prior to the shear test starts to ensure undrained conditions, and thus no volume change of the specimen during the shear phase. The loading of the specimen is carried out by applying a continuously strain-controlled vertical load. Hence, according to SVV, a strain rate around 2 %/hour is recommended for compressive triaxial tests (Statens Vegvesen, 2016).

However, before the shear test is initiated, one must take into account that the height of the specimen has changed during the consolidation and saturation phases. Therefore, the change in height during the consolidation must be considered when calculating the strain rate for the shear phase. Equation (3.11) shows the calculation method for determining the strain rate, equivalent to 2 %/hour, which is often given as input in mm/min.

$$\dot{\varepsilon} = \frac{0.02}{60} \cdot (H_0 - \delta_a) \quad [\text{mm/min}] \tag{3.11}$$

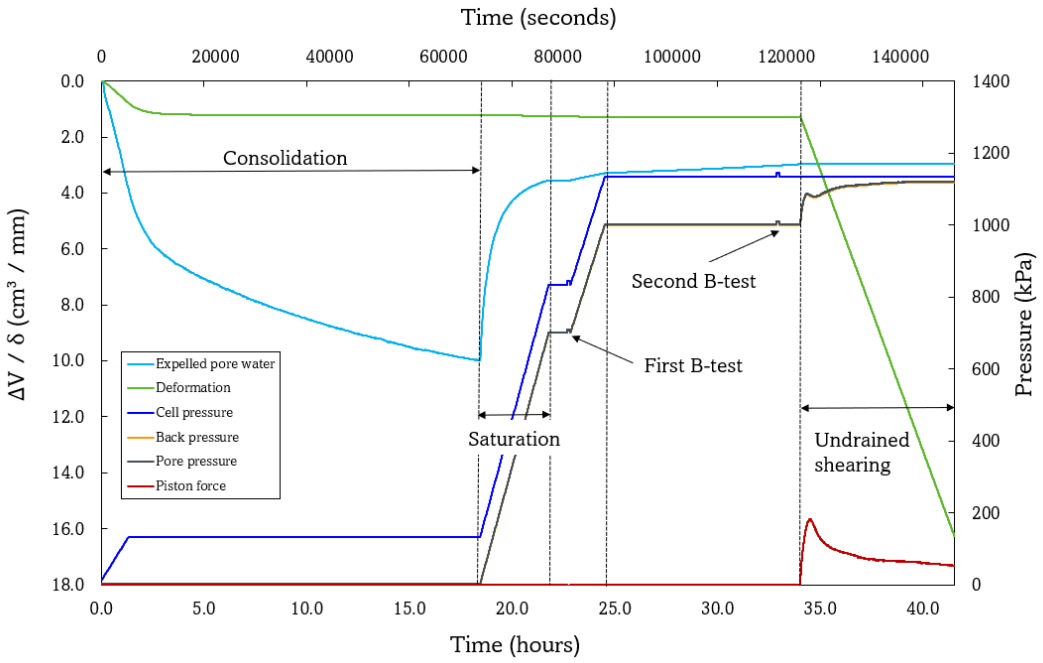

Figure 3.10: Procedure of a typical consolidated, undrained triaxial shear test. The timeline follows every stage, and visualizes the application of both cell and back pressure during consolidation and saturation. Two stages of B-tests are marked after each saturation phase. The red curve shows how the piston force develops during the shear stage for developing the axial strain rate defined for the test. Figure admiringly inspired by Sigurdur Mal Valsson, SVV.

The shear test is considered complete when the failure criterion, often between 10−15% axial strain, is met. Figure 3.11 shows three different samples immediately after the completion of a shear test. Once the shear test is completed, measured stress and strain values throughout the different phases are subject to the interpretation of the mechanical soil response. Interpretation of results obtained from conducting triaxial tests is further described in detail in section 3.5.7.

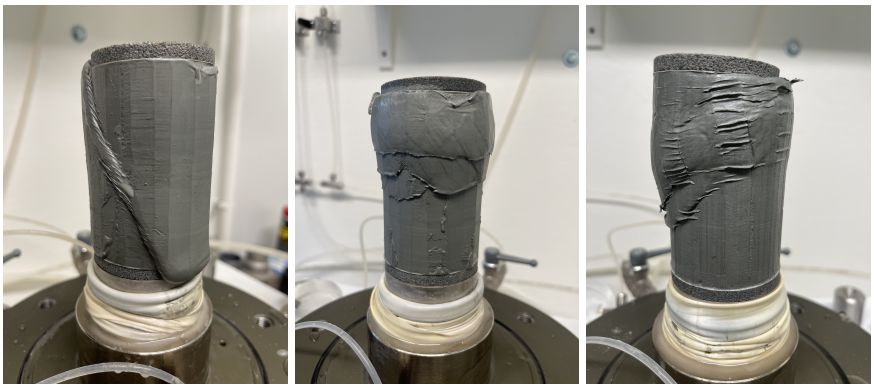

Figure 3.11: Developed failure planes from quick clay samples during this test series after meeting the 15 % failure strain.

Drained shearing

The drained shearing follows the same procedure as the undrained shear test prior to the shear stage. Thus, the drained shear test may be consolidated both isotropically and anisotropically, further denoted CIDC and CADC. The procedure for the drained shearing follows ISO 17892-9 Standard Norge (2018). The specimen is allowed to drain both at the top and bottom and sheared at a strain rate that causes no significant build-up of pore pressure. ISO 17892-9 clarifies that the choice of the axial strain rate has to be such that the pore pressure does not differ by more than 4 % of the cell pressure. As per this claim, paper strips surrounding the specimen from top to bottom may produce better drainage during shearing.

Similar to the undrained shearing, the drained shearing takes place until the specimen reaches 10-15 % axial strain and the soil specimen has failed and developed a significant amount of shear strains.

3.5.7 Interpretation of results

Stress controlled parameters during test execution

The specimen experiences several different phases during the actual triaxial test before the desired failure strain is achieved. The volume change of the specimen, i.e. the amount of expelled pore water, will be subject to interpretation after different test phases. Continuous measurement of this quantity, as well as the axial deformation of the specimen, enables us to follow the specimen's deformation pattern throughout the entire test series. After consolidation is executed, the amount of expressed pore water and axial deformation are parameters used to "update" the specimen's current geometry and volume before the shear test takes place. As a result of the consolidation stresses applied to the specimen, the specimen's response to compression will be described by changes in height, area, volume, and strains throughout the consolidation phase. The GDS triaxial equipment measures vertical deformation continuously throughout the test so that stress components are continuously updated during the different phases.

$$H = H_0 - \delta_a \tag{3.12}$$

Equation 3.12 describes the change in height of the specimen. The axial deformation, δ_a, is continuously estimated during the experimental phases using an electric deformation gauge that communicates with the GDS software.

$$V_{kons} = \Delta V \tag{3.13}$$

The amount of expelled pore water, ΔV, is measured during the consolidation phase. The area correction, described in Equation 3.14 for the consolidation phase, is further carried out using the volume change of the specimen. If any axial deformation takes place after the consolidation, e.g. through the saturation or B-check, the sample height is as well updated prior to shearing.

$$A_{kons} = A_0 - \Delta A = A_0 \cdot \left(1 - \frac{2}{3}\frac{\Delta V}{V_0}\right) \tag{3.14}$$

Equation 3.14 shows the samples' area correction throughout the test. For undrained shear tests, it's especially during the consolidation phase that the sample experiences significant volume change due to the expulsion of pore water. However, both the saturation phase and the resting period after consolidation, as described in section 3.5.2, will not be undrained, and a smaller amount of pore water may therefore be squeezed out of the sample. The GDS software continuously corrects for this, even after the consolidation phase, so that accurate values for both cross-sectional area, sample volume, and axial deformation will be precisely employed at the start of the shear test.

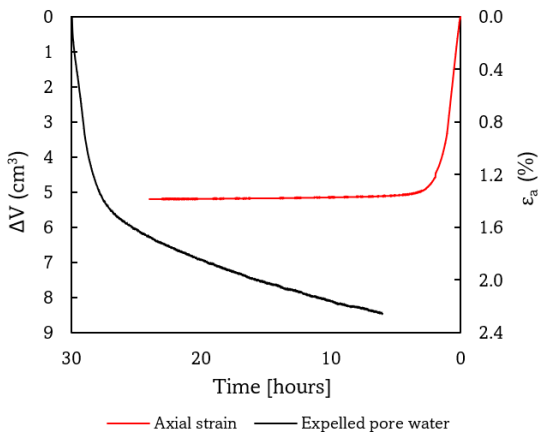

(a) Expelled pore water and axial strain during drained consolidation from this test series.

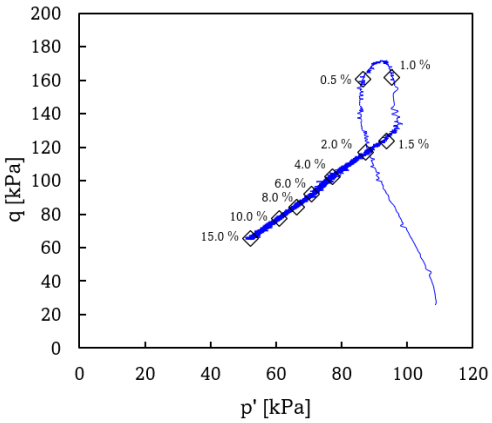

(b) p':q plot of an anisotropically consolidated undrained shear test from this test series.

Figure 3.12: Expelled pore water and axial strain during consolidation and CAUC stress path.

Figure 3.12 illustrates the amount of expelled pore water and axial deformation during the consolidation phase for a randomly selected specimen from this thesis' laboratory study, as well as an example of an arbitrary stress path from an undrained shear phase, here presented in an p'-q stress space.

During the shear phase, the sample will be loaded at a constant axial strain rate. This will result in a continuous aerial cross-section change throughout the shear phase. Samples subjected to undrained shearing will not experience any volume change. Therefore, the area correction during the shear test is based on axial, radial, and volumetric strains. To ensure that the stress values are calculated most accurately during the shear test, the deviator stress is used as the controlling parameter through equation (3.15). The axial strain, ε_a, radial strain, ε_r, and the volumetric strain, ε_{vol}, are further found as presented in Equation 3.16 to 3.18.

$$q = \frac{P}{A_{kons}} \cdot \frac{1-\varepsilon_a}{1-\varepsilon_{vol}} \tag{3.15}$$

$$\varepsilon_a = \frac{\delta_a}{H_0} \tag{3.16}$$

$$\varepsilon_r = \frac{\Delta r}{r_0} = \frac{\frac{V_0}{2A_0} - \frac{\Delta V}{2A_{kons}}}{r_0} \tag{3.17}$$

$$\varepsilon_{vol} = \varepsilon_a + 2 \cdot \varepsilon_r \tag{3.18}$$

By using the deviator stress as the governing stress parameter throughout the shear test, one can efficiently find the mobilized shear stress in the sample, as shown in Equation 3.19.

$$\tau = \frac{q}{2} \tag{3.19}$$

The estimation of the effective mean stress is further performed by considering the continuously updated cross-sectional area throughout the shear test, denoted as A_{shear}. σ_c represents the selected cell pressure for conducting the triaxial test.

$$p' = \frac{1}{3} \cdot (\sigma_a + 2\sigma_c) - u_b = \frac{1}{3} \cdot \left(\frac{P}{A_{shear}} + 2\sigma_c \right) - u_b \tag{3.20}$$

Strength parameter interpretation

By utilization of the stress-controlled parameters obtained in the above section, the strength parameters for the clay sample are subject to interpretation. Undrained shear strength, friction angle, attraction, and cohesion are all strength parameters that may be interpreted from the resulting triaxial stress path. For an optimized interpretation of the strength envelope of a soil deposit, several performed stress paths obtained from samples extruded at different depths are desired due to sample disturbance and local variations. Figure 3.13, as well as Equation (3.21) to (3.22) shows the procedure for obtaining the different parameters.

$$c_u = \tau_{max} \tag{3.21}$$

$$tan\varphi' = \frac{S_f}{\sqrt{1 + 2S_f}} \tag{3.22}$$

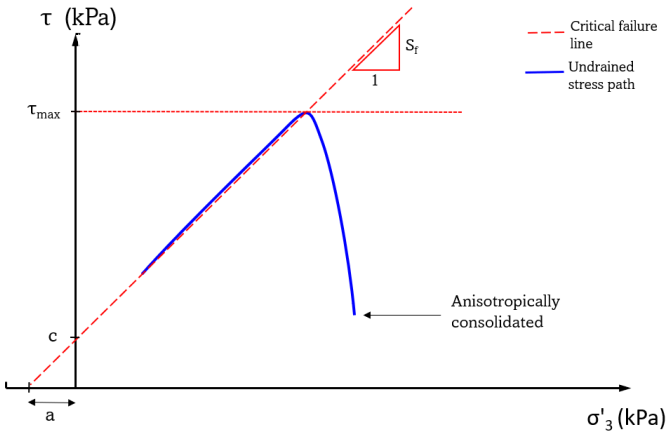

Figure 3.13: Triaxial strength parameter interpretation, based on the Coloumb envelope. Here shown by an undrained stress path in the σ_3':τ stress space.

Identification of yield mechanism

The interpretation of the yield point after the culmination of the constant K_0' test is carried out by coordinating for which p' value the change in both void ratio and volume strain adjusts drastically. Equation 3.23 links the amount of expelled pore water and aerial cross-section correction, and shows the procedure for estimating the specific volume and void ratio. Volume strain is estimated based on equation 3.18. As described in detail in chapter 2.5.1, the yield point is identified for several parameters in the K_0' consolidation. In this master's thesis, the yield points are identified by coordinating a severe shift in specific volume and volumetric strains, to satisfactorily describe when the strains develop plastically.

$$v = 1 + e = 1 + \frac{V_p}{V_s} = 1 + \frac{A_{kons} \cdot H(V_0 - \Delta V) - m_s/\rho_d}{m_s/\rho_d} \tag{3.23}$$

For a further interpretation of yielding, different stress-strain relations are correlated and compared against each other. In the p'-q - space, the volumetric, ε_p,- and deviatoric strain, expressed in equation (3.24), relate respectively the development of plastic strains to its stress component.

$$\varepsilon_q = \frac{2}{3}(\varepsilon_a - \varepsilon_r) \tag{3.24}$$

By uncovering the volumetric- and deviatoric strains, one could as well obtain the bulk- and shear stiffness of the soil specimen. By these stiffnesses in the elastic region, one could couple the strain increments when crossing the yield locus. This procedure is shown in equation 3.25 to 3.28.

$$G = \frac{\Delta q}{3\Delta \varepsilon_q} \tag{3.25}$$

$$K = \frac{\Delta p'}{\varepsilon_p} \tag{3.26}$$

$$\delta {\varepsilon_q}^{el} = \frac{\delta q}{3G} \tag{3.27}$$

$$\delta {\varepsilon_p}^{el} = \frac{\delta p'}{K} \tag{3.28}$$

For undrained triaxial tests, there is no volume change during shearing, and the strain components links to the shear modulus as it follows from equation 3.29.

$$\varepsilon_q = \varepsilon_a \Rightarrow E_u = \frac{\Delta q}{\Delta \varepsilon_a} \Rightarrow G = \frac{E_u}{3} \tag{3.29}$$

Because the clay not being an isotropic material (Länsivaara, 1995; Nordal, 2020; Wood, 1990) the above-listed bulk- and shear modulus interpretation are not sufficient for obtaining the total strain increment when reaching the yield locus. A semi-graphic procedure, proposed by Graham et al. (1983), is in this thesis utilized for the estimation of the total plastic strain increment when reaching an interpreted yield mechanism. This technique is illustrated in figure 3.14, and the total plastic strain increments are from all samples found for a standardized stress change of $0.1 \cdot \sigma'_{cv}$ related to each specimen. The corresponding values of $\delta p'$, δq and $\delta \varepsilon_p$, $\delta \varepsilon_q$ may be evaluated from the chosen stress path (Graham et al., 1983).

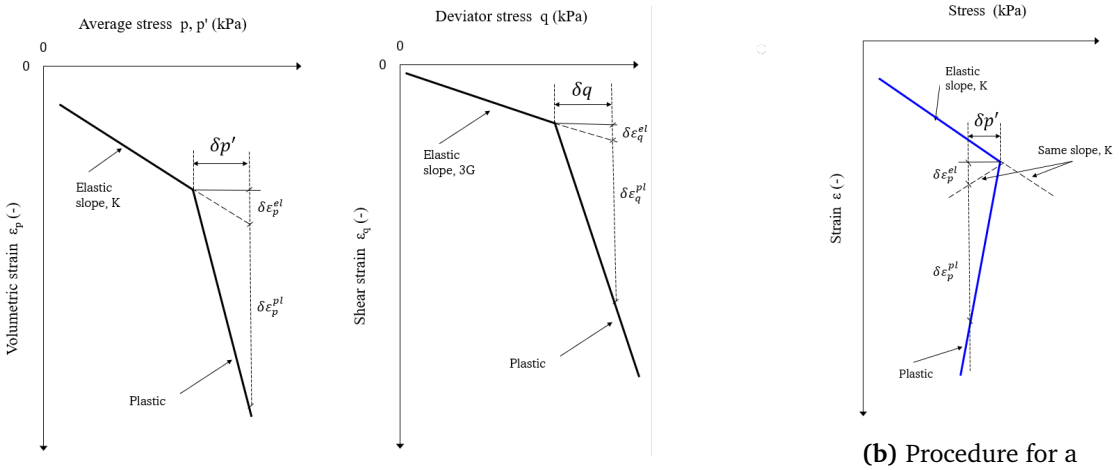

(a) Procedure for a progressive and stiffer structural yield response, with increasing stress values after yield.

(b) Procedure for a strain-softening yield response.

Figure 3.14: Semigraphic procedure for obtaining the total plastic strain increments when crossing the yield envelope. Figure and method inspired by Graham et al. (1983).

3.6 Oedometer tests

The oedometer test is conducted to determine the deformation properties of soil samples. The results from the oedometer test are generally used in practice to estimate the settlements and deformation behavior of a soil layer. The test material, which is prevented from radial deformation during the test, is subjected to increasing axial compressive loads. This one-dimensional loading condition results in a measurable axial deformation under known pressure loads at the laboratory (Statens Vegvesen, 2016).

3.6.1 Equipment

Figure 3.15 shows both NTNU's oedometer equipment, as well as a schematic drawing of an oedometer setup, taken from (Statens Vegvesen, 2016). The sample is surrounded by an oedometer ring, which has a diameter of 50 mm and a height of 20 mm. Saturated porous filters are used at the top and bottom surface of the specimen, and an electric device continuously measures the pore pressure during the oedometer test.

The execution of the oedometer tests in this master thesis follows the procedures developed by SVV (Standard Norge, 2017). The procedure for sample preparation and selection of user-defined test conditions is explained in more detail in the following sections.

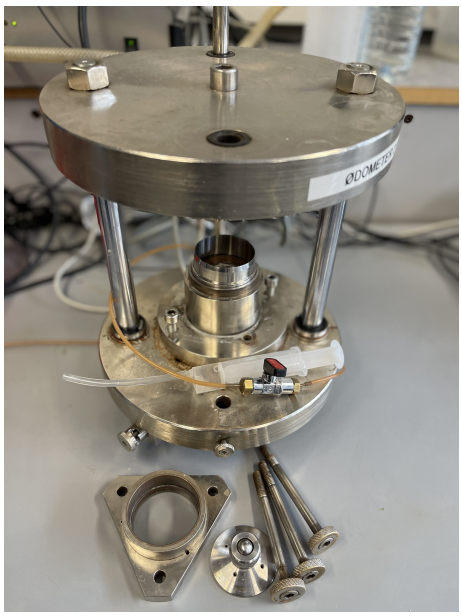

(a) Oedometer apparatus at NTNU lab.

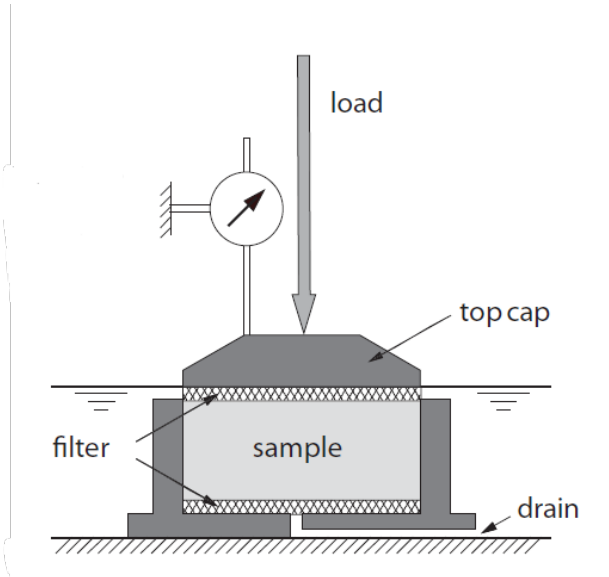

(b) Sketch of oedometer apparatus. Pore pressure measurements are obtained from the bottom drain. Taken from Sandven et al., 2017.

Figure 3.15: Oedometer test setup, equipment, and cross-sectional sketch.

Mounting and preparation

Before cutting the oedometer sample, undisturbed soil material is selected for conducting the oedometer test. A custom-made apparatus is used together with the oedometer ring, which is pre-lubricated with silicone oil, to press the soil sample into the oedometer ring. After the oedometer ring is pressed in, external soil material is removed, and the end faces are trimmed and made flat using a wire saw. The oedometer ring is weighed both before and after trimming to determine the density of the soil sample (Statens Vegvesen, 2016).

The bottom drain of the oedometer pedestal is filled from bottom to top with distilled, air-free water to ensure that there aren't any air bubbles in the system which may disturb pore pressure measures. The lower porous filter is placed gently on the bottom in such a way that air is not trapped under the filter stone. The oedometer ring containing the soil sample slides in above the sealing ring, before the upper porous filter is placed centered above the oedometer ring. Both filter stones should be cleaned in a UV bath and stored in air-free water prior to the experiment. The top cap is mounted over the oedometer sample and saturated with distilled, air-free water.

3.6.2 CRS - test

Constant rate of strain oedometer tests (CRS) are conducted by subjecting the clay sample to a predefined constant strain rate dependend on the soil type (Sandven et al., 2017). For sensitive clay samples, SVV recommends a deformation rate of $0.0033 - 0.0067$ mm/min to obtain reliable results and a pore pressure-to-stress ratio below 50%, $u_b/\sigma_a < 0.5$. This strain rate is recommended due to the low residual strength which is typical for brittle soils. In this experimental study, the oedometer tests are therefore conducted with a strain rate equivalent to 300 μm $= 0.005$ mm/min $= 1.5\%$/hour.

3.6.3 Interpretation of results

From oedometer tests, there is mostly the interpretation of the yield preconsolidation stress, σ'_{cv}, which is central to this master's thesis. However, obtaining not only the oedometer curve, but also the modulus, M_{oed}, is essential both for the accompanying interpretation of the pre-consolidation stress, but also for evaluating the sample quality. This section presents the central expressions for maintaining the desired results from CRS oedometer tests.

$$\varepsilon = \varepsilon_a = \frac{\delta_a}{H_0} \tag{3.30}$$

Due to the oedometer ring that encloses the oedometer sample, the deformation pattern of the sample is limited to only vertical deformation. Equation (3.30) describes the sample's vertical strain. Axial deformation is continuously measured throughout the test, and the original height of the oedometer sample is $H_0 = 20mm$.

$$\sigma'_m = \sigma_a - \frac{2}{3} \cdot u_b \tag{3.31}$$

The factor $\frac{2}{3}$ correlated to the pore pressure in Equation 3.31 refers to a correction factor that takes into account a parabolic pore pressure distribution in the oedometer sample during the implementation of CRS tests, with drainage only allowed against the top and pore pressure readings done in the bottom. This approximation has previously been shown to work well as long as $\frac{u_b}{\sigma'_v} < 0.20$ throughout the test (Sandven et al., 2017). Thus, σ'_m represents the average effective stress in the oedometer sample throughout the test.

There haven't been developed any exact expressions for obtaining the oedometer modulus during CRS oedometer tests (Sandven et al., 2017). Thus, the standard definition of stiffness is recommended, seen in Equation (3.32). The vertical coefficient of consolidation is estimated as seen in Equation (3.33). Secondary effects, such as creep, affect the deformation pattern on soft soils significantly (Sandven et al., 2017). Even though CRS-test applies a continuous load to the specimen, the opposite of the incremental loading test, it should be noted that the coefficient of consolidation is sensitive for soft soils.

$$M_{oed} = \frac{d\sigma'_m}{d\varepsilon} \tag{3.32}$$

$$c_v = \frac{d\sigma'_m}{dt} \cdot \frac{1}{u_b} \frac{[H_0(1-\varepsilon)]^2}{2} \tag{3.33}$$

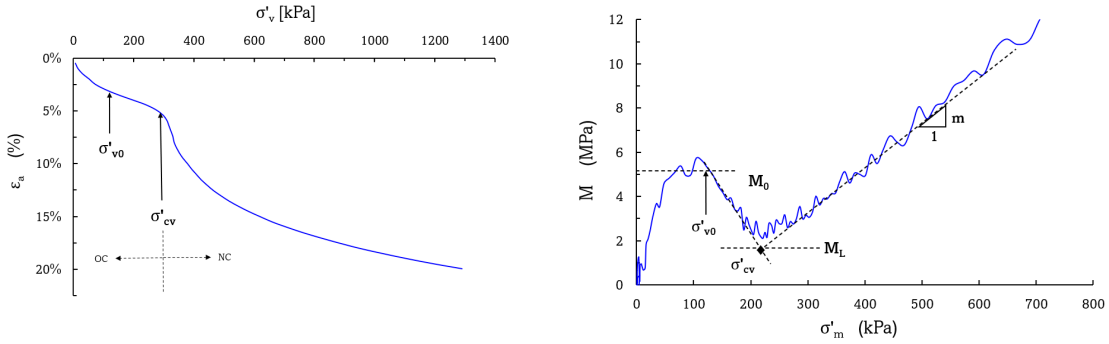

(a) Stress-strain path from oedometer test. Pore pressure measured at the bottom. Interpretation of σ'_{cv} marked.

(b) Obtained oedometer modulus by the procedure described in 3.6.3. Pore pressure obtained as parabolic. Corresponding σ'_{cv} marked.

Figure 3.16: Interpretation of oedometer test results.

Chapter 4

Tiller-Flotten research site

Concerning the Norwegian GeoTest Site (NGTS) research project, financially supported by the Norwegian Research Council, a research area has been established at Tiller-Flotten, south of Trondheim, for geotechnical studies of a more than 50-meter deep, sensitive clay layer. Chapter 4 presents and describes relevant geotechnical and geological data from the current testing site, Tiller-Flotten. An area description, geological history, and relevant engineering properties from the research site are presented. Relevant and extensive geotechnical field, routine, and strength parameters from the previously published report 20160154-20-R, (L'Heureux et al., 2019), are introduced for the current quick clay deposit.

4.1 Area description

The Tiller-Flotten test site is as mentioned above, located around 10 km south of Trondheim in Trøndelag and approximately 700 meters west of the Nidelva River. The research site, marked inside the red ellipse in Figure 4.1, is situated about 127 m.a.s.l. and drains east towards the lower situated Nidelva River. The area surrounding the Nidelva River may be characterized as a valley, stretching from Trondheim to Klæbu in the south-east. Figure 4.2 shows the terrain profile from the test site towards Nidelva River in the east, through insition A-A. The site has for several years been utilized as a quick clay research site due to its deep and highly sensitive clay deposit, further defined as a pure quick clay site through the NGTS project. Through NGTS, quick clay sampling and other geotechnical site investigations are easily accessible for research purposes.

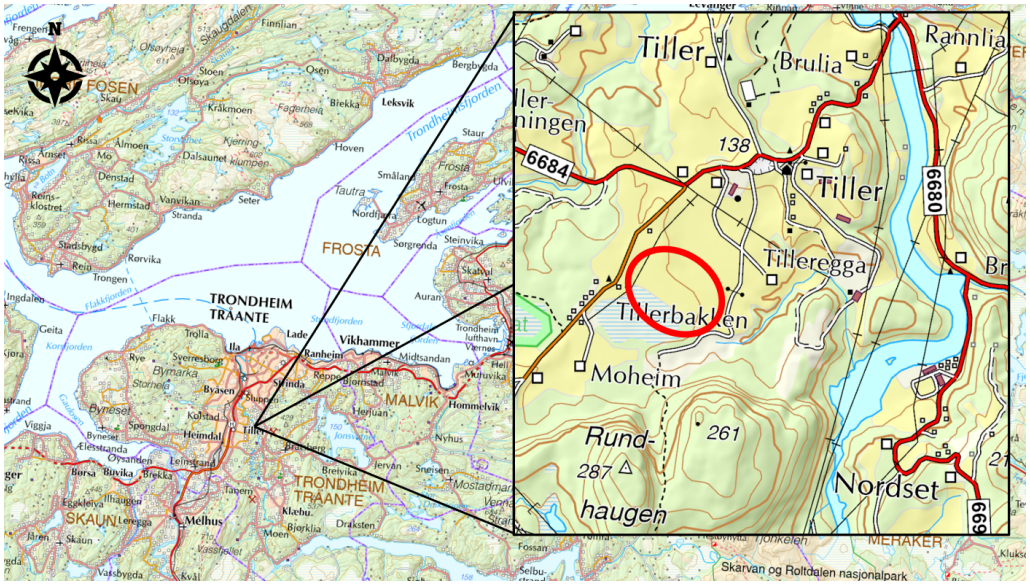

Figure 4.1: Overview of the site location, ("Norgeskart," 2023).

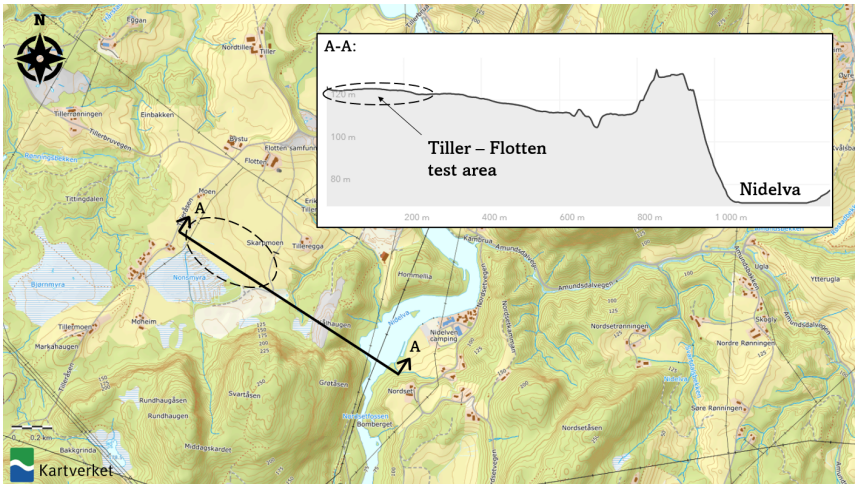

Figure 4.2: Terrain profile from the test site towards Nidelva river in the east, ("Norgeskart," 2023).

Figure 4.3 presents both a historic overview of the site from 1957, 4.3a, as well as a present aerial photo, 4.3b. Tiller-Flotten, as well as surrounding areas, have upon the years been widely used for agricultural purposes due to its convenient location by the river. In modern times the location surrounding the test site, marked within white rectangles in Figure 4.3, is as well utilized for storage of excavated materials.

(a) Historic overview of the Tiller test site. **(b)** Present overview of the Tiller test site.

Figure 4.3: Historic and present overview of test site. Taken from "FINN Kart" (2023).

As may be seen from the Quaternary map presented in Figure 4.4, the area surrounding the test site consists predominantly of marine deposits. Marine deposits often interfere with fine-grained, clayey soils, frequently with large thicknesses. In its southwest corner, the presence of some more vegetated areas and bog masses dominate. The fluvial and till masses found in slopes and elevations around the Tiller area may refer to the last ice age and the glacier retreat. Due to its height above sea level, the test site is situated below the marine limit, which, according to Norway's National Geological Survey (NGU), has a marine limit of approximately 175 m above sea level. Marine deposits in fjord-like environments below the marine limit may often interfere with marine, sensitive soils. However, the presence of sensitive marine deposits is quite common in Norwegian valleys, especially when the groundwater drainage conditions are as seen at Tiller-Flotten, with a downward potential and drainage from higher situated levels.

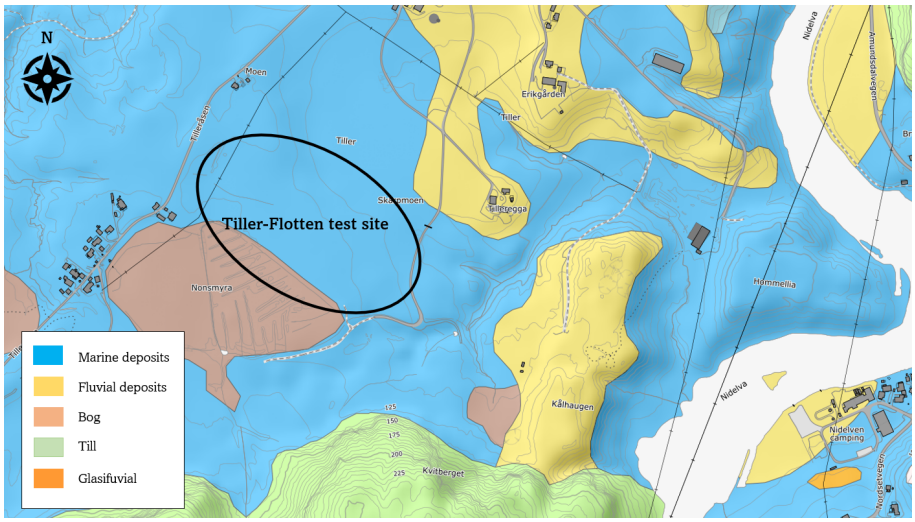

Figure 4.4: Excerpt of NGU's Quaternary deposits map from the Tiller-Flotten test area, marked inside the black ellipse. Taken from NGU (2022).

4.2 Geological history

The Tiller-Flotten test site is located approximately 700 meters west of the Nidelva River. Hence, according to L'Heureux et al. (2019), the site drain towards the Nidelva River in the east due to its elevation and potential. The presence of moraine ridges along the local elevations in the area is a consequence of the glaciers' activity before their retrograde, around 10,300 years ago. Figure 4.5 presents a reconstructed composition of the marine limit and the glacier placement around 10.300 years ago (Reite et al., 1999). The relatively rapid retreat of glaciers towards the east explains the relatively high measurements of the overconsolidation ratio in the first meters of the clay deposit. Based on the modern terrain formations and its' history, it is likely that the sediments found in the Tiller area today were deposited in a fjord-like environment, around 30-40 meters below sea level at that time (L'Heureux et al., 2019).

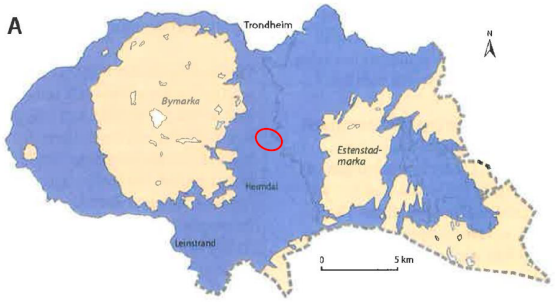

Figure 4.5: Reconstructed composition of the marine limit, approximately 10.300 years ago. The tiller-Flotten test area is marked within the red circle. Taken from Reite et al. (1999).

As processes such as land uplift and complementary lowering of the sea level advanced, the saline clay deposit was exposed to drainage. Freshwater penetrated the clay deposit and released the strong-bonded salt ions from the clay particles. The result over a longer time perspective with drainage is a sensitive clay layer with low residual strength, which is a characteristic of marine deposits in Norway, (Rosenqvist, 1953).

Hence, such sensitive clay deposits may be classified as brittle materials, in some cases quick clay. The Tiller-Flotten research site is well identified as a deep quick clay deposit by L'Heureux et al. (2019), for the soil masses of the experimental area deeper than 7 meters below ground level. In more recent times, it is known that a large quick clay landslide, later known as the Tiller landslide, was triggered in the area northeast of the experimental area in 1816. This may be indicated in Figure 4.6, presenting lidar data from the area surrounding the research site. Further interpretation of the lidar data may also reveal indications of scars in the landscape only a few hundred meters north of the experimental area, which may indicate other landslides from elder times.

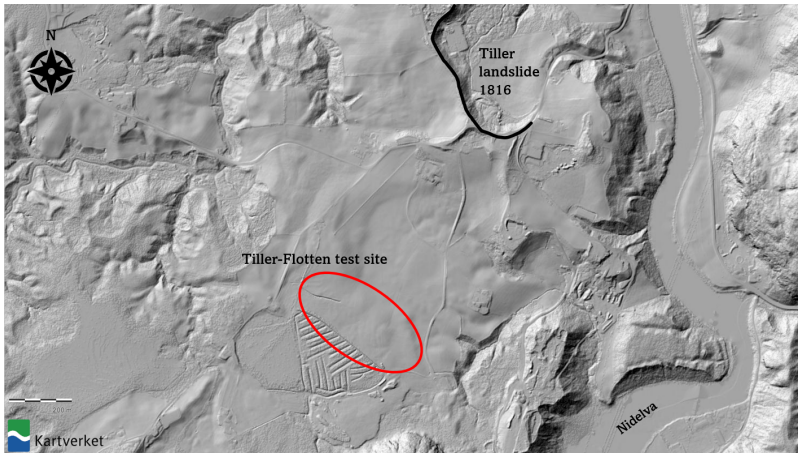

Figure 4.6: Lidar overview above the Tiller-Flotten test site, excerpt from "Høydedata" (2023). Blue ellipse marks the test site, and black line defines the Tiller landslide from 1816.

4.3 Soil and deposit characteristics

Soil parameters and engineering properties from report 20160154-20-R, L'Heureux et al. (2019), are below presented and further utilized for defining relevant parameters and distributions for the relevant depths the soil samples used in this thesis are extracted from.

4.3.1 Stratigraphy and structure

Figure 4.7 shows the presented stratigraphy and relevant index parameters from the Tiller-Flotten quick clay site, previously presented by L'Heureux et al. (2019). Due to extensive geotechnical site and laboratory investigations, the stratigraphy at the site is characterized as a clayey, dry crust followed by a low to medium-sensitive clay layer down to around 7 meters below the ground surface. From this depth, the following clay layer is defined as very sensitive quick clay, based on several correlations obtained from laboratory and site investigations.

The bulk density weight of the clay deposit varies between $\gamma_s \approx 17 - 18.5 kN/m^3$, while the water content of the soil is reported around $w \approx 37 - 50\%$. The particle density, ρ_d, is found to be relatively accurate for the clay deposit around $2.85 g/cm^3$. One may also notice the relatively low salinity values reported below 7 meters depth, all below 5 g/l.

The reported values for the liquidity index, I_L, sensitivity, S_t, and the remolded shear strength, c_{ur}, all support the presence of quick clay from around 7 meters depth. As described in Section 2.1, a liquidity index above 1.6 indicates the presence of quick clay. Together with the utmost sensitivity values and low remolded strength values, the clay layer below 7 meters is defined as highly sensitive and further quick clay if the c_{ur} are below $0.33 kPa$.

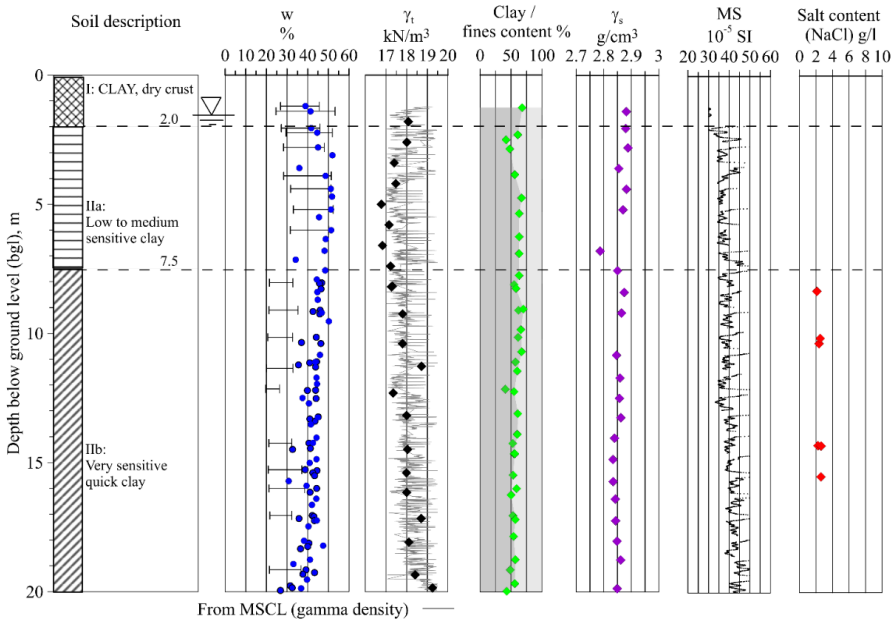

Figure 4.7: Stratigraphy: Rutine and index parameters from the Tiller-Flotten clay deposit. From L'Heureux et al. (2019)

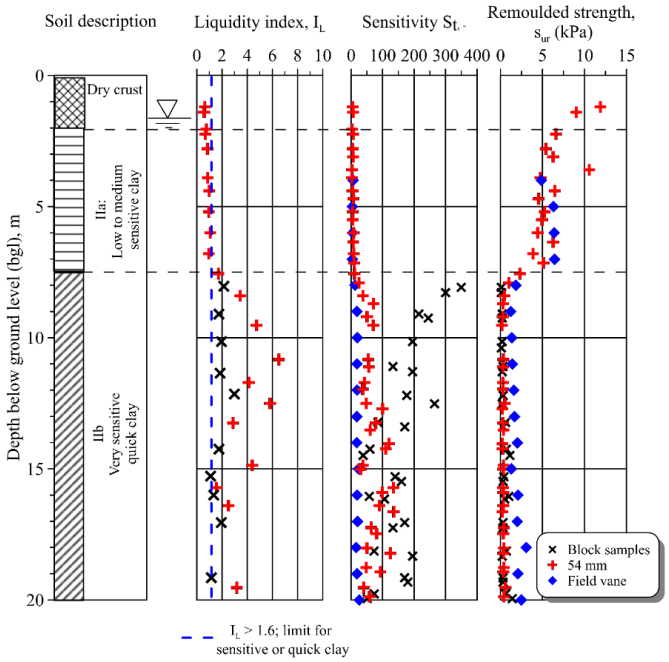

Figure 4.8: Liquidity index, sensitivity, and remolded shear strength obtained from the Tiller-Flotten research site.From L'Heureux et al. (2019)

4.3.2 In-situ stress and history

Figure 4.9 shows the current pore pressure distribution and resulting effective stress profile for the borehole to which the test series in this master's thesis is extracted. The profiles are sketched based on previously reported piezometer measurements, reported weights and densities, as well as oedometer tests presented in report 20160157-20-R (L'Heureux et al., 2019). The pore pressure is distributed below hydrostatic pressure from around 4 meters below the ground surface, with a groundwater level at around 1-2 meters depth. The variation of the surrounding elevations and the drainage conditions may affect the descending gradient from around 4 meters depth, also supporting the steady downward groundwater flow towards the Nidelva River.

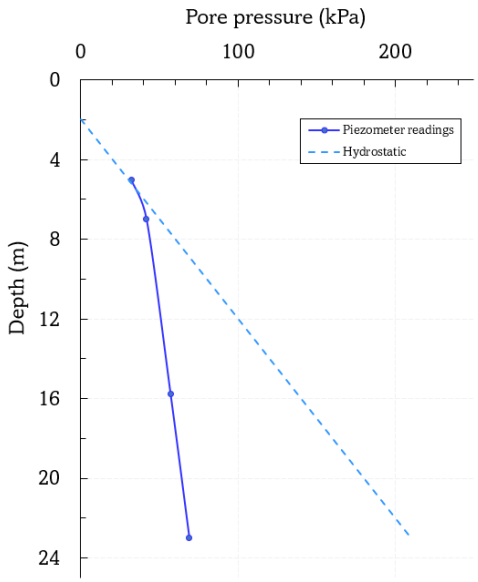

(a) Earlier reported piezometer readings and the resulting pore pressure distribution.

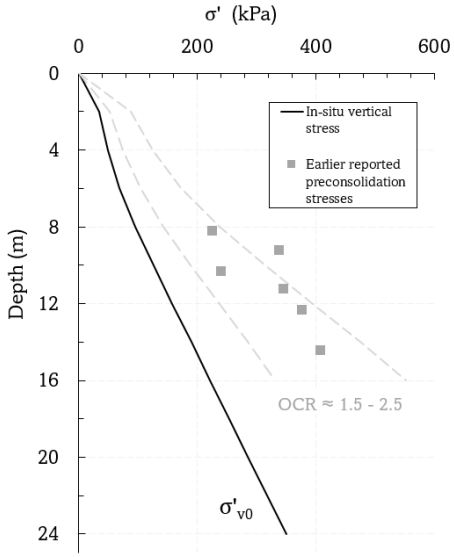

(b) Resulting effective overburden stress and earlier reported preconsolidation stresses.

Figure 4.9: Pore pressure and effective overburden stress at Tiller-Flotten test site. Reported parameters from L'Heureux et al. (2019), are used for obtaining the distributions.

The effective stress distribution is obtained due to the reported density and weight of the soil and the resulting pore pressure distribution. CRS oedometer tests reveal an overconsolidation ratio of around $OCR \approx 1.5-2$ for the quick clay layer, supporting the geological history of the glacier activity in the area. The groundwater flow, and also the groundwater level, (Bjerrum & Aitchison, 1973), which may have changed during the retraction of the glaciers and the resulting Nidelva river, may also influence the tendency of higher preconsolidation stress values than the current effective stress at the site.

4.3.3 Engineering properties

The yield stress, or the preconsolidation stress identified from oedometer tests, is reported as nearly twice the current effective stress at the site. Results from CRS oedometer test on high-quality block samples, together with performed piezocone penetration tests (CPTU-soundings), suggest an OCR around 2. The ratio between the horizontal and vertical stress, also called the earth pressure coefficient at rest, K_0', are from laboratory tests and CPTU soundings found to decrease from 1.2 at the top clay layer, to around 0.7 at 23 meters depth. On average, $K_0' \approx 0.8$ for the very sensitive quick clay layer (L'Heureux et al., 2019).

The shear strength data presented in Figure 4.10 are obtained through performing consolidated triaxial compression and extension tests from mini block samples, as well as routine tests like unconfined compression tests and falling cone tests. The best-fit effective strength parameters are reported to be around $\varphi' \approx 28-31^o$ with a small cohesion of $5kPa$, (L'Heureux et al., 2019). The undrained strength parameters reveal an increasing distribution, with the minimum obtained shear strengths at the beginning of the very sensitive quick clay layer. Routine tests, such as falling cone and unconfined compression tests, reveal undrained shear strength values both inside and below the NC envelope ($s_u/\sigma_0' = 0.2-0.3$). However, the conducted triaxial compression tests performed with a confining pressure by L'Heureux et al. (2019) reveal a normalized shear strength profile of $s_u/\sigma_0' = 0.40-0.61$ for the very sensitive quick clay layer.

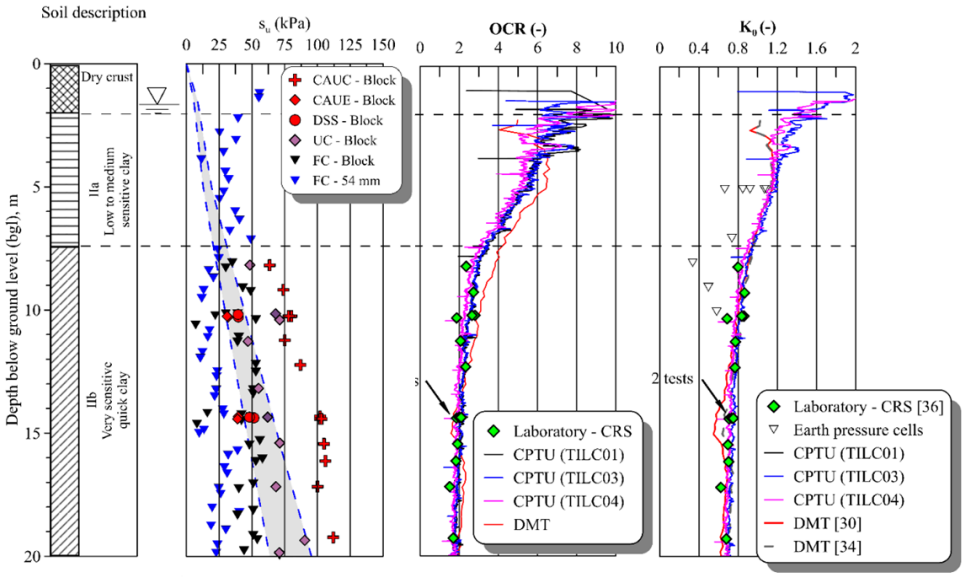

Figure 4.10: Engineering properties: Rutine and index parameters from the Tiller-Flotten test site. From L'Heureux et al. (2019)

Chapter 5

Laboratory testing and procedures

Chapter 5 describes how the laboratory testing series has been selected to be carried out, based on consolidation approaches and preferred results. As described in chapter 4, the quick clay from Tiller-Flotten has previously been thoroughly geotechnically identified, and large quantities of valuable laboratory and field data have been collected. Triaxial equipment was primarily used throughout this experimental series. In addition, oedometer tests were also conducted to primarily identify the preconsolidation stress and rate dependencies. General routine tests were carried out for coordination with previously reported index parameters. Each sub-chapter clarifies why and to what extent the chosen conditions, especially for the implementation of triaxial procedures, have been selected and theoretically prepared to support the experimental results.

5.1 Identification of yield surface

As pointed out by Graham et al. (1983), the mechanical behavior of clays, including anisotropy and memory effects, may favorably be identified through minimally disturbed clay samples. Therefore, the experimental series organized to identify the yield surface and the mechanical behavior of quick clay from the Tiller-Flotten area was carried out using high-quality mini-block samples.

Figure 5.1 illustrates some principles on the experimental setup for identifying the yield surface of the quick clay from Tiller-Flotten. A combination of various triaxial test setups enables an interpretation of the yield surface and its properties when reaching various yield mechanisms. Both consolidated undrained and drained shear tests, along with K_0' tests, will form the basis for the analysis together with the CRS oedometer tests. All shear tests used for identifying the yield surface are initially consolidated to the respective in-situ effective stress to maintain the comparison equal throughout the sample series in terms of both sample quality and expelled pore water during the consolidation. The experiments are carried out on specimens from different depths, and the test series is thereby organized to provide a common basis for comparing the quality of the samples after the experiments.

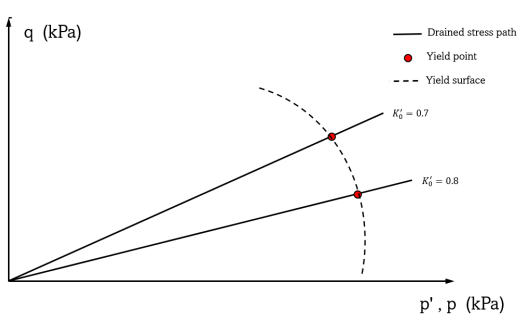

(a) Yield point identification from constant K'_0 triaxial tests.

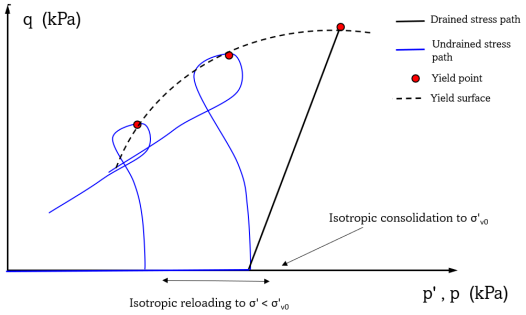

(b) Yield point identification from drained and undrained triaxial shearing.

Figure 5.1: Yield identification from different triaxial tests performed in the test series.

As per section 2.5.1, the yield locus for samples from different depths will vary in size due to differences in their stress and overburden history. However, even though the size of the locus varies, Graham et al. (1983) states that the shape of the yield locus is similar. Therefore, oedometer tests are performed on all samples for the normalizing purpose of the stress plane and thereby comparison of the samples from different depths through each sample's respective preconsolidation stress.

The analysis of yield point placements inferred from the triaxial tests performed in this master's thesis warrants thorough consideration of the specific test methodologies employed, including both undrained and drained conditions. The yield mechanisms observed during the triaxial tests are likely influenced by strain- and stress rates and are further complicated by the presence of highly sensitive quick clay which may affect the interpretation of the obtained yield points. The interpretation of yield points is, therefore, predicated upon the detection of marked changes in the material behavior across different compression tests, both shear and K'_0 tests, which are further highlighted by the relevant initial- and boundary conditions. Because of the anisotropic behavior of the natural clay material (Graham et al., 1983; Länsivaara and Nordal, 1998; Wood, 1990) the use of the elastic relations of K, G and ε_p, ε_q are not utilized for finding the total plastic strain increments in this thesis. The principle presented by Graham et al. (1983), presented in section 3.5.7, is instead utilized for the analysis of the direction of the strain increments.

Only mini block samples have been interpreted to identify the yield surface because of their superior sample quality and observed material behavior. The normalization of stress- and strain paths are in Chapter 6 normalized by utilization of the reference preconsolidation pressure, $\sigma'_{cv,ref}$, found from the reference CRS oedometer tests, shown in section 6.2. The meaning of reference samples is, in this case, the mini block samples tested immediately after sampling, which show relatively larger preconsolidation pressures than the samples tested 21-28 days after sampling.

5.2 Isotropic versus anisotropic consolidation to p'

The overall test series conducted in connection with this master's thesis was conducted on 54 mm piston samples as well as mini-block samples. The specimens extracted for this laboratory study represent two different depths - approximately 9.5 and 12.5 m below terrain level. Table 5.1 shows the selected consolidation stresses for the different depths, based on available laboratory data and pore pressure measurements at Tiller-Flotten, (L'Heureux et al., 2019).

As shown in table 5.1, the consolidation test series focuses on consolidating samples from the same depths to the same effective mean stress level, p', for both isotropic and anisotropic conditions. The mean stress level for Tiller-Flotten clay is based on an earth pressure coefficient at rest, K_0', equal to 0.8, further elaborated in Section 4.3.3.

The effective mean stress, p', is represented by an average, effective, stress state for the specimen. For the specimen's state in the triaxial cell, the mean stress is determined utilizing the principal stress state. The principal stresses applied to the clay specimens in this study are calculated from the in-situ stress state of the specimens, which is in turn calculated from density measurements and piezometer data previously reported in report 20160154-20-R (L'Heureux et al., 2019). Equations 5.1 to 5.4 show the procedure for the determination of the current stress situation in-situ, based on the chosen earth pressure coefficient at rest, $K_0' = 0.8$.

$$\sigma'_{v0} = \gamma_s \cdot z - u_b \tag{5.1}$$

$$\sigma'_{h0} = K_0' \cdot \sigma'_{v0} \tag{5.2}$$

$$q = \sigma_1 - \sigma_3 = \sigma'_{v0} - \sigma'_{h0} \tag{5.3}$$

$$p' = p - u_b = \frac{1}{3} \cdot (\sigma_1 + 2\sigma_3) - u_b = \frac{1}{3} \cdot (\sigma'_{v0} + 2\sigma'_{h0}) \tag{5.4}$$

Isotropic triaxial tests are commonly carried out by applying the current in-situ vertical stress, σ'_{v0}, both vertically and horizontally to the specimen. This stress application puts the specimen in an isotropic stress state, where both vertical and horizontal stresses on the specimen are equal. This results in the specimen not being subjected to shear stresses during the consolidation phase, thereby eliminating the potential of the specimen failing prior to the shear test. For clay samples extracted from shallow depths, close to the terrain surface, isotropic consolidation is seen as a gentle stress application, as horizontal stresses can often be assumed to be approximately equal to vertical stresses close to the terrain surface (Statens Vegvesen, 2022).

For clay samples taken from deeper layers, however, the in-situ stress state is usually not representative as an isotropic condition. The coefficient of lateral earth pressure, which is often less than 1.0, indicates that horizontal in-situ effective stresses are often lower than vertical in-situ stresses. Therefore, anisotropic consolidation is considered as a more suitable representative

stress state for specimens taken from deeper layers. The specimen is therefore subjected to higher axial stresses than horizontal stresses in the triaxial cell. Shear strains are thus applied during this procedure by a higher deviatoric stress level, q.

This experimental study has therefore examined the differences between isotropically consolidating quick clay samples to the same mean stress level as achieved by anisotropic consolidation. Isotropic consolidation to the effective average mean stress level thus results in an overall slightly lower stress condition than traditional isotropic consolidation to vertical overburden stress, σ'_{v0}. Table 5.1 shows the estimated stress levels for the extracted quick clay samples utilized in this laboratory study.

In-situ values				**CIUC**		**CAUC**	
Depth, z	σ'_{v0}	K'_0	σ'_{h0}	p'	q	p'	q
(m)	*(kPa)*	*(-)*	*(kPa)*	*(kPa)*	*(kPa)*	*(kPa)*	*(kPa)*
9.5	125	0.8	100	108	0	108	25
12.5	155	0.8	124	134	0	134	31

Table 5.1: Chosen consolidation stresses from best in-situ correspondence for the chosen depths. Shown in terms of effective average stress, p' and deviator stress, q.

5.3 Pore pressure response in undrained conditions

Throughout the autumn of 2022, the author of this thesis conducted a thorough series of experiments on medium-sensitive clay from the upper terrain layer of Tiller-Flotten. The overall theme of the research project focused on triaxial tests, with a main emphasis on the choice of consolidation stresses and resulting undrained shear strength. Several key phases in the execution of the triaxial tests were highlighted throughout the experimental series, particularly the resulting pore pressure response from the B-test.

None of the six triaxial tests conducted during the autumn of 2022 achieved a B-value in accordance with the Norwegian Public Roads Administration's requirements, $B > 0.95$. A pore pressure response equivalent to $B = \Delta u_b / \Delta\sigma = 1.0$ would theoretically indicate a completely undrained state for fully saturated specimens. Lower B-values suggest a pore pressure response to stress increases that do not correspond to undrained loading theory and is believed to indicate trapped air in the system. The air may be in the sample, the valves or the tubes. The selected saturation conditions for the experimental series conducted in the autumn of 2022 were a back pressure corresponding to 500 kPa and a rest period of 60 minutes after achieving back pressure. Recent studies (e.g. Wild et al., 2017; Giger et al., 2018) suggest that the pore pressure response may be improved after the initial B-test by increasing the cell and back pressure to a higher level, as well as increasing the rest period after achieving back pressure to stabilize the stress state in the soil specimen. Using a high back pressure may dissolve air bubbles into the water and provide a more satisfactory undrained response. These measures were not implemented during the autumn of 2022 due to the time constraints of the experiment

and limited time for execution.

The experimental series carried out in connection with this master's thesis has implemented Wild & Giger's recommendations during the execution of the triaxial tests. All reported B-values, as seen in section 6.3, have been attempted to be improved through three measures; increased back pressure to 700-1000 kPa, increased rest time for the sample after desired back pressure is attained, and an increase in cell and back pressure to a higher level if the first B-test yields an insufficient pore pressure response. Figure 5.2 illustrates how back pressure, rest time, and B-tests were conducted in this experimental series.

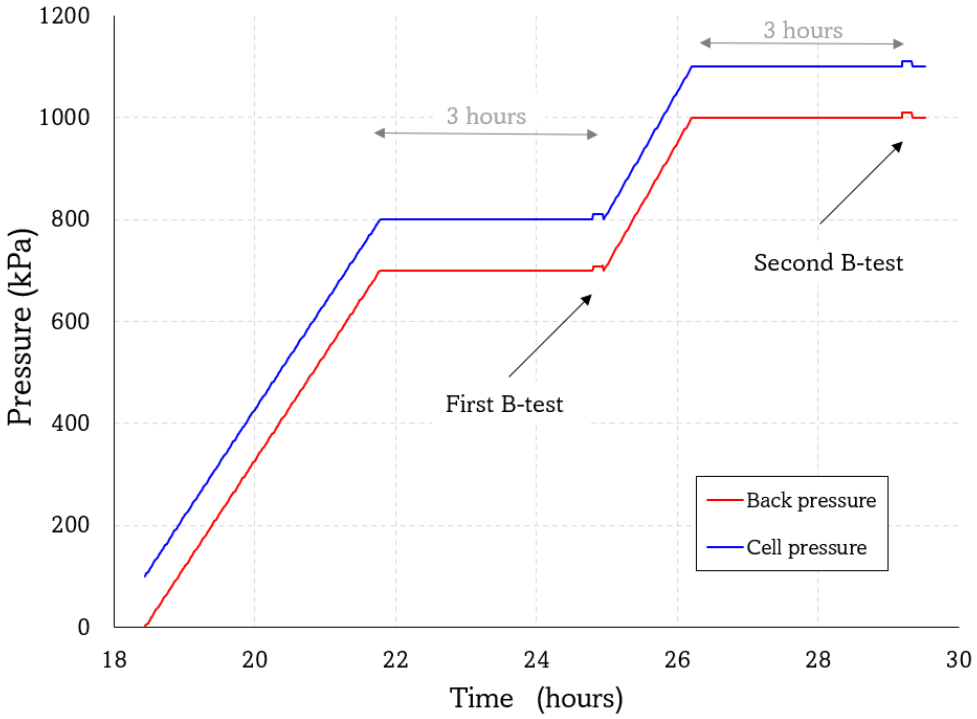

Figure 5.2: Procedure for the saturation stage for improving the pore pressure response in undrained conditions.

Chapter 6

Results

This chapter provides a comprehensive exposition of the laboratory testing results undertaken in conjunction with this thesis, including both the corresponding results and interpretations. Additionally, relevant diagrams are presented with explicit connections to the overall thesis theme. Individualized examinations of each respective test are available for reference within the appendix, A, B and C.

6.1 Rutine and index tests

Samples investigated in this study were collected from around 9 and 12 meters below the ground surface. The water contents for the clay samples from these depths vary between $40.1 - 46.3\%$, averaging at about 42%. The resulting water content is presented for all test specimens in table 6.1. The mean water content represents the average value based on several tests conducted to extract the water content from different locations in the test cylinder/block specimen. For cylinder specimens, the water content was tested relatively at the top, middle, and bottom of the cylinder. The plasticity index is found to vary around $5.0 - 6.4\%$, which identifies the clay as low plastic. We also observe that the liquidity index values vary between $2.0 - 3.3\%$, all exceeding 1.6%, which are seen to be an identification for quick clay, as the remolded shear strength is suggested to be below $0.5kPa$, by Equation (2.5), (Leroueil et al., 1983). The obtained values for the water contents and the plastic- and liquid limits correlates well with the previously reported values presented by L'Heureux et al. (2019) in report 20160154-20-R.

Test ID	Type	Depth	Storage	Av. water content	Atterberg-limits			
		(m)	*(months)*	w *(%)*	w_L *(%)*	w_P *(%)*	I_P *(%)*	I_L *(%)*
U67	54 mm	9.4 m	0	46.3	32	26	5.9	3.30
U172	54 mm	9.5 m	1	40.1	32	27	5.0	3.00
MB-1	Mini block	9.2 m	0	43.2	31	25	6.2	3.00
MB-3	Mini block	9.6 m	1	41.6	34	28	6.2	2.00
L20	54 mm	12.3 m	0	41.3	30	24	6.4	2.70
U195	54 mm	12.6 m	1	42.4	31	25	6.0	2.89
MB-2	Mini block	12.1 m	0	41.5	30	25	5.4	3.10
MB-4	Mini block	12.6 m	1	41.7	31	25	6.18	2.68

Table 6.1: Resulting index parameters for all samples.

The undrained shear strength values determined from the falling cone test are presented in Table 6.2. From the samples collected from 9 meters below the ground surface, the undrained shear strength varies around 26.7−37.4 kPa, while samples collected from 12 meters below the ground surface show values varying between $25.2 - 41.8$ kPa. The remolded shear strength is significantly low for all samples, all below 0.33 kPa, obtaining an all-around ”very high sensitivity” and therefore identifying the clay as a quick clay.

One could also notice that all listed index parameters do not vary significantly when comparing the storage time for the samples. Half of the samples were stored for around 1 month in the laboratory before the tests were conducted. Some deviations are seen for the different samples, which are found to be normal - both in terms of the implementation of the tests and local variations of the clay deposit.

Test ID	Type	Depth	Storage	Falling cone		
		(m)	*(months)*	c_{ufc} (kPa)	c_{urfc} (kPa)	S_t (-)
U67	54 mm	9.5	0	26.7	0.16	164
U172	54 mm	9.5	1	37.4	0.12	312
MB-1	Mini block	9.2	0	31.4	0.27	118
MB-3	Mini block	9.6	1	28.5	0.14	210
L20	54 mm	12.2	0	25.2	0.23	110
U195	54 mm	12.3	1	41.8	0.18	232
MB-2	Mini block	12.1	0	34.8	0.22	159
MB-4	Mini block	12.6	1	31.9	0.15	213

Table 6.2: Resulting shear strength from falling cone.

6.2 Oedometer tests

The oedometer test program consists of CRS tests performed on each sample reported in this thesis. All CRS tests have been run with a vertical strain rate equivalent to 1.5% per hour. In addition, two CRS tests have been performed with both lower and higher strain rates, hereby 0.75% and 3.0%, presented in Figure C.11 and C.12. A comprehensive collection of the oedometer results may be found in Appendix C, similar as Figure 6.1.

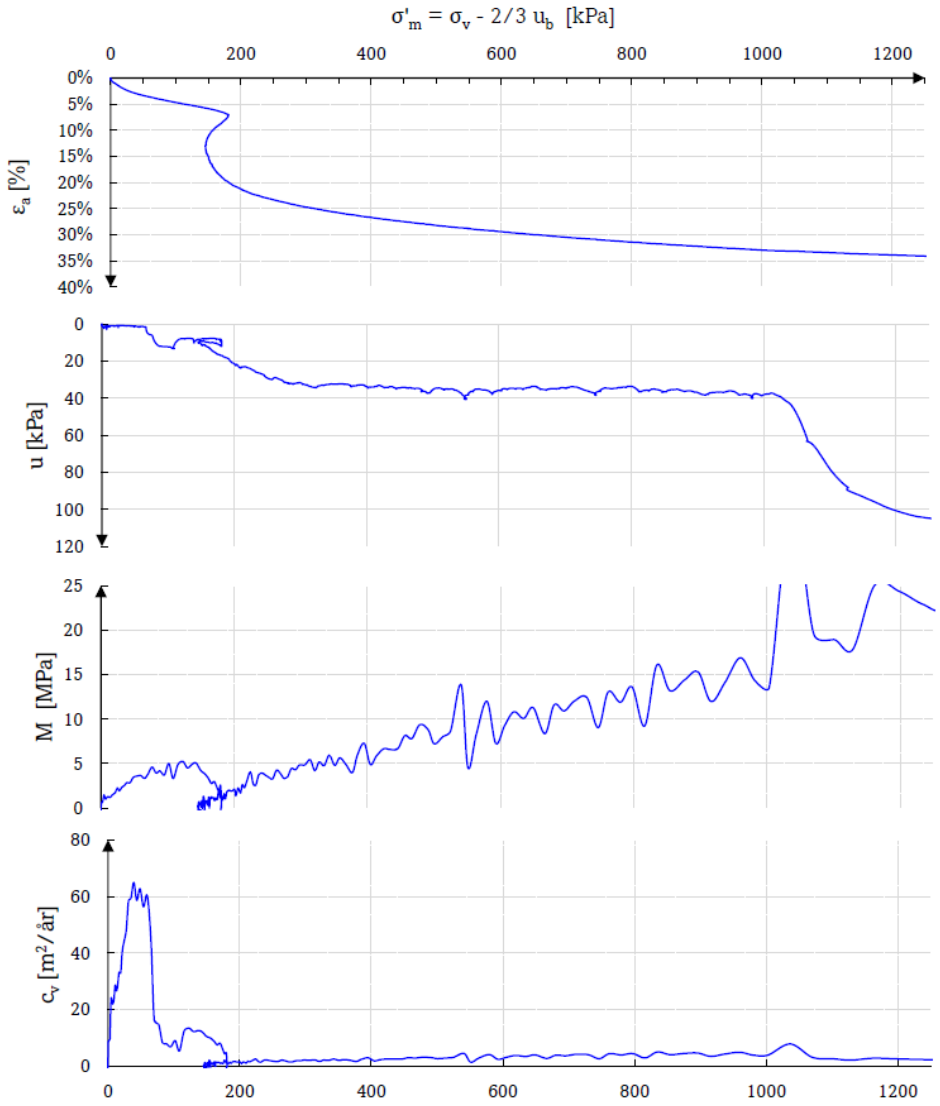

Figure 6.1: CRS results from sample MB-2. Every tested sample may correspondingly be found in Appendix C.

Figure 6.2a and 6.2b presents the oedometer curves obtained from the samples collected from 9 and 12 meters depth in a semilogarithmic scale. From figure 6.2a one may observe a tendency of a clearly larger preconsoliation stress from the mini block samples, with a peak around $\sigma'_{cv} = 315kPa$ for the mini block samples. The piston samples reveals a preconsolidation stress at approximately $185kPa$. The oedometer curves from the samples collected from 12 meters depth, seen in figure 6.2b, also give varying preconsolidation values. Every oedometer test is run with the same strain rate, $\dot{\varepsilon} = 1.5$ %/hour. The peak preconsolidation stress for the samples collected from 12 meters depth is around $\sigma'_{cv} = 325kPa$.

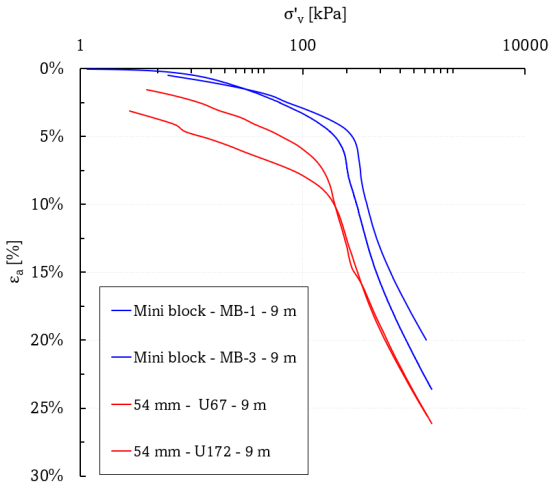

(a) Oedometer curves for all samples taken from 9 m depth. Semilogarithmic plot.

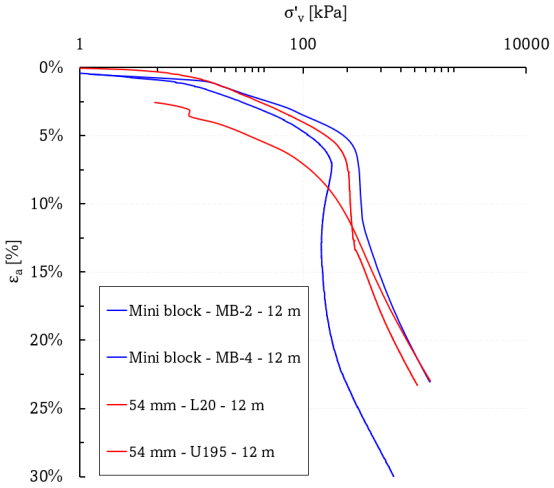

(b) Oedometer curves for all samples taken from 12 m depth. Semilogarithmic plot.

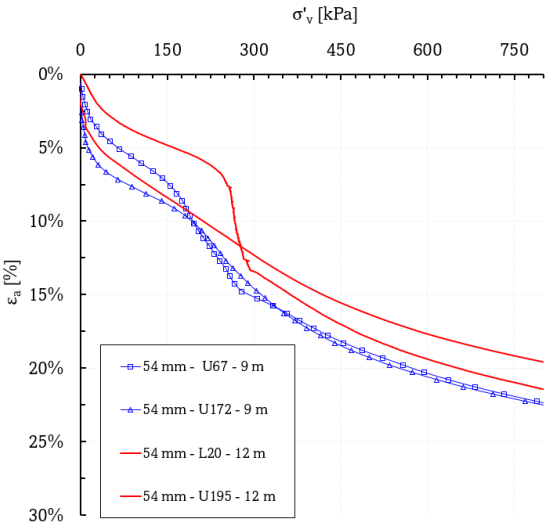

(c) Oedometer curves for every 54 mm piston samples. Linear plot.

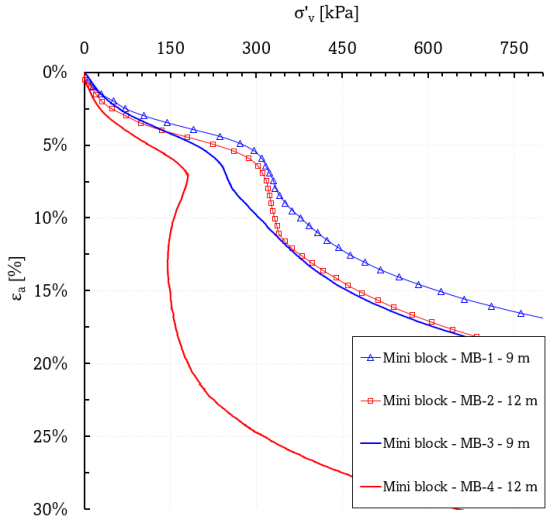

(d) Oedometer curves for every mini block sample. Linear plot.

Figure 6.2: Oedometer results for samples from 9 m and 12 m.

From Figure 6.2c, piston sample L20 reveals the peak preconsolidation stress around 260 kPa. A more apparent collapse plateau is as well identified for the L20 sample compared to the rest of the piston samples. As seen from the above semilogarithmic plots, Figure 6.2d supports the tendency of higher preconsolidation stress identified from the mini block samples. Variations in obtained preconsolidation plateau are as well observed between the respective mini block samples, as well as a significant snap-back at collapse for the stress-strain curve obtained from sample MB-4.

All oedometer curves from every oedometer test can further be seen, separated into 54 mm and mini block samples, in Figure 6.3. Compared to the piston samples, more significant collapse mechanisms as well as higher preconsolidation stresses are observed from the test series on the mini block samples. A smaller strain development is as well seen as a tendency from the mini block test series. This results in higher constrained modulus, visualized in Figure 6.4.

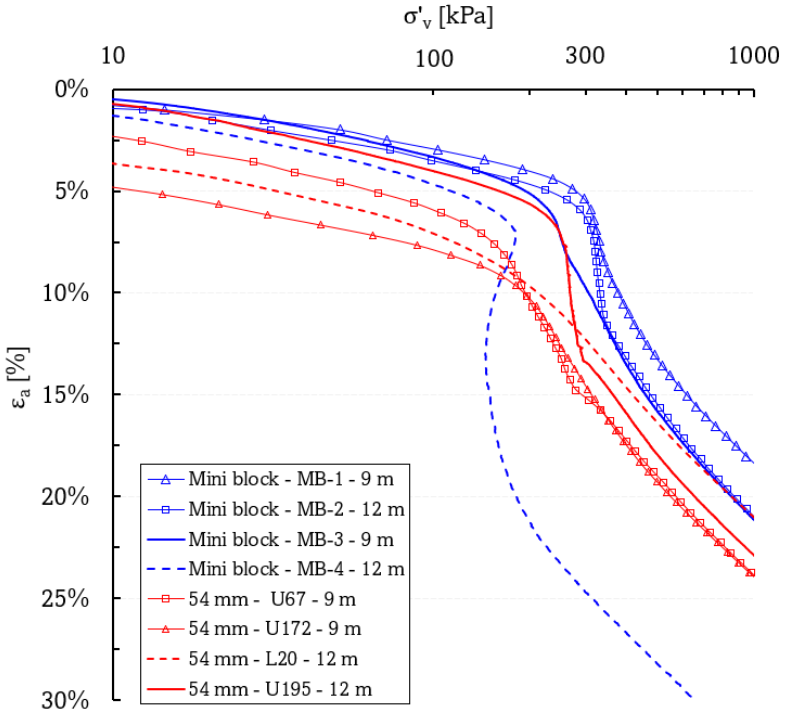

Figure 6.3: Oedometer results for all samples. Semilogarithmic plot.

The resulting sample qualities may be seen from Figure 6.5, both in terms of the modulus criteria, M_0/M_L, and void ratio criteria, e_0/e. The mini block samples tested immediately after sampling shows the best quality, both in terms of stiffness and void ratio. Around 1 month storage of the mini block samples reveals a decreasing quality in terms of e_0/e, but stays inside the ”really good to excellent” by the M_0/M_L - criteria. Storage effects aren't observed from the piston samples in this test series.

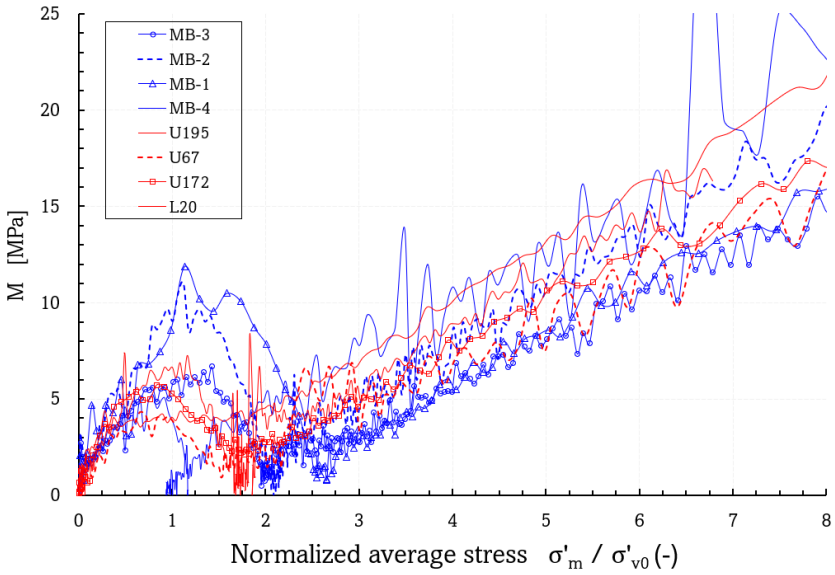

Figure 6.4: Modulus curves for every performed CRS oedometer test in a normalized stress space.

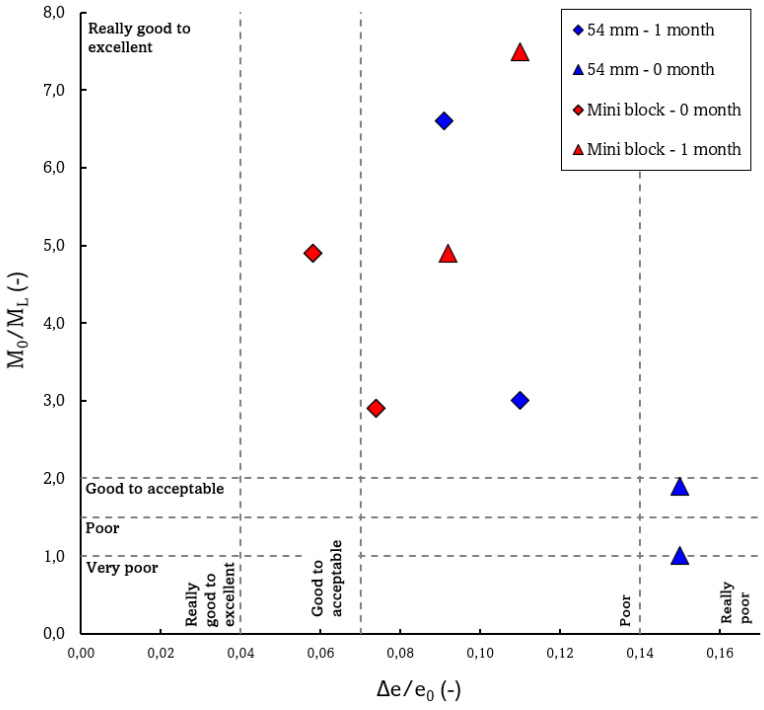

Figure 6.5: Resulting sample quality for every oedometer test, both in terms of change in oedometer module and change in void ratio.

Strain rate variation

In Figure 6.6 two different strain rates are presented by the stress-strain curves from the CRS tests. The stress-strain paths are obtained from the same mini block sample, which eliminates any variation in the soil and variations in sample disturbance, which by Länsivaara (1999), is stated of significant importance. From the beginning of the test, a stiffer response is observed from the test run with the highest strain rate, as well as a higher preconsolidation stress. The softening mechanism observed after passing the preconsolidation stress tends to be more extreme for the test performed with the highest rate, with the vertical effective stress decreasing while the axial strain drastically increases.

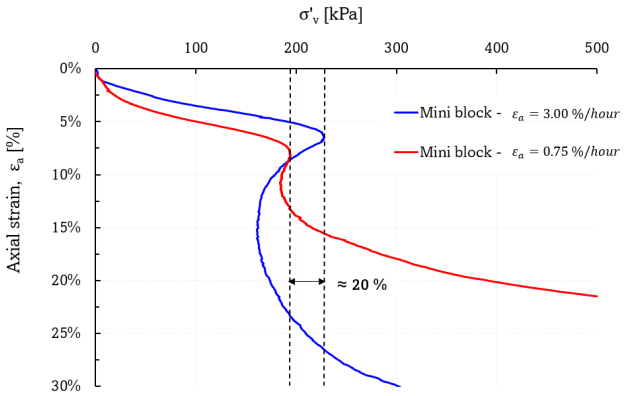

(a) Mini block samples subjected to both slower and faster strain rates than normally used in this thesis, respectively 0.75 and 3.00 % per hour.

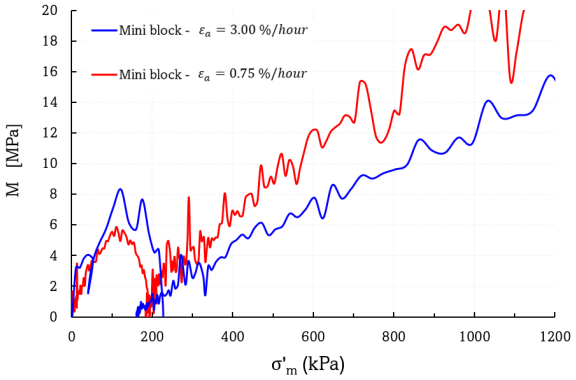

(b) Corresponding oedometer modulus for the two different strain rates. Note the difference in the initial and post preconsolidation stiffness.

Figure 6.6: Strain rate variation for the samples run with both lower and higher strain rates than recommended by SVV.

6.3 Triaxial tests

The triaxial test program consists of both isotropic and anisotropically consolidated undrained and drained shear tests, as well as triaxial consolidations with both constant K_0' and K_0'-consolidations with zero radial strains. A comprehensive collection of every single triaxial test may be found in Appendix B, just as Figure 6.7.

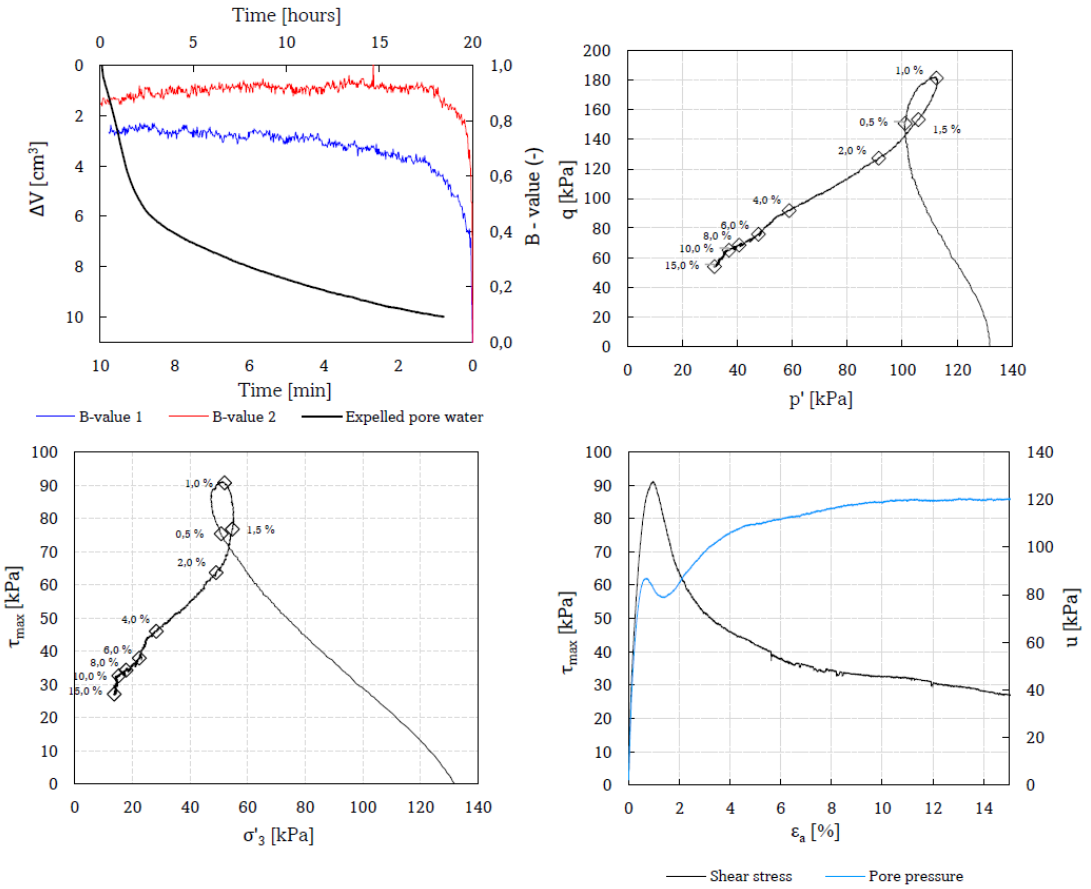

Figure 6.7: Comprehensive result from one undrained shear test. Every triaxial test result may correspondingly be found in Appendix B.

6.3.1 Isotropic versus anisotropic consolidation to p'

Figure 6.8a shows the resulting p':q - stress paths for the mini block samples tested during this reconsolidation study. The strain-softening behavior when reaching the maximum mobilized shear stress in the sample is evident, with a failure strain around 0.75−1.1%. The normalized shear strength observed for the block specimens unveils a normalized shear strength (s_u/σ_0') between 0.56 - 68. The stress paths from the mini block sample series unveil a tendency of a moderately constant undrained shear strength for the chosen effective average stress level for both consolidation procedures. The characteristic dilative loop close to failure stands out

when compared to the stress paths from the 54 mm piston samples, seen in Figure 6.8b. The contractive response when reaching the peak deviator is common for all piston samples. Failure strains around 1.4—2.0 % are observed from the 54 mm piston samples, as well as a normalized shear strength (s_u/σ'_0) between 0.33 - 0.49.

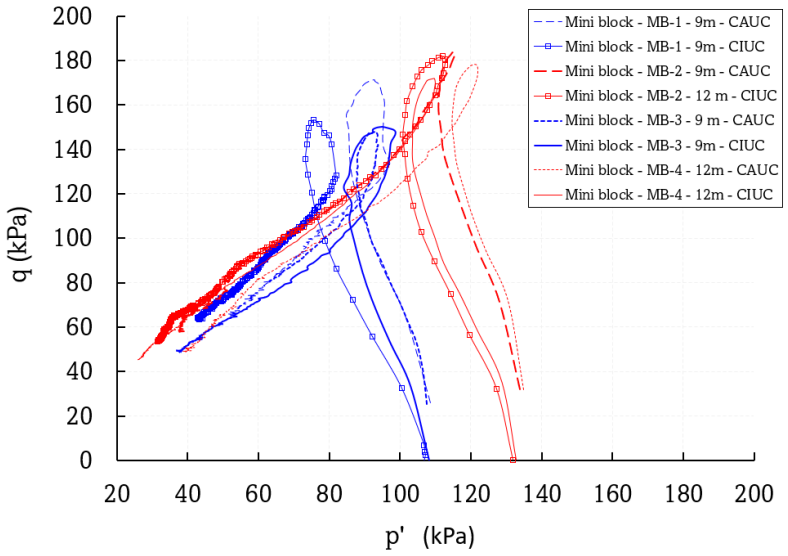

(a) Resulting stress paths from the undrained test series on mini block samples.

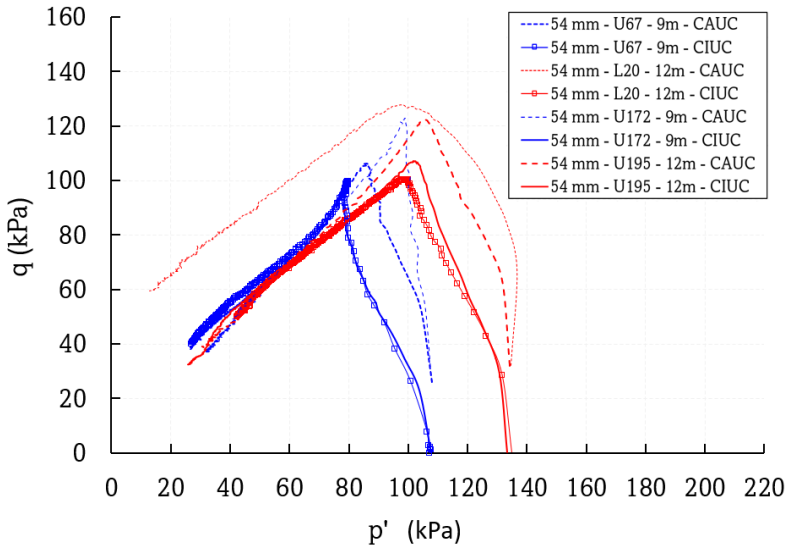

(b) Resulting stress paths from the undrained test series on mini block samples.

Figure 6.8: All CAUC/CIUC stress paths from this laboratory study presented in a p':q stress space. Blue paths present the samples from 9 m depth. Red paths present the samples from 12 m depth.

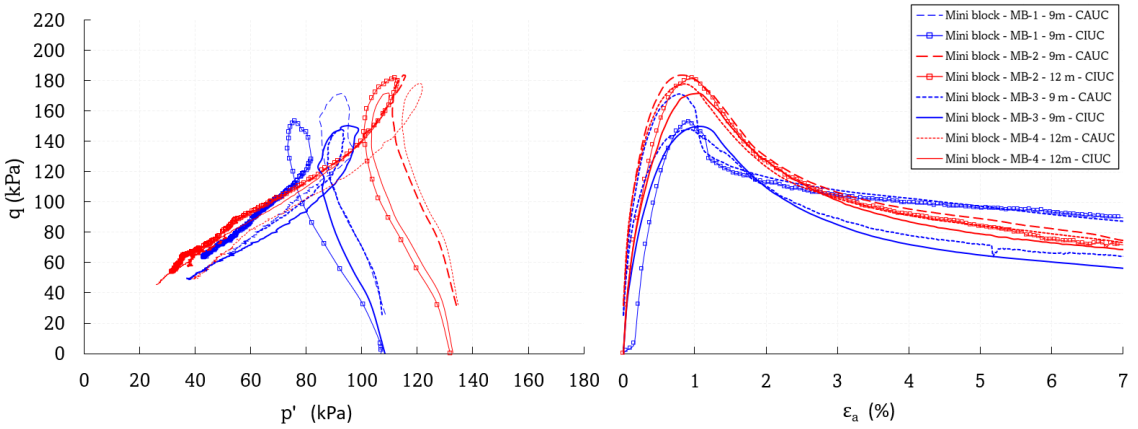

Figure 6.9: Stress- and strain paths every mini block samples tested during this laboratory study. Blue paths present the samples from 9 m depth. Red paths present the samples from 12 m depth.

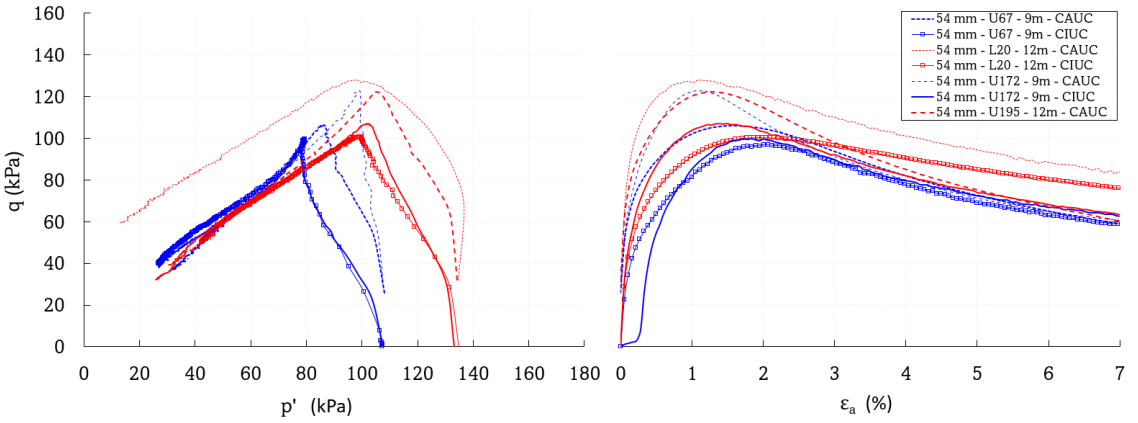

Figure 6.10: Stress- and strain paths every 54 mm piston samples tested during this laboratory study. Blue paths present the samples from 9 m depth. Red paths present the samples from 12 m depth.

Figure 6.9 and 6.10 presents both the resulting stress paths in addition to the corresponding strain development during shear. The piston samples' loss of the dilative loop prior to failure comes quite clear when comparing the two sampling methods. An average of 40 % lower undrained shear strength are observed for the piston samples, compared to the mini block samples.

In terms of the consolidation procedures, the isotropically consolidated mini block samples appear to obtain approximately the same undrained shear strength as the anisotropically consolidated samples. From the test series performed on the piston samples, the anisotropically consolidated samples give around 20 % higher undrained shear strength. However, the similarity between both sampling methods during the reconsolidation study is lower failure strains for the anisotropically consolidated samples for every sample. Table 6.3a and 6.3b summarize

the obtained undrained shear strengths and failure strains from the isotropic versus anisotropic consolidation study.

Type *(-)*	**Depth** *m*	**Test** *(-)*	c_u *(kPa)*	ε_f *(%)*
MB-1	9 m	CIUC	76	0.90
MB-1	9 m	CAUC	85	0.75
MB-2	12 m	CIUC	90	0.96
MB-2	12 m	CAUC	91	0.90
MB-3	9 m	CIUC	75	1.10
MB-3	9 m	CAUC	74	0.91
MB-4	12 m	CIUC	87	1.00
MB-4	12 m	CAUC	89	0.90

(a) CIUC/CAUC results for mini block samples.

Type *(-)*	**Depth** *m*	**Test** *(-)*	c_u *(kPa)*	ε_f *(%)*
U67	9 m	CIUC	48	2.00
U67	9 m	CAUC	53	1.61
L-20	12 m	CIUC	50	2.00
L-20	12 m	CAUC	63	1.40
U172	9 m	CIUC	49	1.76
U172	9 m	CAUC	61	1.55
U195	12 m	CIUC	53	1.50
U195	12 m	CAUC	61	1.48

(b) CIUC/CAUC results for 54 mm piston samples.

Table 6.3: Undrained shear strength and failure strains from the CAUC/CIUC reconsolidation study.

Figure 6.11 shows the development of pore water expulsion during the isotropic- and anisotropic reconsolidations for every mini block sample. The plot doesn't show any characteristic dissimilarities or similarities to further separate the two consolidation procedures by means of gentle stress application and sample response during the reconsolidation stage. The amount of expelled pore water at the end of both isotropic- and anisotropic consolidation seems to be varied for the procedures applied during this laboratory study.

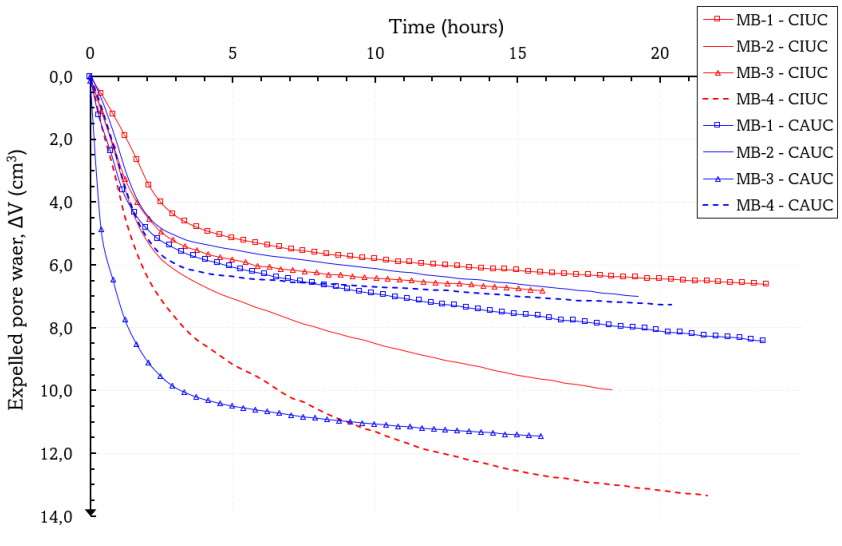

Figure 6.11: Expelled pore water during reconsolidation to p' for every mini block specimens. Red curves present the isotropically consolidated samples. Blue curves present the anisotropically consolidated samples.

The effect of the expelled pore water from the consolidation procedures is also shown in Figure 6.12, both in terms of the $\Delta V/V_0$ and $\Delta e/e_0$. One could notice the slight variation in sample disturbance, both for 54 mm piston samples and the mini block samples. The variation in the sample disturbance plots does rather not appear to coincide with any further relation between anisotropically and isotropically consolidation, which are a result of the varied amount of expelled pore water seen in Figure 6.11.

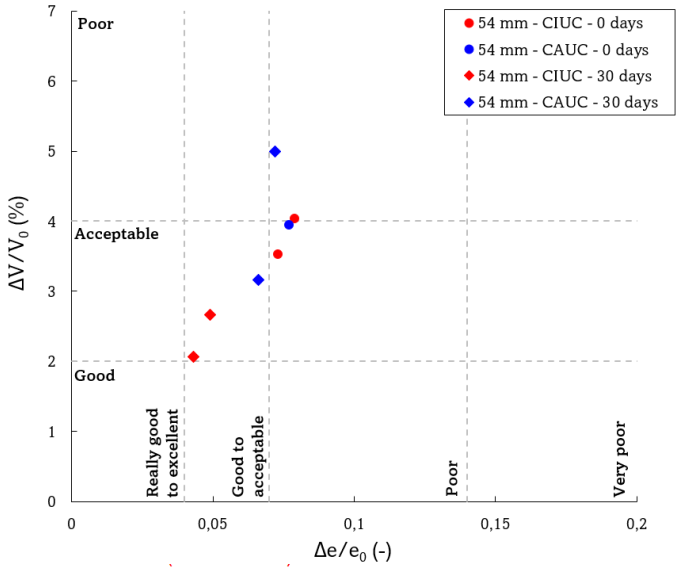

(a) Sample quality for every 54 mm undrained tests.

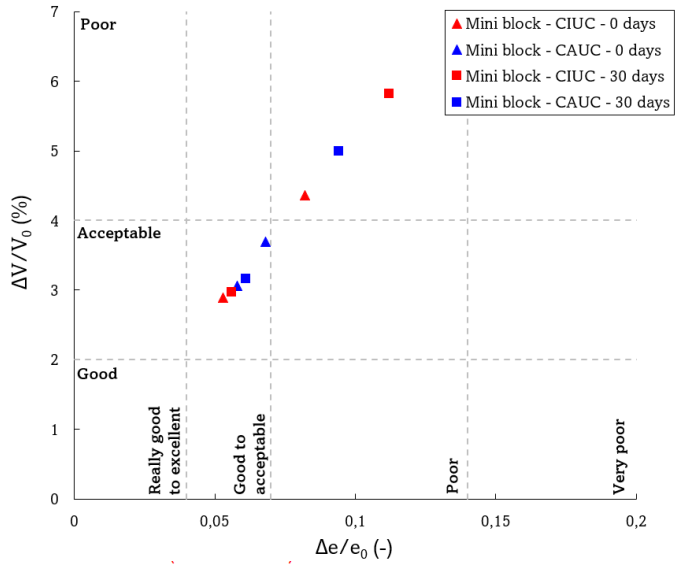

(b) Sample quality for every undrained mini block tests.

Figure 6.12: Sample quality for every undrained triaxial tests. Several tests are defined as poor in terms of both the amount of expelled pore water and the void ratio.

6.3.2 Pore pressure response in undrained conditions

For the undrained shear tests, the procedure described in Section 5.3 was performed for the samples that did not obtain a sufficient B-value for the first B-test. Figure 6.13 shows a plot of the obtained B-values from the two undrained tests for sample MB-4. The overall tendency from the test series reveals an appriximate 20% increase of the pore pressure response to the initial, after increasing the back pressure from 700 to 1000 kPa and letting the specimen stabilize and rest for 3 hours.

Test	1st back pressure (kPa)	1st B-value (-)	2nd back pressure (kPa)	2nd B-value (-)	Increase (%)
MB-1: CIUC	700	0.75	1000	0.88	17
L20: CIUC	700	0.62	1000	0.91	51
MB2: CIUC	700	0.70	1000	0.92	31
MB2: CAUC	700	0.71	1000	0.91	28
MB4: CIUC	700	0.74	1000	0.89	20
MB4: CAUC	700	0.86	1000	0.89	3

Table 6.4: Reported B-values for the tests run with an additional saturation stage.

Table 6.4 shows the increase in the pore pressure response for each sample when increasing the back- and cell pressure in the saturation stage after the first performed B-test. Every sample that was subjected to this approach shows an improved pore pressure response, even though the total increase in undrained pore pressure response for each sample seems fairly random and does not present any homogeneous growth.

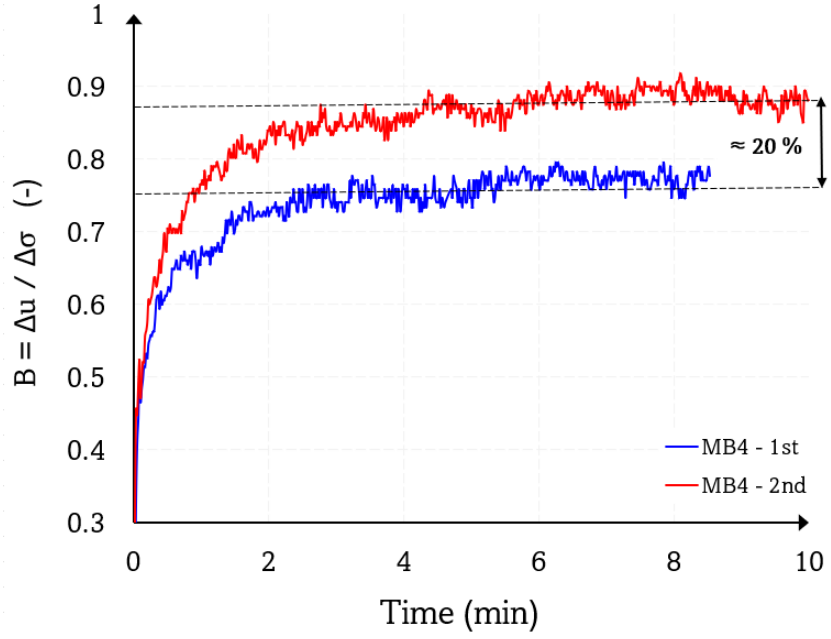

Figure 6.13: Increased B-value from the undrained triaxial test on sample MB-4.

6.4 Yield identification

Identification of yield mechanisms

Figure 6.14 presents the utilized methodology for interpretation of the yield mechanism observed from consolidated undrained shear tests. The distinctive and contractive yield mechanism observed for the Tiller-Flotten quick clay is consistent throughout every compression test performed, further seen in Appendix B. The yield interpretation from the undrained compression test series is emphasized on the basis of the structural yield, observed near the peak deviator stress in the dilative loop. The progressive shear failure development occurring after passing the peak deviator rapidly accumulates strains in the shear plane, which makes the interpretation of any plastic strain increments sensitive.

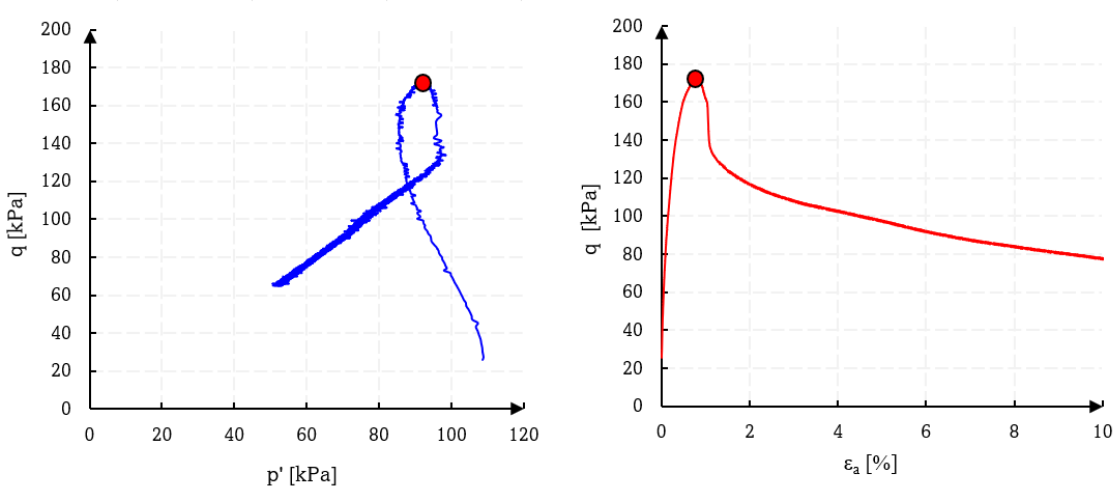

Figure 6.14: Method for yield point identification from the undrained triaxial tests. Red dots marks the interpreted yield mechanism.

Three different undrained effective stress paths are shown in Figure 6.15a, where the correlated volume change by means of the expelled water during the isotropic consolidation is presented in 6.15b. The samples shown are from the same depths, but isotropically unloaded to a lower confining stress prior to the undrained shearing. Every sample was initially isotropically consolidated to the same in situ average stress level prior to the two shown isotropic unloadings to the lower stress levels. One may notice the dropping peak deviator stress values for the correlated decreasing confining stress values, whereas the inclination of the failure lines coincides. The rise of the failure line from the sample consolidated to the highest stress, shown in 6.15a, is due to the extreme development of the shear fraction across the sample. This makes the sample not deform uniformly after reaching failure.

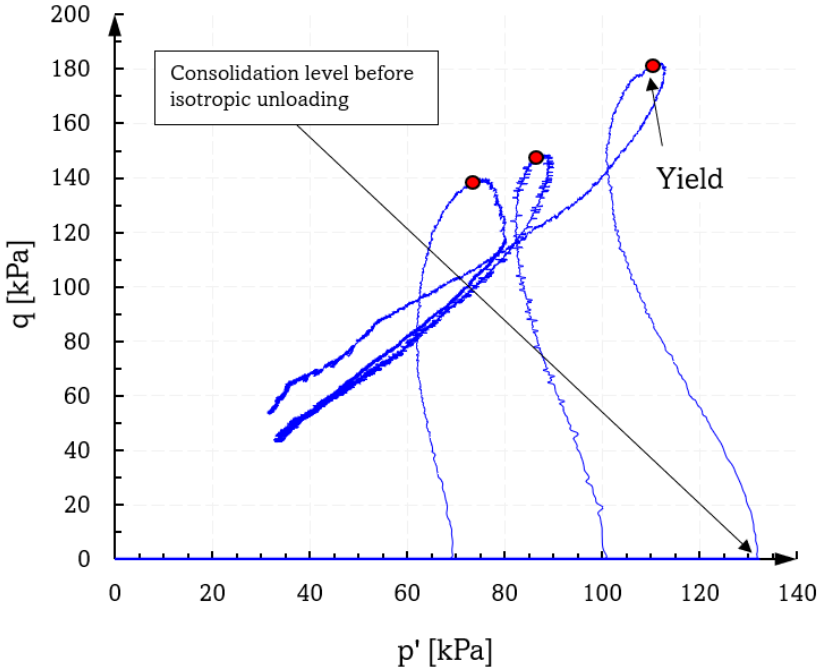

(a) Stress paths from undrained compression tests consolidated to the same average effective stress level before isotropic unloading.

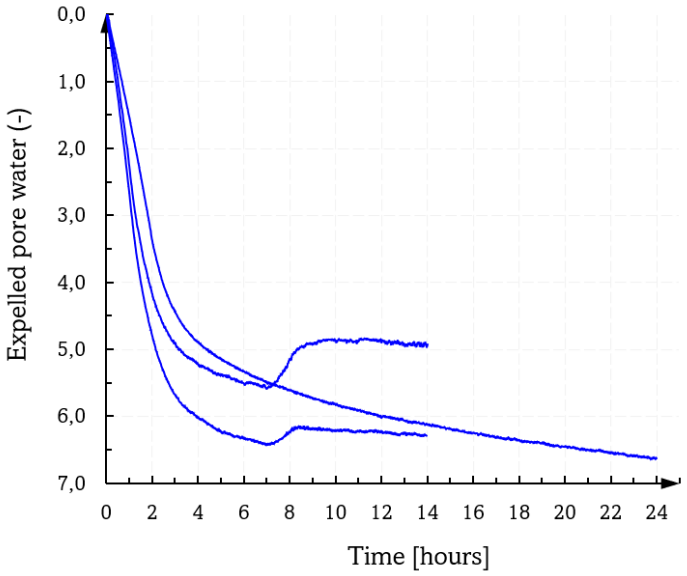

(b) Expelled pore water during the consolidation of the isotropic loading and the further isotropic unloading.

Figure 6.15: Yield identification and correlated volume change for undrained compression tests during isotropic consolidation.

The principle behind the identification of the yielding mechanism for the drained shearing can be seen in figure 6.16. A stiff response, both in p and q are observed before approaching a significant development of plastic strains, and a clear yielding mechanism is observed prior to the progressive failure for the quick clay. The typical strain-softening behavior for highly sensitive clays is in addition to the undrained shear tests also observed from the CIDC triaxial test.

Even though the yielding mechanism from the drained triaxial tests comes quite clear from the presented stress-strain relations, one could as well identify the plastic mechanism developing for the sample by utilization of the concept of external work. Figure 6.17 visualizes how the external energy required to reach a yield mechanism is developed for the drained shearing. Notice how the curves from both the energy required to reach and the stress-strain paths coincide in the terms of both the average stress,p, and the deviatoric stress, q.

From figure 6.16 and 6.17 one may notice the coinciding yield identification at $p \approx 200kPa$ for both a comparison of the required energy and the development of deviatoric and volumetric strains. As one may see from the external work required to develop stresses during shearing, a more significant drop is identified after failure for the deviatoric stress component. This corresponds with a smaller axial stress for the further development and accumulation of strains after reaching yielding and later failure.

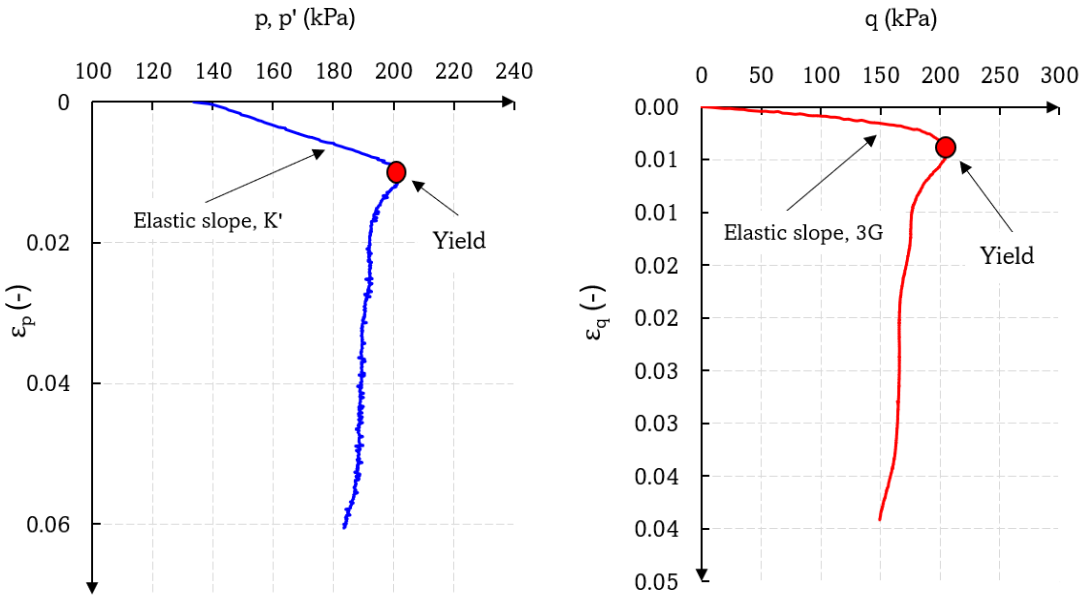

(a) Yield mechanism interpreted by use of the volumetric strain-stress path from the drained triaxial test.

(b) Yield mechanism interpreted by use of the deviatoric strain-stress path from the drained triaxial test.

Figure 6.16: Yield identification by use of the stress-strain paths from the drained triaxial test.

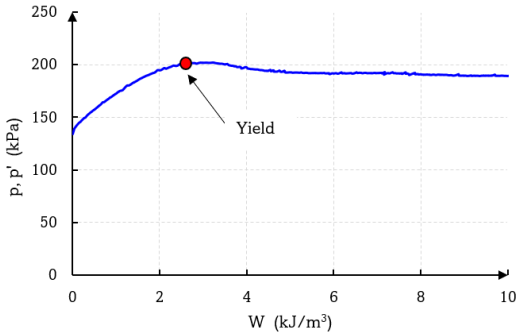

(a) Yield mechanism interpreted by use of the principle of external work and volumetric stress path.

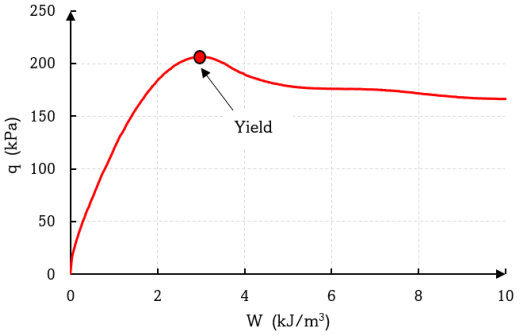

(b) Yield mechanism interpreted by use of the principle of external work and deviatoric stress path.

Figure 6.17: Yield identification by use of the principle of external work from the drained triaxial test.

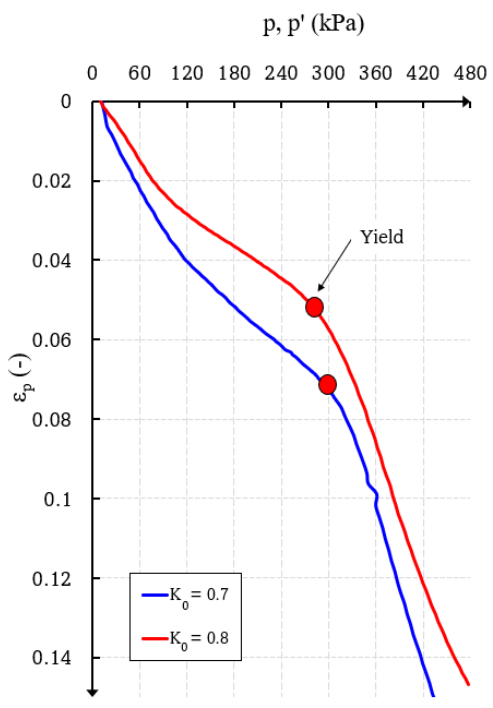

(a) Yield mechanism interpreted by the volumetric stress-strain - path from the constant K_0'-triaxial tests.

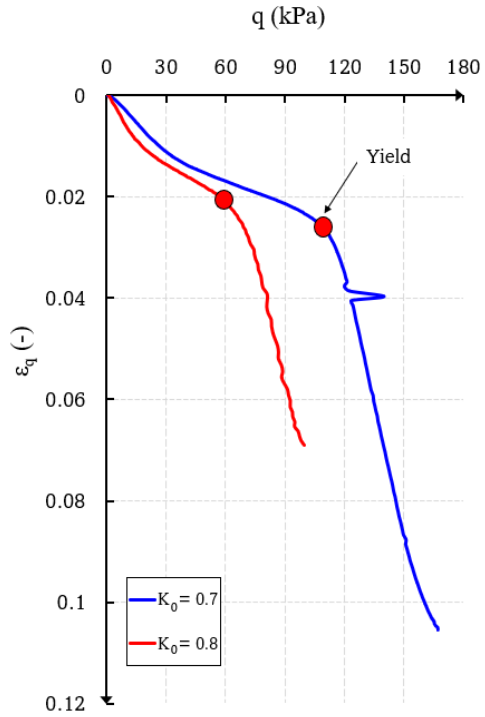

(b) Yield mechanism interpreted by the deviatoric stress-strain - path from the constant K_0'-triaxial tests.

Figure 6.18: Interpreted yield mechanism from both triaxial tests carried out with constant K_0.

From the test series performed with constant K_0', the accumulation of volumetric and deviatoric strains are shown in Figure 6.18a and 6.18b. Clear indications of the plastic mechanism developed for both tests may be interpreted from the accumulated strains, where the different levels of yield in p' and q comes from the fact that the samples are from different depths and loaded with different values of K_0'.

The K_0'-consolidation stress paths can be seen in figure 6.19, and the corresponding axial strain development in figure 6.20. The stress paths are here normalized and presented regarding the reference preconsolidation pressure found from the oedometer tests for the respective mini block samples. These experiments were carried out under the condition that the amount of expelled pore water ensures that no radial strains are developed. Both experiments are characterized by an initial stiff response, followed by subsequent slowly increasing deviator stress which identifies a structural yielding behavior for the quick clay samples. The stress paths eventually follow the NC K_0'-line after an approximately constant deviatoric plateau when reaching the yield mechanism.

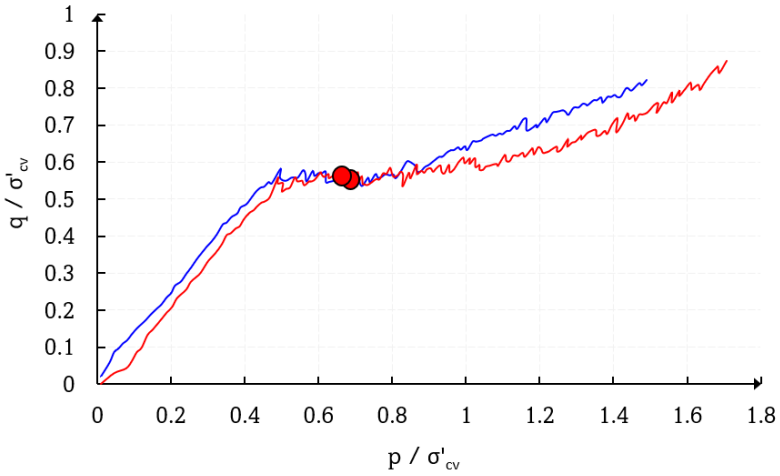

Figure 6.19: Yield mechanism interpreted from the normalized stress path from the K_0'-consolidation tests.

The structured yielding observed from both the K_0'-consolidations as well as the constant K_0' tests appears different than the yielding prior to failure for the shear tests. Progressive failures observed from all triaxial shear tests, both undrained and drained, reveal some yielding differentials when compared to the drained loadings. The significant strain-softening behavior as identified from the triaxial shear tests is not that present after yielding in drained K_0' compression tests. The slow pore water drainage during the drained K_0' compressions is one effect causing this difference in yield behavior between the different triaxial procedures.

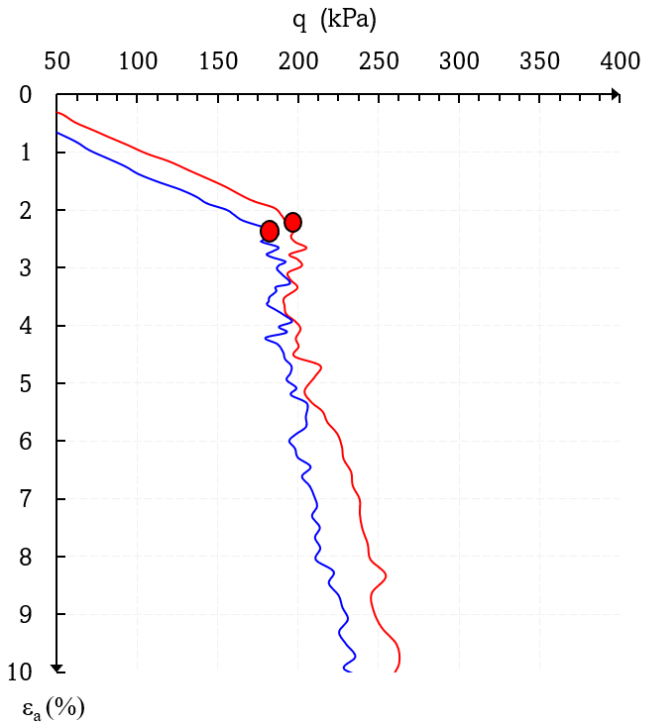

Figure 6.20: Yield mechanism from the K_0'-consolidation tests interpreted from deviatoric stress and axial strain development.

Identification of an incipient yield mechanism for the K_0'-consolidation tests is also supported by the development of axial strains. Figure 6.20 shows that for both experiments, a yield mechanism is interpreted as the deviatoric stress approaches 200 kPa.

Table 6.5 shows the decrease in the sample sensitivity immediately after performing the two K_0'-consolidations for this laboratory study. It must be mentioned that the sensitivity presented in the table was obtained after the sample had reached 10% axial strain and experienced around $30cm^3$ volume change due to the expelled pore water.

Sample	Initial S_t	S_t after test
MB-3	210	35
MB-4	165	30

Table 6.5: Sample sensitivity immediately after execution of the triaxial K_0'-consolidations.

Resulting yield surface

Figure 6.21 shows the distribution of every identified yield point from the triaxial test series, normalized by the chosen reference preconsolidation stress for the mini block samples. The total strain increments at yielding are also presented, where one may notice the ratio

$d\varepsilon_q/d\varepsilon_p = 2/3$ from the K_0'-consolidations as a consequence of the test setup which does not allow any radial strain development during compression. All undrained yield points localize conveniently at the dry side of the p':q stress space, and indicate the corresponding direction for the total strain increments. The drained triaxial tests reveal yield points at the wet side of the stress space. The placements of the yield points obtained from the constant K_0'-tests refer to the chosen loading paths, by means of the chosen values for K_0'. The drained shear tests, reconsolidated to in situ condition, reveals the peak yield point.

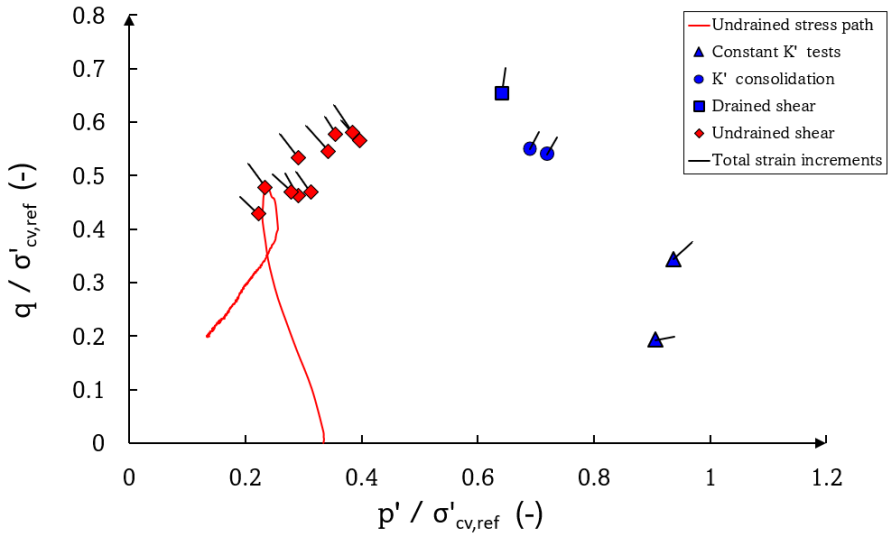

Figure 6.21: Plot of every yield point deducted from every triaxial test performed, normalized by the reference preconsolidation stress. In addition, one undrained stress path is presented.

Correlation to proposed material models

The observed plastic strain increments upon crossing the yield state indicates for every correlated yield surface, presented in Figure 6.22, that the assumption of associated flow is a reasonable assumption in the proposed material models, also for the highly sensitive quick clay from Tiller-Flotten. The conclusion on whether the yield surface for the quick clay from Tiller-Flotten may be described as symmetrical around the p'-axis can not be made, because of missing yield points at the tension side of the p':q-diagram, as well as missing yield identification along the isotropic p'-axis. The total strain increments upon crossing the yield surface do, however, indicate a clear relation from the observed material behavior to the material models used today.

One could notice the coinciding placement of the MCCM-surface against the plotted yield points, presented in 6.22a. Yield points deducted from the undrained and drained triaxial tests are fairly spaced around the defined yield surface, plotted for a friction angle of $\rho = 30^o$, giving the critical state line inclination $M = 1.2$. The proposed yield surface for soft clays by Länsivaara, shown in 6.22b, does coincide well with the yield points interpreted from the undrained

shear test series. However, the yield points interpreted from the drained tests show a clear deviation from the model. The two hyper-viscoplastic material surfaces proposed by Dadras-Ajirloo, plotted with two different values of R, may be seen in 6.22c. The hyper-viscoplastic surfaces shown in the figure are plotted with $\gamma = 1$, which gives the convex form and indicates strain-softening behavior. One could as well as for the MCCM surface observe a somehow good correlation for the proposed yield surface, besides leaving some of the undrained yield points at the dry side outside the surface.

The yield surfaces from the models presented in this master's thesis are shown together with the interpreted yield points from the Tiller-Flotten quick clay in Figure 6.23. Both the MCCM and the hyper-viscoplastic material model seem to correlate well to the obtained surface of the Tiller-Flotten quick clay. The yield points determined from the drained triaxial tests, both the shear test and the consolidations, are placed outside the normalized rotated elliptic surface, and do not seem to correlate with the model proposed by Länsivaara.

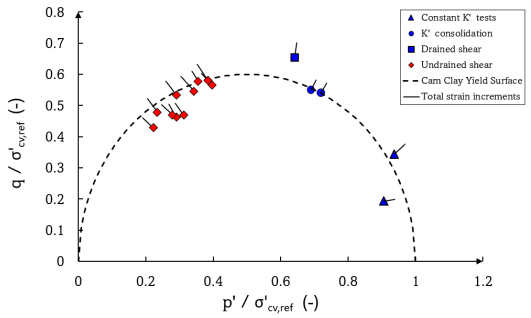

(a) Obtained yield points and the MCCM yield surface.

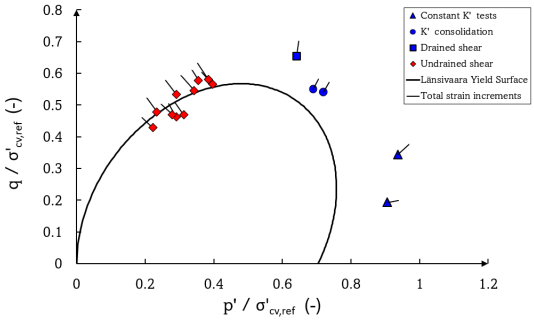

(b) Obtained yield points and the adjusted Länsivaara yield surface.

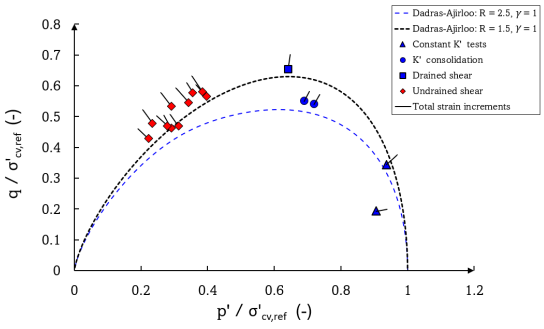

(c) Obtained yield points and two hyper-viscoplastic yield surfaces.

Figure 6.22: Obtained yield points and different correlated yield surfaces.

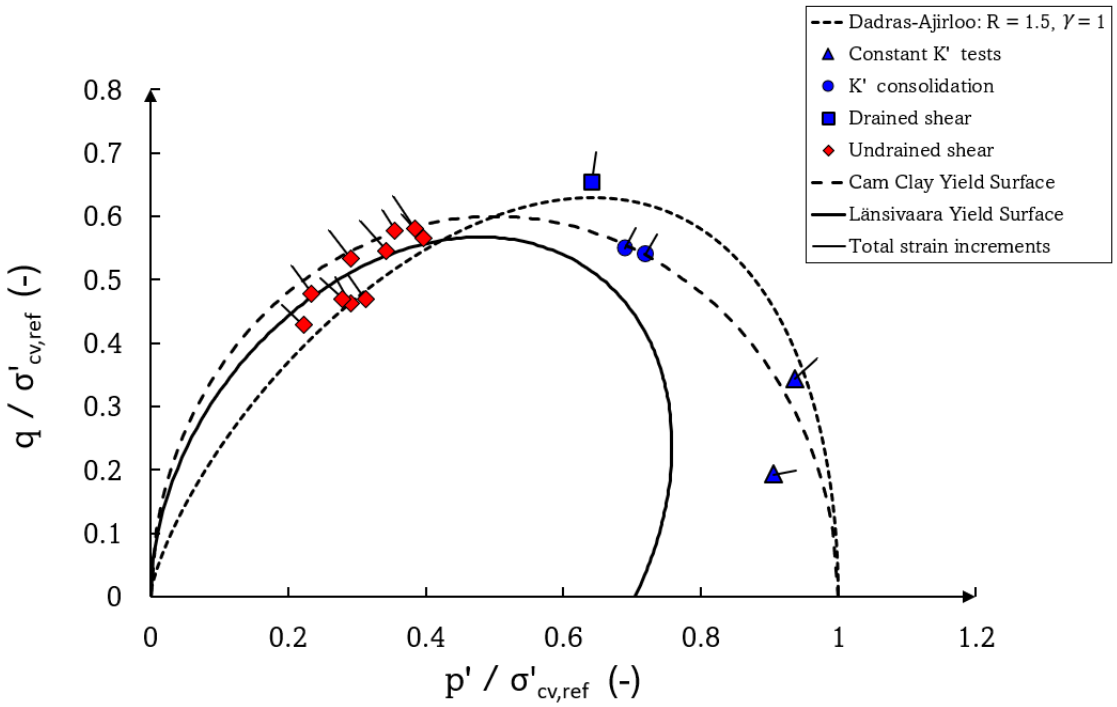

Figure 6.23: Every yield surface and the obtained yield points.

Chapter 7

Discussion

The observed material behavior for the Tiller-Flotten quick clay during oedometer and triaxial compressions are examined in further sections. Distinctive collapse and yield mechanisms observed from the various laboratory tests are compared, both for undrained and drained conditions. The interpretation of yielding and the complementary yield points from the various tests and their localization correlated to each other in the normalized stress space are also debated in terms of the observed material behavior and the different test procedures. In addition, sample quality and strength parameters obtained from the isotropic versus anisotropic reconsolidation procedures are debated, as well as the obtained pore pressure response in undrained conditions.

7.1 Compression and collapse characteristics

During this laboratory test series, several oedometer tests reveal a significant material behavior at collapse for the Tiller-Flotten quick clay. The highly sensitive quick clay indicates a distinctive collapse when reaching the preconsolidation plateau, characterized by a decreasing effective stress path. This effect is from here noted ”snap-back”, and seen in Figure 7.1. The pore over-pressure at failure points to a structural collapse of the soil skeleton which leads to the rapid accumulation of axial strains in the test specimen. These results correspond well with the strain-softening material behavior also seen from triaxial shearing. The snap-back effect clearly states that the clay particles are floating in their own pore water after reaching the collapse mechanism. Despite that it’s not a liquefaction that is occurring, as seen for silts and sands, parallels may be drawn because of the build-up pore pressure. Since the oedometer setup allows one-way drainage, the effective stress path eventually increases during the further loading of the specimen, and the non-linear normal consolidated path is exposed.

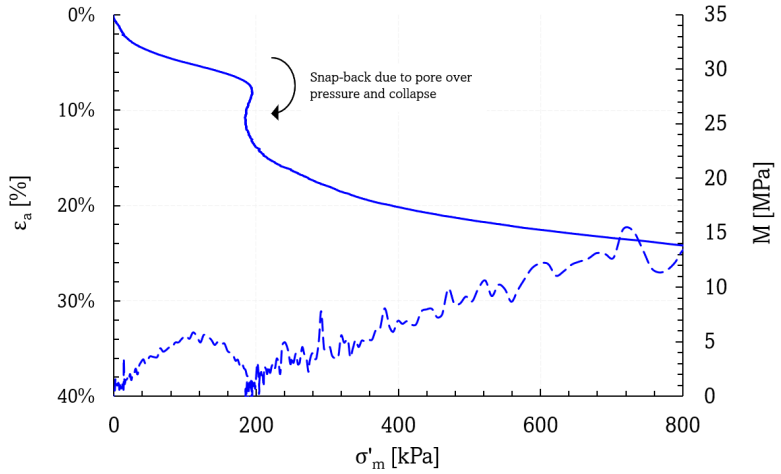

Figure 7.1: Oedometer and modulus curve from one CRS oedometer test performed on mini block sample.

As expected due to lower sample quality, the 54 mm piston samples reveal both lower stiffness in the OC area, as well as lower preconsolidation values. The oedometer and modulus paths obtained from two mini block and two piston samples are seen in Figure 7.2. The inclination of the stiffness path in the normal consolidated area, m, seems to coincide for the two sampling methods and remain fairly steady. Significant deformations at the start of the test for the piston samples may additionally confirm the lower quality results from the disturbed piston samples. Thus, a more distinct collapse mechanism are observed from the mini block samples at failure. Despite the fact that these effects are previously studied by several authors, the Tiller-Flotten quick clay also reveal the same tendency.

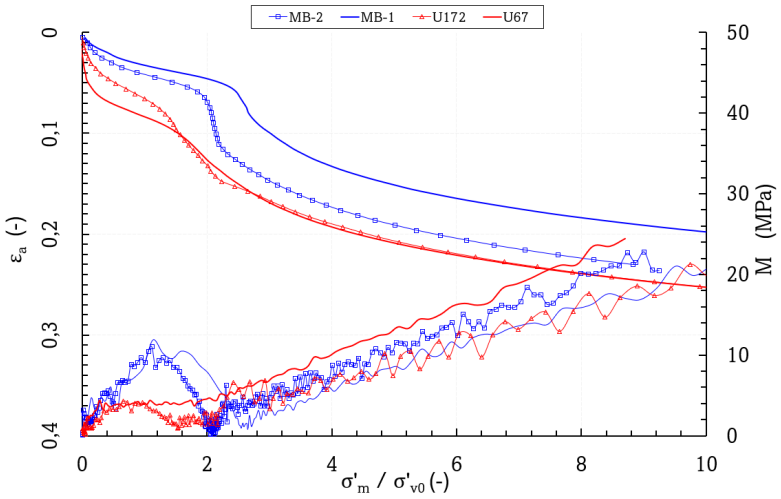

Figure 7.2: Observed differences between 54 mm and mini block samples during CRS oedometer tests.

The behavior seen from the 54 mm piston samples, by means of loss of the dilative peak strength, are visualized in Figure 7.3. Regardless, the piston samples reveal the contractive and strain-softening response, typical for quick clay and sensitive clays. Thus, the curves obtained from mini block samples more sufficiently confirm that the Tiller-Flotten quick clay behaves in an undisturbed and structured way by the highly brittle and progressive failures. Overconsolidated clays are expected to inherit a dilative behavior prior to failure in shear, which is confirmed by the high-quality mini block samples. Undrained strength values and the correlated difference between the sampling methods are due to interpretation. Thus, the effective stress paths from undrained triaxial shear tests confirm the superior quality of the mini block samples. The lower failure strains obtained from mini block samples also support this. The figure also shows the effect of isotropic versus anisotropic consolidation to best guess in situ stresses.

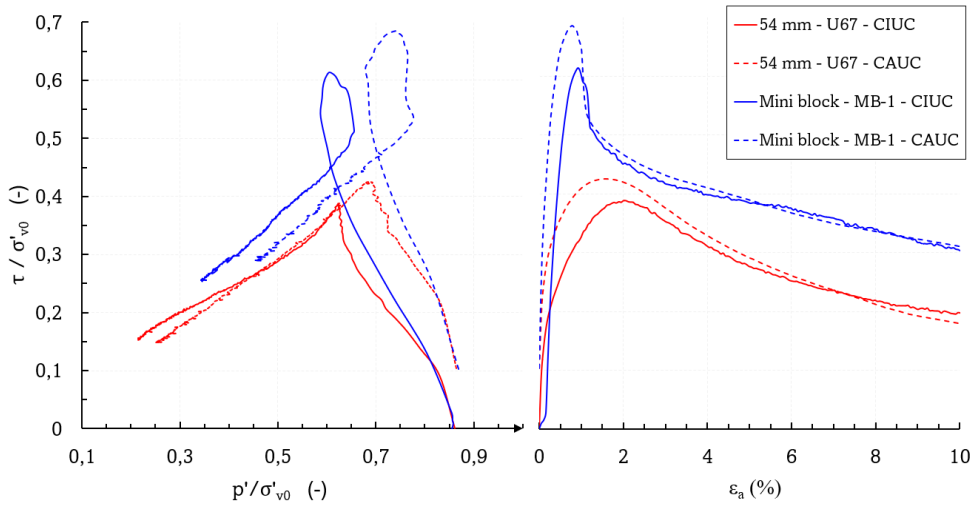

Figure 7.3: Stress paths from CIUC and CAUC triaxial tests on mini block sample MB-1 and 54 mm piston sample U67.

In Appendix B, pictures of the sheared quick clay samples and the developed shear bands are attached to each test report. Each specimen throughout the laboratory study developed significant shear planes at failure. Some of the specimens showed the characteristic $\approx 45^o$ failure plane, despite some abnormalities of barrel-shaped specimens. Figure 7.4 shows the development of the deviator stress component and the axial strain close to failure during undrained shearing for the isotropic and anisotropic consolidated mini block sample MB-1. Following the brittle failure at peak deviator, one could notice the '"sudden" drop in the deviator stress. Figure B.6 and B.7 show how the specimen has developed shear strains during the test. The specimen and its' progressive failure are thus characterized by a sudden development of a failure plane. This characteristic quick clay behavior is typical for the Tiller-Flotten clay tested during this laboratory study when subjected to triaxial shear.

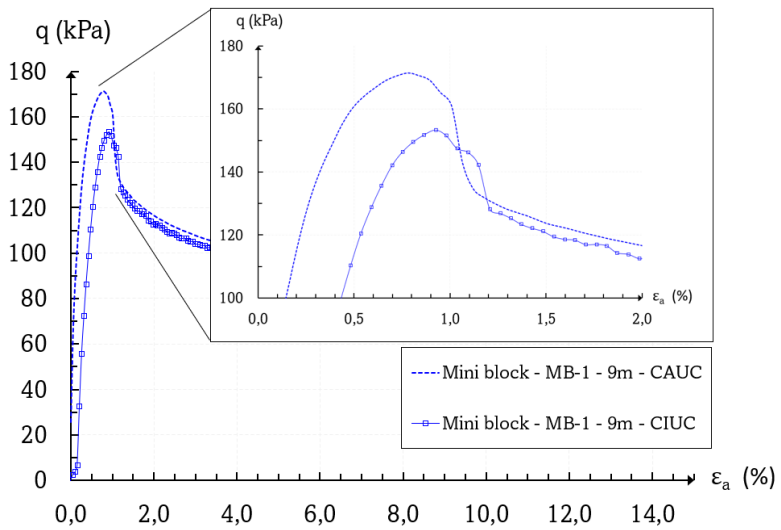

Figure 7.4: Collapse during undrained shear after passing maximum deviator in terms of strain development for mini block sample MB-1.

7.2 Isotropic versus anisotropic consolidation to p'

Based on the problem of determining the most suitable consolidation procedure, in this thesis especially for highly sensitive quick clay from Tiller-Flotten, there are several approaches for consideration. Both sample quality, mechanical behavior, and resulting strength parameters may reveal the difference between the two procedures. The traditional procedures for performing consolidated, triaxial compression tests are to apply an anisotropic stress state which is relevant to the samples' in-situ state or representative of the design problem. Isotropic consolidation stresses are normally only applied to samples extracted from shallow depths to prevent surpassing the shear strength prior to the shear phase. The two different procedures do result in different loading scenarios, leaving the anisotropically consolidated samples at higher axial compression.

The clay samples are all reconsolidated back to their best interpreted in-situ effective stress state. However, both for the isotropic and anisotropic consolidations, one could notice the coinciding amount of expelled pore water during the consolidation phases. Because of the difference in the applied deviator stress for the two consolidation procedures, the initial thought was that the anisotropically consolidated samples would release more pore water during the consolidation. In the overview of the amount of expelled pore water, seen in Figure 6.11, there is no clear tendency that may reflect which consolidation procedure that is most gentle to the soil specimen. This does also reflect the results of the sample disturbances, which in this thesis are found on the basis of the expelled pore water and the change in the void ratio.

The amount of expelled pore water during the two consolidation procedures seems to be fairly arbitrary in this study. The different specimens are due to different amounts of expelled pore water regardless of the same consolidation stresses. Thus, it seems like the deviation in volume

change does not have a significant impact on the interpreted strength parameters when examining the different stress paths and peak values. The isotropically consolidated samples, which introduce less axial stresses than the anisotropically consolidated samples, seem not quite to reach the peak stress values compared to the anisotropically consolidated samples. This comparison is somewhat more apparent for the 54 mm piston samples, leaving the isotropically consolidated samples at a lower peak undrained shear strength before a significant contractive, strain softening behavior appears. This tendency does also occur for the mini block samples, but at a lower level. The structured, dilative loop past the critical line for the mini block samples reveals some small deviations in the observed peak strength, but the coinciding intersection with the failure line seems to be more or less at the same level for the two consolidation procedures.

The tendency for every test performed in the consolidation study, both for the 54 mm piston samples and the mini block samples, reveals that the isotropically consolidated samples do have a higher failure strain when reaching the peak deviator stress. One could imagine that this behavior may coincide with the fact that the isotropically consolidated samples do not have any shear stresses introduced prior to the shear phase. When the shear phase starts, the strain rate, which is higher than the stress rate in the consolidation phase, introduces shear strains to the sample at a higher rate than for the anisotropically consolidated samples. The yielding and failure behavior that further occurs does then happen at slightly different time intervals for the two different procedures, leaving the discussion of rate dependencies open for interpretation.

However, the interpreted effective strength parameters seem to vary. One can clearly observe the major difference in the interpreted friction angle and attraction values between the mini block samples and the 54 mm piston samples, which apparently comes from the mini blocks' superior sample quality. Comparing the two consolidation procedures, the tendency for both the piston and mini blocks samples reveals a higher obtained friction angle for the anisotropically consolidated samples. On the other hand, the isotropically consolidated samples reveal a higher attraction to the material. However, the effective strength parameters interpreted from the failure paths in this study need to be compared with care due to the major strain-softening behavior when reaching the yield state. The shear fracture, which can be seen for each quick clay sample in Appendix B, does introduce clear and large fractures to each sample, which are normal for sensitive clays with low residual strength. This leads the calculation and interpretation of axial strains and thereby stress parameters being somewhat uncertain because of the accumulated strains along the surface of the shear band. However, the observed tendency from this consolidation study seems to support the thought of the effect of the structured, dilative loop for the mini block samples to have an impact on the failure path. This, as mentioned, leaves the effective strength parameters interpreted from mini block samples at a higher level than the 54 mm piston samples which does not seem to reveal the dilative behavior prior to failure.

The best-fit effective strength parameters from the undrained triaxial tests are shown in Figure 7.5. One could notice that the two consolidation procedures results in narrowly different inclinations for the failure path, both for the mini block samples and the 54 mm piston samples, where the anisotropically consolidated samples tend to give a moderately higher friction

angle. On the contrary, the isotropically consolidated samples indicate a higher material attraction. Notice that friction angles obtained from the mini block samples are above the results given by the 54 mm piston samples. Even though the 54 mm piston samples do not seem to show the dilative response when getting close to failure, the inclination on the failure path also appears to be somewhat below the mini block samples.

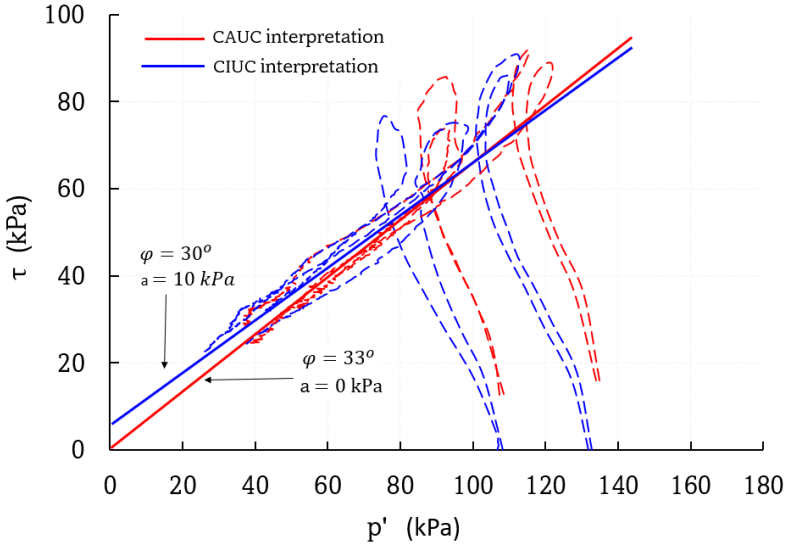

(a) Obtained values for the friction angle and attraction from the mini block samples.

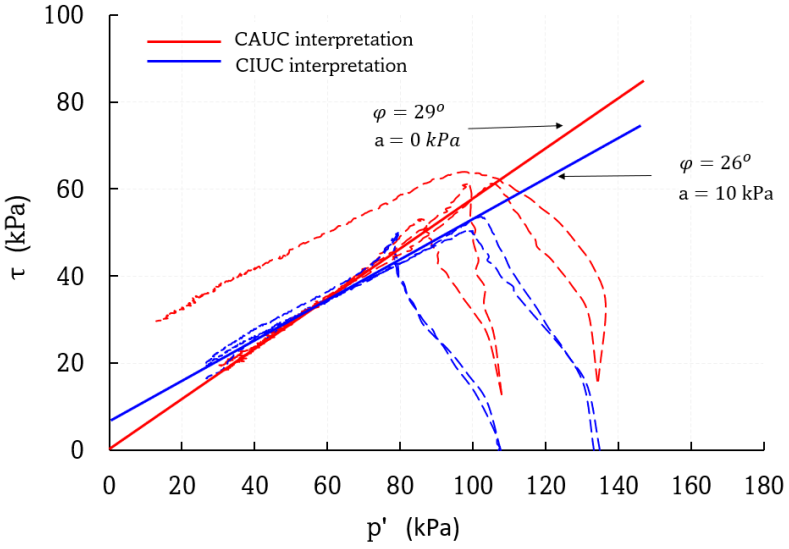

(b) Obtained values for the friction angle and attraction from the 54 mm piston samples.

Figure 7.5: Interpreted best-fit effective strength parameters from all undrained triaxial tests, both mini block samples and 54 mm piston samples.

7.3 Pore pressure response in undrained conditions

During this laboratory study, it turned out to be difficult to achieve satisfactory B-values above the stated 0.95. During the pre-work of this master's thesis, during the fall of 2022, the same problem also appeared during several undrained triaxial tests. An increase of the back pressure to 700 kPa was then done, to further compress any remaining air in the system. Nevertheless, several B-values through this test series were not even close to reaching the theoretical undrained condition. The procedure described in Section 3.5.5, by further increasing the back pressure to 1000 kPa subsequently to the first B-test and letting the sample rest for 3 hours, made the pore pressure response increase significantly.

There might be several factors that influence the unsatisfactory pore pressure response in the system. The procedure for mounting the specimen into the cell and the subsequent flushing of the system was done in hand with communication with geotechnical laboratories and traditional methods, followed by standards and Norwegian guidelines. The cleaning procedure for the porous filters in UV bath and the subsequent saturation in the desiccator is also done according to traditional methods. Different use of vents and pipes in the triaxial apparatus, hereby not fully sealed and tight connections, must, of course, be mentioned as a central factor that may cause disturbance in the pore pressure readings. However, the increased B-values after performing the described procedure did make the pore pressure response significantly better, implying that any system disturbance might not be the biggest reason for the first obtained unsatisfactory B-values.

The reconsolidation procedure when establishing a relevant effective stress state to the sample will force the internal pore water to expell. The internal structure in the clay sample, seen in the emphasis of the particle structure, will change due to the drained consolidation. Norwegian clays extracted from below the groundwater table are in practice seen to be fully saturated (L'Heureux et al., 2019), leaving a gap of pore water expulsion from the samples' original state when the consolidation procedure is finished. The application of back pressure, also called the saturation stage, is done to secure a fully saturated system - by the meaning of porous filter stones, equipment pipes, and the soil sample itself. The application of back pressure is in standards and guidelines defined at relatively high rates, forcing air-free water into the system. For the low permeability of clays, one can imagine that if the B-test is performed directly after reaching the back pressure target, the clay sample has not closed the gap of the "missing", expelled pore water from the consolidation, and thereby is not fully saturated. The results of the improved B-values after leaving the system for 3 hours in this thesis may seem to agree with this statement.

Standards and guidelines for performing undrained compression tests reveal that an increase of 10 kPa of the confining pressure is recommended for performing the B-test for soft clays. During this laboratory study, this recommendation was followed, and the B-test was for every sample performed following the consolidation. One could discuss the procedure for checking the pore pressure response, whether it should take place before or after the consolidation phase, or even if the increase in the confining pressure when performing the B-test may be at a higher level than the recommended 10 kPa. If the consolidation stage is performed prior to the saturation and B-check, any further increase of the confining pressure will introduce a

higher total stress state to the sample than desirable after reaching the target consolidation state. If the saturation stage is performed prior to the consolidation, one could perform the B-check within the range of an effective stress state far below the desirable consolidation stresses, causing no further disturbance to the soil specimen, even with a higher cell pressure increase than the recommended 10 kPa.

7.4 Yield characteristics

The interpreted yield mechanisms from this laboratory study are due to different criteria and methods for establishing plastic mechanisms. The amount of expelled pore water during compression tests, accumulated shear strains, and significant drops in stress-strain-related paths are all examples of methods used for obtaining the mechanical material response to the subjected loadings. Because of the test series' different test procedures, individually with different initial conditions, the placement and comparison of the obtained yield points relative to each other may be insufficiently justified.

However, the Tiller-Flotten quick clay significantly develops yield mechanisms during all performed compression tests. Even though the yield mechanisms developed from the triaxial consolidations are less distinctive than those from the shear tests, the placement of the yield points obtained from these consolidations is well reported on the basis of several contexts and approaches. One may notice the low residual strength from the significant, and representative for quick clay samples, contractive strain-softening drop after reaching the peak deviator from the shear tests. The brittle collapse observed at maximum deviator during shear stands out from the yield mechanisms observed during drained compressions. Thus, the shear tests state the obvious difference between a total collapse and a pure yield mechanism, as seen from the K_0' compression tests. The yield mechanism developed during the drained K_0' compressions is characterized by the slower stress application and the correlated drainage of the pore water. On the other hand, the triaxial shear tests are run with higher stress rates. The correlation between the yield points deducted from the respective test methods needs to be taken with care.

The further interpretation of, and especially the definition of yielding, may be carefully utilized due to the brittle failure observed for the quick clay specimens when subjected to shearing. The accumulated strains and stresses when developing large shear strains may result in inadequate and inaccurate values of the stress-depending parameters. The failure planes and shear bands developed during shearing have a large extent, and may not lead to a sufficient and reliable calculation of the developed strains due to the inhomogeneous geometry and deformation of the test specimen. The smaller friction around the developed shear plane could therefore lead to uncertain results after the brittle collapse seen from the shear tests.

Thus, the total strain increments from the undrained shear tests should be carefully interpreted when reaching the peak mobilized shear strength. The shear fraction of the specimen may cause disturbance in the calculation of the accumulated plastic strains on the dry side of the yield envelope in the p':q space. Together with the uncertainty regarding the obtained stress and strain variables at yielding in shear, the simplified procedure for obtaining the plastic strain

increments does as well cause uncertainty, both for the direction and the length of each strain vector. The presented strain paths for the shear tests do reveal this effect quite clearly because of the different stress levels the strains are developing from after the strain-softening failure (different CSL inclinations). The fragile structure of the Tiller-Flotten quick clay might also affect this observation, and the different developed fraction patterns may further explain the different CSL inclinations. However, the directions of the total strain increments found from this laboratory study seem to coincide pretty well with the yield surfaces from the proposed material models which are reproduced to simulate clay behavior.

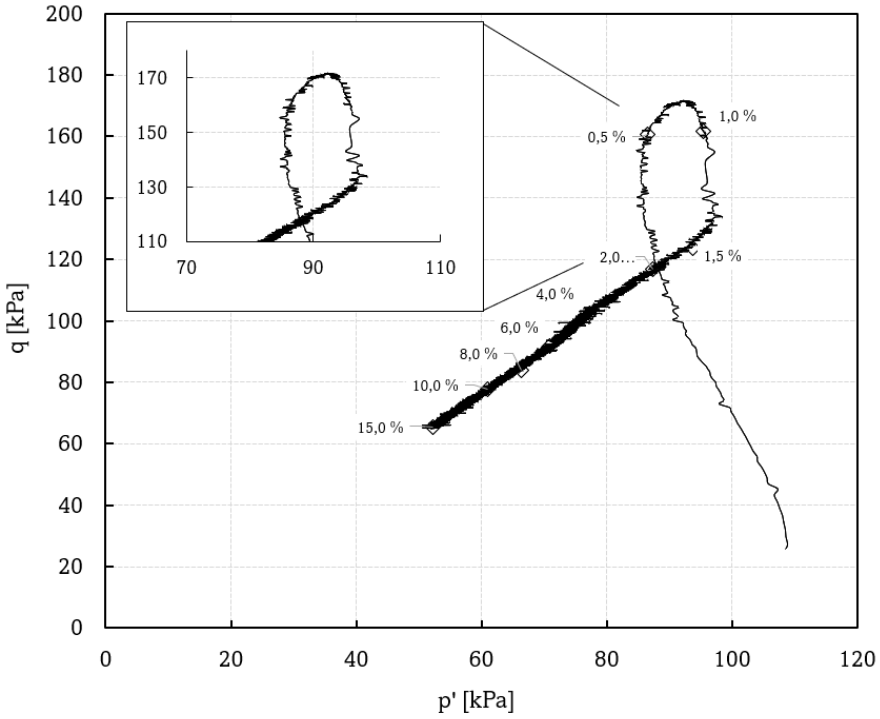

Figure 7.6: The spesific and characteristic structured dilative loop prior to undrained failure for mini block samples from Tiller-Flotten.

The characteristic structured loop seen from the undrained shear tests on mini block samples may introduce a discussion on how to perform adequate yield interpretation. The differentiation of yielding and collapse for the brittle quick clay is challenging. From the triaxial shear tests, the brittle failure mechanism makes the general yield interpretation based on the change in stiffness hard to observe. The observed dilative behavior for the mini block specimens prior to reaching the peak deviator, also presented in Figure 7.6, may be of significant importance when trying to understand how the material is responding and affects the mechanical properties of the clay specimen. When taking a closer look at the increase in effective average stress close to yielding, the soil structure is likely to be affected by the observed dilative response. Thus, the original structure of the sample is being restructured, and the placement of the coinciding yield point may be disturbed, in roughly the same way as creep effects also seem to

”move” the yield surface. Equivalent results are seen from the oedometer tests, where a significant strain-softening response is observed after reaching the yield plateau and decreasing vertical effective stress. These uncertainties may affect the natural yield surface of the material, and the interpreted yield points from the undrained test series must be read with care.

The overall tendency from the undrained test series on the mini block samples does according to the characteristic loop reveal a decreasing pore pressure prior to reaching the peak deviator stress. This is presented in Figure 7.7 from one undrained shear test, but represents the overall tendency from every undrained shear test, especially for the mini block samples. Even though the pore pressure decrease close to failure is normal for high-sensitive soils, the discussion on whether the peak pore pressure may represent the optimal position for interpreting a structured yield of the clay specimen might suggest a central aspect. The drop in pore pressure close to collapse may therefore suggest a structural yield mechanism. The definition of yield and failure may therefore be considered as two separate stages as discussed above, which for the Tiller-Flotten quick clay seems to coincide rather closely than for other low-sensitive clays. The subsequent decrease in pore pressure after this peak, and prior to the peak deviator, may indicate a structural collapse between the soil particles.

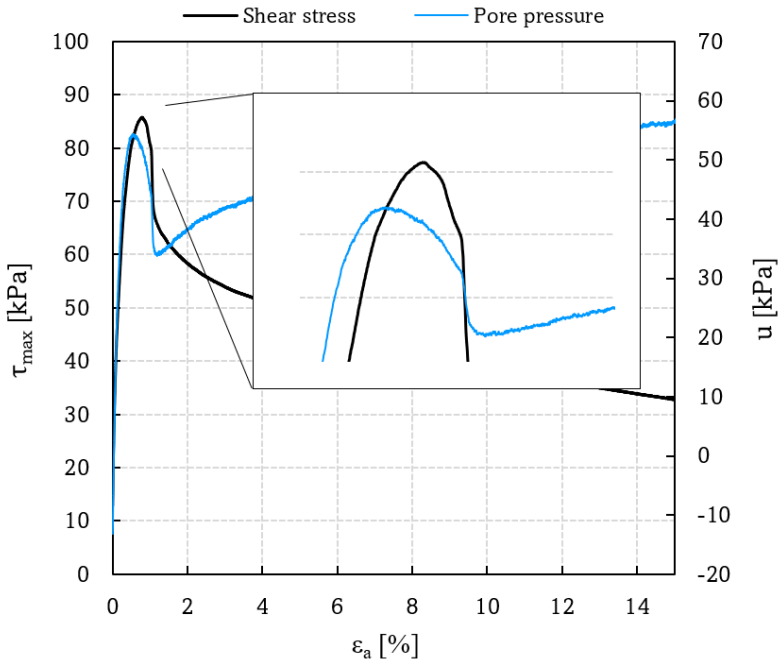

Figure 7.7: The overall tendency for pore pressure development during undrained shear tests on mini block samples.

The drained triaxial tests performed during this laboratory study, especially the consolidation tests, will continuously cause pore water expulsion during the continually increased compression stresses. As reported in Table 6.5, which presents the sample sensitivity immediately after execution of the K_0'-consolidations, the sensitivity of the specimen decreases significantly as

pore water is drained out of the specimen. Hence, the interpretation of a yield plateau is correspondingly tougher to define and correlate to undrained behavior. This is one of the factors that makes the identification of yielding from the consolidations more challenging than the shear tests. We observe that the consolidations give clear indications from developing the yielding mechanism, but the inaccuracy of the yield point position in the p':q-space needs to be taken into account when discussing the yield surface for the material.

Because of the decreasing sensitivity during drained consolidation, one might as well discuss how this volume change affects the drained shear test. The undrained shear tests do as well experience pore water expulsion during the consolidation stage, but the application of back pressure puts the specimen and system in a somehow ”back to basics” state. The drained shear test does lose pore water from the consolidation, as well as pore water losses during the drained shear. One may discuss if the position of the yield point from the drained shear test should be identified and placed at a lower level due to the decrease in the sample sensitivity. However, on the path of trying to understand the behavior of this complex material, we might have to accept the limitations we're forced to undergo when performing laboratory tests. As geotechnical engineers, our understanding of material behavior comes fairly from laboratory experiments. The soil behavior and corresponding response because of the loading scenarios we define are due to interpretation and need to be taken with care. The in situ stress state is challenging to reproduce in the laboratory. Samples are as well extracted from large depths and have further experienced several stress reliefs and suction effects during the sampling procedure. In laboratory studies, we might have to accept the uncertainty of the test results, and further use our knowledge for obtaining reliable results and conservative conclusions.

The majority of the proposed material models are due to experimental studies of clay samples extruded with traditional cylindrical tube samplers. The clear indication of the disturbed material behavior when subjected to compression for the 54 mm piston samples, seen in this study as well as earlier reported from (Amundsen et al., 2015; Berre, 2012; Emdal, Amundsen, Kåsin, et al., 2016), reveals lower values of strength data from triaxial shear tests. However, the entry of mini block samples, and thereby lower disturbed specimens, may not give any special increases to the overall predoncolidation-normalized yield surfaces. This is due to the overall better sample quality which also gives higher preconsolidation values interpreted from the oedometer tests. Even though the mini block samples do reveal a significant increase for the undrained shear strength when compared to piston samples, the normalized yield data from Tiller-Flotten seems to coincide pretty well in compression compared to other strength data from clays with approximately equal friction angles, seen in Figure 2.5.

7.5 Rate effects

The performed drained and undrained shear tests are not run with the same strain rates as the triaxial consolidation tests. Rate dependencies when defining yield characteristics are earlier discussed by several authors, e.g. Wood (1990) and Länsivaara (1999), and will probably highly affect the interpretations of the developed yield mechanisms observed from this laboratory study. This implies that the correlated placement of the presented yield points may not interfere with the exact location of the normalized yield envelope for the Tiller-Flotten quick

clay.

The drained consolidations were performed mainly to secure no significant pore pressure build-up. This was obtained by defining a low stress rate during the K_0' compression tests. Drainage was allowed only at the top surface of the specimen, and the pore pressure was thereby measured at the specimen's bottom surface. The sample height could have been decreased for making the drainage length significantly lower, and thereby apply stresses at a rate closer to the rates used in the shear tests.

For the drained consolidations, the procedure proposed by Berre (2012) may be a better approach for an approximation of the compression rate of the specimen. The procedure for obtaining the preferred rate of strain for the K_0'-consolidations with drainage at both the top of the specimen, proposed by Berre (2012) may be a preferred choice for relating the strain rate from the shear compression tests to the consolidations, seen in Equation (7.1), where γ_w refers to the unit weight of the pore water and k_V equals the coefficient of permeability in the vertical direction.

$$\Delta u_{b,max} = \frac{1}{2}\frac{\dot{\varepsilon}_{vol}}{k_V} \cdot \left(\frac{H}{2}\right) \cdot \gamma_w \tag{7.1}$$

Rate effects seen from performing the CRS oedometer tests also reveal rate dependencies for the Tiller-Flotten quick clay. Comparing the performed compression tests, one may clearly see the difference between the obtained preconsolidation stresses and stiffness relations, as well as the mechanical behavior after reaching the yield plateau. Figure 7.8 shows the variation in the obtained oedometer curves from every mini-block sample. Collapse when surpassing the yield stress complies with a highly contractive behavior for the actual quick clay specimens.

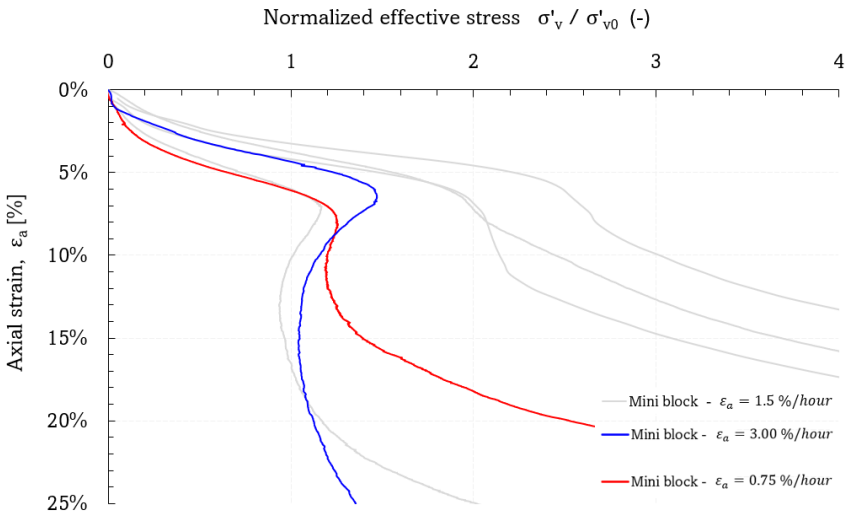

Figure 7.8: Rate effects in the CRS test series on the mini block samples.

Related to the yield points presented in this master's thesis and the proposed material model by Länsivaara, one could notice the position of the drained yield points outside the defined yield surface and outside the highest theoretical values for the chosen reference preconsolidation pressure ($\sigma_1 = 1$). This might be due to rate dependencies, but hardly as much as observed in Figure 7.9. The chosen preconsolidation pressure for normalizing the placement of the yield points may interfere at a higher level, leaving questions about the linking of the preconsolidation pressure found from the oedometer tests to triaxial strength results from the same samples.

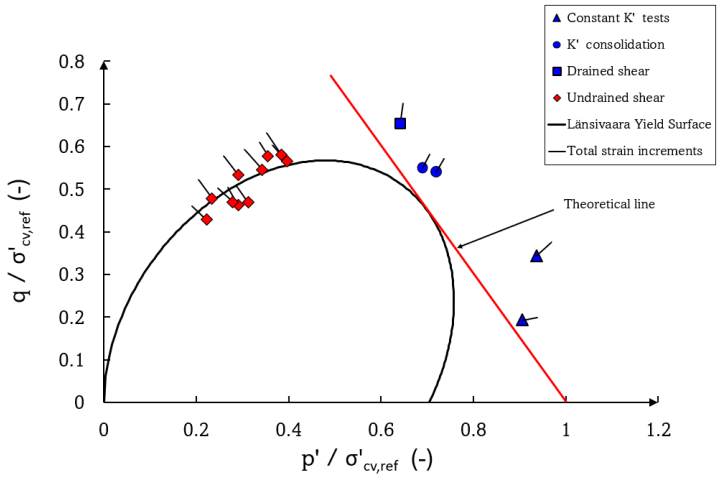

Figure 7.9: The placement of the drained yield points interpreted from drained triaxial tests outside the theoretical range in terms of the chosen reference preconsolidation pressure.

7.6 Sample disturbance

The sample quality is measured for each individual sample throughout this laboratory study, both for oedometer and triaxial tests. The majority of the undrained shear tests are planned for obtaining the difference in consolidation procedure, but as well for mapping the sample difference due to unavoidable storage time for the samples. Some of the samples were stored, for up to one month, in the laboratory cooling room before the tests could be conducted. For the oedometer tests, especially from the mini block series, a tendency of a decreasing preconsolidation level is observed for the stored samples. This seems reasonable, due to the reconsolidation process that takes place for the quite large sample which is stored only with wrapped plastic around the radial edges, which also is reported from Amundsen et al. (2015). The reconsolidation and suction effects seem to rather give a high impact on the oedometer results, with a decreasing preconsolidation level after storage. In terms of the criteria based on M_0/M_L, every CRS test from mini block samples may identify as 'really good to excellent", but in terms of $\Delta e/e_0$, a lower quality is revealed for the stored samples. However, the obtained undrained shear strengths interpreted from triaxial tests seem not to be influenced as much as the preconsolidation level. Even though some mini block samples are identified as poor

quality in terms of $\Delta V/V_0$, the difference in the achieved undrained shear strength seems to differ less. The choice of using the reference preconsolidation pressure ($\sigma'_{cv,ref}$) from the samples showing the best quality was therefore made.

The sample quality derived from every performed undrained shear test does not present any linear tendency in terms of the amount of expelled pore water. The amount of expelled pore water seems to be rather variable, even though the application of the consolidation stresses was done to the same level and with the same stress-application technique, both in terms of time and procedure. By the obtained values for the peak undrained shear strength, one may notice that the sample quality evaluation, only based on expelled pore water during consolidation, does not seem to reflect the strength values. The application of back pressure upon reaching the finished consolidation will cause an in-flow of air-free water from the back pressure controller, both to the sample and the surrounding filters, but also to the pipes connected to the back system. This in-flow will cause a pore water volume increase for the specimen, which is not taken into account when evaluating the sample quality. The sample quality criteria, based on $\Delta V/V_0$ has to be used for comparing the overall volume change during consolidation back to the sample's in-situ stresses for a reliable consolidation level.

Regarding the sample quality obtained from the triaxial tests, based on the criteria of expelled pore water during consolidation to in situ conditions, $\Delta V/V_0$, both mini block samples and piston samples reveal disorganized results. Despite the difference in expelled pore water during consolidation, the resulting stress paths do reveal a significant difference in sample quality when comparing the two sampling methods. The material behavior obtained from the mini block samples does reveal a significantly lower disturbance, and the criteria based on $\Delta V/V_0$ prove to be insufficient for comparing the two sampling methods. However, the $\Delta V/V_0$ criteria need to be utilized for the assessment of the quality and reliability of test results when it comes down to the reconsolidation of the samples' in situ condition.

Concerning the sample quality on a general matter, the laboratory work and handling of the sample are of course central. Several oedometer tests reveal results that may suggest a "false" deformation at the beginning of the tests. This might be a result of a slightly disturbed material surface, caused by improperly cut of the specimen during mounting. Such effects, caused by rough sample handling at the laboratory, need, of course, to be mentioned as a significant source of error when assessing the quality and reliability of laboratory results.

7.7 Further work

To further complete the study of yielding characteristics for the quick clay from Tiller-Flotten, several additional tests have to be performed. Isotropic consolidations ($K'_0 = 1$) have to be performed to identify where the yield surface cuts the p'-axis. Triaxial extension tests will as well identify yield characteristics at a negative deviator, which may reveal any additional anisotropy effects and/or suggest a rotated yield surface.

Additional tests series, both for oedometer and triaxial conditions, performed with different strain rates will further identify the differences in yielding and resulting strength parameters.

If the oedometer as well may measure the amount of expelled pore water during compression, further comparison between triaxial compression in terms of void ratio could be made.

For a further study regarding the pore pressure response during undrained conditions, it's desirable to conduct a more structured test series. A test series where the B-check is performed momentaneously after the desired back pressure is achieved, as well as for selected time increments, may reveal any time dependency for the system regarding the removal of air and gasses. The saturation may as well be tried to be done prior to the consolidation, to address any effect of applying higher confining stress ($\Delta\sigma_c > 10$ kPa) during the B-check.

Chapter 8

Summary and conclusion

This thesis has documented the variation in results by performing both isotropic and anisotropic consolidation procedures to the same average effective stress level p' for undrained triaxial tests and also mapped the mechanical behavior of Tiller-Flotten quick clay. Technical aspects of performing the triaxial tests have been investigated and attempted to improve by pursuing suggested measures, especially for the undrained conditions in the triaxial cell. This relates to obtaining a B-value close to 1.

8.1 Yield surface identification

The Tiller-Flotten quick clay shows clear yielding characteristics both during shear compression tests and general compression in both oedometer and triaxial conditions. The typical strain-softening and progressive failure, typical for quick clay, is identified from both undrained and drained shear tests. Structural yield defines the material behavior during the drained K_0' compressions.

High-quality mini block samples reveal a temporary dilating response prior to reaching contraction failure at the ultimate strength. This characteristic loop in the p':q-space suggests a structured material of significantly better quality compared to the responsively contractive behavior identified from 54 mm piston samples.

The identification of yielding and strength are related to the achieved stress level during re-consolidation to in situ conditions of the samples prior to undrained and drained shearing, which also points to the initial sample volume and the correlated amount of expelled pore water during the consolidation phase. Structural yielding are identified from the drained K_0' compression tests.

The positions of the interpreted yield points on the compressive side of the p':q stress space position the mechanical manners for the Tiller-Flotten quick clay at a reasonable similar strength plateau as earlier studies performed on clays with approximately equal friction angle. A comprehensive shape of the yield locus for the Tiller-Flotten quick clay is challenging to define due to the lack of isotropic compression and triaxial extension tests.

The proposed soil models presented in this thesis and their arrangement of the yield surface are found to correlate reasonably well with the yielding characteristics in compression found in this laboratory study. The total strain increments at yield seem to orthogonally intersect the proposed surfaces, even though these increments have to be interpreted with care due to the extreme strain-softening behavior and the explicit shear bands, especially found from the undrained and drained shear tests.

The typical rate dependencies seem to be valid as well for Tiller-Flotten clay, both when performing oedometer tests and when conducting different loadings in the triaxial cell. The pore overpressure causing the progressive "snap-back" response when yielding in the oedometer, also at different strain rates, suggests a sudden collapse characterized by significantly low residual strength. The mini block samples reveal this "snap-back" effect at a higher stage than seen from 54 mm piston samples.

8.2 Isotropic versus anisotropic consolidation to p'

There are not identified any linear dependencies in sample quality after comparing isotropically and anisotropically consolidations to the in situ average effective stress level, p', in terms of the $\Delta V/V_0$ and $\Delta e/e_O$ criteria. The amount of expelled pore water during the reconsolidations are found to be variable, even though the stresses are applied at equal rates.

54 mm samples are found to reveal higher strength parameters for the anisotropically consolidated samples. The shear strength obtained from the test series performed on mini block samples seems to be approximately equivalent for the two consolidation procedures. Typical for both sample types are higher failure strains from the isotropically consolidated samples to the same stress level. Even though isotropic stress applications are simpler and show approximately comparable results, traditional anisotropic reconsolidations are preferred.

The interpreted effective strength parameters are found to vary by different slopes from the failure paths. The anisotropically consolidated samples reveal slightly higher friction angles. Thus, higher values for the material attraction are identified from the isotropically consolidated samples.

8.3 Pore pressure response in undrained conditions

Each sample that initially reveal unsatisfactory values for the pore pressure response does show a B-value increase when applying a higher back pressure and allowing the sample to rest for three hours before the following B-check. Even though no linearity is identified through the test improvements, an average increase of 25 % is found when the back pressure is increased from 700 (first test) to 1000 kPa (second test). Air bubbles in vents and cranes contribute to unsatisfactory pore pressure response and are considered to be accountable for low B-values. Effective procedures for satisfactory saturation of the specimen, cranes, and vents together with substantial back pressure and resting time for the specimen are recommended.

References

Amundsen, H. A., Thakur, V., & Emdal, A. (2015). Comparision of the sample assessment methods applied to oedometer test results.

Barnhart, T. (2014). *Three musketeers in soils testing: Atterberg, casagrande, and terzaghi*. AASHTO.

Berre, T. (2012). Triaxial testing of soft rocks. *Geotechnical Testing Journal*, *34*(1).

Bishop, A. W., & Bjerrum, L. (1960). *The relevance of the triaxial test to the solution of stability problems*. NGI.

Bjerrum, L. (1955). Stability of natural slopes in quick clay. *Geotechnique*, *5*(101).

Bjerrum, L., & Aitchison, G. D. (1973). Problems of soil mechanics and construction on soft clays and structurally unstable soils | semantic scholar. *International Conference on Soil Mechanics and Foundation Engineering*, (8).

Cotecchia, F., & Chandler, R. J. (2000). A general framework for the mechanical behaviour of clays. *Géotechnique*, *50*(4), 431–447.

Dadras-Ajirloo, D., Grimstad, G., & Ghoreishian Amiri, S. A. (2022). On the isotache viscous modelling of clay behaviour using the hyperplasticity approach. *Géotechnique*. https://doi.org/10.1680/jgeot.21.00245

Días-Rodríguez, J. A., Leroueil, S., & Alemán, J. D. (1992). Yielding of mexico city clay and other natural clays [ISSN: 0733-9410]. Retrieved February 21, 2023, from https://ascelibrary.org/doi/epdf/10.1061/%28ASCE%290733-9410%281992%29118%3A7%28981%29

Emdal, A. (2022). Introduksjon til geoteknikk.

Emdal, A., Amundsen, H. A., Kåsin, K., & Long, M. (2016). Mini-block sampler. *Canadian Geotechnical Journal*, *53*(8), 1235–1245.

Emdal, A., Amundsen, H. A., & Thakur, V. (2016). Sample disturbances in block samples of low plastic soft clays.

FINN kart. (2023, February 28). http://kart.finn.no

Giger, S. B., Russel, T. E., Favero, V., Stankovic, R., & Keller, L. M. (2018). Consolidated-undrained triaxial testing of opalinus clay: Results and method validation.

Graham, J., Noonan, M. L., & Lew, K. V. (1983). Yield states amd stress-strain relationships in a natural plastic clay.

Gregersen, O. (2008). Program for økt sikkerhet mot leirskred - Metode for kartlegging og klassifisering av faresoner, kvikkleire.

Grimstad, G., Dadrasajirlou, D., & Ghoreishian Amiri, S. A. (2020). Modelling creep in clay using the framework of hyper-viscoplasticity. *Géotechnique Letters*, *10*(3), 404–408.

Helle, T. E. (2017). Quick-clay landslide mitigation using potassium chloride.

Høydedata [Høydedaa]. (2023). Retrieved December 16, 2022, from https://hoydedata.no/

Karlsrud, K., & Hernandez-Martinez, F. G. (2013). Strength and deformation properties of norwegian clays from laboratory tests on high-quality block samples. *Canadian Geotechnical Journal*, *50*(12).

Länsivaara, T. (1995). A critical state model for anisotropic soft soils [Publisher: Danish Geotechnical Society]. *The Interplay between Geotechnical Engineering and Engineering Geology, Proceedings of the Eleventh European Conference on Soil Mechanics and Foundation Engineering, Copenhagen, 28 May - 1 June, DGF-Bulletin*, 101–106.

Länsivaara, T. (1999, January 1). *A study of the mechanical behavior of soft clay* (Doctoral dissertation). https://doi.org/10.13140/RG.2.1.2842.0641

Länsivaara, T., & Nordal, S. (1998). A soil model for the overconsolidated region of clays. https://doi.org/10.1007/978-3-7091-2512-0_33

Leroueil, S., Tavenas, F., Samson, L., & Morin, P. (1983). Preconsolidation pressure of champlain clays. part II. laboratory determination [Publisher: NRC Research Press]. *Canadian Geotechnical Journal*, *20*(4), 803–816. https://doi.org/10.1139/t83-084

L'Heureux, J.-S. (2012). *A study of the retrogressive behavior and mobility of norwegian quick clay landslides*.

L'Heureux, J.-S., Gundersen, A. S., D'Ignazio, M., Smaavik, T., Kleven, A., Rømoen, M., Karlsrud, K., Paniagua, P., & Hermann, S. (2018). Impact of sample quality on CPTU correlations in clay – example from the rakkestad clay.

L'Heureux, J.-S., Lindgård, A., & Emdal, A. (2019). *The tiller – flotten research site: Geotechnical characterization of a very sensitive clay deposit* (Report 20160154-20-R) [Accepted: 2019-12-06T09:56:35Z]. Norges Geotekniske Institutt. Retrieved October 12, 2022, from https://ngi.brage.unit.no/ngi-xmlui/handle/11250/2632134

Lunne, T., Berre, T., & Strandvik, S. (1997). SAMPLE DISTURBANCE EFFECTS IN SOFT LOW PLASTIC NORWEGIAN CLAY. Retrieved November 16, 2022, from https://trid.trb.org/view/476476

Lunne, T., Berre, T., Andersen, K. H., Strandvik, S., & Sjursen, M. (2011). Effects of sample disturbance and consolidation procedures on measured shear strength of soft marine norwegian clays. *Canadian Geotechnical Journal*, *43*(7).

NGF. (2013). NGF melding 11 - prøvetaking.

NGI. (2013). State of the art: Blokkprøver.

NGU. (2022). Forekomst - eller ikke - av marin leire. Retrieved December 16, 2022, from https://www.ngu.no/emne/forekomst-eller-ikke-av-marin-leire

Nordal, S. (2020). Geotechnical engineering: Advanced course.

Norgeskart [Norgeskart]. (2023). Retrieved May 9, 2023, from https://www.norgeskart.no/

NVE. (2019). Sikkerhet mot kvikkleireskred.

Reite, A. J., Sveian, H., & Eriksen, E. (1999). Trondheim fra istid til nåtid - landskapshistorie og løsmasser | norges geologiske undersøkelse. Retrieved December 17, 2022, from https://www.ngu.no/publikasjon/trondheim-fra-istid-til-n-tid-landskapshistorie-og-l-smasser

Rosenqvist, I. (1953). Considerations on the sensitivity of norwegian quickclays.

Sandven, R., Nordal, S., Emdal, A., Janbu, N., Grande, L., & Amundsen, H. A. (2017). Geotechnics: Field and laboratory investigations.

Standard Norge. (2017). *Geotekniske felt- og laboratorieundersøkelser - laboratorieprøving av jord - del 6: Konusprøving NS-EN ISO 17892-6:2017*.

Standard Norge. (2018). *Geotekniske felt- og laboratorieundersøkelser - laboratorieprøving av jord - del 9: Konsolidert treaksial trykkprøving av mettet jord NS-EN ISO 17892-9:2018*.

Statens Vegvesen. (2016). *Håndbok r210 laboratorieundersøkelser*. Vegdirektoratet.

Statens Vegvesen. (2022). *Håndbok V220 Geoteknikk i vegbygging*. Vegdirektoratet.

Tavenas, F., Leroueil, S., LaRochelle, P., & Roy, M. (1978). Creep behaviour of an undisturbed lightly overconsolidated clay. *Canadian Geotechnical Journal*, *15*(3), 402–423.

Wild, K. M., Barla, M., Turinetti, G., & Amann, F. (2017). *A multi-stage triaxial testing procedure for low permeable geomaterials applied to opalinus clay*. CSRME.

Wood, D. M. (1990). *Soil behaviour and critical state soil mechanics*. Cambridge University Press.

Yong, R. N., & McKyes, E. (1971). Yield and failure of a clay under triaxial stresses. *ASCE*, *97*(1), 159–176. https://doi.org/10.1061/JSFEAQ.0001513

Appendix A

Results: Rutine tests

Sample ID	Type	Depth	Storage	Water content	Density	Falling cone			Atterberg			
			(months)	w *(%)*	γ (kN/m^3)	s_{ufc} (kPa)	s_{urfc} (kPa)	S_t (-)	w_L (%)	w_P (%)	I_P (-)	I_L (-)
U67	54 mm	9 - 9.7 m	0	46.3	18.6	26.7	0.16	164	32	26	5.9	3.3
U172	54 mm	9 - 9.7 m	1	40.1	17.7	37.4	0.12	312	32	27	5.0	3.0
MB-1	Miniblokk	9 - 9.3 m	0	43.2	21.1	31.4	0.27	118	31	25	6.2	3.0
MB-3	Miniblokk	9.3 - 9.6 m	1	41.6	17.6	28.5	0.14	210	34	28	6.2	2.2
L-20	54 mm	12 - 12.7 m	0	41.3	18.1	25.2	0.22	113	30	22	6.5	2.7
U195	54 mm	12 - 12.7 m	1	x	19.1	29.3	0.19	154	31	24	6.9	x
MB-2	Miniblokk	12 - 12.3 m	0	41.5	17.9	34.8	0.22	159	30	25	5.4	3.1
MB-4	Miniblokk	12.3 - 12.6 m	1	x	18.3	37.9	0.23	165	31	25	6.1	x

Table A.1: Results: rutine tests

Appendix B

Results: Triaxial tests

TRIAXIAL TESTS: CONSOLIDATION PROCEDURES

Sample ID	Type	Depth [m]	Storage [months]	Test	B-value $\Delta u/\Delta\sigma_c$	p' [kPa]	c_{uA} [kPa]	ε_f [%]	Figure
U67	54 mm	9.3	0	CIUC	0.88	108	48	2.00	B.4
U67	54 mm	9.6	0	CAUC	0.91	108	53	1.61	B.5
MB-1	Mini block	9.2	0	CIUC	0.87	108	76	0.90	B.6
MB-1	Mini block	9.2	0	CAUC	0.92	108	85	0.75	B.7
U172	54 mm	9.4	1	CIUC	0.91	108	49	1.76	B.8
U172	54 mm	9.6	1	CAUC	0.88	108	61	1.55	B.9
MB-3	Mini block	9.4	1	CIUC	0.92	108	75	1.10	B.10
MB-3	Mini block	9.4	1	CAUC	0.94	108	74	0.91	B.11
L-20	54 mm	12.6	0	CIUC	0.91	134	50	2.00	B.12
L-20	54 mm	12.3	0	CAUC	0.62	164	63	1.40	B.13
MB-2	Mini block	12.2	0	CIUC	0.92	134	90	0.96	B.14
MB-2	Mini block	12.2	0	CAUC	0.91	134	91	0.90	B.15
U195	54 mm	12.4	1	CIUC	0.94	134	53	1.50	B.16
U195	54 mm	12.3	1	CAUC	0.90	134	61	1.48	B.17
MB-4	Mini block	12.2	1	CIUC	0.89	134	87	1.00	B.18
MB-4	Mini block	12.2	1	CAUC	0.89	134	89	0.90	B.19

Table B.1: Results: Triaxial tests to identify consolidation difference.

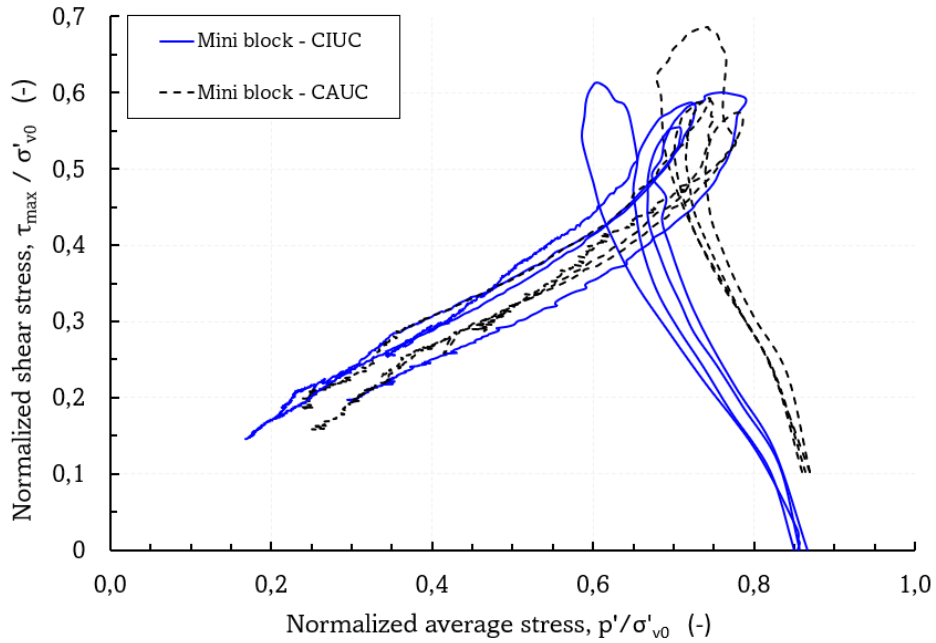

Figure B.1: Resulting normalized stress paths from the undrained shear tests on mini block samples.

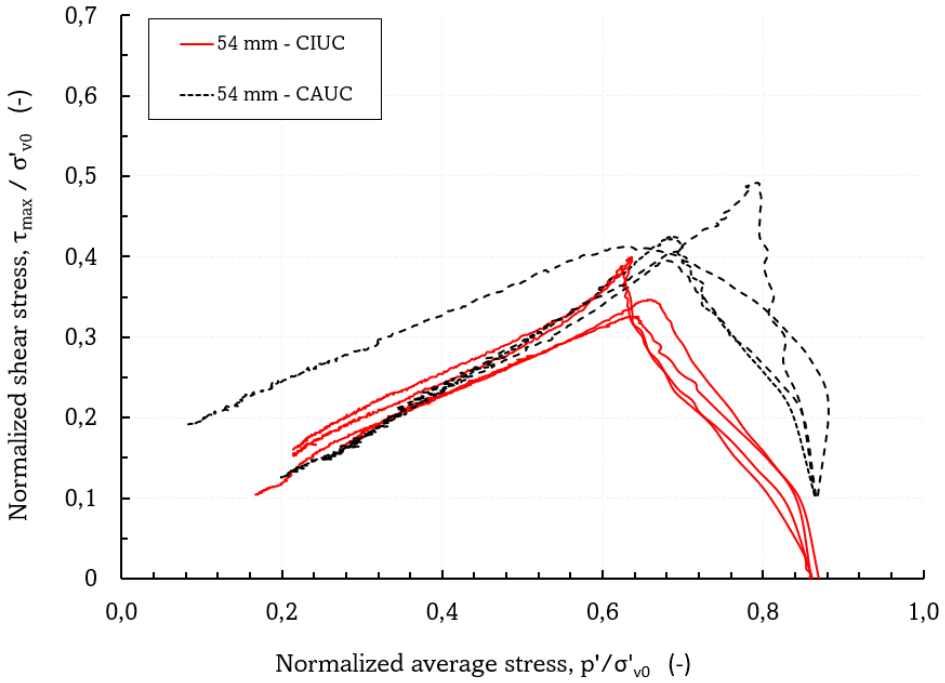

Figure B.2: Resulting normalized stress paths from the undrained shear tests performed from 54 mm piston samples.

TRIAXIAL TESTS: IDENTIFICATION OF YIELD SURFACE

	General				Yield					
Test	Sample ID	Depth (m)	$\sigma'_{cv\,ref}$ (kPa)	w (%)	p' (kPa)	q (kPa)	$d\varepsilon_q/d\varepsilon_p$ (-)	q/p' (-)	W (-)	Figure
$K_0 = 0.7$	MB-3	9.5	320	42	310	108	0.21	2.9	1.8	B.20
$K_0 = 0.8$	MB-3	9.5	320	42	300	77	0.12	3.9	2.1	B.21
$K_0 - cons$	MB-3	9.4	320	42	245	198	0.67	1.2	2.4	B.22
$K_0 - cons$	MB-4	12.5	315	42	224	194	0.67	1.2	2.2	B.23
CIDC	MB-4	12.4	315	42	202	205	2.48	1.01	0.89	B.24
CIUC	MB-4	12.5	315	42	77	140	0.89	1.82	0.77	B.25
CIUC	MB-4	12.5	315	42	85	147	0.78	1.73	0.91	B.26

Table B.2: Triaxial tests to primarily identify yield surface. The undrained shear tests perfomed on the mini block samples shown in Table B.1 are also part of the interpreted yield surface in this thesis.

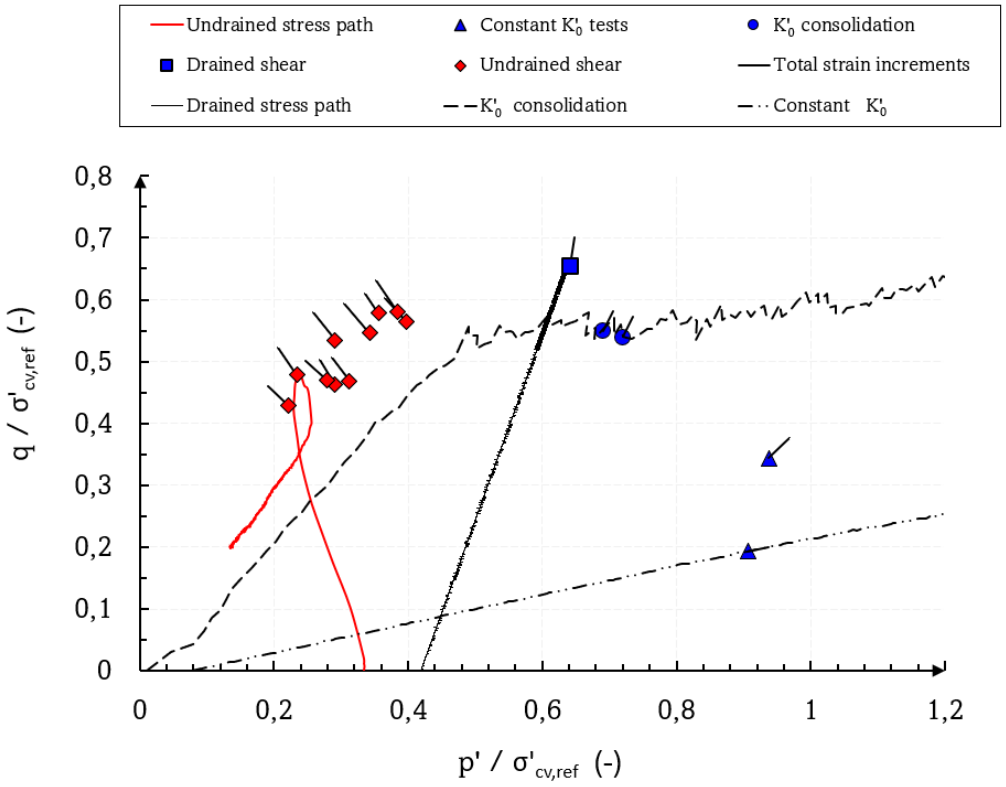

Figure B.3: Plot of every yield point deducted from every triaxial test performed, normalized by the reference preconsolidation stress. In addition, one undrained stress path is presented.

Triaxial test - U67 - CIUC

Depth :	9,3	m
Sampling date :	31.01.2023	
Opening date :	03.02.2023	
Test date :	03.02.2023	
ΔV :	9,24	
Vertical strain rate $\dot{\varepsilon}$:	2	(% / hour)
ε_v :	4,0	(%)
B-value :	0,88	(-)
σ'_{v0} :	125	kPa
K'_0 :	1	(-)
p' :	108	kPa
γ :	18,6	kN/m^3
w :	46	%

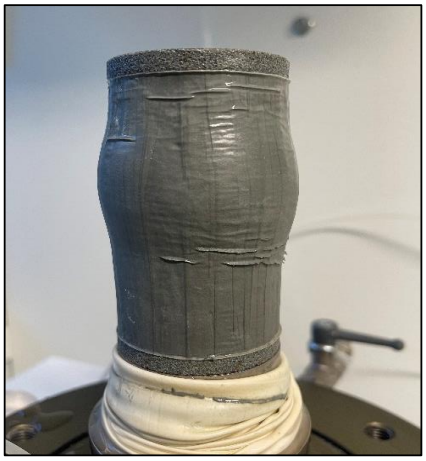

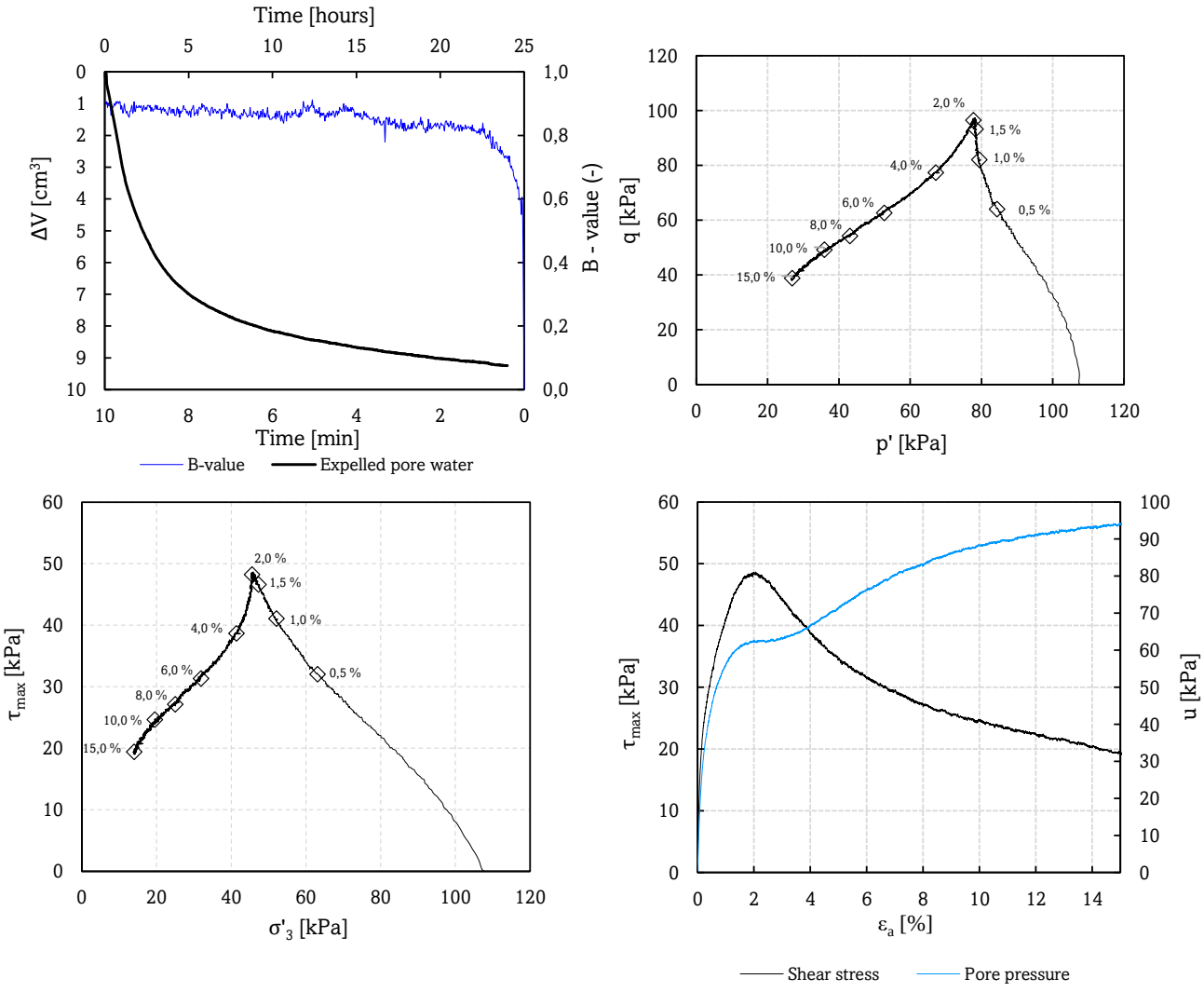

Figure B.4: CIUC - U67 - 54 mm

Triaxial test - U67 - CAUC

Depth :	9,6	m
Sampling date :	31.01.2023	
Opening date :	03.02.2023	
Test date :	03.02.2023	
ΔV :	9,02	
Vertical strain rate $\dot{\varepsilon}$:	2	(% / hour)
ε_v :	3,9	(%)
B-value :	0,91	(-)
σ'_{v0} :	125	kPa
K'_0 :	0,8	(-)
p' :	108	kPa
γ :	18,6	kN/m^3
w :	46	%

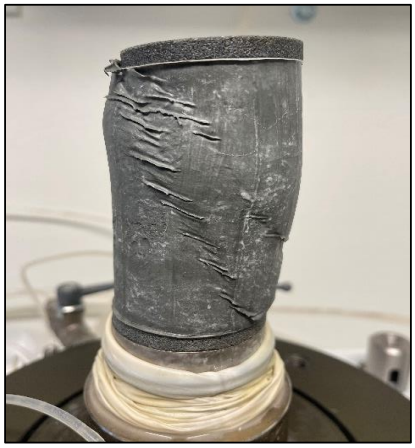

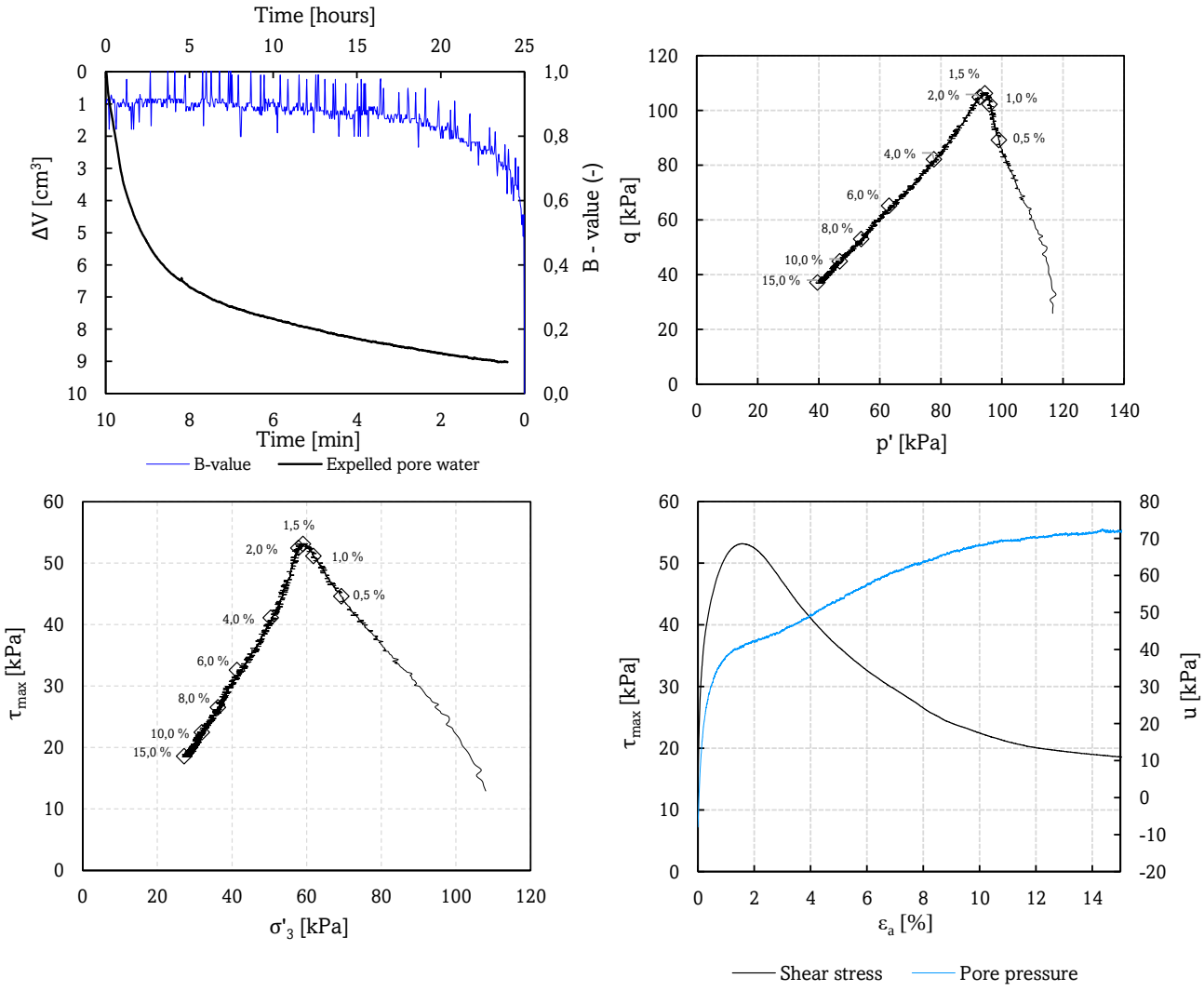

Figure B.5: CAUC - U67 - 54 mm

Triaxial test - MB-1 - CIUC

Depth :	9,2	m
Sampling date :	11.02.2023	
Opening date :	11.02.2023	
Test date :	11.02.2023	
ΔV :	6,62	cm^3
Vertical strain rate $\dot{\varepsilon}$:	2	(% / hour)
ε_v :	2,9	(%)
B-value :	0,87	(-)
σ'_{v0} :	125	kPa
K'_0 :	1	(-)
p' :	108	kPa
γ :	21	kN/m^3
w :	43	%

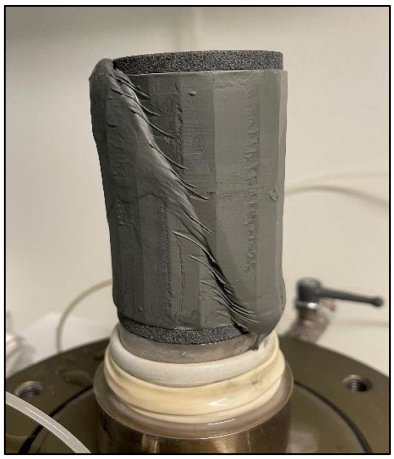

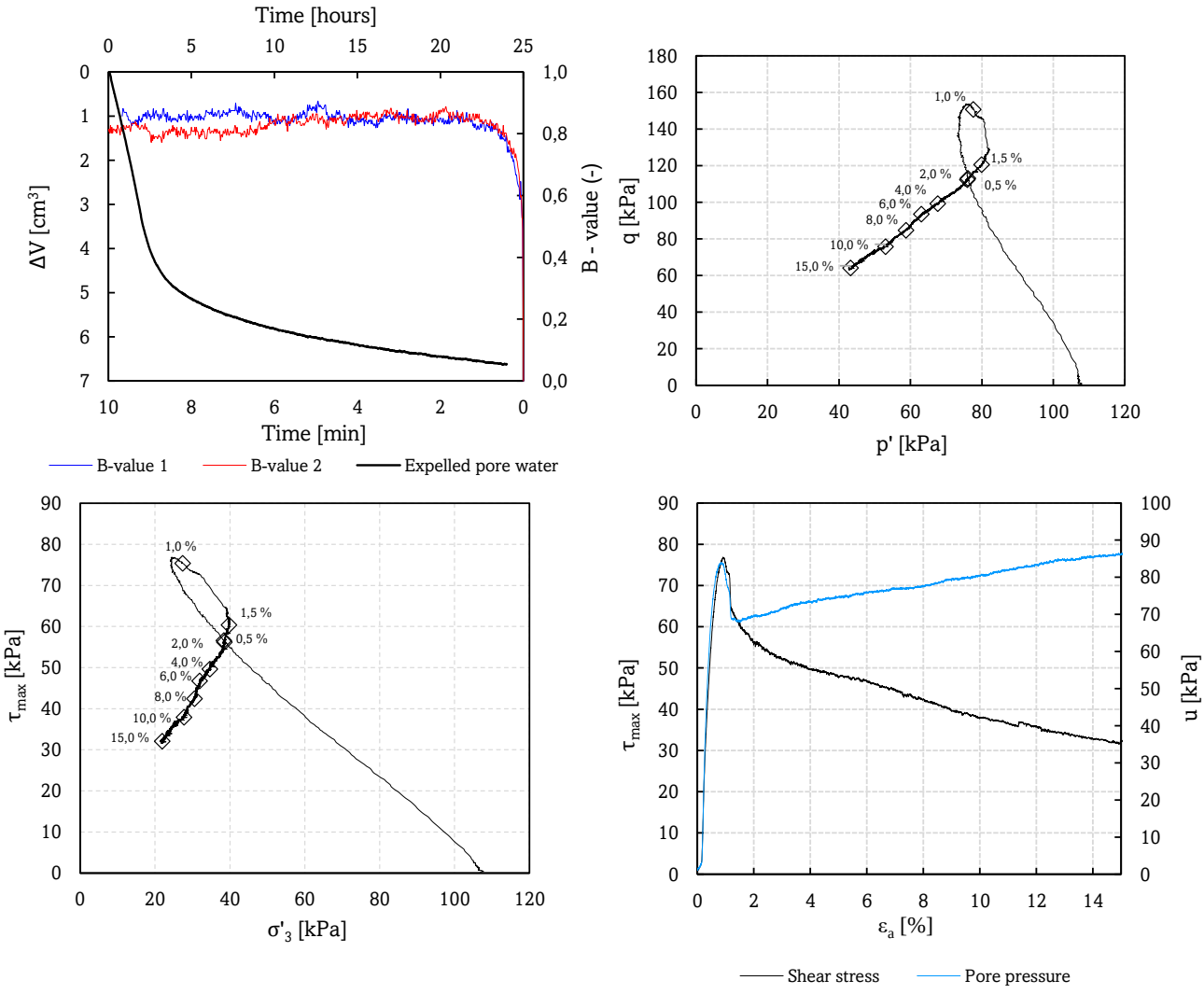

Figure B.6: CIUC - MB-1 - Mini block

Triaxial test - MB-1 - CAUC

Depth :	9,2	m
Sampling date :	11.02.2023	
Opening date :	11.02.2023	
Test date :	11.02.2023	
ΔV :	8,45	
Vertical strain rate $\dot{\varepsilon}$:	2	(% / hour)
ε_v :	3,7	(%)
B-value :	0,92	(-)
σ'_{v0} :	125	kPa
K'_0 :	0,8	(-)
p' :	108	kPa
γ :	21	kN/m^3
w :	43	%

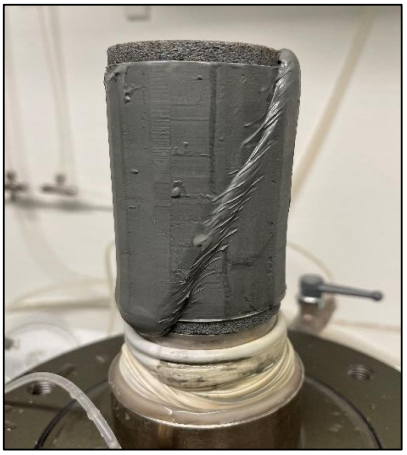

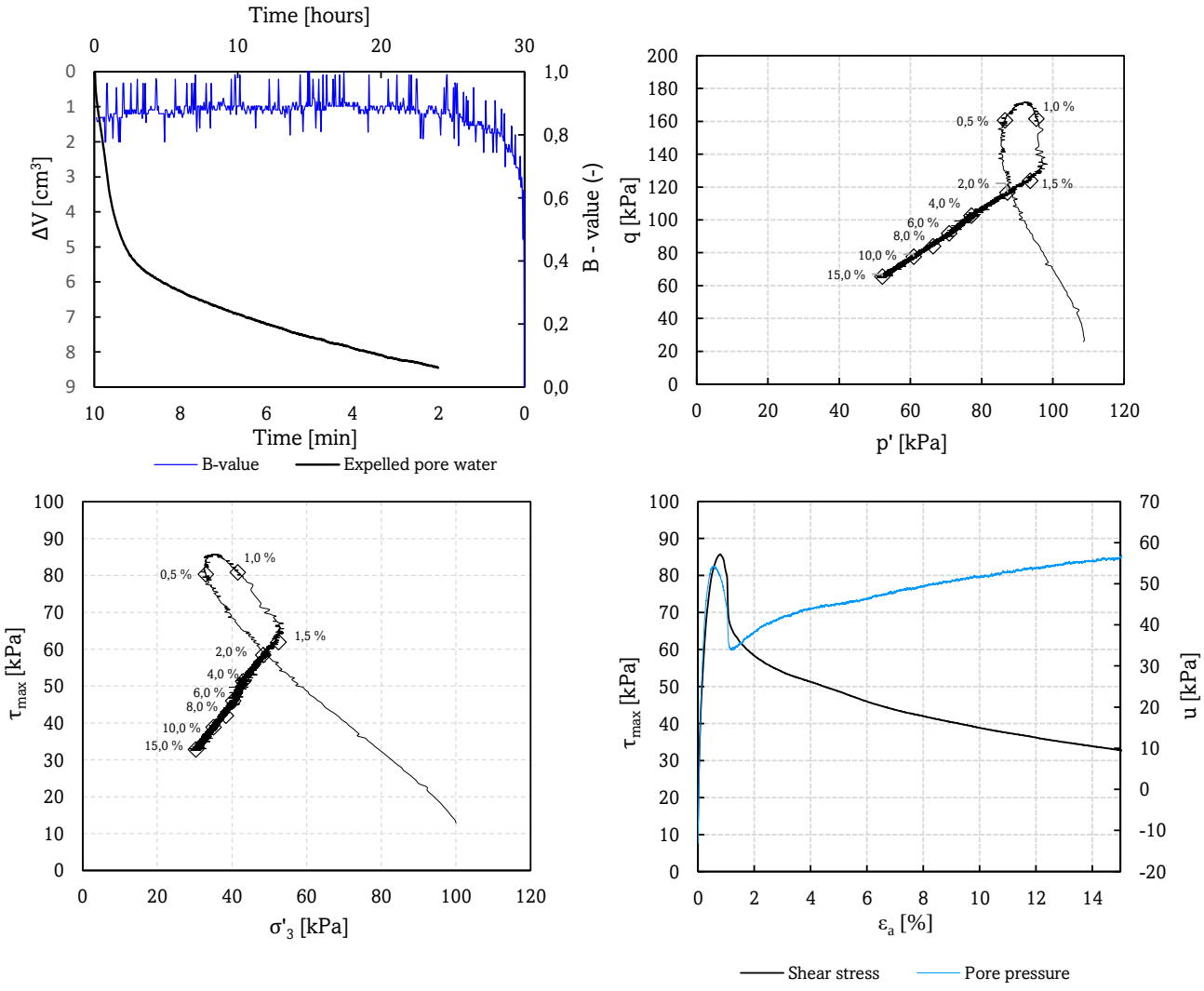

Figure B.7: CAUC - MB-1 - Mini block

Triaxial test - U172 - CIUC

Depth :	9,4	m
Sampling date :	22.12.2022	
Opening date :	30.01.2023	
Test date :	30.01.2023	
ΔV :	4,73	cm^3
Vertical strain rate $\dot{\varepsilon}$:	2	(% / hour)
ε_v :	2,1	(%)
B-value :	0,91	(-)
σ'_{v0} :	125	kPa
K'_0 :	1	(-)
p' :	108	kPa
γ :	18,1	kN/m^3
w :	41	%

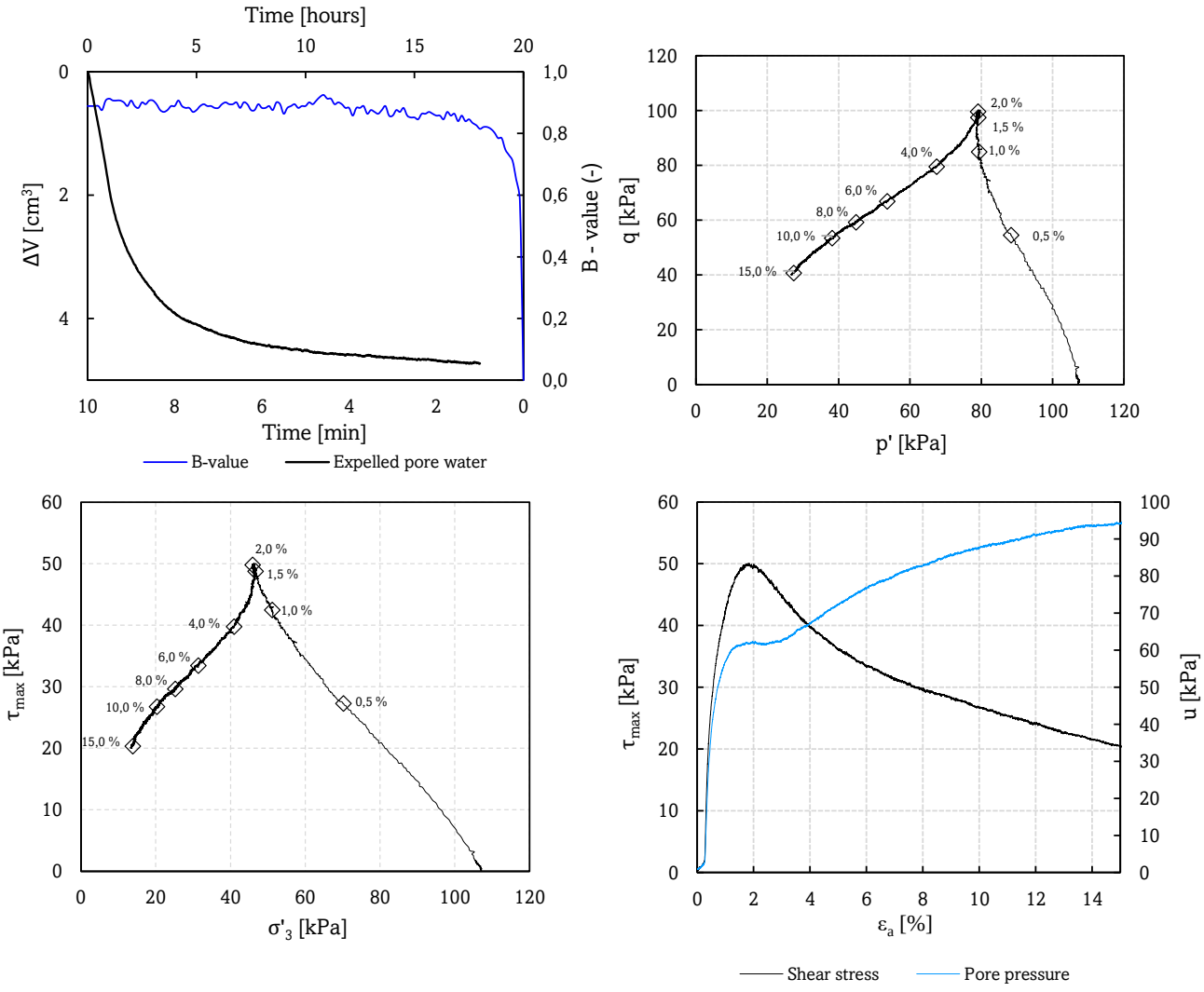

Figure B.8: CIUC - U172 - 54 mm

Triaxial test - U172 - CAUC

Depth :	9,6	m
Sampling date :	22.12.2022	
Opening date :	30.01.2023	
Test date :	30.01.2023	
ΔV :	7,42	cm^3
Vertical strain rate $\dot{\varepsilon}$:	2	(% / hour)
ε_v :	3,2	(%)
B-value :	0,88	(-)
σ'_{v0} :	125	kPa
K'_0 :	0,8	(-)
p' :	108	kPa
γ :	18,1	kN/m^3
w :	41	%

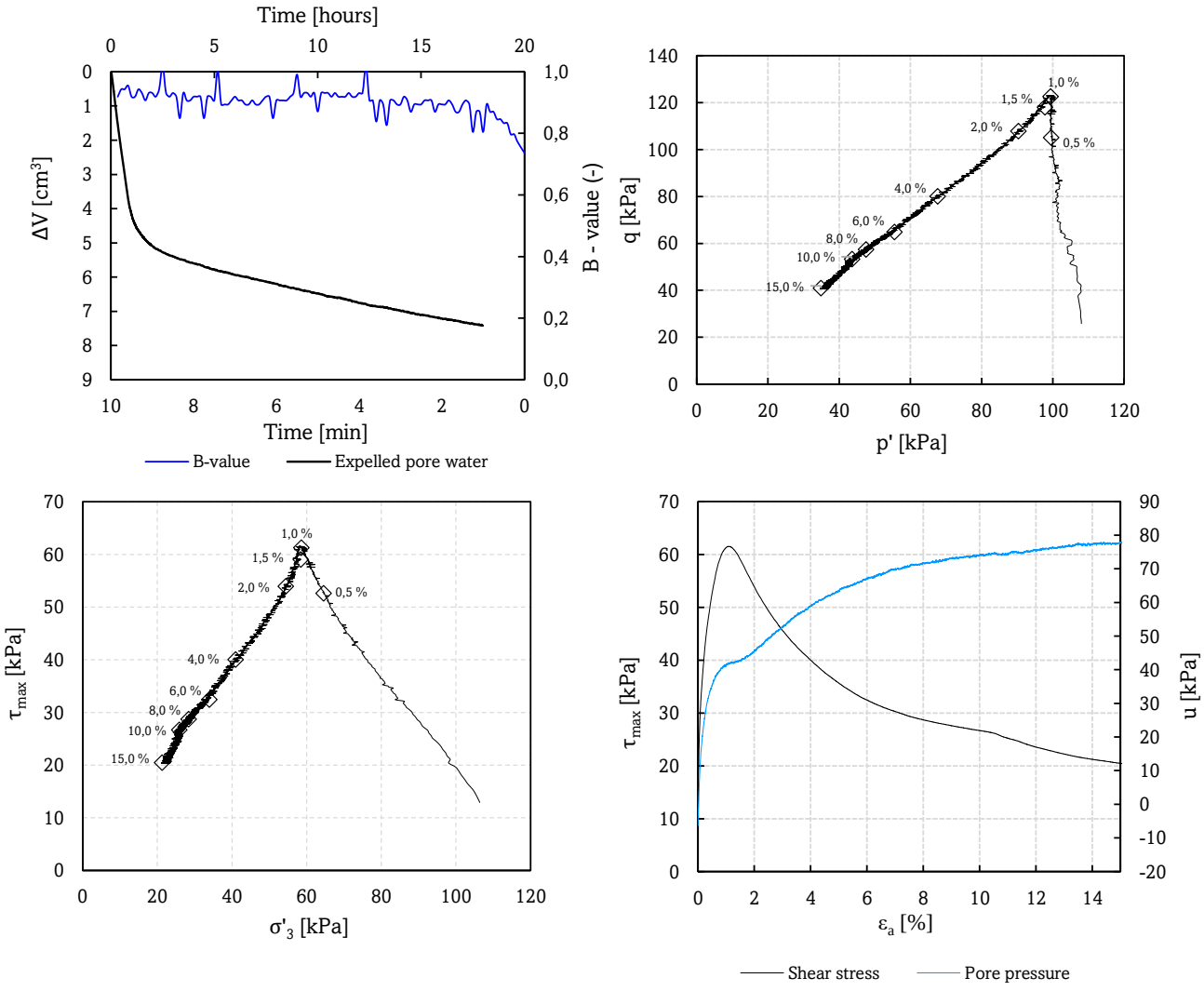

Figure B.9: CAUC - U172 - 54 mm

Triaxial test - MB-3 - CIUC

Depth :	9,4	m
Sampling date :	11.02.2023	
Opening date :	27.02.2023	
Test date :	27.02.2023	
ΔV :	6,81	cm^3
Vertical strain rate $\dot{\varepsilon}$:	2	(% / hour)
ε_v :	3,0	(%)
B-value :	0,92	(-)
σ'_{v0} :	125	kPa
K'_0 :	1	(-)
p' :	108	kPa
γ :	18	kN/m^3
w :	42	%

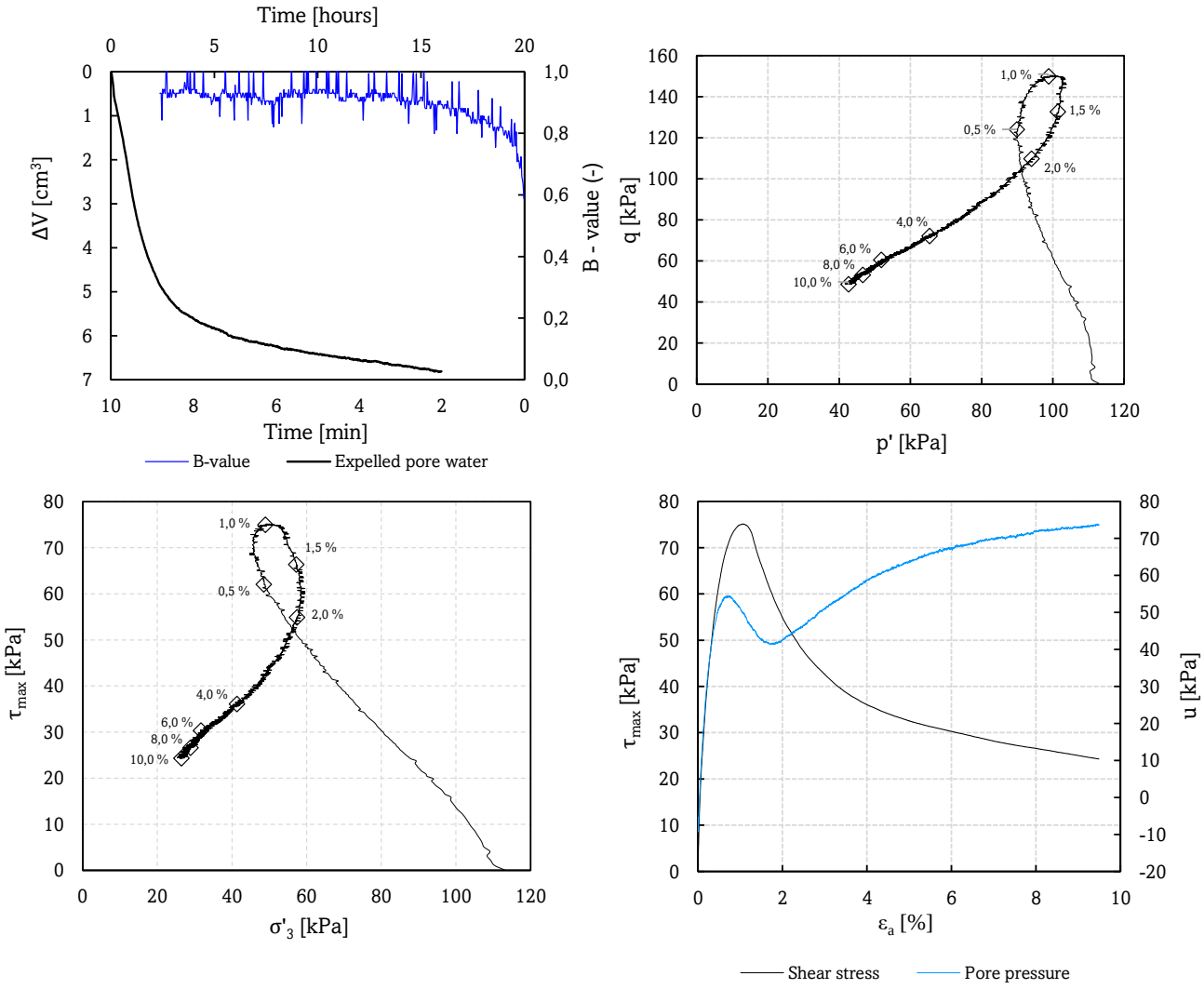

Figure B.10: CIUC - MB-3 - Mini block

Triaxial test - MB-3 - CAUC

Depth :	9,4	m
Sampling date :	11.02.2023	
Opening date :	27.02.2023	
Test date :	27.02.2023	
ΔV :	11,46	cm^3
Vertical strain rate $\dot{\varepsilon}$:	2	(% / hour)
ε_v :	5,0	(%)
B-value :	0,94	(-)
σ'_{v0} :	125	kPa
K'_0 :	0,8	(-)
p' :	108	kPa
γ :	18	kN/m^3
w :	42	%

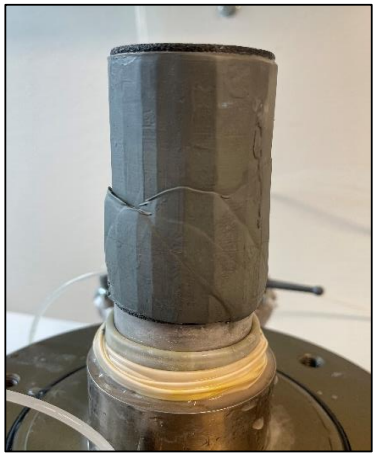

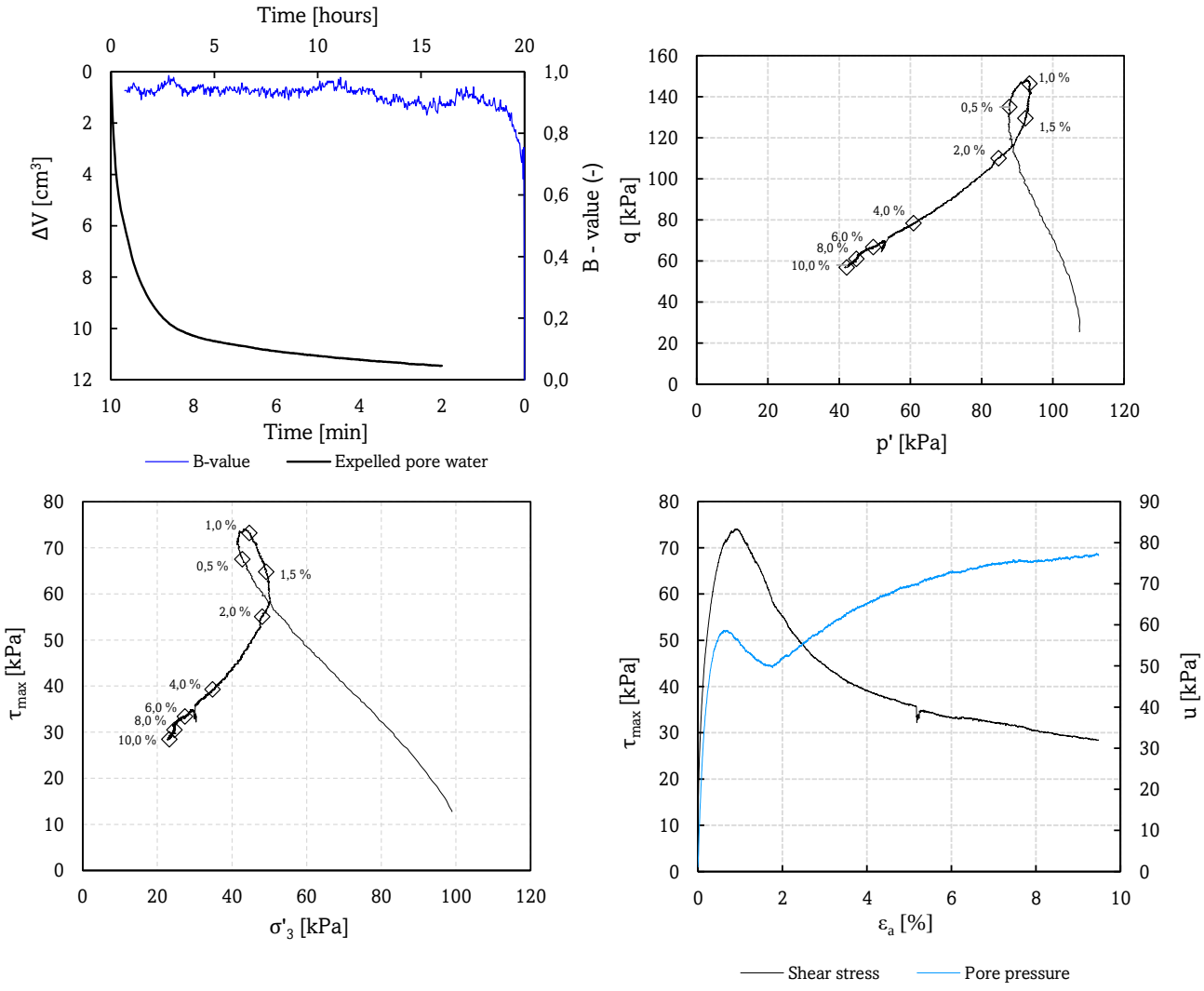

Figure B.11: CAUC - MB-3 - Mini block

Triaxial test - L20 - CIUC

Depth :	12,6	m
Sampling date :	16.01.2023	
Opening date :	24.01.2023	
Test date :	24.01.2023	
ΔV :	8,08	cm^3
Vertical strain rate $\dot{\varepsilon}$:	2	(% / hour)
ε_v :	3,5	(%)
B-value :	0,91	(-)
σ'_{v0} :	155	kPa
K'_0 :	1	(-)
p' :	134	kPa
γ :	18,1	kN/m^3
w :	41	%

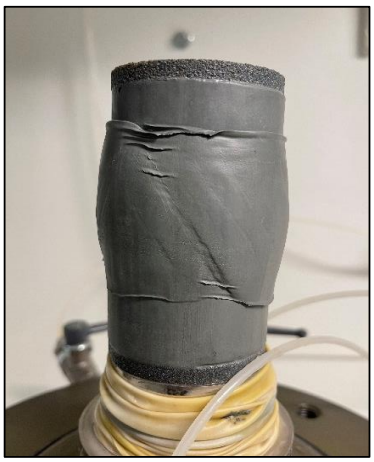

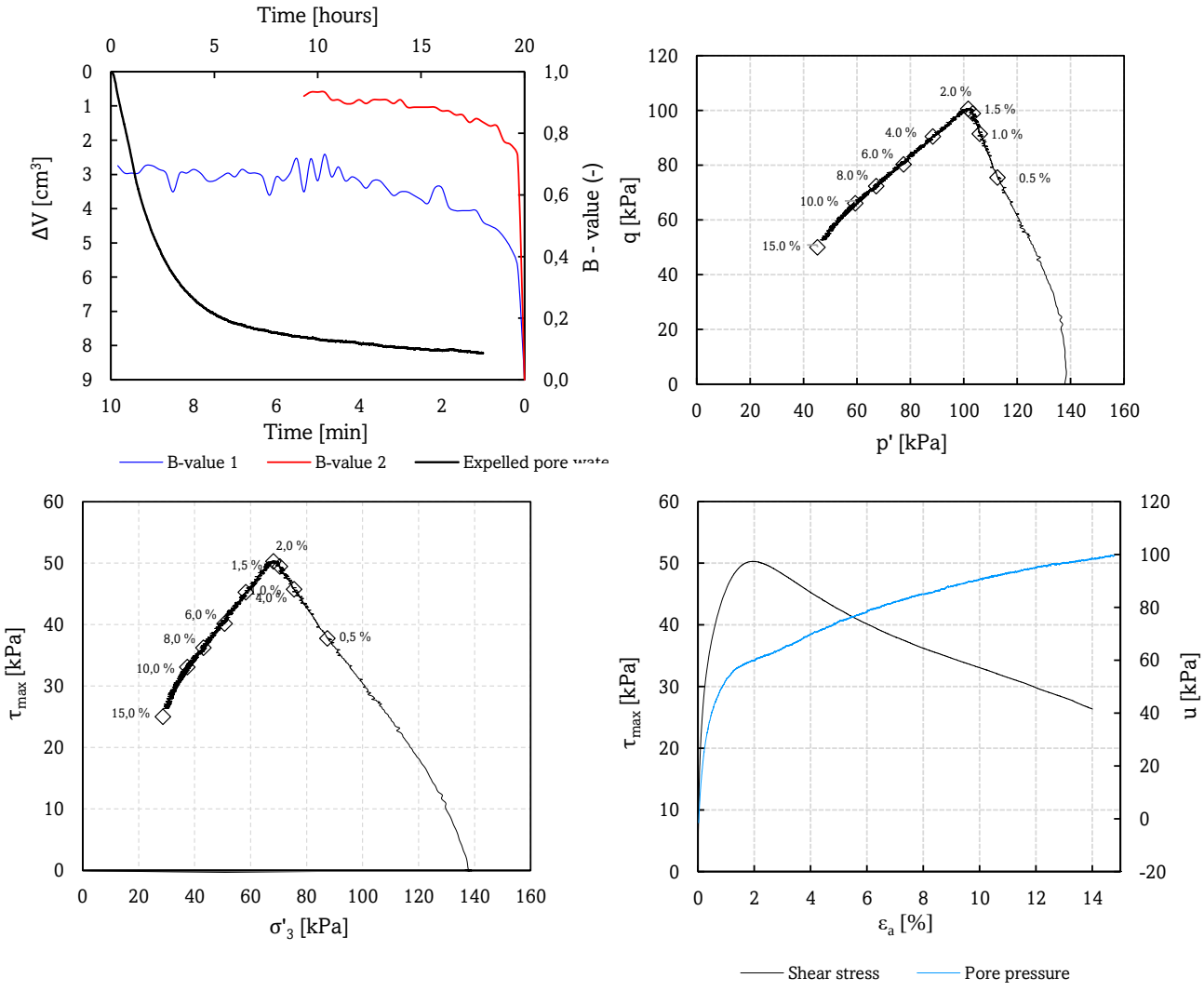

Figure B.12: CIUC - L20 - 54 mm

Triaxial test - L20 - CAUC

Depth :	12,3	m
Sampling date :	16.01.2023	
Opening date :	24.01.2023	
Test date :	24.01.2023	
ΔV :	26,92	cm^3
Vertical strain rate $\dot{\varepsilon}$:	2	(% / hour)
ε_v :	11,8	(%)
B-value :	0,62	(-)
σ'_{v0} :	155	kPa
K'_0 :	0,8	(-)
p' :	162	kPa
γ :	18,1	kN/m^3
w :	41,3	%

Comment:
Higher consolidation stresses than intended.

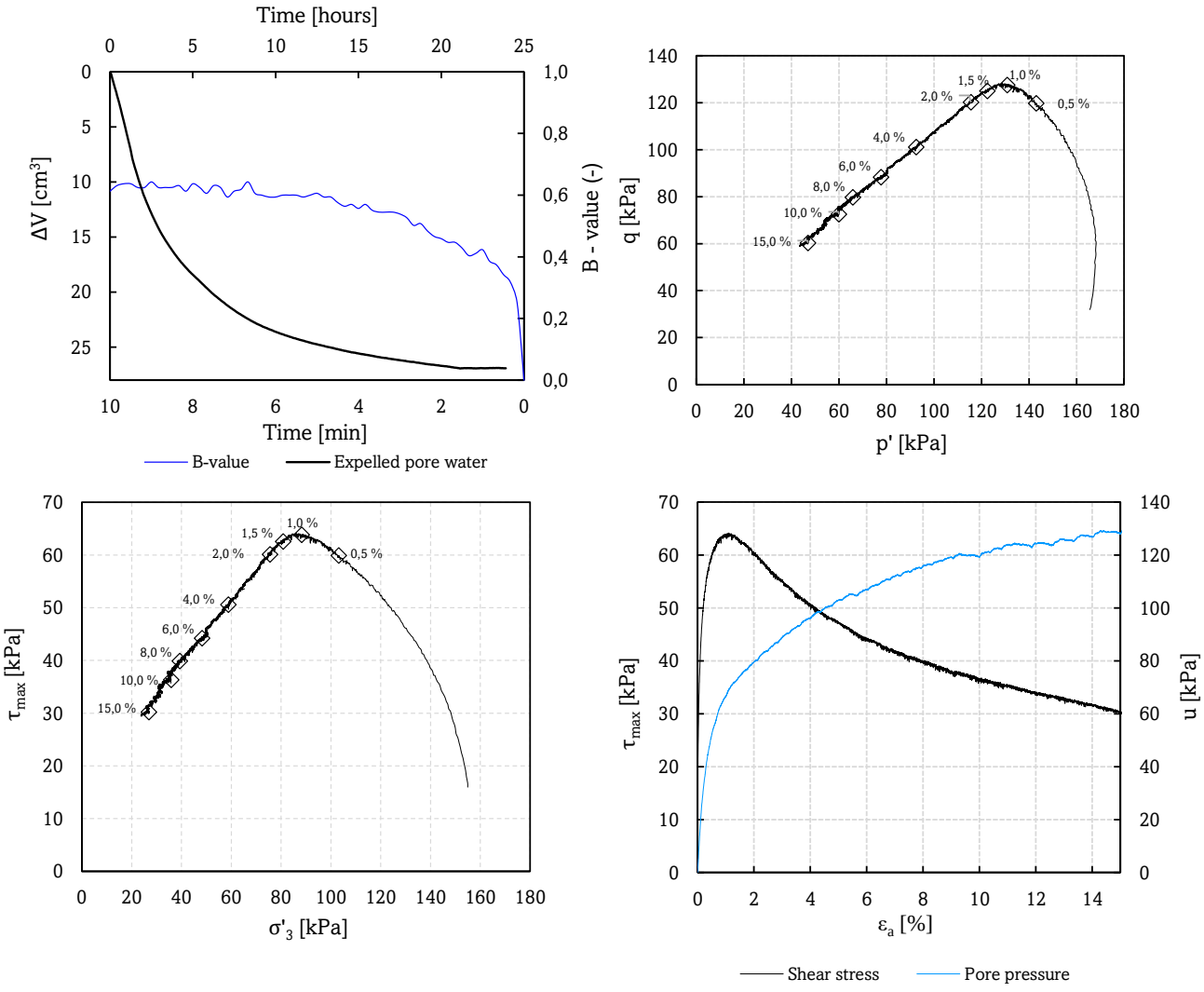

Figure B.13: CAUC - L20 - 54 mm

Triaxial test - MB-2 - CAUC

Depth :	12,2	m
Sampling date :	16.02.2023	
Opening date :	16.02.2023	
Test date :	16.02.2023	
ΔV :	9,99	cm^3
Vertical strain rate $\dot{\varepsilon}$:	2	(% / hour)
ε_v :	4,4	(%)
B-value :	0,92	(-)
σ'_{v0} :	155	kPa
K'_0 :	1	(-)
p' :	134	kPa
γ :	18,9	kN/m^3
w :	41,5	%

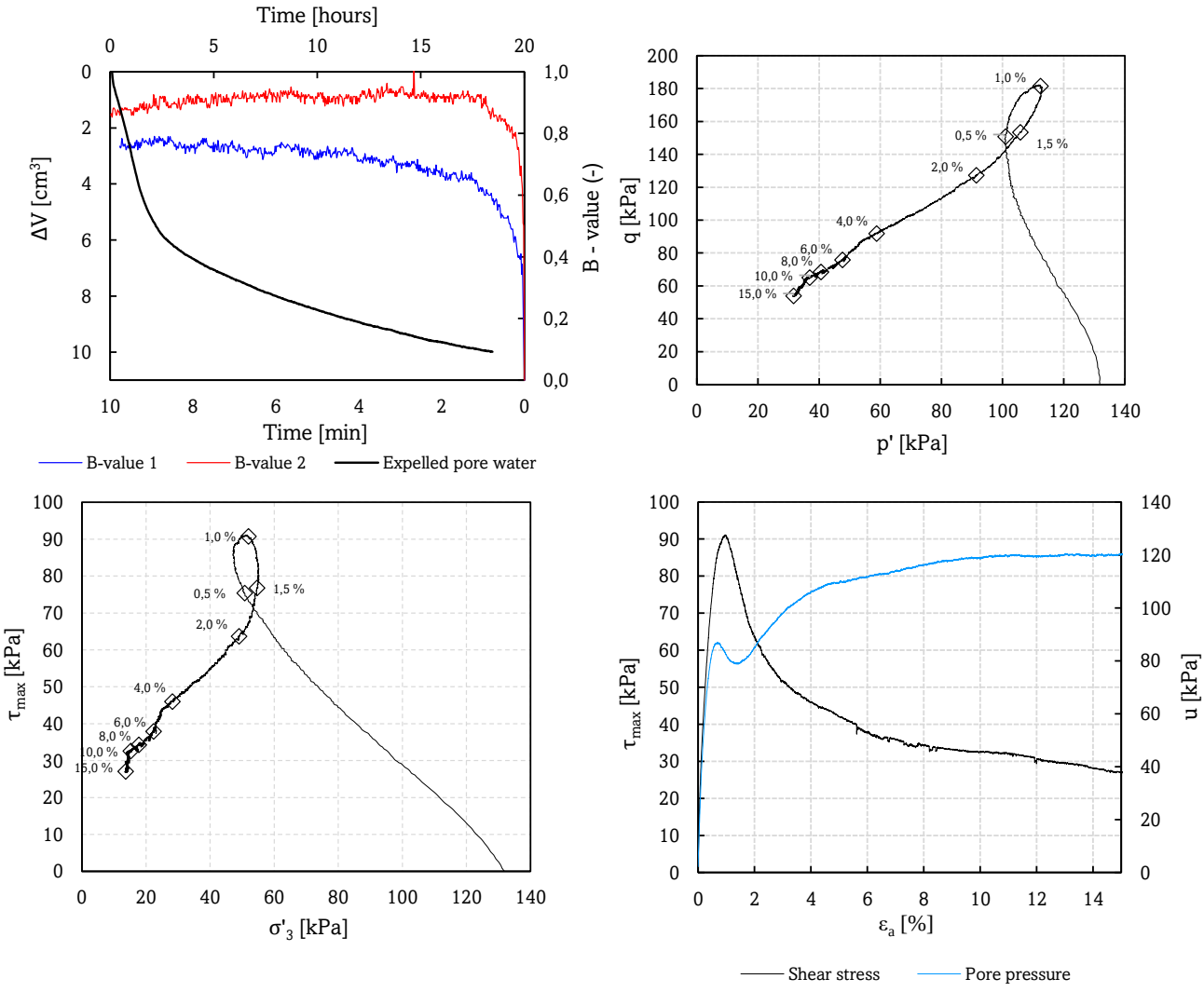

Figure B.14: CIUC - MB-2 - Mini block

Triaxial test - MB-2 - CAUC

Depth :	12,2	m
Sampling date :	16.02.2023	
Opening date :	16.02.2023	
Test date :	16.02.2023	
ΔV :	7,01	cm^3
Vertical strain rate $\dot{\varepsilon}$:	2	(% / hour)
ε_v :	3,1	(%)
B-value :	0,91	(-)
σ'_{v0} :	155	kPa
K'_0 :	0,8	(-)
p' :	134	kPa
γ :	17,16	kN/m^3
w :	41,5	%

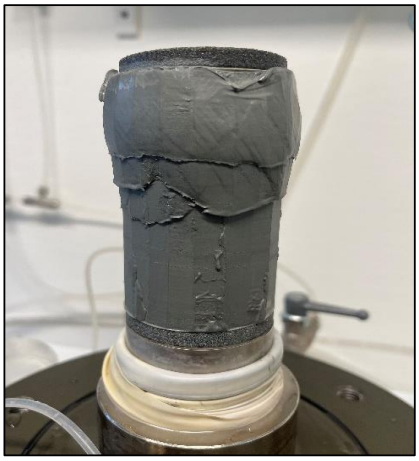

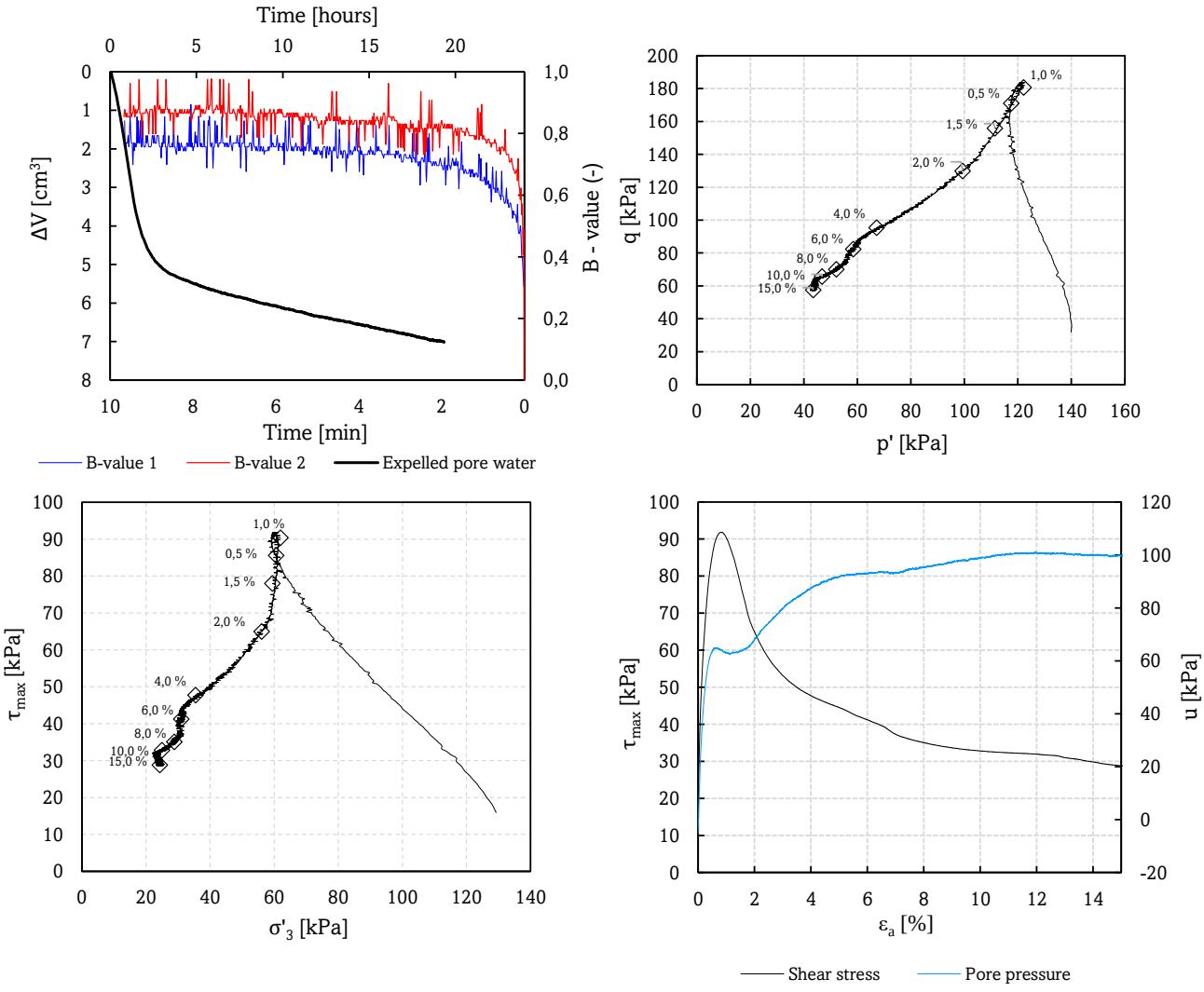

Figure B.15: CAUC - MB-2 - Mini block

Triaxial test - U195 - CIUC

Depth :	12,4	m
Sampling date :	31.01.2023	
Opening date :	03.03.2023	
Test date :	03.03.2023	
ΔV :	6,11	cm^3
Vertical strain rate $\dot{\varepsilon}$:	2	(% / hour)
ε_v :	2,7	(%)
B-value :	0,94	(-)
σ'_{v0} :	155	kPa
K'_0 :	1	(-)
p' :	134	kPa
γ :	19,1	kN/m^3
w :	42	%

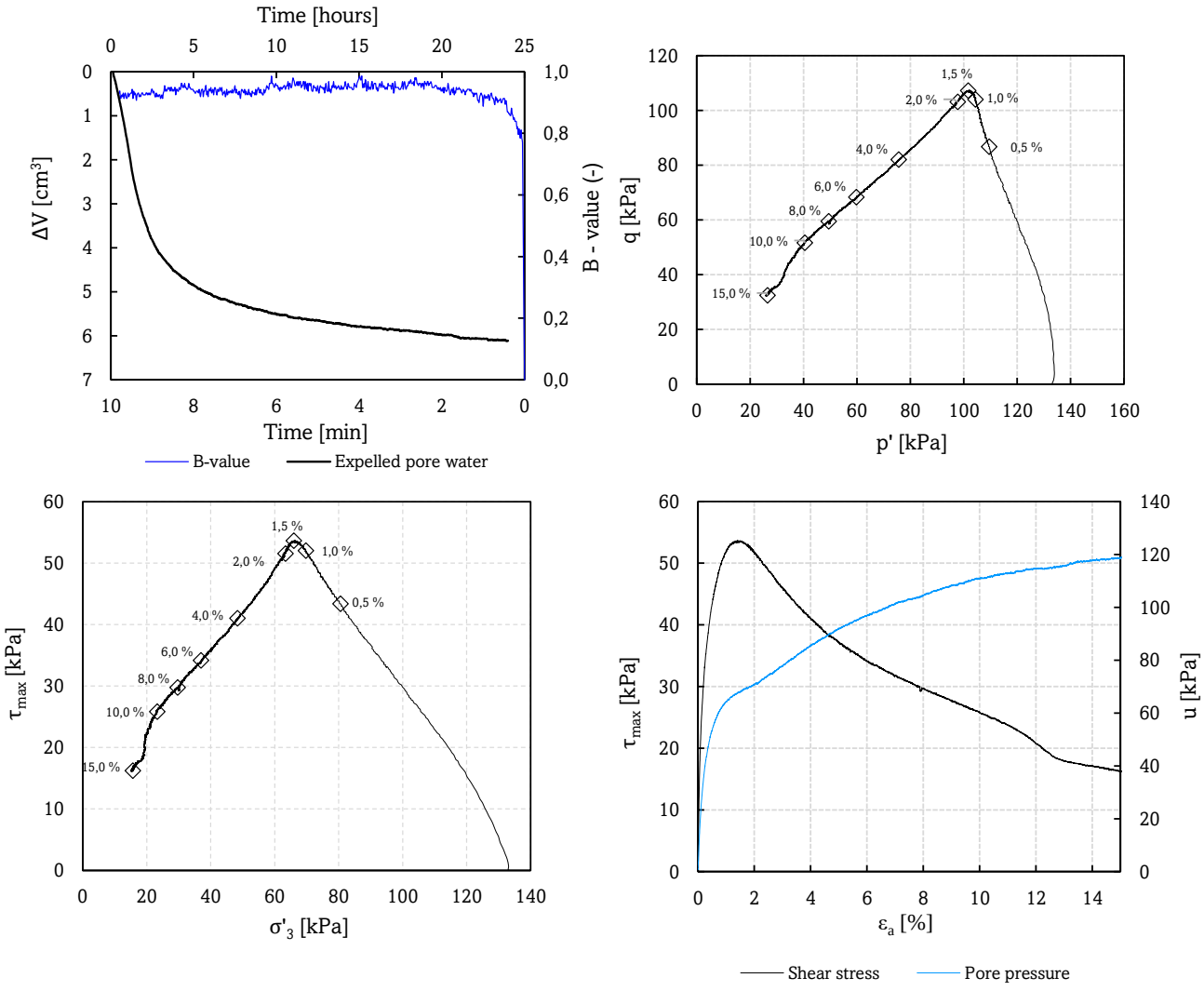

Figure B.16: CIUC - U195 - 54 mm

Triaxial test - U195 - CAUC

Depth :	12,3	m
Sampling date :	31.01.2023	
Opening date :	03.03.2023	
Test date :	03.03.2023	
ΔV :	9,02	cm^3
Vertical strain rate $\dot{\varepsilon}$:	2	(% / hour)
ε_v :	3,9	(%)
B-value :	0,9	(-)
σ'_{v0} :	155	kPa
K'_0 :	0,8	(-)
p' :	134	kPa
γ :	19,1	kN/m^3
w :	42	%

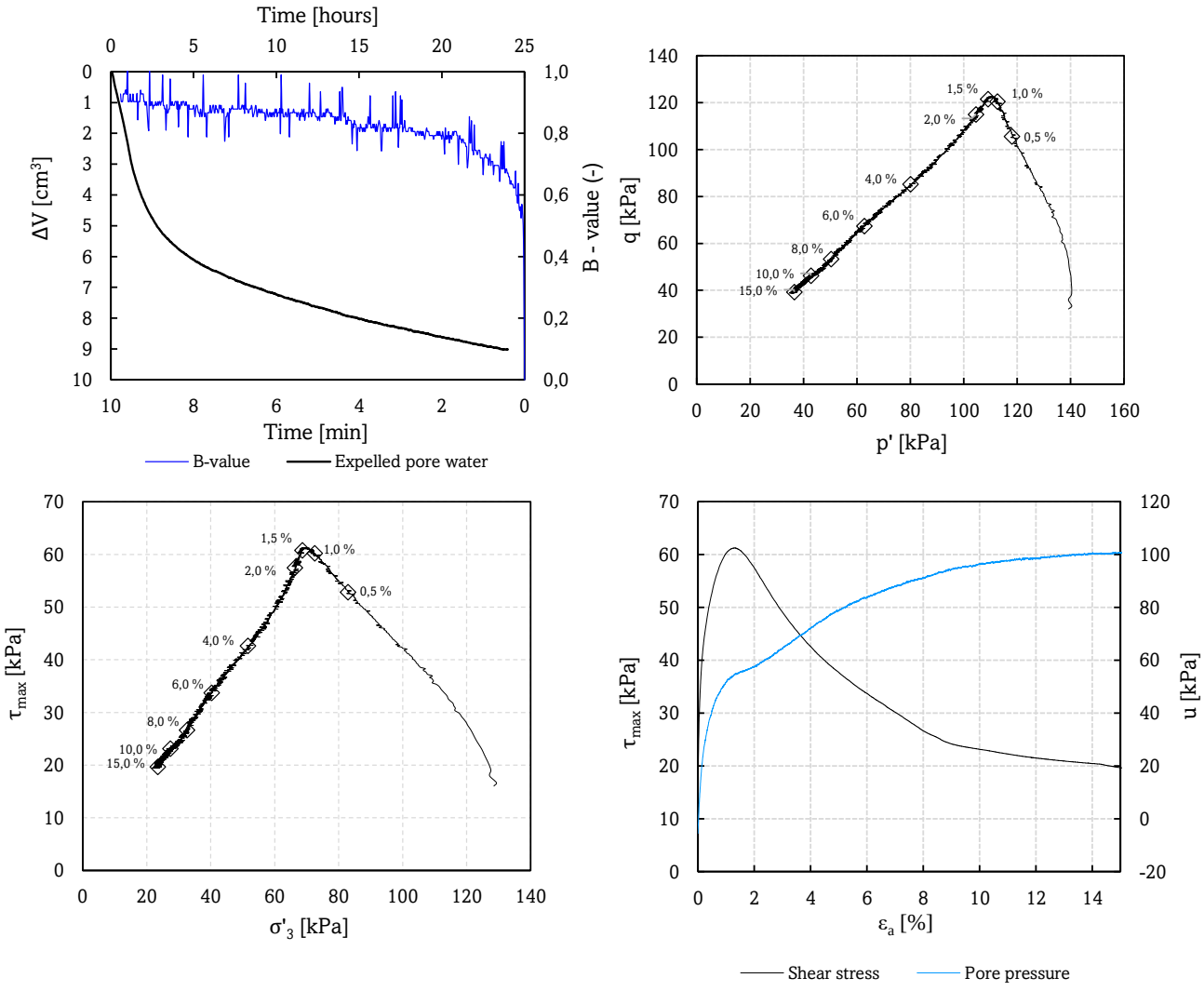

Figure B.17: CAUC - U195 - 54 mm

Triaxial test - MB-4 - CIUC

Depth :	12,2	m
Sampling date :	16.02.2023	
Opening date :	06.03.2023	
Test date :	06.03.2023	
ΔV :	13,3	cm^3
Vertical strain rate $\dot{\varepsilon}$:	2	(% / hour)
ε_v :	5,8	(%)
B-value :	0,89	(-)
σ'_{v0} :	155	kPa
K'_0 :	1	(-)
p' :	134	kPa
γ :	18,3	kN/m^3
w :	42	%

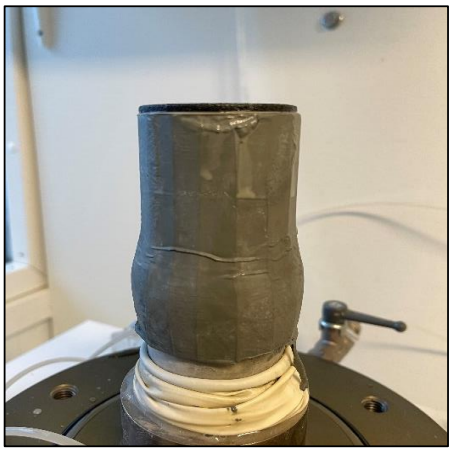

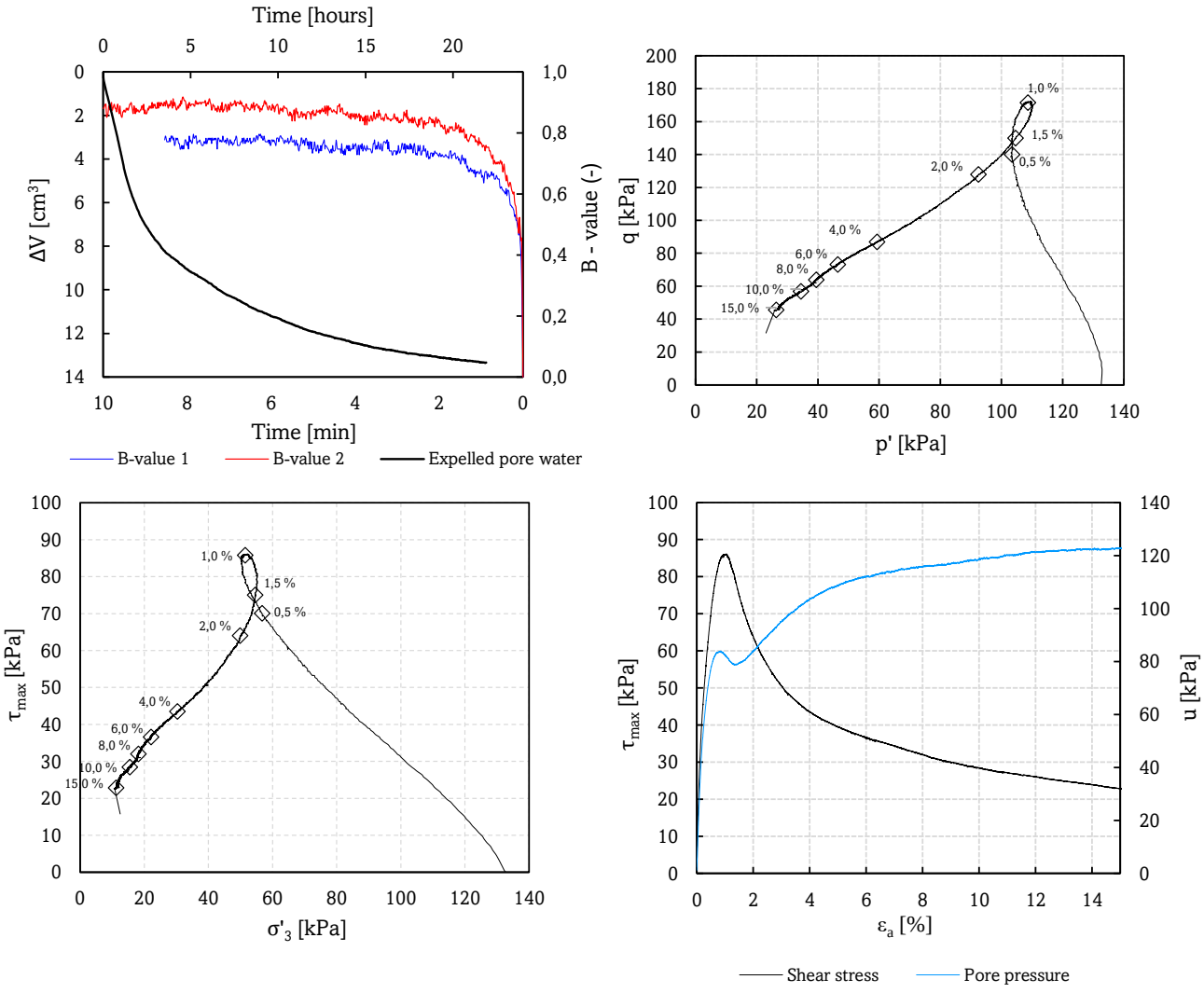

Figure B.18: CIUC - MB-4 - Mini block

Triaxial test - MB-4 - CAUC

Depth :	12,2	m
Sampling date :	16.02.2023	
Opening date :	06.03.2023	
Test date :	06.03.2023	
ΔV :	7,25	cm^3
Vertical strain rate $\dot{\varepsilon}$:	2	(% / hour)
ε_v :	3,2	(%)
B-value :	0,89	(-)
σ'_{v0} :	155	kPa
K'_0 :	0,8	(-)
p' :	134	kPa
γ :	18,3	kN/m^3
w :	42	%

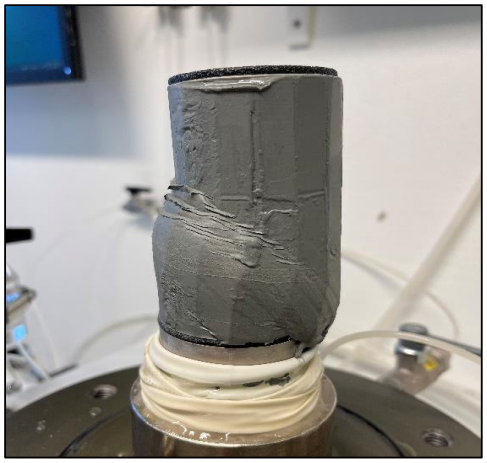

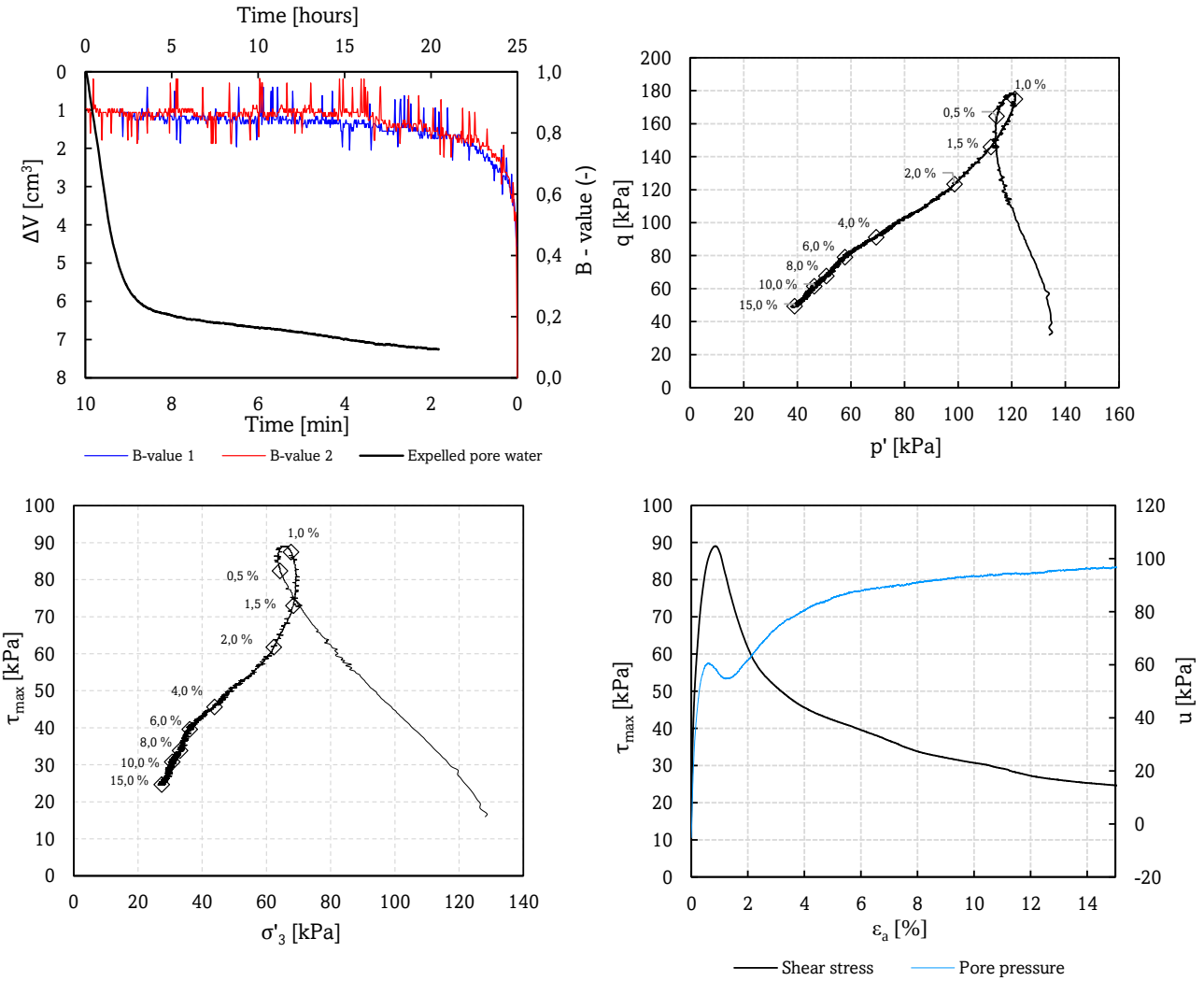

Figure B.19: CAUC - MB-4 - Mini block

Treaksialforsøk

Dybde:	9,5	m	σ'_{v0} :	125	kPa
Prøvetakingsdato:	11.02.2023		K'_{0} :	0,7	(-)
Prøveåpningsdato:	11.02.2023		γ :	18,5	kN/m^3
Testdato:	01.03.2023		w :	42	%
Test ID:	MB-3		$\dot{\sigma}$	0.2	kPa/min

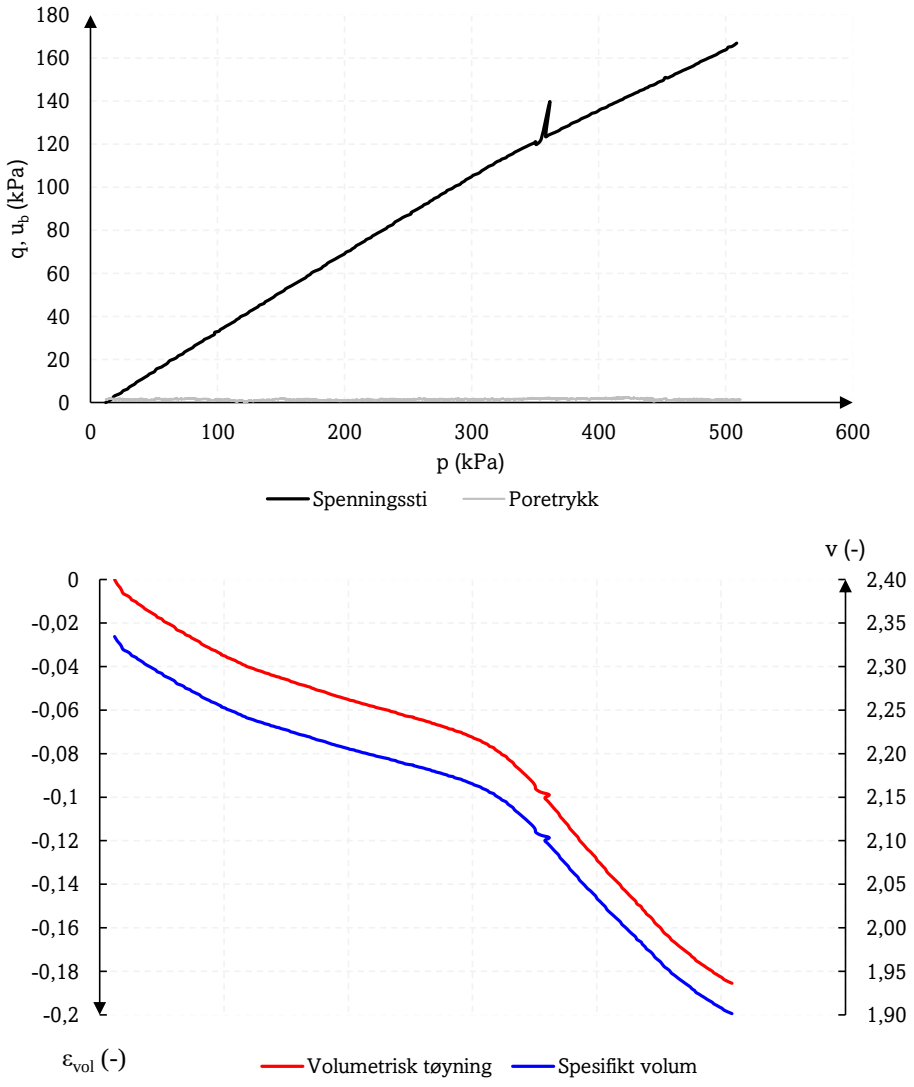

Figure B.20: Constant K'_0 - MB-3 - Mini block

Treaksialforsøk

Dybde:	9,5	m	σ'_{v0} :	125	kPa
Prøvetakingsdato:	11.02.2023		K'_{0} :	0,8	(-)
Prøveåpningsdato:	01.03.2023		γ :	18,5	kN/m^3
Testdato:	01.03.2023		w :	42	%
Test ID:	MB-3		$\dot{\sigma}$	0.2	kPa/min

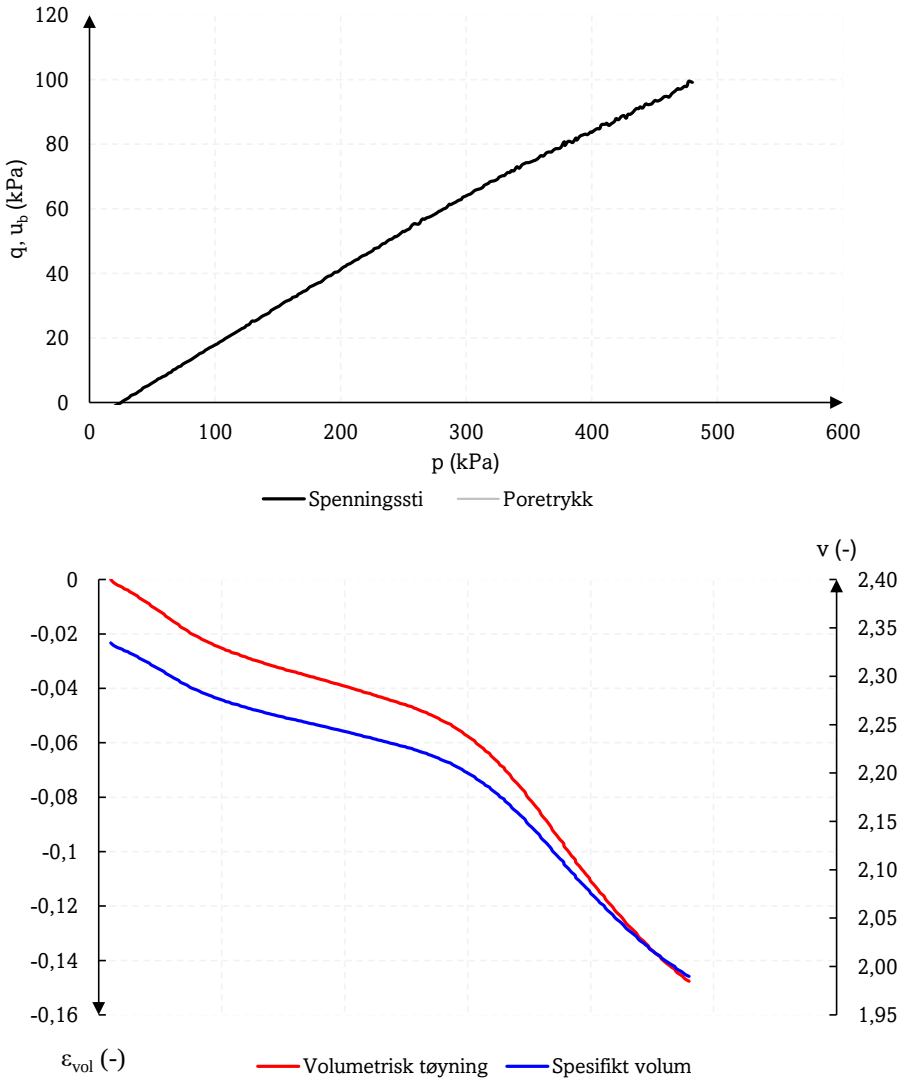

Figure B.21: Constant K'_0 - MB-3 - Mini block

Triaxial test - K'_0 consolidation - MB-3

Depth:	9,5	m	σ'_{v0} :	125	kPa
Sampling date:	11.02.2023		K'_{0} :	≈	(-)
Test opening date:	01.03.2023		γ :	18,5	kN/m^3
Test date:	01.03.2023		w :	42	%
Test ID:	MB-3		$\dot{\sigma}$	0.2	kPa/min

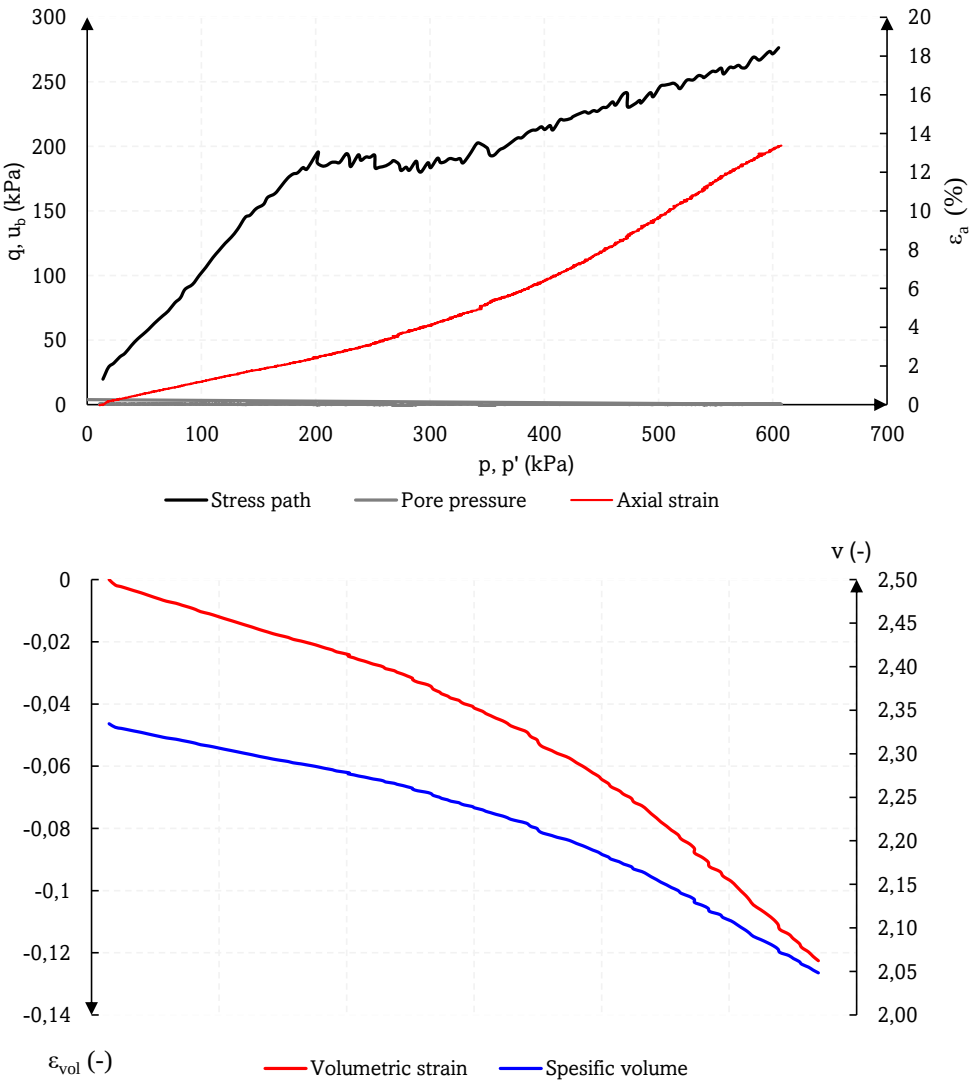

Figure B.22: K'_0-consolidation - MB-3 - Mini block

Triaxial test - K_0' consolidation - MB-4

Dybde:	12,5	m	σ'_{v0} :	155	kPa
Prøvetakingsdato:	16.02.2023		K'_{0} :	-	(-)
Prøveåpningsdato:	06.03.2023		γ :	18,3	kN/m^3
Testdato:	08.03.2023		w :	42	%
Test ID:	MB-4		$\dot{\sigma}$	0.2	kPa/min

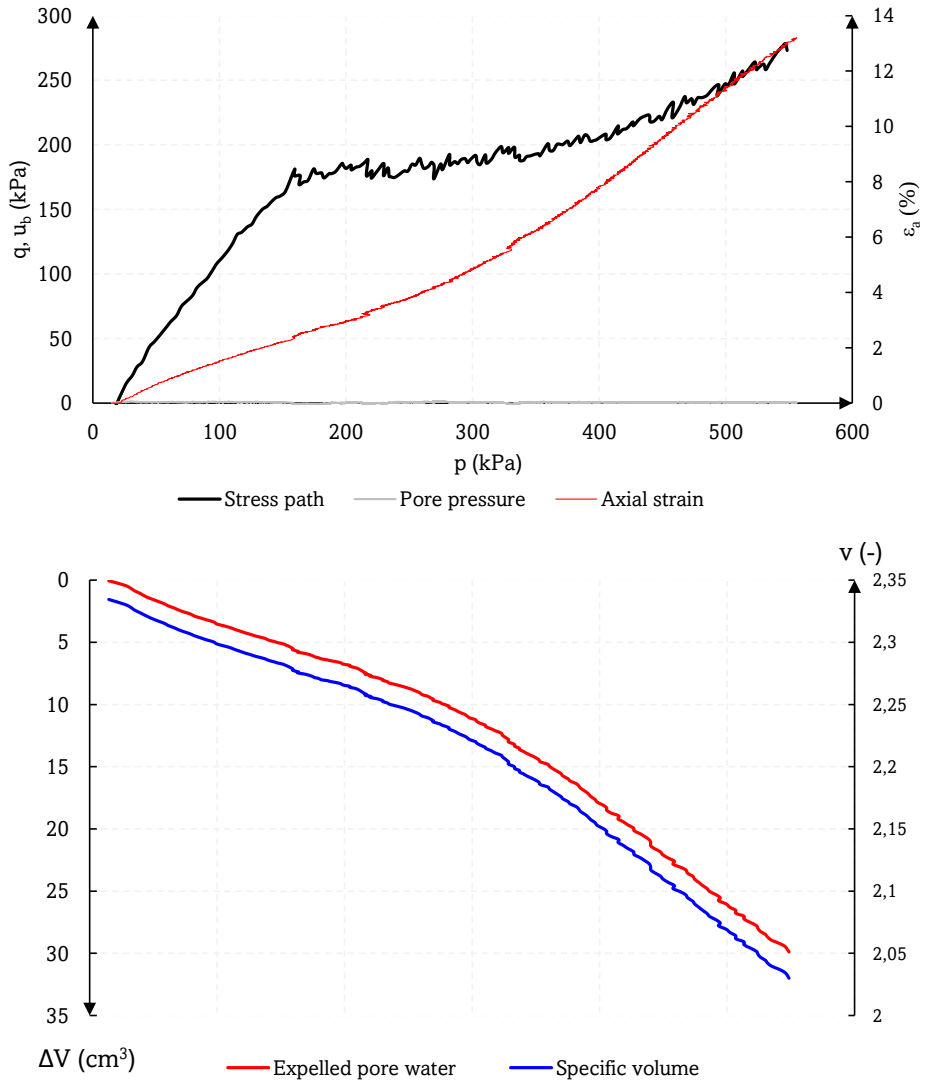

Figure B.23: K_0'-consolidation - MB-4 - Mini block

Triaxial test - MB-4 - CIDC

Depth :	12,4	m
Sampling date :	16.02.2023	
Opening date :	06.03.2023	
Test date :	08.03.2023	
ΔV :	5,69	cm^3
Vertical strain rate $\dot{\varepsilon}$:	2	(% / hour)
ε_v :	2,5	(%)
B-value :	-	(-)
σ'_{v0} :	155	kPa
K'_0 :	-	(-)
p' :	134	kPa
γ :	18,3	kN/m^3
w :	42	%

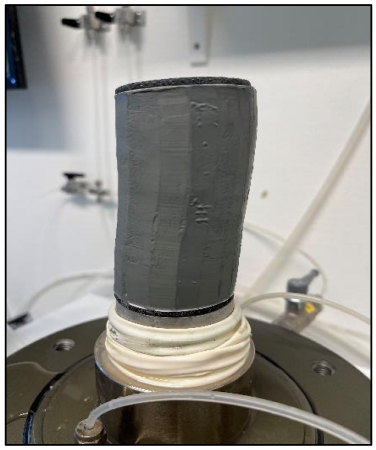

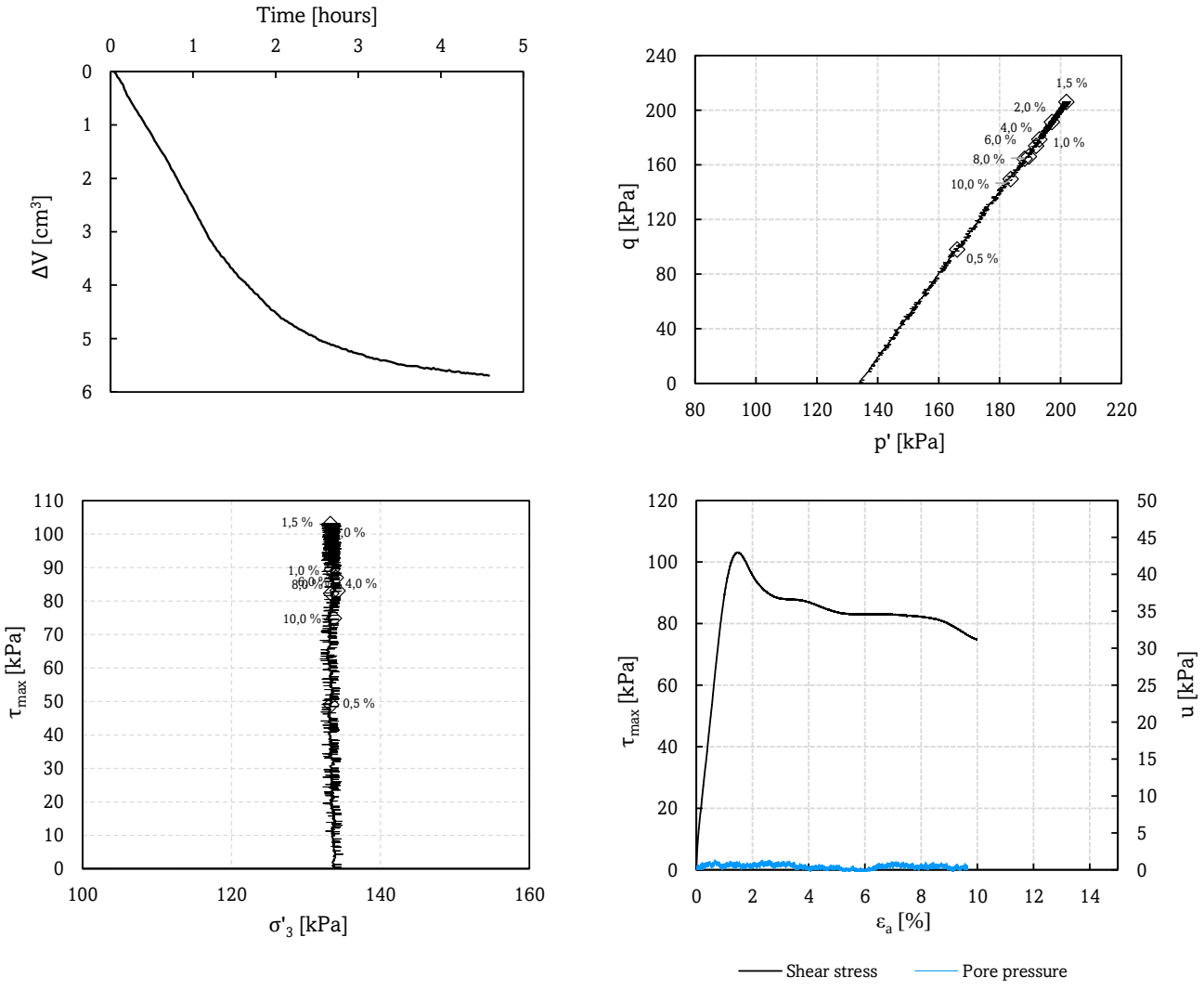

Figure B.24: CIDC - MB-4 - Mini block

Triaxial test - MB-4 - CIUC

Depth :	12,5	m
Sampling date :	16.02.2023	
Opening date :	06.03.2023	
Test date :	10.03.2023	
ΔV :	4,92	cm^3
Vertical strain rate $\dot{\varepsilon}$:	2	(% / hour)
ε_v :	2,1	(%)
B-value :	0,94	(-)
σ'_{v0} :	155	kPa
K'_0 :	1	(-)
p' :	134	kPa
γ :	18,1	kN/m^3
w :	42	%

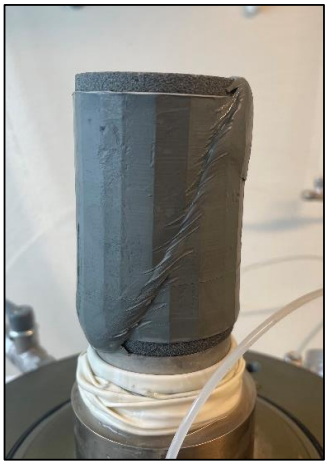

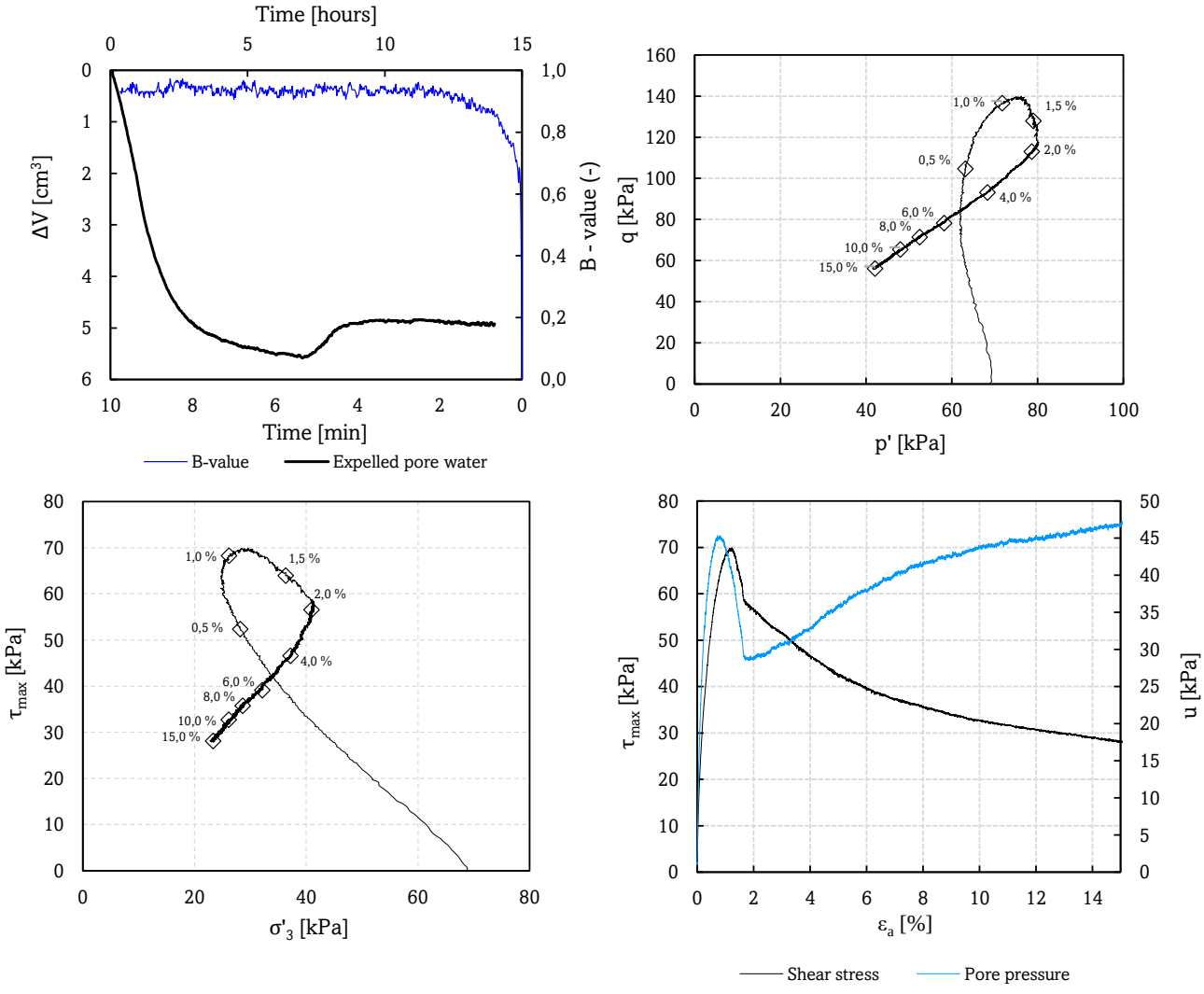

Figure B.25: CIUC - MB-4 - Mini block - Isotropically unloaded

Triaxial test - MB-4 - CIUC

Depth :	12,5	m
Sampling date :	16.02.2023	
Opening date :	06.03.2023	
Test date :	10.03.2023	
ΔV :	6,28	cm^3
Vertical strain rate $\dot{\varepsilon}$:	2	(% / hour)
ε_v :	2,7	(%)
B-value :	0,93	(-)
σ'_{v0} :	155	kPa
K'_0 :	1	(-)
p' :	134	kPa
γ :	18,1	kN/m^3
w :	42	%

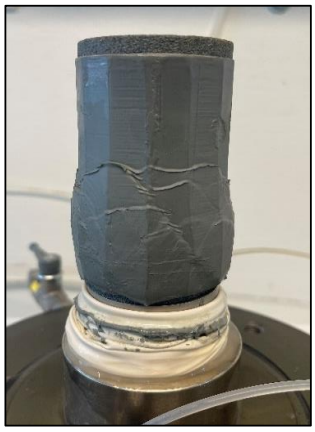

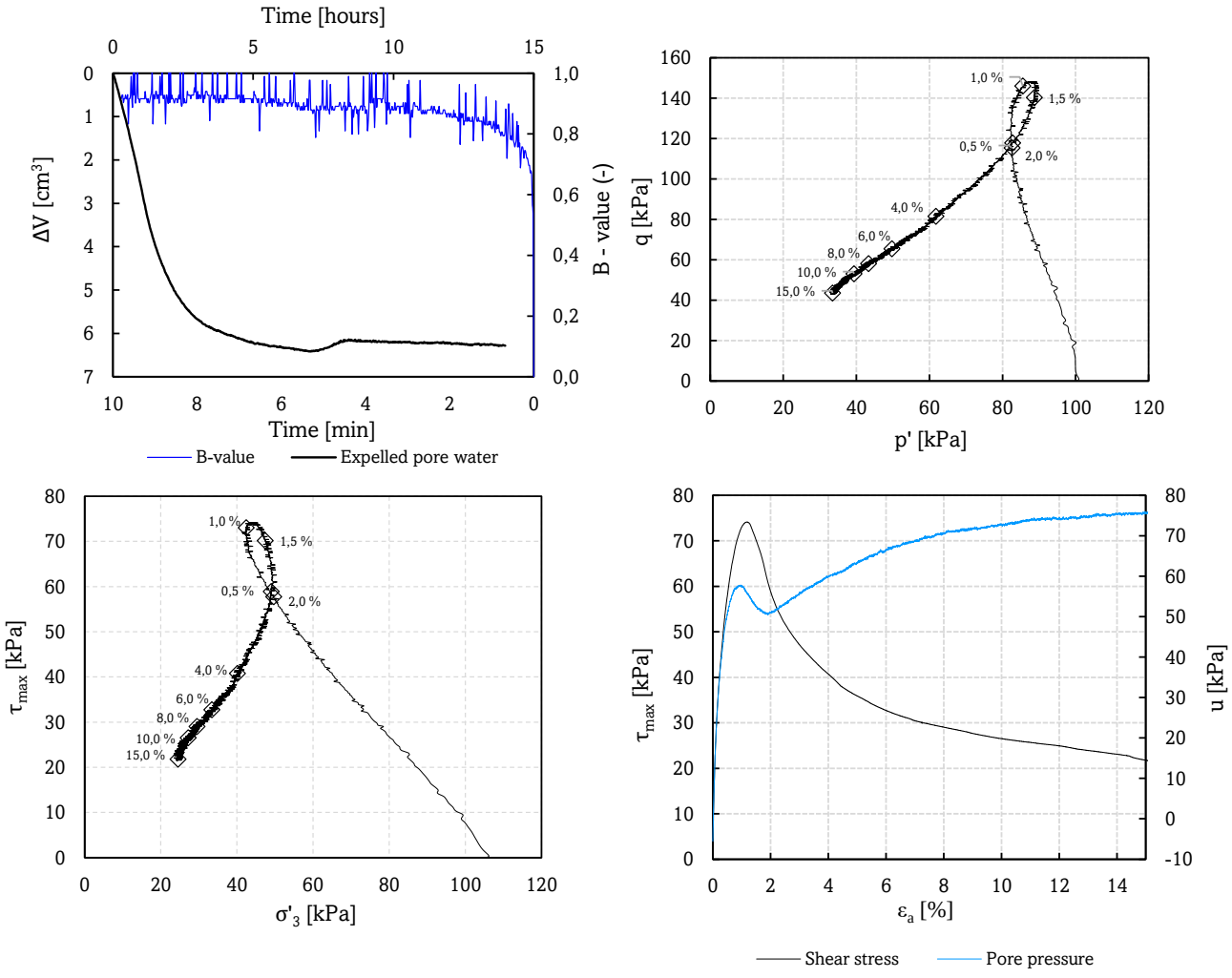

Figure B.26: CIUC - MB-4 - Mini block - Isotropically unloaded

Appendix C

Results: Oedometer tests

Sample ID	Type	Depth *(m)*	Storage *(months)*	Type	σ'_{v0} *(kPa)*	σ'_{cv} *(kPa)*	OCR *(-)*	$\dot{\varepsilon}$ (%/hour)	M_0/M_L (-)	Figure
U67	54 mm	9.5	0	CRS	125	170	1.36	1.5	3.0	C.3
MB-1	Mini block	9.2	0	CRS	125	315	2.52	1.5	4.9	C.4
U172	54 mm	9.5	1	CRS	125	210	1.68	1.5	1.9	C.5
MB-3	Mini block	9.4	1	CRS	125	245	1.96	1.5	2.9	C.6
L-20	54 mm	12.6	0	CRS	155	225	1.45	1.5	1.0	C.7
MB-2	Mini block	12.3	0	CRS	155	320	2.06	1.5	7.5	C.8
U195	54 mm	12.6	1	CRS	155	250	1.61	1.5	6.6	C.9
MB-4	Mini block	12.2	1	CRS	155	185	1.19	1.5	4.9	C.10
MB-3	Mini block	9.4	1	CRS	125	195	1.56	0.75	5.0	C.11
MB-3	Mini block	9.5	1	CRS	125	230	1.84	3.0	4.2	C.12

Table C.1: Results: oedometer tests

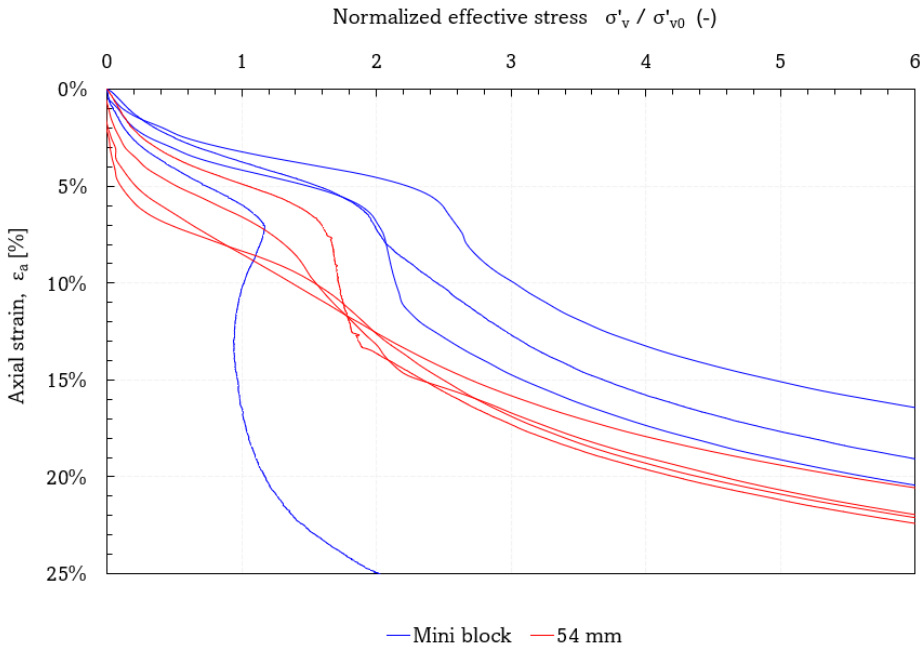

(a) Every oedometer curves from the CRS test series run by $\dot{\varepsilon} = 1.5$ %/hour.

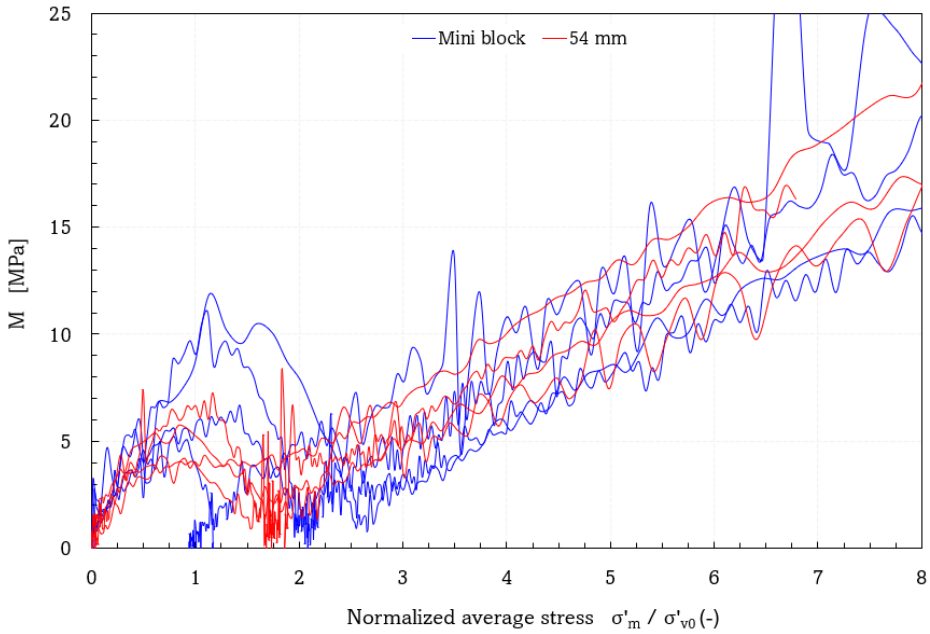

(b) Every modulus curves from the CRS test series run by $\dot{\varepsilon} = 1.5$ %/hour.

Figure C.1: Every oedometer and modulus curves obtained from the CRS test series run by $\dot{\varepsilon} = 1.5$ %/hour.

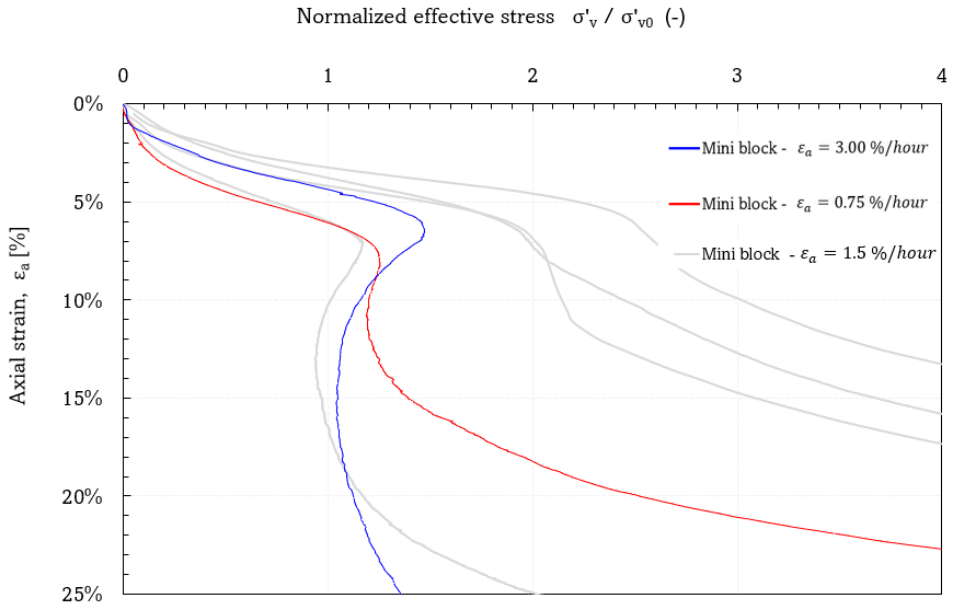

(a) Every oedometer curves from the CRS test series run by both lower and higher strain rates.

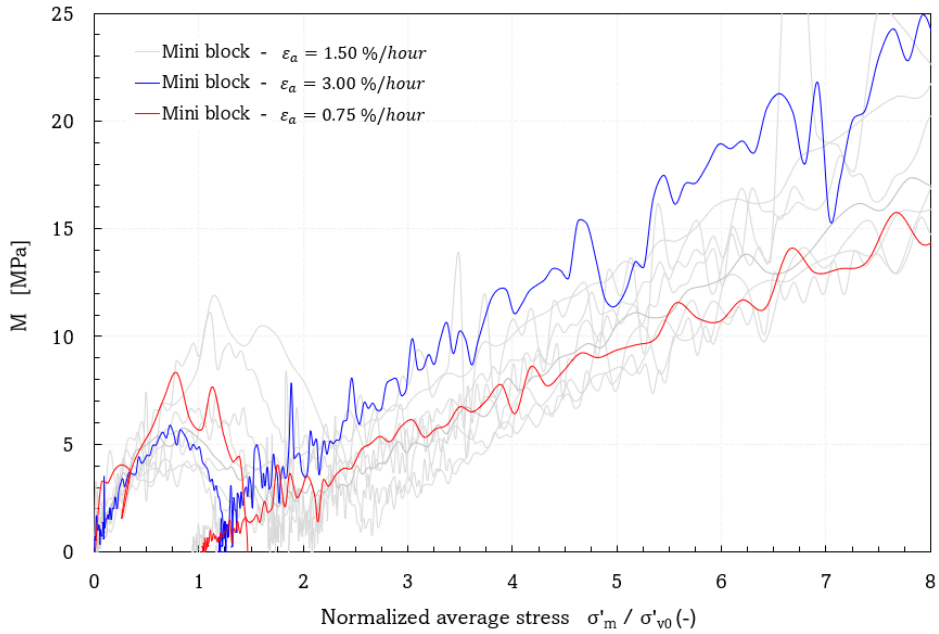

(b) Every modulus curves from the CRS test series run by both lower and higher strain rates.

Figure C.2: Every oedometer and modulus curves obtained from the CRS test series run by lower and higher strain rates.

Oedometer test - U67 - 54 mm - CRS

Depth :	9,5	m	σ'_{v0}	125	kPa
Sampling date :	31.01.2023		σ'_{cv}	180	kPa
Opening date:	03.02.2023		OCR	1,44	[-]
Test date :	03.02.2023		Strain rate, $\dot{\varepsilon}$	1,50	%/hr
γ :	18,6	kN/m^3	M_0/M_L	3,00	[-]
w :	46,0	%	$\Delta e/e_0$	0,11	[-]

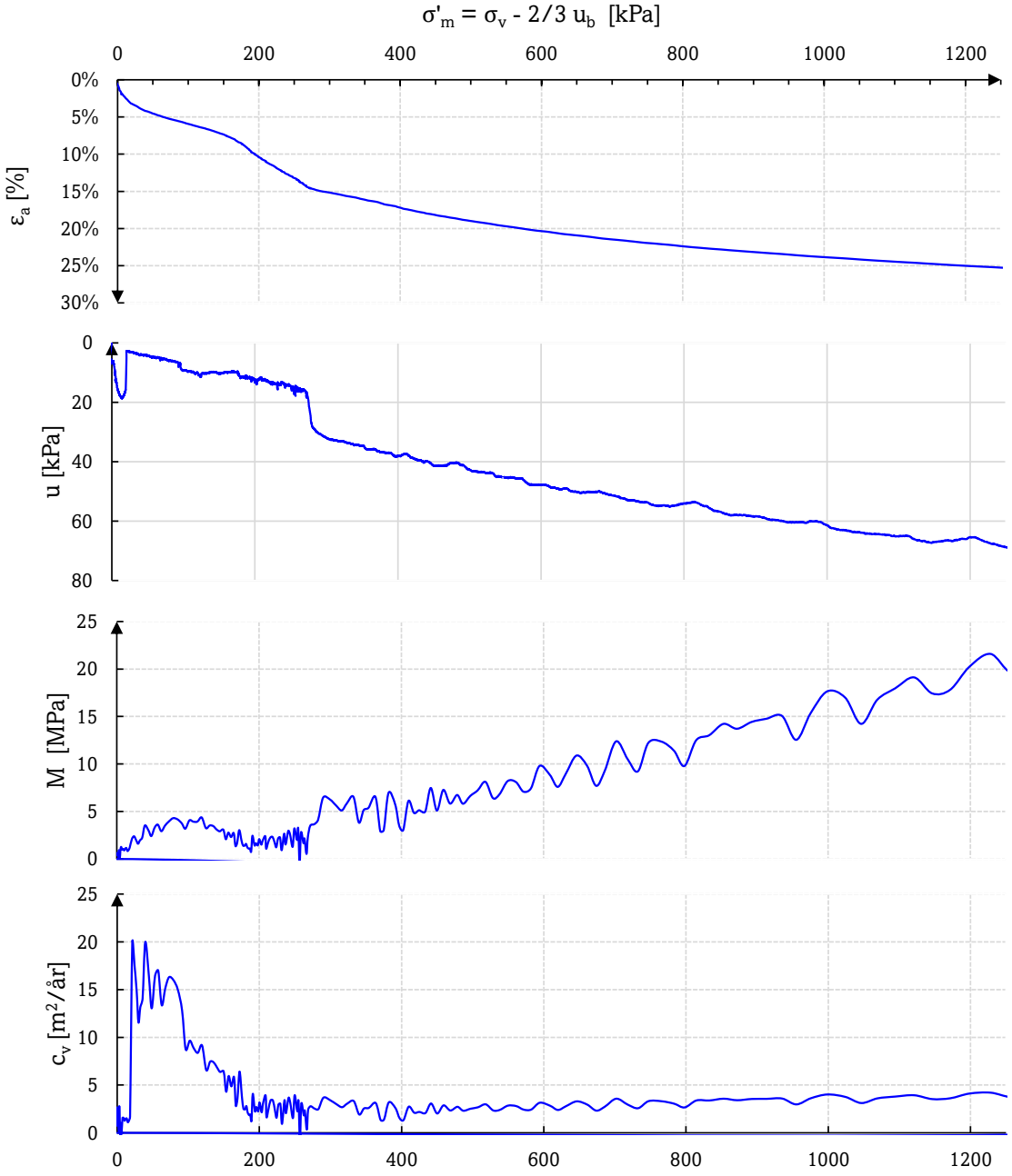

Figure C.3: CRS - U67 - 54mm

Oedometer test - MB-1 - Mini block - CRS

Depth :	9,2	m	σ'_{v0}	125	kPa
Sampling date :	11.02.2023		σ'_{cv}	320	kPa
Opening date:	11.02.2023		OCR	2,56	[-]
Test date :	11.02.2023		Strain rate, $\dot{\varepsilon}$	1,50	%/hr
γ	21,0	kN/m^3	M_0/M_L	4,86	[-]
w :	43,2	%	$\Delta e/e_0$	0,058	[-]

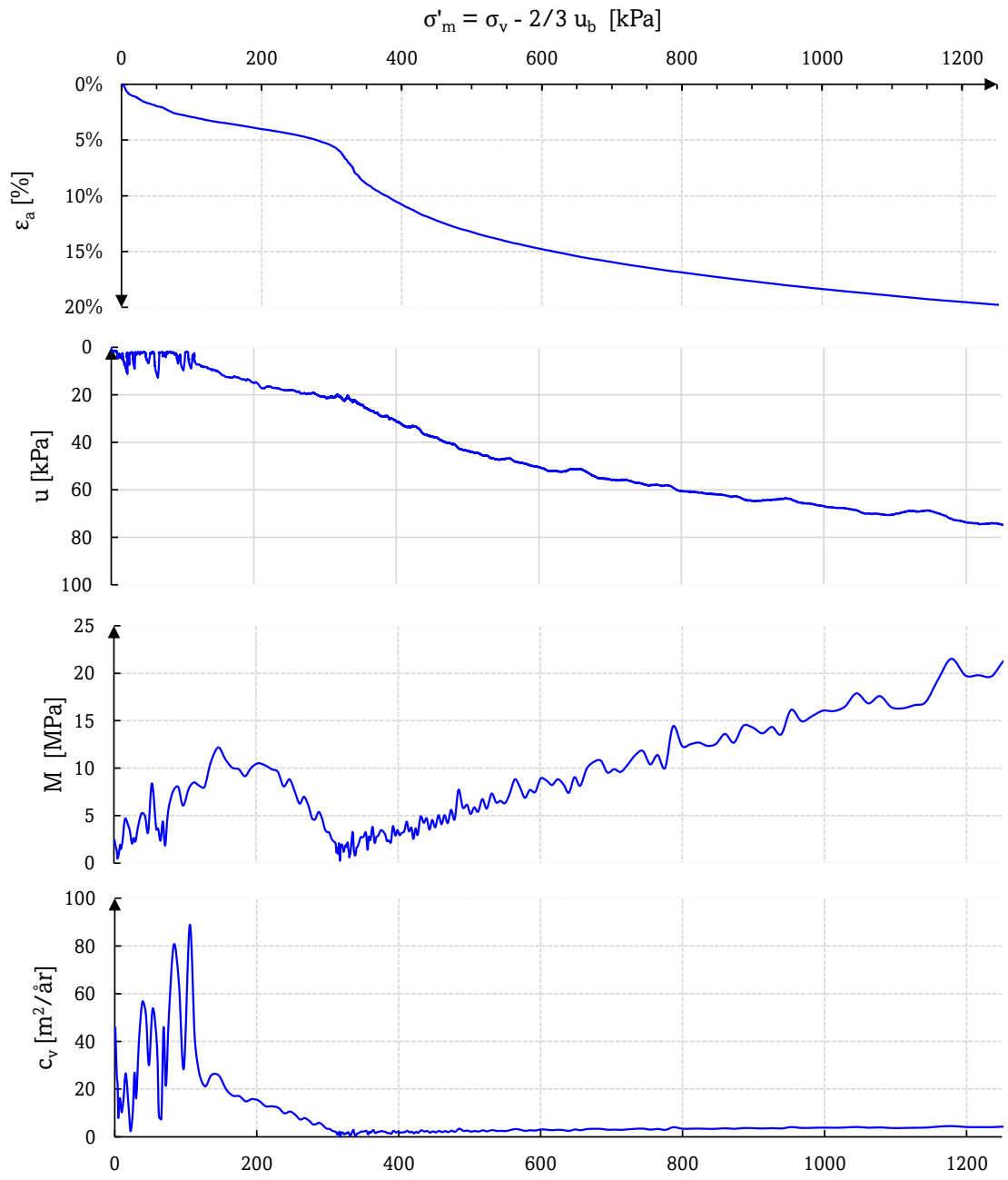

Figure C.4: CRS - MB-1 - Mini block

Oedometer test - U172 - 54 mm - CRS

Depth :	9,6	m	σ'_{v0}	125	kPa
Sampling date :	22.12.2022		σ'_{cv}	215	kPa
Opening date:	30.01.2023		OCR	1,72	[-]
Test date :	30.01.2023		Strain rate, $\dot{\varepsilon}$	1,50	%/hr
γ	17,7	kN/m^3	M_0/M_L	1,89	[-]
w :	40,1	%	$\Delta e/e_0$	0,15	[-]

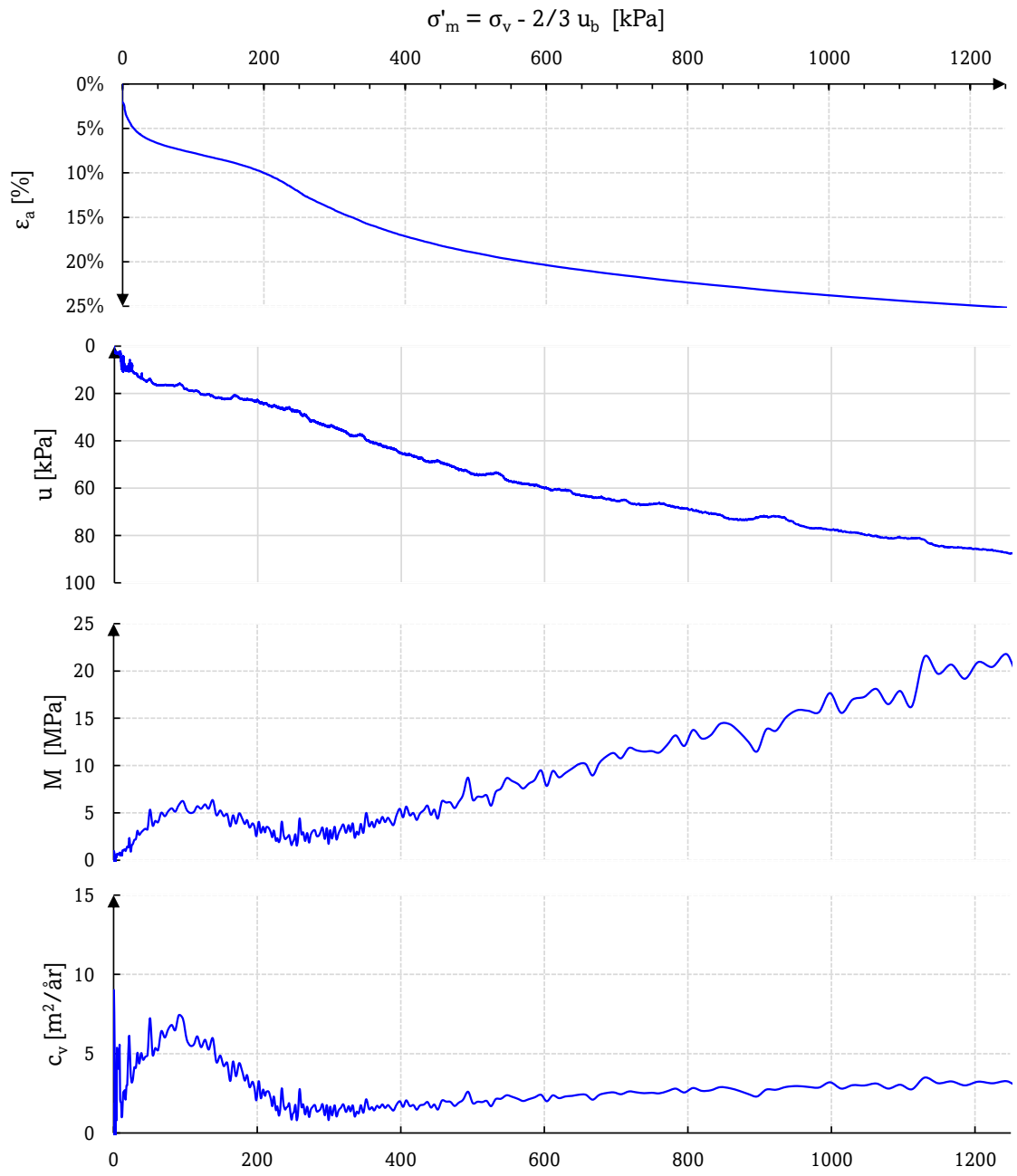

Figure C.5: CRS - U172 - 54mm

Oedometer test - MB-3 - Mini block - CRS

Depth :	9,4	m	σ'_{v0}	125	kPa
Sampling date :	11.02.2023		σ'_{cv}	190	kPa
Opening date:	27.02.2023		OCR	1,52	[-]
Test date :	27.02.2023		Strain rate, $\dot{\varepsilon}$	1,5	%/hr
γ	19,1	kN/m^3	M_0/M_L	2,94	[-]
w :	41,6	%	$\Delta e/e_0$	0,11	[-]

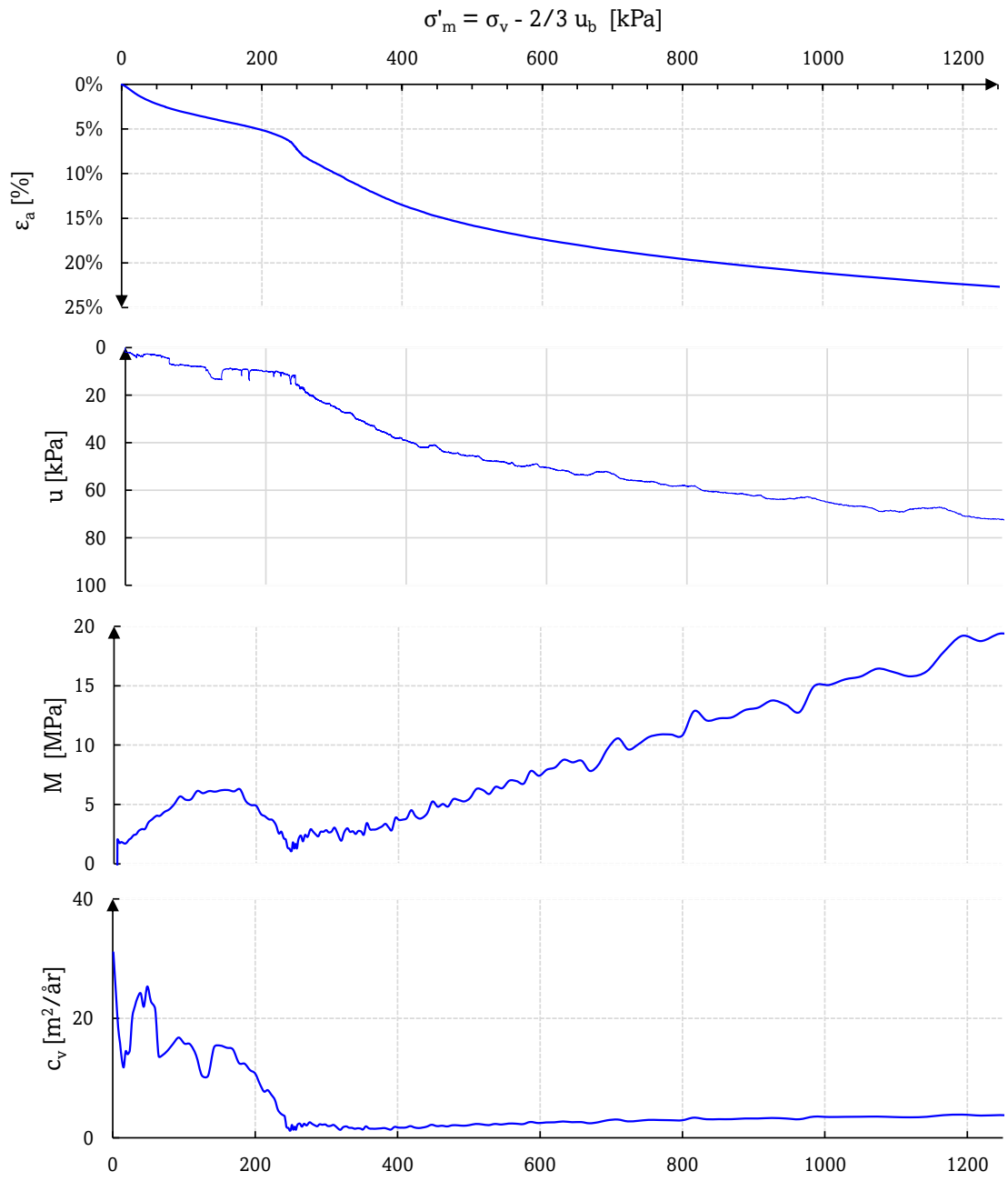

Figure C.6: CRS - MB-3 - Mini block

Oedometer test - L20 - 54 mm - CRS

Depth :	12,7	m	σ'_{v0}	155	kPa
Sampling date :	16.01.2023		σ'_{cv}	240	kPa
Opening date:	24.01.2023		OCR	1,55	[-]
Test date :	24.01.2023		Strain rate, $\dot{\varepsilon}$	1,50	%/hr
γ	18,1	kN/m^3	M_0/M_L	1,00	[-]
w :	41,3	%	$\Delta e/e_0$	0,15	[-]

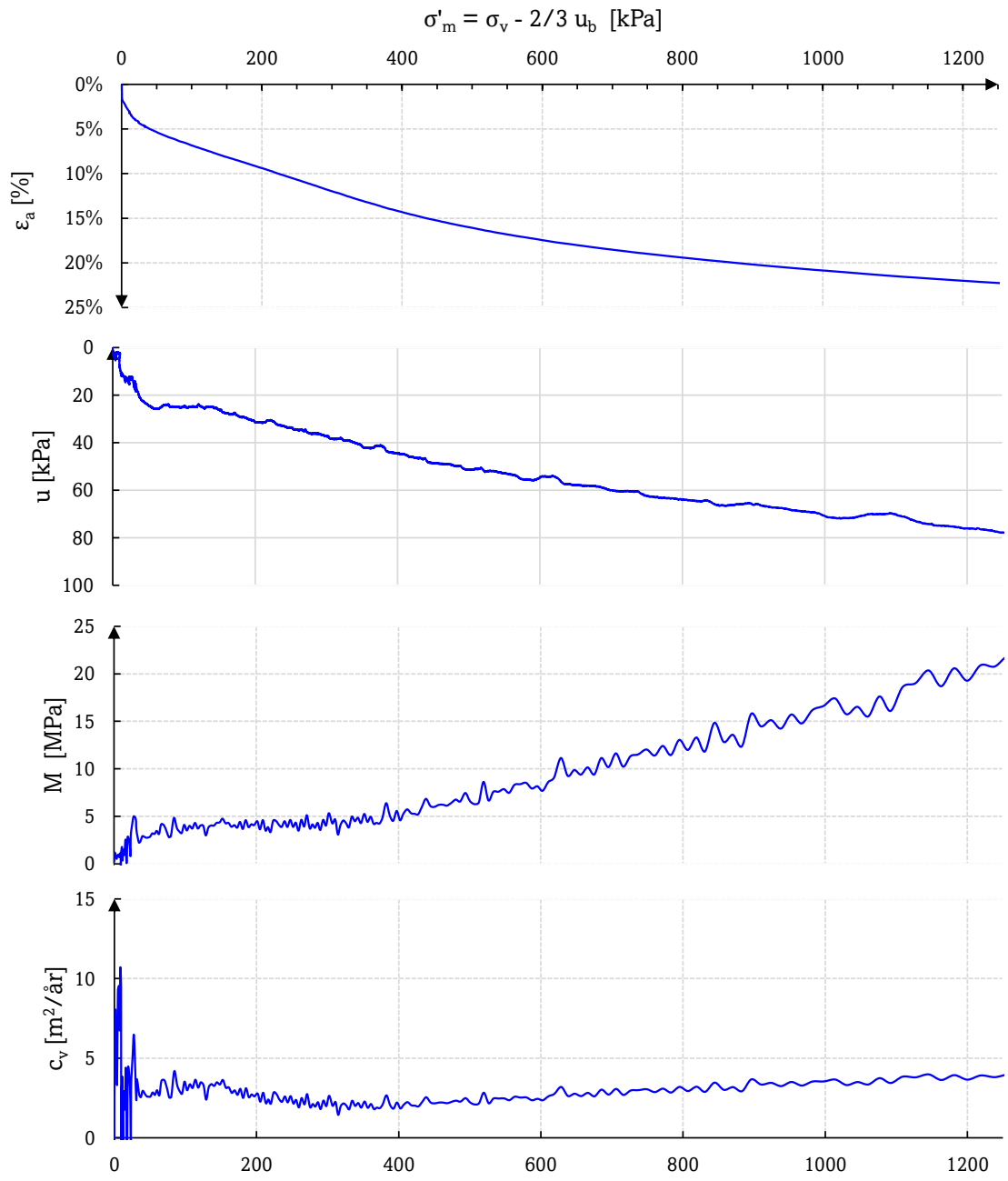

Figure C.7: CRS - L20 - 54mm

Oedometer test - MB-2 - Mini block - CRS

Depth :	12,3	m	σ'_{v0}	155	kPa
Sampling date :	16.02.2023		σ'_{cv}	320	kPa
Opening date:	16.02.2023		OCR	2,06	[-]
Test date :	16.02.2023		Strain rate, $\dot{\varepsilon}$	1,50	%/hr
γ	17,9	kN/m^3	M_0/M_L	7,50	[-]
Comment :	41,5	%	$\Delta e/e_0$	0,074	[-]

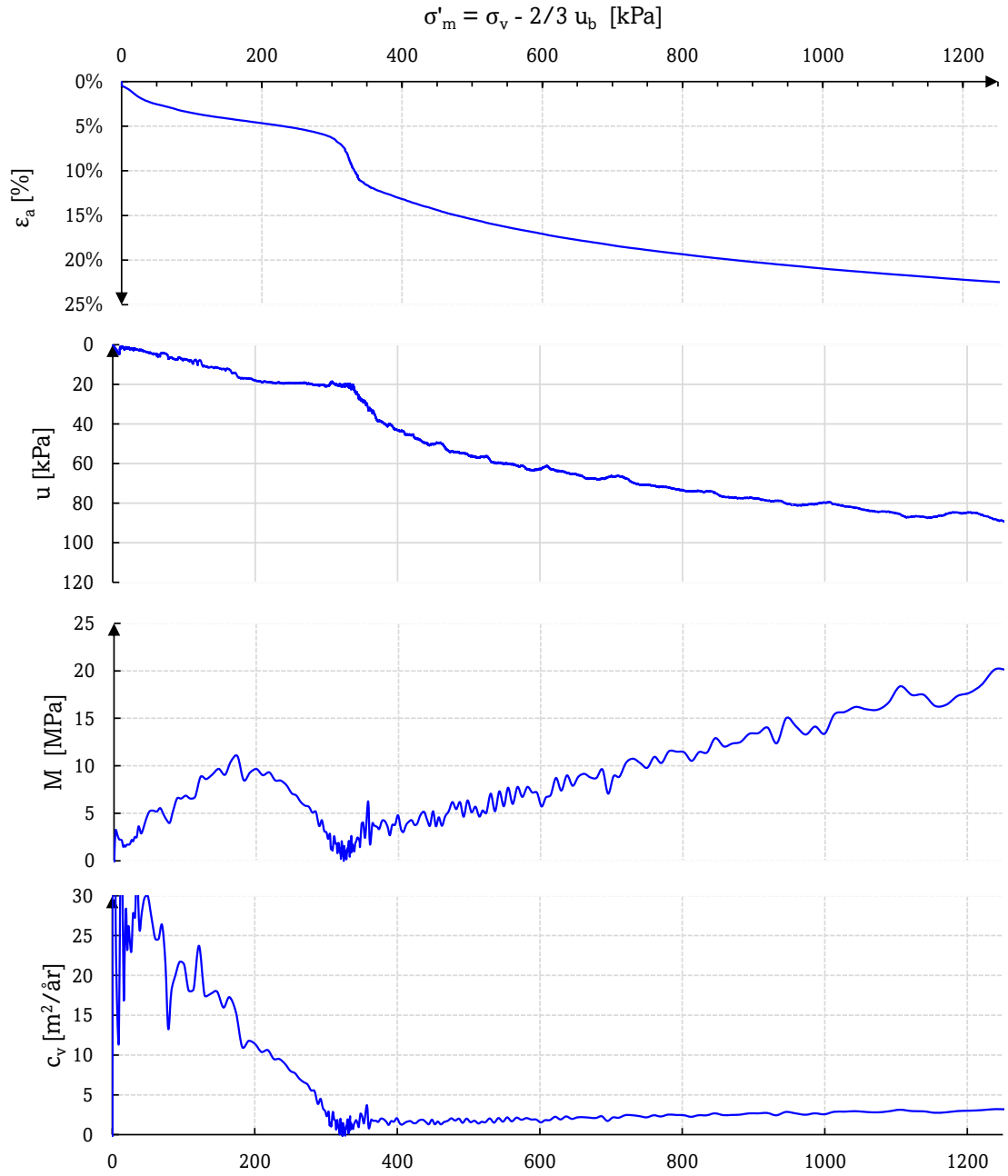

Figure C.8: CRS - MB-2 - Mini block

Oedometer test - U195 - 54 mm - CRS

Depth :	12,6	m	σ'_{v0}	155	kPa
Sampling date :	31.01.2023		σ'_{cv}	260	kPa
Opening date:	03.03.2023		OCR	1,68	[-]
Test date :	03.03.2023		Strain rate, $\dot{\varepsilon}$	1,50	%/hr
γ	19,1	kN/m^3	M_0/M_L	6,60	[-]
w :	42,4	%	$\Delta e/e_0$	0,091	[-]

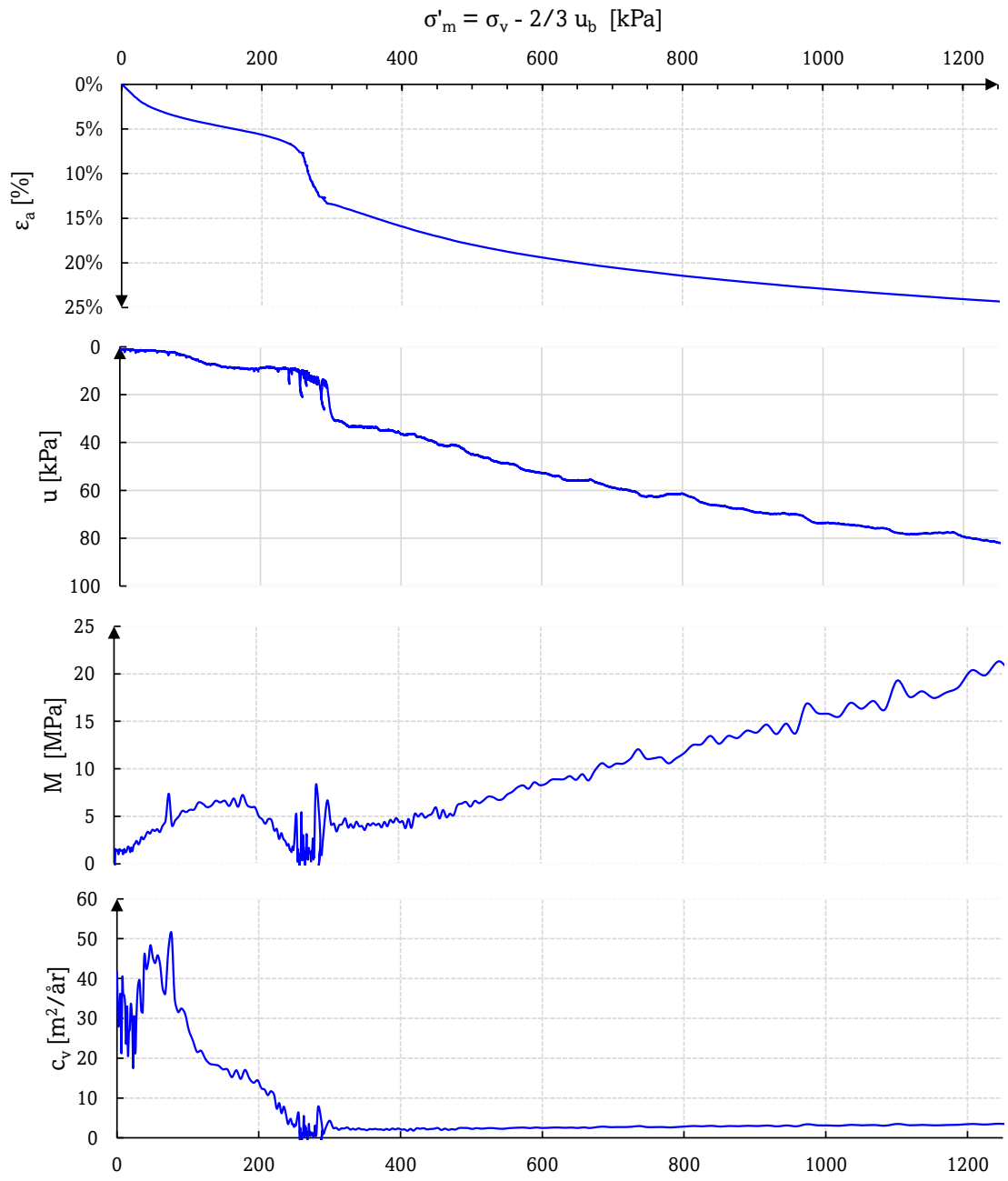

Figure C.9: CRS - U195 - 54 mm

Oedometer test - MB-4 - Mini block - CRS

Depth :	9,2	m	σ'_{v0}	155	kPa
Sampling date :	16.02.2023		σ'_{cv}	185	kPa
Opening date:	03.03.2023		OCR	1,19	[-]
Test date :	03.03.2023		Strain rate, $\dot{\varepsilon}$	1,5	%/hr
γ	18,45	kN/m^3	M_0/M_L	4,9	[-]
w :	42	%	$\Delta e/e_0$	0,092	[-]

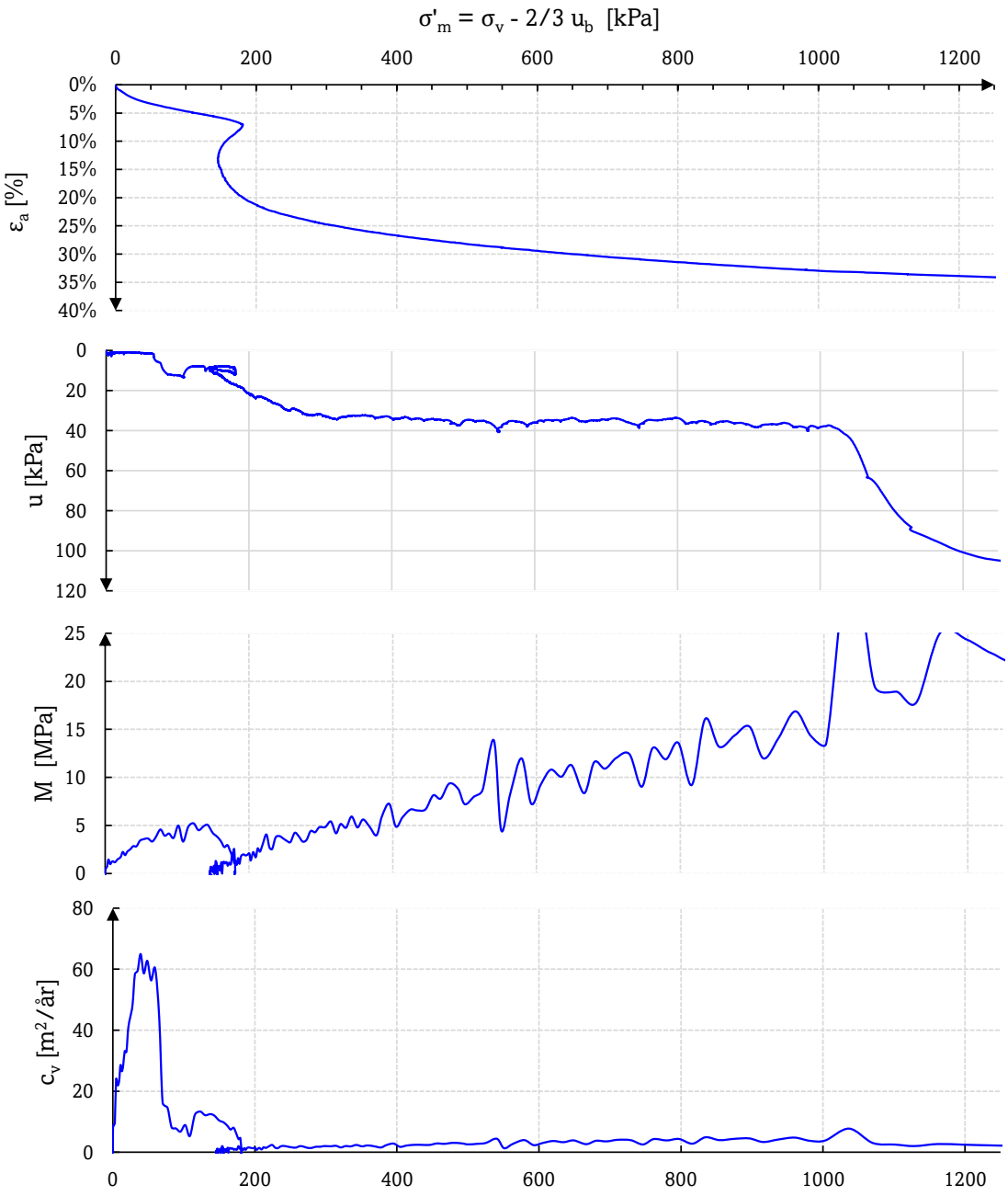

Figure C.10: CRS - MB-4 - Mini block

Oedometer test - MB-3 - "Slow" CRS

Depth :	9,40	m	σ'_{v0}	125	kPa
Sampling date :	16.02.2023		σ'_{cv}	195	kPa
Opening date:	06.03.2023		OCR	1,56	[-]
Test date :	08.03.2023		Strain rate, $\dot{\varepsilon}$	0.75	%/hr
γ	18,1	kN/m^3	M_0/M_L	5,01	[-]
w :	41,6	%	$\Delta e/e_0$	0,105	[-]

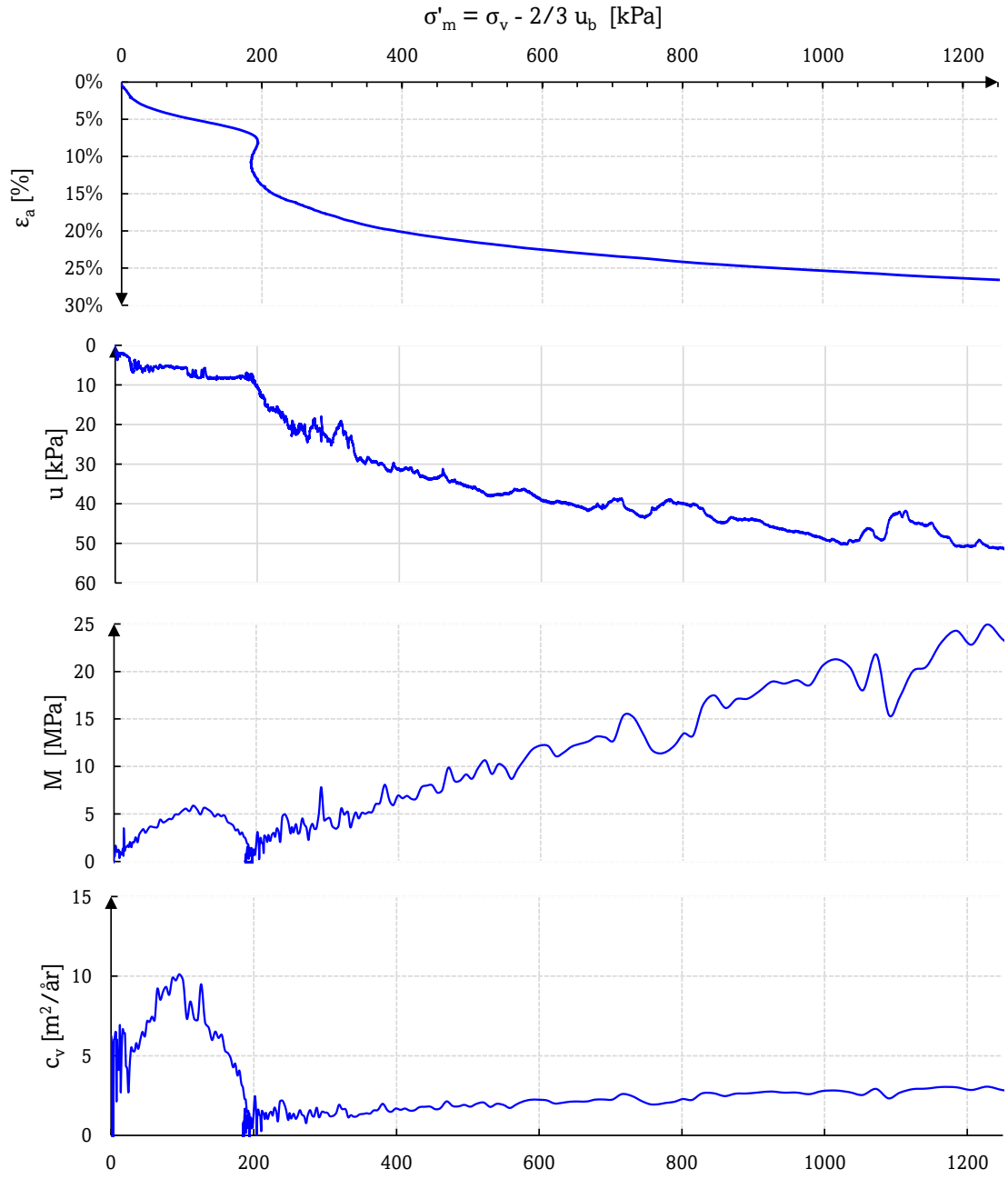

Figure C.11: CRS - MB-3 - Mini block - Slow rate

Oedometer test - MB-3 - Mini block - "Fast" CRS

Depth :	9,5	m	σ'_{v0}	125	kPa
Sampling date :	11.02.2023		σ'_{cv}	230	kPa
Opening date:	01.03.2023		OCR	1,84	[-]
Test date :	01.03.2023		Strain rate, $\dot{\varepsilon}$	3,00	%/hr
γ	18,5	kN/m^3	M_0/M_L	4,20	[-]
w :	41,6	%	$\Delta e/e_0$	0,074	[-]

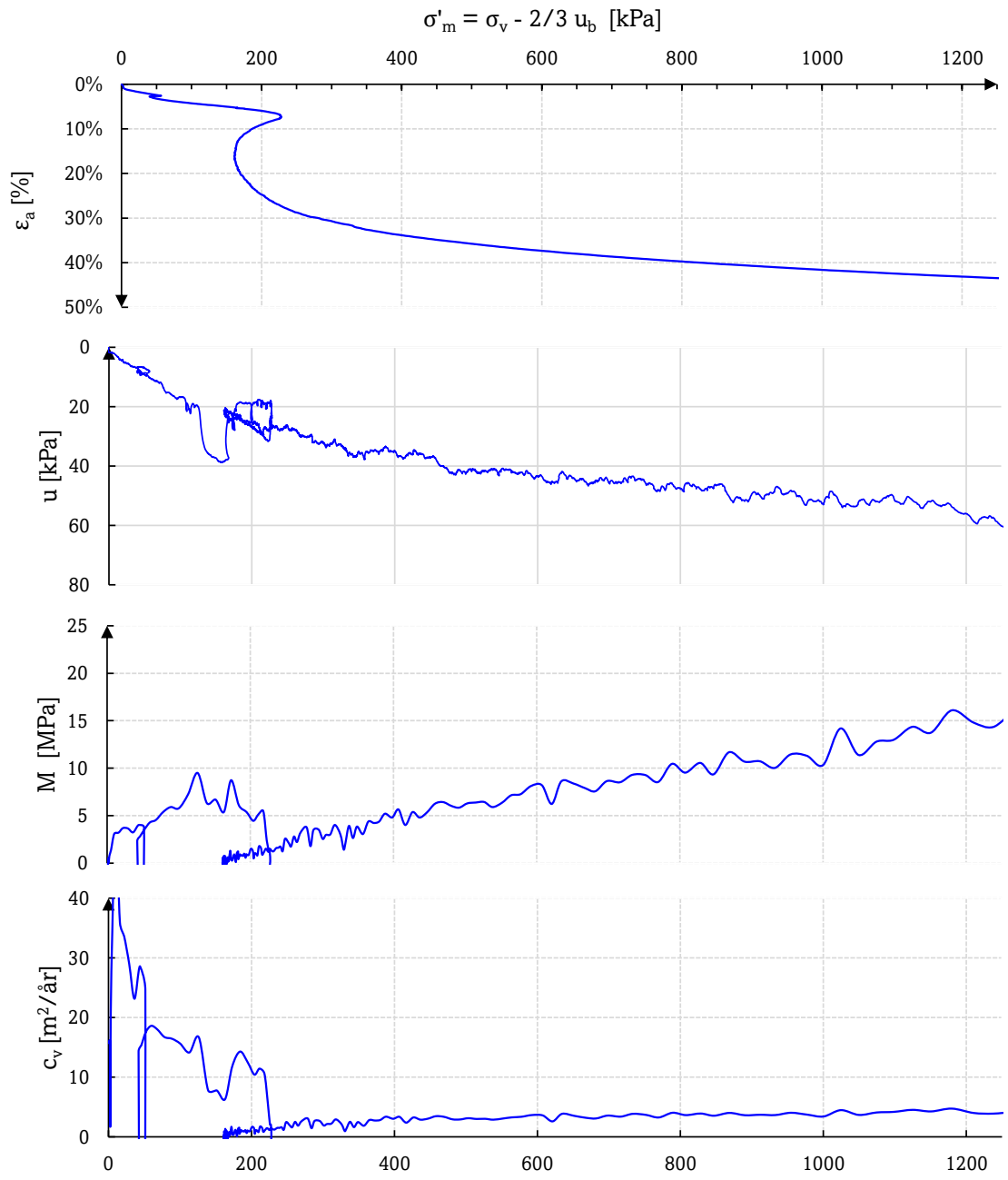

Figure C.12: CRS - MB-3 - Mini block - Fast rate

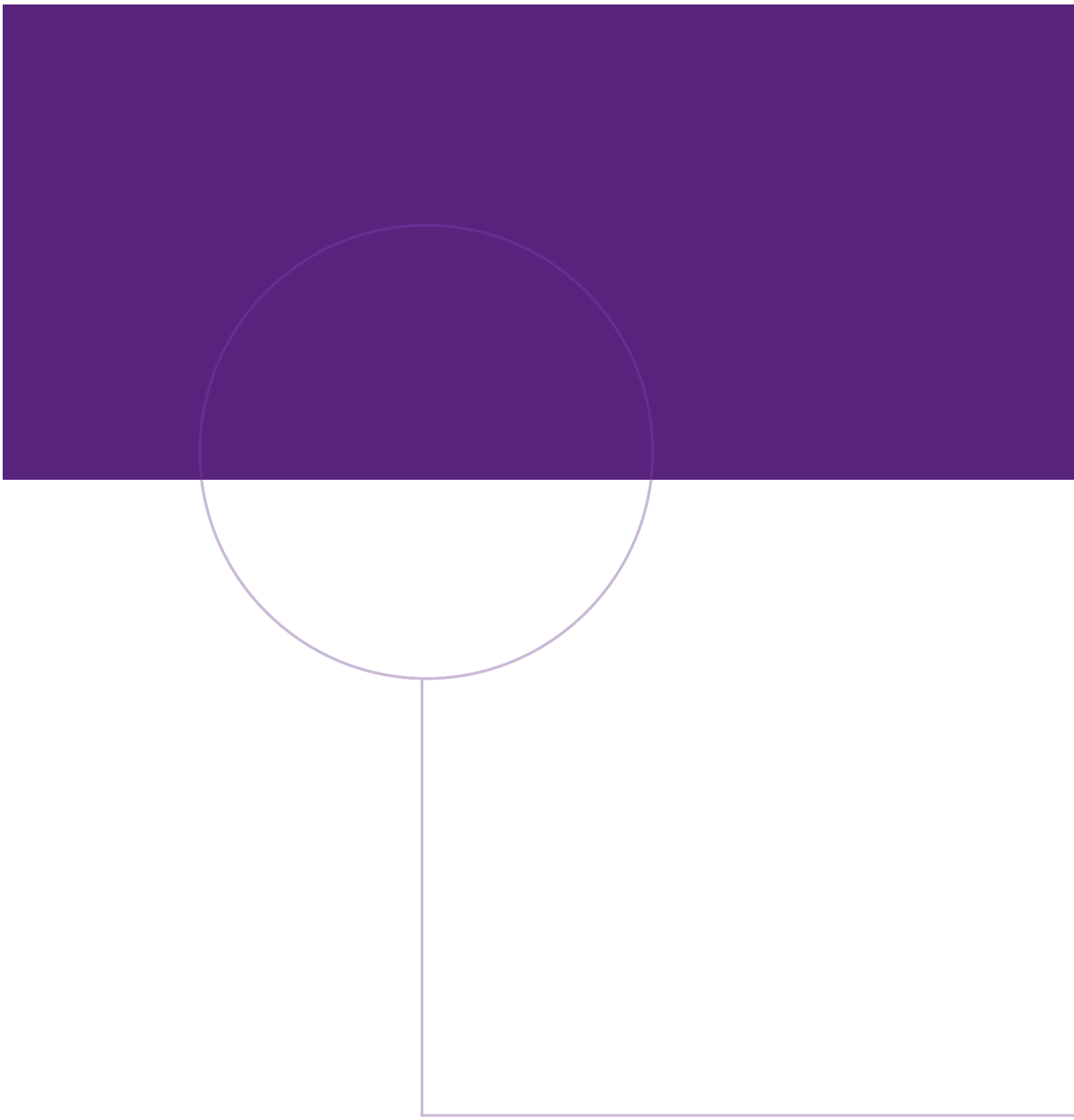

NTNU

Norwegian University of
Science and Technology